Università degli Studi di Modena e Reggio Emilia
Diparimento di Ingegneria "Enzo Ferrari"

PhD SCHOOL in
HIGH MECHANICS AND AUTOMOTIVE DESIGN & TECHNOLOGY
Cycle XXV - Dean: Prof. Eng. Antonio Strozzi

Lightweight Hybrid Structures: Nickel Aluminides and Carbon Nanotubes for High Temperature Applications

Candidate:
Elena Colombini

Supervisor:
Prof. Giorgio Poli

Co-Advisor:
Prof. Eng Paolo Veronesi

Modena, 22nd March 2013

Dissertation Presented in Partial Fulfillment of the Requirements for the Degree Doctor of Philosophy in the Graduate School of the University of Modena and Reggio Emilia

Ai miei genitori

Acknowledgments

Many people have contributed to this dissertation in countless ways, and I am indebted to all of them.

First and foremost, I would like to thank my primary advisor, Prof. Giorgio Poli, for making it possible for me to pursue my PhD at the University of Modena and Reggio Emilia. And a special ‘thank you’ must go to Prof. Paolo Veronesi. You have been a steady influence throughout my Ph.D. career with your patient guidance, support and encouragement, helping me develop new ideas and overcome difficulties. It has been a pleasure to work with you. Your ability to select and tackle challenging research problems, your high scientific standards and your hard work are an example to all.

I am also indebted to Ferrari S.p.A for having given me the invaluable opportunity to spend a year at the Department of Aeronautics and Astronautics, Massachusetts Institute of Technology (M.I.T), USA, where I was able to work with the research team of Prof. Brian L. Wardle, to whom I also extend my thanks. It has been a great privilege to get to know and work with all of them.

Many thanks also to all my colleagues, and to Silvia Gaiani in particular, for providing me with opportunities to learn all about working methods and approaches for problem solving with regard to materials. My thanks too to Andrea and Katia, for their daily patience, helpfulness and kindness.

And last, but not least, I would like to extend my deepest gratitude to my family: my parents, Pier Luigi and Anna Maria, my aunt and uncle, Paola and Andrea, and my grandparents, for their unwavering love, encouragement and support throughout my life. Thank you for believing in me.

Table of Contents

List of Figures

Chapter 2 MACS: Microwave Activated Combustion Synthesis

State of Art

Chapter 3 C/C/CNT: Carbon Nanotube on Crbon Matrix Carbon Fiber Composite State of Art

List of Tables

Chapter 2 MACS: Microwave Activated Combustion Synthesis
State of Art

Chapter 2 MACS: Microwave Activated Combustion Synthesis
Methods & Results

Chapter 3 C/C/CNT: Carbon Nanotube on Crbon Matrix Carbon Fiber Composite
Methods & Results

Symbols and Abbreviations

A	pre-exponential factor
Al_2O_3	Alumina (aluminium oxide)
$AlCl_3$	Aluminum Chloride
Ar	Argon
ATI	Aluminum triisopropoxide, $Al(OC_3H_7)_3$
ATSB	Aluminum tri-*sec*-butoxide, $Al(OC_4H_9)_3$
c	specific heat capacity [J/kgK]
C	Species concentration [$mol \cdot m^{-3}$]
c_0	Initial species concentration [$mol \cdot m^{-3}$]
C	carbon
C/C	carbon/carbon composite
CF	carbon fiber
C_i	liquid composition of precipitate matrix interface
C_xH_y	hydrocarbon fuel (Ethylene (ethene) or Acetylene (ethyne) or Methane)
C_m	far-field composition of liquid alloy
CNT	carbon nanotube
CO_2	carbon dioxide
$conc_{catalyst}$	reference concentration of catalyst
C_s	molar volume of solid metal powder
CS	combustion synthesis
CVD	chemical vapor deposition
$c_{\beta\alpha}^{eq}$	equilibrium concentration gradient
$c_{\beta\gamma}^{eq}$	equilibrium concentration gradient
$c_{\beta\alpha}$	concentration gradient
$c_{\beta\gamma}$	concentration gradient
c(x,y,t)	conserved Shvab-Zeldovich
D	Diffusion coefficient [$m^2 \cdot s^{-1}$]
d	sample diameter
D_0	pre-exponential diffusion coefficient
$\widetilde{D}_\beta$	chemical interdiffusion coefficient
E	Young's modulus
E_a	activation energy [kJ/mol]
EM	electric magnetic
E_{rms}	electric field intensity [V/m]
E_x	electric field x direction
f(n)	function of order reaction
f	frequency [Hz]
$Fe(NO_3)_3$	Iron(III) nitrate
h	lateral heat transfer
H	enthalpy [kJ/mol]
H_2	hydrogen
He	helium
HNO_3	nitric acid
H_2O	water
H_3PO_4	phosphoric acid
h-PSMA	poly(styrene-*alt*-[maleic acid])

h_p	Plank's constant
H_{rms}	magnetic field intensity [V/m]
ΔHsl liquid	latent heat of formation of
H_2SO_4	sulfuric acid
IPA	2-propanol (isopropanol)
K_2CO_3	potassium carbonate
K-PSMA	poly(styrene-*alt*-[dipotassium maleate])
$K_{\beta a}$, $K_{\beta \gamma}$	costant
L	sample length
L	phase transformation enthalpy
MACS	microwave activated combustion synthesis
MW	microwave
MWNT	multi-wall carbon naotube
n	equation order
n_r	order of reaction
N	nitrogen
P_i	products
p	gas pressure
Pd	power density [$W \cdot m^{-3}$]
q	heat source [W/m^3]
q_{ign}	ignition power [$cal \cdot cm^{-2} \cdot s^{-1}$]
q_s	heat flow across the surface
Q	thermal effect of reaction
$\dot{q}^i_{chem}$	heat release
r	initial radius of particle
R	gas constant
R_0	radius of cylindrical sample
R_R	reaction rate [mol/m3·s]
R_i	reactants
RF	radio frequency
$\dot{r}^A_\beta$	state flow rate
S	entropy [J/(mol·K)]
SAR	specific absorption rate [W/kg]
sccm	Standard cubic centimeters per minute = $cm^3\ min^{-1}$ = mL min^{-1}
SEM	Scanning electron microscopy
SiO_2	silica (silicon oxide)
SHS	self propagation high temperature synthesis
SWNT	single-wall carbon nanotube
t_1	best time chosen for CO_2 process
$t_{catalyst}$	reference dipping time into catalyst solution
t_{growth}	growth time
t_{H2}	flow time of hydrogen
t_{opt}	best time chosen for dipping sample into catalyst solution
t_r	reference time to reduce catalyst
T	temperature
T_0	initial temperature
T_1	best temperature chosen for CO_2 process
T_a	room temperature
T_{ad}	adiabatic temperature
T_c	combustion temperature
T_{cr}	crystallization temperature
T_i	intermediate temperature
T_{ig}	ignition temperature
T_p	maximum temperature reached [K]

T_s	surface temperature [K]
T_s	surface temperature
T_ρ	adiabatic temperature at ρ density
t	time
t_{ign}	ignition delay time
TE	thermal explosion
TE	transverse electric
TM	transverse magnetic
TACS	thermal activation combustion synthesis
U	burning velocity [$cm \cdot s^{-1}$]
V_{ad}	adiabatic steady-state velocity
$V_{M\ out}$	velocity prior to quenching
u,v,w	spatial coordinate system
x,y,z	spatial coordinate system
α	effective coefficient of heat transfer
δ_{ts}	time scale factor
δs	skin depth
ε''_{eff}	effective loss factor
ε	emissivity
ε_0	permittivity of free space
ε'	dielectric constant
ε"	loss factor
ε*	complex permittivity
η	degree of conversion
η_s	stochiometry ratio
θ	stability of CS
k_0	pre-exponential factor
λ_0	wavelength of incident MW
λ	thermal conductivity [W/m·k]
λe	effective thermal conductivity
λs	average thermal conductivity of unreacted powder
λr	thermal conductivity reactants
λp	thermal conductivity of fluid in pores
μ'	permeability
μ"	magnetic loss factor
μ'_r	relative permeability
μ''_{eff}	effective magnetic permeability
μ_r	relative permeability
Ξ	coordinate variable
ρ	density [kg/m^3]
Φ	kinetic function
σ	time range
σ	Stefan-Boltzmann constant
σ	electrical conductivity [S/m]
ώ	rate of heating of the substrate with the wave
ω	angular frequency (2πf) [Hz]
X	molar fraction

Abstract

The aim of the activity is focused on laboratory scale production methods of two different lightweight hybrid structures for high performance automotive application and on understanding the influence of several process parameters on the composite final characteristics.

Hybrid materials include composites reinforced by fibers or particles, foams and lattices, and almost all natural materials. The goals of hybrid structures are the combination of different material properties, maximization of structural efficiency, weight and costs reduction. In the present study two types of hybrid materials showing different structures and target applications were analyzed.

The first one is an intermetallic, in particular a nickel aluminide, produced through combustion synthesis (CS) activated by microwaves. This lightweight intermetallic, in details aluminide, is applied as joining material between heterogeneous base metals, like inconel and titanium, and it can also be used to *in-situ* repair damaged components and for assembling components presenting dissimilar characteristics, which need to be simultaneously exposed to different environments and/or temperature and/or mechanical stresses.

The latter is a nanostructured composite where carbon nanotubes (CNTs) are grown on substrates made of carbon-matrix reinforced with carbon-fibers, by means of chemical vapor deposition. The benefits expected from the use of CNT-containing hybrid structures are related to the possibility to control expansion coefficient of the final components, and meanwhile to improve wear resistance, hydrophobicity and thermal conductivity. Thanks to high wear resistance at elevated temperature, carbon-matrix carbon-fiber composite are currently used for high performance brake and clutch manufacturing in automotive applications.

The two hybrid materials have been investigated using two different approaches.

With respect to nickel aluminides, the main research purpose is focused on developing a predictive and mathematical model of microwave ignited and sustained CS of micrometric metal powders. The simulation couples, for the first time, chemical, thermal and electromagnetic models to overcome the difficulty, or impossibility, to perform non perturbative temperature measurements during microwave initiated CS. The combustion synthesis process has been chosen as joining technique because is based on the highly exothermic reaction by reactants, which, if properly ignited, spontaneously turn into products. In addition the activation by microwave heating is particularly efficient because is based on energy transfer instead of heat transfer. Thus it allows continuous heating during and after the ignition, varying the cooling rate and leading to a more rapid

temperature increase of the whole reaction zone. Numerical simulation is also used to estimate the heating and cooling rates in each portion of the reactants and products volume, as well as of the surrounding substrates and supporting materials. As a consequence it is demonstrated the variation of microstructure and the minimization of heat affected zone extension.

Concerning nanostructured carbon composites, two different experimental approaches that allow the synthesis of CNT on carbon-based substrate have been developed. One method exploits a barrier layer between substrate and CNTs, the other grow CNTs directly on the carbon-matrix carbon-fiber composite. Both techniques were successfully developed but the desirable aligned CNTs is achieved only by the barrier approach, indeed high-yield but unaligned CNTs have been obtained by the no-barrier approach. Optimization studies of growth parameters yielded preliminary materials that were processed into carbon-CNT matrices via infusion and pyrolysis. In all cases porosity of the material from one infusion is too high, revealing that further infusion studies need to be developed. The results indicate that CNTs on C/C composite is a promising approach for improving the mechanical, electrical and thermal properties of structural composites. However, further developments are necessary before evaluating wider issues concerning the new composite material like infiltration with the carbon matrix precursors and optimization of such process.

Riassunto

Questa attività di ricerca è focalizzata sullo studio dei metodi produttivi su scala di laboratorio di due differenti strutture ibride a bassa densità per applicazioni nel settore *automotive*, con lo scopo di valutare l'influenza di diversi parametri di processo sulle caratteristiche finali del materiale composito.

I materiali ibridi comprendono compositi con rinforzo mediante fibre o particelle, schiume e lattici, e quasi tutti i materiali naturali. L'interesse scientifico di questi materiali è orientato sulla loro capacità di combinare diverse proprietà, massimizzare l'efficienza strutturale, minimizzare il peso ed i costi di produzione.

In questo studio sono state analizzate due tipologie di materiali ibridi con differenti strutture ed applicazioni. Il primo materiale è un intermetallico, nello specifico un alluminuro di nichel, che viene prodotto attraverso sintesi per combustione (CS) attivata da microonde. Esso viene impiegato come elemento di giunzione fra materiali eterogenei, come inconel e titanio, e risulta essere adatto sia per riparare componenti *in-situ* sia per assemblare componenti con diverse caratteristiche, che devono, per esempio, essere contemporaneamente esposti ad ambienti o sforzi meccanici differenti.

Il secondo è invece un composito nanostrutturato dove nanotubi di carbonio (CNTs) sono fatti accrescere, mediante tecnica di Chemical Vapor Deposition, su di un substrato a matrice di carbonio rinforzato con fibre di carbonio. I benefici nell'impiego di tali strutture ibride sono la possibilità di controllare il coefficiente di espansione termica del componente finale, migliorandone la resistenza all'usura, l'idrofobicità e la conducibilità termica. Grazie alla resistenza all'abrasione ad elevata temperatura, i compositi in matrice di carbonio rinforzata con fibre di carbonio vengono impiegati nel gruppo freno e/o frizione nel settore delle competizioni automobilistiche.

I due materiali sopra descritti sono stati analizzati utilizzando due diversi approcci.

Nel caso degli alluminuri di nichel, lo scopo principale della attività di ricerca è basato sullo sviluppo di un modello matematico predittivo della CS di polveri metalliche micrometriche innescata da microonde. La sintesi per combustione è stata scelta come tecnica di giunzione grazie alla sua capacità di sfruttare reazioni chimiche fortemente esotermiche che, una volta innescate, si autopropagano fino a completo esaurimento delle specie reagenti. Inoltre grazie al riscaldamento a microonde, che si basa sul trasferimento di energia invece che sul trasporto di calore, una volta innescata la reazione, è possibile continuare a generare calore nei prodotti, riscaldandoli e minimizzando la zona termicamente alterata. La simulazione ha accoppiato il modulo chimico, termico ed elettromagnetico al fine di ottenere informazioni altrimenti difficilmente misurabili per via sperimentale. In tal modo è possibile valutare sia la

variazione composizionale e delle temperature sia la cinetica di reazione durante il procedere della sintesi, dimostrando come l'applicazione delle microonde durante e dopo la sintesi possa alterare la velocità di raffreddamento dei prodotti e, di conseguenza, la loro microstruttura.

Nello studio dei compositi in carbonio nanostrutturati si sono invece analizzati due differenti approcci sperimentali che permettano la sintesi di CNT su substrato a base carbonio, i quali differiscono per la presenza o meno di uno strato intermedio di allumina tra componente e rivestimento. Entrambe le tecniche sono state sviluppate con successo, ma se da un lato l'allineamento dei nanotubi di carbonio sul substrato è stato raggiunto esclusivamente dal sistema che sfrutta lo strato di allumina, una buona distribuzione e una buona aderenza con il substrato sono state ottenute in entrambi i sistemi.

L'ottimizzazione dei parametri di crescita ha prodotto un materiale preliminare, il quale può essere elaborate tramite pirolisi per ottenere il composito C/C/CNTs. In tutti i casi analizzati la porosità del materiale ottenuto usando solamente una o due infusioni è troppo elevata, pertanto ulteriori studi di questa fase del processo devono essere condotti. I risultati ottenuti indicano che la crescita di CNTs un approccio promettente per migliorare le proprietà meccaniche, elettriche e termiche di compositi strutturali. Tuttavia, il presente lavoro costituisce solamente uno studio preliminare di una tematica più ampia nell'ambito dello sviluppo di un nuovo materiale composito, come l' infiltrazione in resina e l'ottimizzazione di tale processo.

Chapter 1
Introduction

Lightweight materials, their manufacturing and their durability in extreme conditions are important topics in several industries. There are three major application fields where lightweight materials play an important role in products: aerospace, alternative energy, and automotive.

To realize efficient lightweight structures, it is mandatory to develop new materials and cost-effective manufacturing technologies. Often a single material or structure, tough lightweight, does not possess all the required properties, thus hybrid structures are then needed. Tailored materials are manufactured with the purpose to combine different properties demanded for a specific application. Mechanical strength, stiffness, toughness or damage tolerance, electrical and thermal conductivity, thermal contraction/expansion, environmental and corrosion resistance and manufacturability are only few examples of tailorable properties. The optimization of different properties sets is in general more difficult than the achievement of a single material property. Particularly interesting are hybrid structures which combine dissimilar materials, like metal/ceramic or metal/intermetallics. Such hybrid structures exhibit special properties or properties combination, allowing to maximize the structural efficiency and/or minimize weight, while preserving natural resources by limited use of materials, and simultaneously minimizing fabrication and operating costs. Hybrid composite architectures, combining traditional composite materials, offer significant potential mechanical and multifunctional performance benefits.

One of the most relevant processes to realize hybrid structures with dissimilar materials is joining. Industrial and large scale joining of metals (by welding) dates back to 1750 (Industrial revolution), but joining between dissimilar materials such as ceramic and metals is nowadays one of the most challenging aspect in the research field of advanced and high temperatures material applications. Engineering ceramics present appealing applications as structural and electronic materials due to their excellent mechanical properties at high temperature as well as resistance to wear, erosion, oxidation and corrosion. Thus, especially in high temperatures application fields, ceramics and ceramic matrix composites generally present higher performances than metals. Anyway, ceramic materials are usually brittle and difficult to machine, hence it is hard to use them to manufacture complex-shaped parts. Therefore, it is reasonable to manufacture composite parts of ceramics and metals by joining techniques, in order to meet possible project requirements. Joining dissimilar materials is an attractive technique also to both in situ repair damaged components and for applications requiring

components with different characteristics, since, as mentioned above, they will need to be contemporary exposed to different environments and/or temperature and/or mechanical stress.

The most used joining techniques involving ceramics, at the state of the art, are: active metal brazing, diffusion bonding and transient (or partial transient) liquid phase bonding, brazing, arc welding, friction welding, laser welding and many others are used to join also metals and alloys.

1.1. Motivation

The aim of the doctorate research activity is focused on the laboratory study and optimization of two innovative methods to manufacture, with possible scale up at the industrial scale, two different lightweight hybrid structures for high performance automotive applications:

- microwave-synthesized brazing materials to be used to join dissimilar materials like nickel-superalloys and titanium lightweight alloys or titanium and aluminide intermetallics or silicon carbide ceramics
- carbon-matrix carbon-fiber composite coated or reinforced by aligned carbon nanotubes, to obtain a new composite materials suitable for high performance tribological applications, like brakes.

In this work, an innovative microwave-assisted joining process is proposed, using the heat developed during the rapid reaction of metallic powder precursors to generate intermetallic compounds. As a matter of fact, intermetallic compounds are currently being investigated for potential high temperature structural applications. They are lightweight materials, their density is less than half of the superalloys one, and they are highly resistant to oxidation and burning.

Carbon nanotubes are thought to be promising candidates for selective reinforcement of matrix-rich interlaminar regions due to their nanoscale diameter, high aspect ratios and desirable mechanical, electrical, and thermal properties. Carbon nanotube growth on carbon composite surface to create hierarchical carbon structures is a promising approach for improving mechanical, electrical and thermal properties of a structural composite. Due to their extraordinary (and anisotropic) thermal conductivity and mechanical and electrical properties, carbon nanotubes find applications as additives to various structural materials. The benefits expected from the use of carbon nanotube-containing hybrid structures, in this study, are related to the possibility to control expansion coefficient of the final components, and meanwhile to improve wear

resistance, hydrophobicity and thermal conductivity. These characteristics make these materials excellent for lightweight reinforcement for numerous applications, ranging from aerospace to high performance automotive. However, state of the art technologies do not allow to grow aligned carbon nanotubes on industrial substrates, and in this work a new method will be developed and optimized.

As is known from literature, both carbon-based and intermetallic-based materials are applied in aerospace, aircraft, automotive and energy field, where high strength, low weight and high temperature resistance are required. For instance, CNTs are applied in energy storage media, high performance polymer and ceramic composites, electronic components, logic and memory chips, sensors, catalyst support, adsorption media, actuators. Intermetallic materials are currently used in advanced aero-engines and automotive parts for high temperature structural use, in power plants, chemical and nuclear industries thanks to their high temperature resistance. The opportunities of using such materials for aerospace industry are in the field of thermal barrier and wear resistant coatings and sensors that can perform at high temperature, sensors. Other interesting fields are composites, wear resistant tires, improved avionics, satellite, communication and radar technologies.

1.2. Thesis Outline

In this work two types of hybrid materials, showing different structures and target applications and possible innovative processing routes, are analyzed: one involves the microwave assisted combustion synthesis of intermetallics belonging to the aluminides family, to be used for dissimilar material joining (Chapter 2), the other involves the use of advanced deposition techniques to obtain carbon-matrix carbon-fiber composites (C/C) reinforced by aligned carbon nanotubes (CNTs)(Chapter 3).

The first hybrid structure is described in Chapter 2. An intermetallic, in detail a nickel aluminide, produced through combustion synthesis activated by microwaves, has been applied as joining material, between heterogeneous base metals, like inconel and titanium. This approach, besides providing the required joints, can also be used to in-situ repair damaged components and for assembling components presenting dissimilar characteristics, which need to be simultaneously exposed to different environments and/or temperature and/or mechanical stresses. The main research purpose is focused on developing a predictive and mathematical model of combustion synthesis of micrometric metal powders ignited and sustained by microwave, in order to gain understanding and control of such a rapid and extremely exothermic process. This demanding task will require the coupling of electromagnetic, heat transfer and chemical

application modes of the FEM software Comsol Multiphysics® . In the first part of Chapter 2 (Chapter 2.1), an overview of combustion synthesis techniques and intermetallic combustion synthesis is described, in particular from the modeling point of view. Afterwards the microwave ignited combustion synthesis is summarized, focusing on microwave as system to activate combustion synthesis in metal powder mixtures. In the second part of Chapter 2 (Chapter 2.2), the newly developed multiphysic models are described. For the first time, a fully coupled 3D model of the microwave combustion synthesis is proposed, tough in a simplified version due to the lack of reliable temperature dependent properties of the materials involved. In detail, the synthesis of NiAl between different metal substrates and silicon carbide system is investigated, in order to understand how the processing parameters can influence the final products properties and microstructure, as well as the extension of the heat affected zones. Simulation results have been validated experimentally using NiAl synthesis on titanium substrate. The developed model could be useful to forecast behavior of aluminides used for joining of dissimilar materials. Furthermore electromagnetic field distribution, concentration development of powder, compositional and temperature variations, as well as kinetic reactions during the combustion synthesis and the volume of heat affected, if a threshold temperature value depending on joining material is fixed, could be established.

The second hybrid structure, described in Chapter 3, is a nanostructured composite where carbon nanotubes (CNTs) are grown on carbon-matrix carbon-fiber composite, by means of chemical vapor deposition technique. The first part of Chapter 3 (Chapter 3.1) is a background about polymer nanocomposites, carbon nanotube synthesis, growth theories and barrier coating deposition methods, like CVD and sol-gel techniques. In the second part (Chapter 3.2) the optimization of such experimental procedures to coat a carbon/carbon composite by aligned carbon nanotube has been studied. Two different experimental approaches that allow the synthesis of CNT on carbon-based substrate are developed. One method (“barrier”) exploits a barrier layer between substrate and CNTs, while the other (“non-barrier”) is aimed at growing CNTs directly on the carbon-based composite. Both techniques were successfully developed, but the desirable alignment of CNTs is only achieved by the barrier approach, while high-yield but unaligned CNTs are shown by the non-barrier approach. Optimization studies of growth parameters yielded preliminary materials that were processed into carbon-CNT matrices via infusion and pyrolysis. The obtained materials are then characterized in terms of porosity and hardness, showing the different properties deriving by a different degree of alignment.

An overall summary of the achieved results and perspective for future developments are outlined in Chapter 4.

Chapter 2
MACS: Microwave Activated Combustion Synthesis

2.1. Background

Hybrid composite architectures combining traditional composite materials offer significant potential mechanical and multifunctional performance benefits[1]. Joining is a secondary manufacturing procedure exploited to produce parts and devices with wider dimensions and complex geometries. Assembling by joining simpler and/or smaller components to build up complex shaped or large sized items usually reduces production costs. Joining techniques are often necessary in order to in situ repair damaged components, thus leading to time and energy savings. Moreover, joining between dissimilar materials is attracting when a component must own different characteristics since its parts will need to be contemporary exposed to different environments and/or temperatures and/or mechanical stresses. Traditional fusion welding is not suitable to join materials characterized by different properties[2], but today innovative brazing or welding processes are increasingly attracting more attention in industry because they can reduce the material costs and improve the design flexibility[3]. Some of the greatest challenges in the welding or brazing of materials occurs with intermetallics, both as monolithic and as reinforced composite forms[4]. The ability to join either class of material to metals would be extremely beneficial for hybrid structures[5]. The goals of hybrid structures, which combine dissimilar materials metal/ceramic or metal/intermetallic, are numerous: achievement of special properties or properties combination, maximization of structural efficiency and/or minimization of weight, conservation of limited materials resources, minimization of fabrication and operating costs and environmental compatibility[6].

---

1 C. Pascal, R.M. Marin-Ayral, J.C. Tedenac, Joining of Nickel Monoaluminide to a Superalloy Substrate by High Pressure Self-Propagating High-Temperature Synthesis, J. Alloys Comp., 337 (2002) 221-225

2 J.C. Feng, J. Cao, Z.R. Li, Microstructure Evolution and Reaction Mechanism during Reactive Joining of TiAl Intermetallic to TiC Cermet Using Ti–Al–C–Ni Interlayer, J. Alloys Comp., 436, (2007) 298–302

3 H.C. Chen, A.J. Pinkerton, L. Li, Fiber Laser Welding of Dissimilar Alloys of Ti–6Al–4V and Inconel 718 for Aerospace Applications, Int. J. Adv. Manuf. Technol., 52 (2010) 977– 987

4 R.W. Messler *et al.*, Welding with SelfPropagating HighTemperature Synthesis, Welding J., 74 (1995) 37–44

5 R.W. Messler, Joining Advanced Materials, Adv. Mater. Process., 2 (1995) 47–49

6 C. Pascal, R.M. Marin-Ayral, J.C. Tedenac, Joining of Nickel Monoaluminide to a Superalloy Substrate by High Pressure Self-Propagating High-Temperature Synthesis, J. Alloys Comp., 337 (2002) 221-225.

Combustion synthesis (CS) as joining technique offers many attractive features also for advanced materials joining applications. Among these it mainly lies in rapid and highly localized heat generation distinctive of CS processes. The direct consequence of this particular joining procedure appears to be the possibility to limit the extension of heat affected zones (HAZ), thus avoiding excessive thermal damage of heat sensitive substrate microstructures. Moreover, the great chemical compatibility between selected reaction products and the substrates should be mentioned, as the process being used to produce the joint, is often the same as the process that was or could have been used to produce the substrates[7].

2.1.1. Combustion Synthesis

The process of Combustion Synthesis (CS) is a synthetic method for producing a wide class of simple and complex inorganic materials having high chemical purity and excellent physical and mechanical properties. In 1967, Merzhanov, Skhiro and Borovinskaya published[8] the first paper describing the self-sustaining reaction in a condensed phase, which could be applied to synthesize many ceramic and intermetallic materials[9]. The authors studied experimental models of combustion in condensed systems and discovered a process during which all substances (starting, final, and sometimes intermediate) exist in the solid state even at very high combustion temperatures. The phenomenon was called solid flame or solid combustion. The process is based on the highly exothermic reaction by reactants, which, if properly ignited, spontaneously turn into products. Solid flame was first discovered in mixtures of titanium and boron powders, whose interaction was performed in autowave mode as a running wave of the oxygen-free combustion in an inert atmosphere to form titanium monoboride, as the combustion product. The main stages of the process are: initiation (ignition), propagation of the front separating a mixture of the initial reagents from the incandescent combustion product, cooling of final product [10].

---

7 R. Rosa, Microwaves as Ignition Source in the Combustion Synthesis of High Performances Materials, Doctor of Philosophy “High Mechanics and Automotive Design and Technology” at the University of Modena and Reggio Emilia (2010)

8 A.G. Merzhanov, V. M. Shkiro, I. P. Borovinskaya, Synthesis of refractory inorganic compounds, USSR Pat. 255221, 1967; Fr. Pat. 2088668, 1972; US Pat. 3726643, 1973; UK Pat. 1321084, 1974; Jpn. Pat. 1098839

9 W. McCauley, J.A. Puszynski, Historical perspective and contribution of US researchers into the field of self-propagating high-temperature synthesis (SHS)/combustion synthesis (CS): Personal reflections, Int. J. SHS 17 (2008) 58-75

10 A. G. Merzhanov, Reviews: Fundamentals, achievements, and perspectives for development of solid-flame combustion, Russian Chemical Bulletin 46 (1997) 1-27

Combustion synthesis (CS) exploits the propagation of a combustion front across the reactants mixture. The method is based on the ability of an exothermic heterogeneous chemical reaction to become self-sustaining and propagate as a combustion wave through the mixture of the reactants. A reaction will become self-propagating when there is sufficient heat release by the reaction to ignite reactants ahead of the reaction zone [11].

When metallic powders are used as reactants, compared to conventional powder metallurgy techniques, combustion synthesis excludes the requirement for high-temperature sintering; moreover, volatile contaminants or impurities may be eliminated whereas the high-temperature combustion wave propagates through the whole sample. CS is characterized by high reaction temperatures (2000-5000 K), fast combustion rates (0.1-200 cm/s), and high temperature gradients (up to 10^6 K/cm). From these properties, other technologically interesting characteristics follow: high degree of conversion and intrinsic ability to partial self-purification from impurities and synthesis rapidity.[12,13] The steep temperature gradient can also create metastable or non-equilibrium phases which are not accessible by conventional processing.[14,15,16,17]

The CS process encompasses two different sub-processes depending on the way in which the ignition is reached: self-propagating mode, often referred to as SHS and simultaneous combustion mode, often referred to as thermal explosion (TE). In the Self-propagating High-temperature Synthesis (SHS) ignition way, the reaction is ignited at one end of the reactive specimen and it is self-propagated throughout the whole sample, in the form of a propagating combustion wave, thus the wave is driven by exothermic heat generated by an adjacent layer. In the thermal explosion mode the whole volume of the reactive mixture is heated uniformly up to the ignition temperature allowing the reaction to take place simultaneously in the entire sample. The simultaneous combustion mode is generally conducted in a furnace where the entire reactants are heated simultaneously. In both case the combustion reaction wave moves through the reactants

---

[11] C.R. Bowen, B.Derby, Finite-difference modelling of self-propagating high-temperature syntheses of materials, Acta metall. mater., 43 (1995) 3903-3913

[12] M. Arimondi *et al.*, Chemical Mechanism of the $Zr+O_2 \rightarrow ZrO_2$ Combustion Synthesis Reaction, J Phys. Chem. B, 101 (1997) 8059–8068

[13] S. Gennari *et al.*, A new approach to the modeling of SHS reactions: Combustion synthesis of transition metal aluminides, Acta Materialia 54 (2006) 2343–2351

[14] M. Gupta, W.W.L. Eugene, Microwaves and metals, John Wiley and Sons, Singapore, 2007

[15] P.Veronesi *et al.*, Microwave assisted combustion synthesis of non-equilibrium intermetallic compounds, JMPEE, Journal of Microwave Power and Electromagnetic Energy 44 (2010) 45-56.

[16] M. Gupta, W.W.L. Eugene, Microwaves and metals, John Wiley and Sons, Singapore, 2007

[17] M. Arimondi *et al.*, Chemical Mechanism of the $Zr+O_2 \rightarrow ZrO_2$ Combustion Synthesis Reaction, J Phys. Chem. B, 101 (1997) 8059–8068

like a propagating wave without needing further external heat input. Actually, many combustion synthesis reactions lie in the middle of ignition way described. [18,19,20,21]

In the initial studies Merzhanov[22] investigates reactions of direct synthesis from element via the scheme: $R_1+R_2 \rightarrow P+Q$, where R_1 and R_2 are reactants, P is a product and Q is the heat effect of the reaction. Systems and processes studied were divided into two groups. The first includes mixtures of powders (both R_1 and R_2), in which combustion occurs without participation of the gaseous medium (in vacuum or in an inert gas) and does not result in the gasification of reactants. It is the so-called gasless combustion. The second group contained hybrid systems, in which one powder (R_1) is a metal powder, as a filling or moulded sample, and the other, R_2, is a gas. At rather low pressures of the gas, its content in pores of the sample is small, and the self-propagating (frontal) process can occur only due to the spontaneous infiltration of the gas from the environment to the combustion front. The typical parameter values that characterized the process are reported on Table 2.1-1.

Table 2.1-1: Main parameters of SHS process

Initial System		**Process**	
Parameter	Value	Parameter	Value
Size of particle, r [μ]		Burning velocity, U [cm·s^{-1}]	0.1-20
metals non metals	5-100 0.1	Adiabatic temperature, T_{ad} [K]	2300-3800
Relative density of samples, Δ	0.3-0.6	Power of ignition q_{ing} [cal·cm^{-2}·s^{-1}]	10-200
Size of samples diameter, d [mm] length, l[mm]	 5-20 (2-5)d	Delay of ignition, t_{ign} [s]	0.2-1.2
Initial temperature, T_0 [°C]	25-400	Combustion temperature, T_c[K]	800-1200
Pressure of gas, p [atm]	1-150	Rate of heating of the substance in the wave, ώ [deg·s^{-1}]	10^3-10^6

[18] A. Varma, J.P. Lebrat, Combustion Synthesis of Advanced Materials, Chem. Eng. Sci. 47 (1992) 2179-2194

[19] K. Morsi, The diversity of combustion synthesis processing: a review, J. Mater. Sci.,47 (2012) 68-92,

[20] R.W. Messler *et al*., Welding with SelfPropagating HighTemperature Synthesis, Welding J., 74 (1995) 37–44

[21] R.W. Messler, Joining Advanced Materials, Adv. Mater. Process. 2 (1995) 47–49

[22] A.G. Merzhanov, Reviews: Fundamentals, achievements, and perspectives for development of solid-flame combustion, Russian Chemical Bulletin 46 (1997) 1-27

2.1.1.1. Thermodynamics Consideration

The high combustion temperature associated with a CS reaction is related to the enthalpy change between the reactants and products. A general combustion synthesis reaction can be expressed as:

Eq. 1 $$\sum n_i R_i = \sum n_j P_j,$$

where R_i, P_j refer to the appropriate reactants and products respectively, and n_i, n_j are the stoichiometric coefficients of the reactants and products[23].

A schematic representation of a typical temperature-time plot for a combustion synthesis reaction is given in Figure 2.1–1[24].

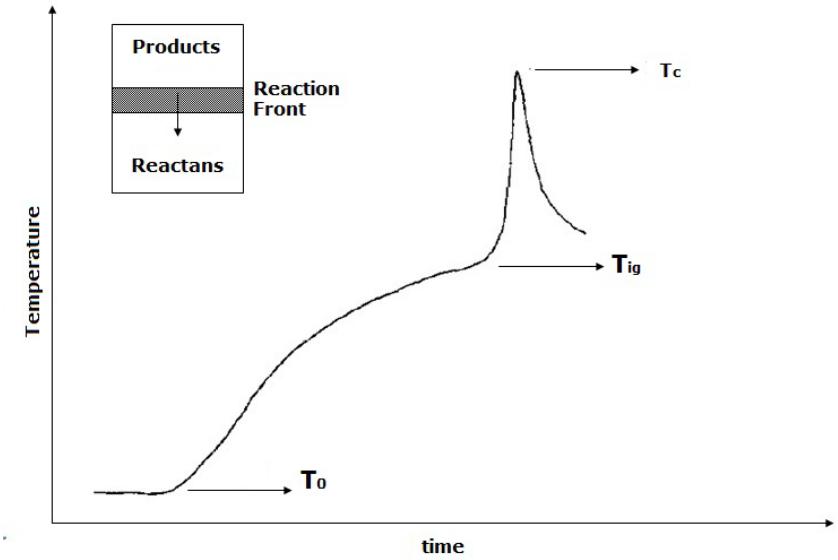

Figure 2.1–1: Schematic representation of the temperature-time curve during an SHS reaction

Combustion synthesis reaction is described by means of four different temperatures, which may affect both the reaction process and final product properties. The typical temperatures are:

1) initial temperature (T_0), i.e. average temperature of reactant sample before the reaction is ignited in the propagation mode;
2) ignition temperature (T_{ig}), i.e. the point at which the SHS reaction is dynamically activated without further external heat supply;

[23] J.J. Moore, H. J. Feng, Combustion synthesis of advanced materials: Part I. Reaction parameters, Progress Mater. Sci. 39 (1995) 243-273

[24] Ibidem

3) adiabatic combustion temperature (T_{ad}), i.e. maximum combustion temperature achieved under adiabatic condition
4) actual combustion temperature (T_c), i.e. maximum temperature achieved normally under non-adiabatic conditions.

The slow step of particles reaction is due to diffusion processes in the solid state, but this is contradicted by the observed burning speed.[25] Moreover, the reagent interaction occurs with a strong delay due to the product formation as a barrier layer between them. For gas combustion, the kinetic reaction lateness associated with burning out of the initial substance is low, and the process is determined by the strong heat acceleration of the reaction. As a consequence, the combustion front is formed at an almost complete reagent transformation in a narrow (compared to the pre-flame zone) zone adjacent to the combustion products. The front propagation speed (V) is determined by the maximum combustion temperature (T_{max}), which can be calculated from thermodynamic concepts. These classical ideas were developed by Zeldovich and Frank- Kamenetskii[26]. In solid flames, the kinetic retardation is strong due to peculiar laws of the interaction of elements (diffusion reaction) and is comparable with the thermal self-acceleration of the reaction. As a result, they compete in the combustion wave. Thereby the burning speed is determined by the incomplete conversion ($\eta<1$) and is related to some intermediate temperature T_i, which is lower than T_{max}. The parameters established that the burning speed cannot be thermodynamically calculated and must be calculated from some additional macrokinetic condition. Thus, the specific features of the solid combustion are caused by high values of the heat effect of the reaction and difficulties in the achievement of completeness of the heat release.

As previously stated, combustion synthesis (CS) arises from enthalpy of formation of the reaction products. If the enthalpy value is high enough, the reaction is self-sustained and does not require any further external energy source in addition to the energy contribution required to reach the ignition temperature, thus reaction starts at a triggering or ignition temperature and it is sustained by self heating of the unreacted portion of the mixture, associated with the release of exothermic formation heat [27] [28].

---

[25] A.G. Merzhanov, Reviews: Fundamentals, achievements, and perspectives for development of solid-flame combustion, Russian Chemical Bulletin 46 (1997) 1-27

[26] A.G. Merzhanov, Reviews: Fundamentals, achievements, and perspectives for development of solid-flame combustion, Russian Chemical Bulletin 46 (1997) 1-27

[27] R.W. Messler et al., Welding with SelfPropagating HighTemperature Synthesis, Welding J., 74 (1995) 37–44

[28] R.W. Messler, Joining Advanced Materials, Adv. Mater. Process. 2 (1995) 47–49

The amount of heat, H(R), needed to perform a CS could be estimated considering an exothermic CS reaction of a reactant powder mix, at an initial temperature T_0, ignited under adiabatic conditions, in the propagating mode, up to T_{ig}. Thus the reactants need to be heated from T_0 to T_{ig}. The equation is given by:

Eq. 2 $$\mathbf{H(R) = \int_{T_0}^{T_{ig}} \sum n_i c(R_i) dT + \sum_{T_0 - T_{ig}} n_i L(R_i)}$$

where $c(R_i)$, $L(R_i)$ are heat capacity and phase transformation enthalpy of the reactants, respectively, if the reactants go through a phase change, e.g. solid to liquid.

The reactant mixture reaches a steady-state at a certain distance from the heat source, from this point $\Delta H(T_{ig})$ only is used to heat the adjacent reactant layer from T_0 to T_{ig}, indeed there is no influence of the heat source on this unreacted layer. Therefore since H(R) is needed to heat the reactants from T_0 to T_{ig}, the amount of heat available to be absorbed by the products under adiabatic conditions is H(P), such that, using the general sign convention for enthalpy:

Eq. 3 $$\Delta H(T_{ig}) = -[H(P) + H(R)]$$

Whereupon, under these conditions, the maximum adiabatic temperature, achievable is dependent on H(P) value. Since all this heat, H(P), is absorbed by the products under adiabatic conditions, the adiabatic temperature will be $T_{ad}(T_0)$. The heat, H(P), required to raise the temperature of the products from T_{ig} to $T_{ad}(T_0)$ is given by:

Eq. 4 $$\mathbf{H(P) = \int_{T_{ig}}^{T_{ad}(T_0)} \sum n_j c(P_j) dT + \sum_{T_{ig} - T_{ad}(T_0)} n_j L(P_j)}$$

where $c(P_j)$, $L(P_j)$ are the heat capacity and the phase transformation enthalpy of the products respectively, as quoted above. Increasing the initial temperature from T_0 to T_1 will decrease H(R), increase H(P) and increase T_{ad} to $T_{ad}(T_1)$. Increasing T_0 to T_{ig} will decrease H(R) to zero and all of $\Delta H(T_{ig})$ will be available to be absorbed by the products, resulting in an adiabatic temperature of $T_{ad}(T_{ig})$. Under these conditions the reaction is ignited under the simultaneous combustion mode. It is, therefore, clear that increasing the extent of pre-heating will increase the adiabatic temperature that can be theoretically achieved by the combustion synthesis reaction. Since reactant and product enthalpies are commonly given at 298 K, and the propagating mode is often initiated at room temperature without any pre-heat, $\Delta H(T_{ig})$ can be calculated using the following relationship:

Eq. 5

$$\Delta \mathbf{H}(\mathbf{T_{ig}}) =$$

$$\mathbf{\Delta H(298)} + \int_{\mathbf{298}}^{\mathbf{T_{ig}}} \left[\sum \mathbf{n_j c}(\mathbf{P_j}) - \sum \mathbf{n_i c}(\mathbf{R_i}) \mathbf{dT} \right] + \left[\sum_{\mathbf{298-T_{ig}}} \mathbf{n_j L}(\mathbf{P_j}) - \sum_{\mathbf{298-T_{ig}}} \mathbf{n_i L}(\mathbf{R_i}) \right]$$

where ΔH(298) is the reaction enthalpy at 298 K. Substituting Eq. 2, Eq. 4 and Eq. 5 into Eq. 3 results in:

Eq. 6 $$\mathbf{\Delta H(298)} + \int_{\mathbf{298}}^{\mathbf{T_{ad}(298)}} \sum \mathbf{n_j c}(\mathbf{P_j}) \mathbf{dT} + \sum_{\mathbf{298-T_{ig}}} \mathbf{n_j L}(\mathbf{P_j}) = \mathbf{0}$$

Considering the relatively low sensitivity of the heat capacity, as a function of temperature, Eq. 6 examination indicates that T_{ad} exhibits a roughly linear relationship with the ratio of $\Delta H(298)/\sum n_j c(P_j)(298)$ at T_0=298 K, for different reactions which undergo no phase transformation. For the formation of compounds, it has been demonstrated empirically that the reaction will not be self-sustaining unless ΔH(298)/Cp(298)≥ 2000 K, which corresponds to T_{ad}≥1800 K. If only pure reactants and products are considered, $\Delta H^0(298)$ will replace ΔH(298) in the above relationships.

2.1.1.2. Combustion Synthesis Modeling

There are two important parts of a CS reaction: one is chemical reaction itself and the other is the physical process. Chemical reaction modeling considers the thermodynamics and kinetics part of reaction, which are related to electron and mass transfer and diffusion on atomic scale, while physical process modeling considers the phenomena associated with ignition, combustion wave and its mechanism of propagation, heat generated and heat lost from the reaction and thermal conductivity of both the reactants and products.[29] Much of the theoretical work on the mode of SHS waves has been based on chemical models derived from the gas-phase homogeneous combustion, including the assumption of a single chemical step. For this reason no information on the influence of the elementary steps involved in the reaction mechanism on the propagation modes has been provided. [30]

The main problem in the CS theory development is the variety of physic and chemical processes which may occur in the combustion zone during reaction.

---

[29] J.J. Moore, H. J. Feng, Combustion synthesis of advanced materials: Part II. Classification, applications and modelling, Progress Mater. Sci. 39 (1995) 275-316.

[30] S. Gennari *et al.*, Combustion Synthesis of Transition Metals Aluminides J. Phys. Chem. B, 110 (2006) 7144-7152

The process is characterized by: chemical reactions in the condensed phase with active gaseous products capable of further conversion, dispersion of a substance due to rapid gasification in the reactive layer of the condensed phase evaporation or sublimation and high-temperature melting. The presence of at least some of the above processes leads to a complex staged pattern of combustion; a multizone structure of the burning front is its characteristic feature.[31] Thanks to technological advantages, combustion synthesis is studied mainly from empirical point of view and a large amount of work on the synthesis and characterization of several materials is published, but knowledge about chemical and microscopic reaction mechanisms of process are still limited. High reaction temperatures and high propagation rates make difficult to investigate experimentally the mechanism involved in the reaction using conventional techniques applied in solid-state reactivity studies. As a consequence experimental data available in literature are restricted. To model and predict the effects on the reaction behaviour of different conditions, compared to experimental ones, is difficult due to lack of knowledge about reaction mechanism. Thus the chemical mechanism investigation is a challenging task because of the lack both of powerful direct investigation methods and simple and unique analytic model. [32,33,34,35,36]

A computer simulation approach becomes a highly desirable tool to investigate the feasibility and mechanisms of combustion synthesis. Simulation tool is able to deal simultaneously with different mechanisms and it determines both under different process variable and at different spatial and time points during CS with the same set of process variables.[37]

To describe the time evolution of CS process, computational methods are described in different papers. [38,39,40] The basis of the model presented try to emulate the process using finite difference mathematics. [41]

---

31 A.G. Merzhanov, The theory of stable homogeneous combustion of condensed substances, Combust. Flame, 13 (1969) 143–156

32 M. Arimondi *et al.*, Chemical Mechanism of the Zr + O2 → ZrO2 Combustion Synthesis Reaction, J Phys. Chem. B, 101 (1997) 8059–8068

33 S. Gennari *et al.*, A new approach to the modeling of SHS reactions: Combustion synthesis of transition metal aluminides, Acta Materialia 54 (2006) 2343–2351

34 Ibidem

35 S. Gennari *et al.*, Self-Propagating High-Temperature Synthesis of Intermetallic Compounds: A Computer Simulation Approach to the Chemical Mechanisms, J. Phys. Chem. B, 107 (2003) 732-738

36 S. Gennari *et al.*, Combustion Modes and Reaction Paths of the Self-Sustained High-Temperature Synthesis of Intermetallic Compounds: A Computer Simulation Study of the Effect of Exothermicity, J. Phys. Chem. B, 108 (2004) 19550–19556

37 F. Maglia, Dynamic behaviour and chemical mechanism in the self-propagating high-temperature reaction between Zr powders and oxygen gas, Phys. Chem. Chem. Phys., 3 (2001) 489-496

38 S. Gennari *et al.*, Self-Propagating High-Temperature Synthesis of Intermetallic Compounds: A Computer Simulation Approach to the Chemical Mechanisms, J. Phys. Chem. B 107 (2003) 732-738

Most of the theoretical models which have been proposed to explain, simulate and predict CS reaction phenomena are based on energy and mass balances and largely ignore chemical reaction details. Experimental investigations on various types of SHS reactions have provided data on wave characteristics and propagation rates which are used to judge whether a model is correct or not. Unfortunately incomplete understanding of CS reactions has limited the development of models. On the other hand, theoretical considerations may predict fairly well a specific type of CS reaction and are useful to help the process understanding.

2.1.1.3. Model Basis

In earlier investigations a simplified reaction mechanism based on the assumption of a single reaction step, derived from homogenous gas phase combustion, has been used.[42] Several efforts have been made to establish theoretical models which could explain and/or predict CS stability and reaction parameter influence. Only recently more complex and realistic reaction mechanisms have been proposed. The parameters controlling the microscopic reaction mechanism are usually optimized in order to obtain a good fit to the experimental results. [43,44] For this purpose[45], it was developed a flexible and general numerical method. The method includes several reaction steps, characterized by different kinetic laws for each of them, and considers chemical kinetics at grains level of the component powders. The weakness of starting models, based on the theory of homogeneous premixed flames, is not to consider the effects of the reacting solid particles size. On the contrary, the simulation of the formation of the intermetallic compound was focused on heterogeneity of the process, thus many different reaction steps have to be considered.[46]

---

[39] M. Arimondi *et al.*, Chemical Mechanism of the Zr + O2 → ZrO2 Combustion Synthesis Reaction, J Phys. Chem. B, 101 (1997) 8059–8068

[40] F. Maglia, Dynamic behaviour and chemical mechanism in the self-propagating high-temperature reaction between Zr powders and oxygen gas, Phys. Chem. Chem. Phys., 3 (2001) 489-496

[41] C.R.Bowen, B.Derby, Finite-difference modelling of self-propagating high-temperature syntheses of materials, Acta metall. mater., 43 (1995) 3903-3913

[42] A.G. Merzhanov, The theory of stable homogeneous combustion of condensed substances, Combust. Flame, 13 (1969) 143–156

[43] A.P. Aldushin, B.I. Khaikin, Combustion of mixtures forming condensed reaction products Comb Expl Shock Waves 10 (1974) 273-280

[44] D. Vrel, J.M. Lihrmann, P. Tobaly, Contribution of solid-state diffusion to the formation of titanium carbide by combustion synthesis, Journal of Materials Synthesis and Processing 2 (1994) 179-187

[45] S. Gennari *et al.*, Combustion Modes and Reaction Paths of the Self-Sustained High-Temperature Synthesis of Intermetallic Compounds: A Computer Simulation Study of the Effect of Exothermicity, J. Phys. Chem. B, 108 (2004) 19550–19556

[46] S. Gennari *et al.*, Combustion Modes and Reaction Paths of the Self-Sustained High-Temperature Synthesis of Intermetallic Compounds: A Computer Simulation Study of the Effect of Exothermicity, J. Phys. Chem. B, 108 (2004) 19550–19556

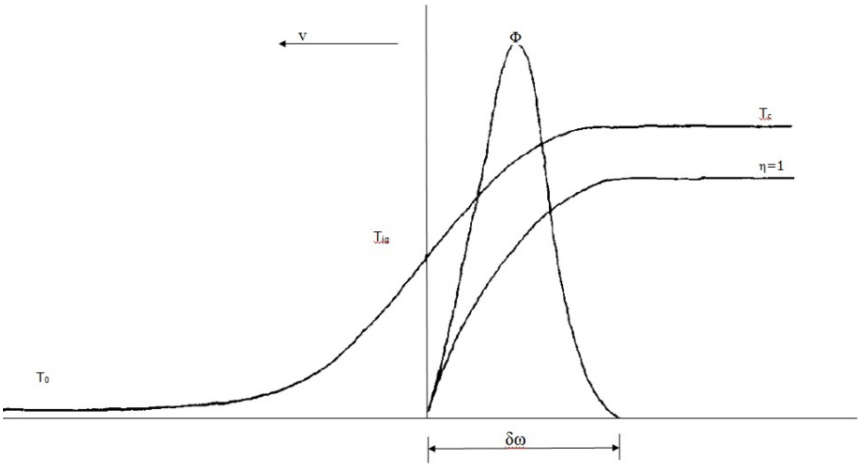

Figure 2.1–2: Schematic representation of reaction parameters for a propagating combustion wave

Since the CS reaction is usually fast, the first assumption is that the process is under adiabatic conditions. The advancing combustion front of the CS reaction is the highest temperature zone with a thickness of $\delta\omega$, where chemical and physical conversions take place. Figure 2.1–2 shows a schematic representation of combustion wave as a plane of reaction propagating through the reactant mixture, as an ideal situation.[47] The unreacted mixture, with initial temperature T_0, is heated up to the ignition temperature. The reaction zone, $\delta\omega$, is the zone where the CS reaction is initiated and completed and, therefore, the thickness of the zone is defined by the degree of completion of the reaction, that is the degree of conversion η, from 0 to 1. The rate of heat evolution, ϕ, will be a maximum at some position within the combustion zone, $\delta\omega$, as indicated in Figure 2.1–2. The thickness of the reaction zone is strongly dependent on the kinetics of the reaction, and may become so wide that the combustion front can be defined by the temperature rather than the degree of completion of the reaction (η). In this latter case, the extent of the effective combustion front is much smaller than the distance between $\eta = 0$ and $\eta = 1$. Under these conditions the section from the end of the effective combustion zone and total completion of the reaction, i.e. $\eta = 1$, is referred to as the after burn region. Based on this simple model and Fourier's heat conduction equation, the rate of propagation of a flat combustion zone can be given by the following equation for a simple basic CS reaction:

Eq. 7
$$c\rho\frac{\partial T}{\partial t} = \lambda\frac{\partial^2 T}{\partial x^2} + Q\phi$$

[47] Z.A. Munir, U. Anselmi-Tamburini, The synthesis of high-temperature materials by combustion, Materials Science Reports, 3 (1989) 277-365

where c is the heat capacity of the product, ρ is the density of the product, λ is the average thermal conductivity of the reaction system, Q is the heat of the reaction, ϕ the reaction rate, and T and t temperature and time respectively.

2.1.1.4. Model based on Ignition Theory

CS reactions show two steps: ignition and propagation of the reaction. The thermal theory has been used to describe ignition processes. However, thermal theory describes only heat generation and conduction without taking account diffusion processes, which take place during reaction. Based on thermal theory, a simple ignition model has been proposed which is based on the following assumptions:

- ignition is induced by the chemical reaction which proceeds in a narrow heated layer;
- layer thickness is lower than sample radius and body size, so that the sample can be treated as a semi-infinite dimension with a flat surface;
- external heating source is the only source used to ignite the sample. There are no volume heat sources in the sample except for the chemical reaction, and no phase transformations and no mass transfer take place in the sample.
- chemical reaction is negligible before ignition takes place and the reaction kinetics are zero-order;
- physical properties in the reaction system, e.g. thermal conductivity, heat capacity etc., are assumed to be constant, as are other properties of the system, such as activation energy for the reaction, heat of reaction, pre-exponential factor and sample heating conditions.

Equation for this basic one dimensional model derived from a consideration of heat balance is similar to Eq. 7 replacing $\phi = \rho K_0 \exp\left(-\frac{E_a}{RT}\right)$

Eq. 8
$$\boldsymbol{c\rho\frac{\partial T}{\partial t} = \lambda\frac{\partial^2 T}{\partial x^2} + \rho Q K_0 \exp\left(-\frac{E_a}{RT}\right)}$$

Assumptions imposed in boundary conditions for ignition technique are:

- constant surface temperature, which is equal to the heat source temperature;
- constant heat flow through reaction system surface

Using simple assumptions, Eq. 8 can be mathematically solved to determine a non-steady temperature field in the reaction system, the ignition delay time and heat amount gained from the source up to the ignition time. Using these two boundary conditions solution result indicates that the ignition delay time, under a constant surface

temperature, is shorter and the ignition temperature is lower than that under the condition of constant heat flow when using a similar heat impulse to ignite the exothermic reaction. However, a non-linear relationship for the heat conduction which takes into account the chemical reaction heat source has not yet been solved analytically. Many researchers have used various approximate methods to solve the equation. In order to simplify calculation, each of these approximate methods included two steps. In the first stage, the chemical reaction is neglected and it is applied an analytical solution of the non-stationary heat conductivity equation for a chemically inert body. In the second stage heat conduction is neglected, different critical conditions for the ignition of the reaction are obtained either from physical considerations or from the results of numerical solution methods. In such approximations, the non-linear equation can be converted into several linear equations at each step and, thus, the equation can be solved by purely mathematical means.

If boundary conditions change during time, instead of assuming a static condition, the ignition regime is dynamic, which is closer to real system. The boundary conditions for the dynamic regime of ignition can be determined by measuring surface temperature changes with time. Merzhanov *et al.*[48] have presented a boundary function of time as a power series of time:

Eq. 9 $$\mathbf{T_s = T_0 + \sum_{K=0}^{S} B_k t^{(K-1)^2}}$$

for the temperature boundary condition, where T_s, is surface temperature and T_0, is the initial temperature of the reactant mixture, B_k is a constant, and the heat flow boundary condition is given as:

Eq. 10 $$\mathbf{q_s = \sum_{K=0}^{S} B_k t^{(K-1)^2}}$$

where q_s is the heat flow across the surface. Furthermore, these individual boundary conditions can be converted into a combined system which follows a fix relationship called a universal curve. The universal dependence of boundary conditions can be used conveniently to analyze the ignition characteristics. The major conclusions from these analyses are:

1) the ignition delay time becomes less dependent on thermophysical and kinetic parameters when the heating rate increases, and t_{ign} will depend only on the dynamics of the outer heat flow using a fast heating rate;

[48] A.G. Merzhanov, A.E. Averson, The present state of the thermal ignition theory: An invited review, Combust. Flame 16 (1971) 89-124

2) the most favourable conditions to measure the kinetic parameters (ignition delay time and activation energy) from experiments are those for which the outer heat flow decreases with time.

The model described above is based on the assumption that there is insignificant reaction prior to the ignition. However, the reaction could occur before the observed ignition process. Taking into account the chemical reaction during the ignition process, the chemical reaction rate has been assumed to be:

Eq. 11 $$\boldsymbol{\phi = \frac{\partial \eta}{\partial t} = \rho K_0 \exp\left(-\frac{E_a}{RT}\right)(1-\eta)^n}$$

The heat balance equation has been modified as follows

Eq. 12 $$\boldsymbol{c\rho\frac{\partial T}{\partial t} = \lambda\frac{\partial^2 T}{\partial x^2} + \rho Q K_0 \exp\left(-\frac{E_a}{RT}\right)(1-\eta)^n}$$

The initial conditions for this equation are: t = 0, T = T_0 and η=0. Since, in this case, the reaction occurs prior to ignition, the reaction rate could be decreased because of product layer formation, which may be a barrier for the subsequent transport of reactant species.

2.1.1.5. Models: State of Art

The basic system of equations which describes[49] the steady combustion of CS systems[50] comprises classical one dimensional equations of the flame propagation, which take into account heat losses for kinetic functions:

- equation of heat conduction (from Fourier's law):

Eq. 13 $$\boldsymbol{\lambda\frac{dT^2}{dx^2} + c\rho\frac{dT}{dx} + Qk_0 \exp\left(-\frac{E_a}{RT}\right)\varphi(\eta) - \left(\frac{2\alpha}{R_0}\right)(T - T_0) = 0}$$

- kinetics equation:

Eq. 14 $$\boldsymbol{-V\frac{d\eta}{dx} + k_0 \exp\left(-\frac{E_a}{RT}\right)\varphi(\eta) = 0}$$

- boundary condition:

[49] A.G. Merzhanov, Reviews: Fundamentals, achievements, and perspectives for development of solid-flame combustion, Russian Chemical Bulletin 46 (1997) 1-27

[50] A.G. Merzhanov, Solid flame propagation in model heterogeneous systems, Dokl. Akad. Nauk, 353 (1997) 504-507

Eq. 15

$$\begin{cases} x = -\infty, T = T_0, \eta = 0 \left(\frac{dT}{dx} = \frac{d\eta}{dx} = 0\right) \\ x = \infty, \left(\frac{dT}{dx} = \frac{d\eta}{dx} = 0\right) \\ \varphi(\eta) = \eta^{-m} e^{-n\eta} \end{cases}$$

where k_0 is the pre-exponential factor, α is the effective coefficient of heat transfer to the surrounding medium, and R_0 is the radius of the cylindrical sample. The solution of this system, which is the simplest in the CS theory, made it possible to discover the main features of the solid combustion: to determine the structure of the combustion wave (temperature and conversion profiles in the wave), to calculate the burning velocity and establish its relationship with the structure of the wave (with parameters of the problem) and to determine combustion limits which appear due to heat losses. The steady-state theory of combustion of CS systems was developed by taking into account various accompanying physicochemical processes, which was expressed as the introduction of additional terms and/or equations in the system mentioned above. The most important result[51] of the experimental diagnostics and theoretical studies is the development of concepts about two limiting mechanisms of CS processes: equilibrium and non-equilibrium. For the equilibrium mechanism, CS processes of the final product phases and formation structures occur simultaneously with the chemical reaction. The reagents interact via the mechanism of diffusion reaction, the reaction product forms at the interface of contact of the reagents and can have a multilayered (according to the phase diagram) structure. By the state of the product, it is a local equilibrium process. It is difficult to obtain this limiting mechanism in a pure form, its features can be seen in solid flames. For the non-equilibrium CS mechanism[52] in the combustion wave, for example, products in the metastable state form, an amorphous substance, melt, or oversaturated solid or liquid solutions; their transformation to the final products occurs far behind the combustion front in the so-called zone of structure formation and exerts no effect (unlike the equilibrium case) on the burning speed. The intermediate phase of tile substance identified in the phase diagram cannot be obtained in non-equilibrium CS processes. The non-equilibrium mechanism is typical of very fast CS processes. The equilibrium approach was popular in early studies of CS processes. Both mechanisms were further specified and formulated more distinctly. An interesting method for diagnostics of the CS

[51] A.G. Merzhanov, Theory and practice of SHS: worldwide state of the art and the newest results, Int. J. of SHS 2 (1993) 113-158

[52] A.G. Merzhanov, Nonequilibrium theory of flame propagation. In: Combustion, Detonation, Shock Waves: Proc. of the Zel'dovich Memorial, Int. Conf. on Combust., Moscow, 12-17 Sept., 1994 / Ed. S.M. Frolov. V.1. Moscow: Russ. Section Combust. Inst. Publ., 1994, p.20-44; Advances in Combustion Science: In Honor of Ya.B.Zel'dovich /Eds. W.A.Sirignano, A.G.Merzhanov, L. De Luca. Aeronaut. and Astronaut. Publ., 1997, p.37-59 (Ser.: Prog. in Astronaut. and Aeronaut., V.173)

mechanisms is based on the determination of the value $\xi_0=Ux_0/a$, where x_0 is the distance from the combustion front to some point characterizing a fast growth of the phase of the final product in the wave and a is the thermal diffusivity of the substance. If $\xi_0 \approx 1$ (i.e., if its order of magnitude is equal to that of the dimensionless width of the combustion zone), the equilibrium mechanism takes place; if $\xi_0 >> 1$, the non-equilibrium mechanism occurs.

An unidirectional steady-state mathematical model[53] for SHS based on heat transfer and chemical kinetics has been formulated. Model assumption[54] are:

1. reaction proceeds in one direction
2. sample is treated as an homogeneous continuum and physical properties are isotropic
3. temperature effect on thermal properties are small (average parameters are used)
4. physical properties do not change significantly upon reaction
5. heat loss to the surrounds is negligible

By performing an energy balance, the following governing equation based on the model assumptions is:

Eq. 16
$$\rho(-\Delta H)\phi = -\frac{\partial}{\partial x}\left(\lambda\frac{\partial T}{\partial x}\right) + \rho c\frac{\partial T}{\partial t}$$

where ϕ is the kinetics function given by

Eq. 17
$$\phi = \frac{d\alpha}{dt} = kf(\alpha)$$

α is the fraction conversion and the rate constant k is given by the Arrhenius equation

Eq. 18
$$k = k_0 exp\left(\frac{-E_a}{RT}\right)$$

with the following boundary condition:

Eq. 19
$$\begin{cases} t \le 0, T = T_o, & \alpha = 0 \\ x = -\infty, T = T_0, \frac{\partial T}{\partial x} = 0, & \alpha = 0 \\ x = \infty, T = T_{ad}, \frac{\partial T}{\partial x} = 0, & \alpha = 1 \end{cases}$$

[53] H.Y. Sohn, X. Wang, Journal Mathematical and experimental investigation of the self-propagating high-temperature synthesis (SHS) of $TiAl_3$ and Ni_3Al intermetallic compounds, Journal of Materials Science 31 (1996) 3281-32888

[54] W.I. Frankhouser *et al.*, Gasless Combustion Synthesis of Refractory Compounds, Noyes Publications, Park Ridge, New Jersey (1985) 5-60

After ignition, the SHS process can be treated as a steady-state problem with the burning front moving at a constant speed. For mathematical convenience, let the solid move in the direction of the distance coordinate at the same rate as the burning front. Then,

Eq. 20 $$\mathbf{u} = \frac{\mathbf{dx}}{\mathbf{dt}}$$

and

Eq. 21 $$\frac{\partial \mathbf{T}}{\partial \mathbf{t}} = \mathbf{u}\frac{\partial \mathbf{T}}{\partial \mathbf{x}}$$

Thus, the following steady-state model is formulated, assuming constant thermal conductivity:

Eq. 22 $$\boldsymbol{\lambda}\frac{\mathbf{d^2T}}{\mathbf{d^2x}} - \boldsymbol{\rho cu}\frac{\mathbf{dT}}{\mathbf{dx}} + \boldsymbol{\rho}(-\Delta \mathbf{H})\mathbf{k_0 f}(\boldsymbol{\alpha})\mathbf{exp}\,(-\frac{\mathbf{E}}{\mathbf{RT}})$$

The boundary conditions remain the same.

Since the rate function ϕ involves fractional conversion α, it is necessary to relate it to other parameters. Integrating Eq. 22 the governing between the limits x = -∞ to any point x using boundary conditions for α, one obtains,

Eq. 23 $$\boldsymbol{\alpha} = \frac{\boldsymbol{\rho cu}(\mathbf{T}-\mathbf{T_0})-\boldsymbol{\lambda}\frac{\mathbf{dT}}{\mathbf{dx}}}{\boldsymbol{\rho}(-\Delta \mathbf{H})\mathbf{u}}$$

with the boundary conditions forms the mathematical model for the unidirectional steady-state combustion for the SHS process. Solving these equations, the temperature profile can be calculated if the kinetic parameters, activation energy, pre-exponential factor, and the form of the conversion factor, are known. There is no analytical solution[55] to the governing equations. Direct numerical solution of the equations is difficult since it involves a stiff problem, which is caused by the steep temperature increase with distance. Because the chemical reaction is highly exothermic, a simplified solution may be used.[56] From the combustion theory the burning rate is determined based on the kinetic parameters such as E_a, k_0, and temperature profile. However, it is more often necessary to obtain the kinetic parameters from the temperature profile and the measured burning rate by applying the theory. A proper approach to the solution is a trial-and-error method with numerical iteration, comparing the calculated results with the

[55] A.A. Zenin, A.G. Merzhanov, G.A. Nersisyan, Investigation of the thermal-wave structure in self-propagating high-temperature systhesis, *Fiz. Goreniya Vzryva,* **17** (1981) 79–90

[56] A.G. Merzhanov, A.E. Averson, The present state of the thermal ignition theory: An invited review, Combust. Flame 16 (1971) 89-124

measured results until the comparison is satisfied. By solving the model equation, the activation energy and the pre-exponential factor for the reaction were computed based on the observed burning rate and temperature profile. The kinetic parameters obtained from the DSC work and the SHS modeling agreed quite well. The model can be used to simulate the SHS process and obtain kinetics information for a unidirectional SHS reaction.

Other work has been carried out on modeling the combustion wave and the influence of processing parameters on it. Merzhanov[57] and Novozhilov[58] derived an analytical expression for the combustion wave which was dependant on the activation energy (E_a) of the reaction.

The wave propagation rate, wave stability and maximum combustion temperature achieved in CS reactions are dependent on heat generation by the reaction and the heat loss from the reaction front. Heat dissipation from the reaction front occurs through heat losses to the environment and heat transfer to the adjacent reactant mixture which is still below the ignition temperature. Hence, any perturbation of these factors can result in a change of the reaction front velocity and stability. Experimentally, combustion synthesis reactions are usually conducted under non-adiabatic conditions, especially in case of self-propagating mode (SHS). Therefore the actual combustion temperature, T_c, is, generally, lower than the maximum theoretical adiabatic combustion temperature. Decreasing heat generation, that means less exothermicity and/or increasing the heat dissipation could create instabilities, which lead to slow down or temporarily stop the propagation of the combustion wave movement, or even quenching out the reaction. Under a steady-state mode the combustion front moves from the ignition surface through the reactants at uniform speed, which varies typically from 1 to 150 mm/s. A non-steady-state mode is defined as a non-uniform rate of the combustion wave with respect to time and/or space. The non-steady-state mode is generally manifested in three forms: oscillating, spinning or spiralling, and repeated combustion wave front movements. In the oscillatory mode, the wave moves in successions of rapid and slow displacements. The propagating wave slows down and almost quenches out at the intersection of two displacements. In the spin mode the reaction proceeds in a spiral motion from one end of the sample to the other. The repeated combustion mode consists of the passage of a second combustion wave through the already reacted substance following the propagation of the first combustion wave in the original reactant materials. Instability of the combustion wave, in the end, could lead to the extinction of the combustion reaction.

---

[57] A.G. Merzhanov, New elementary models of the second kind, Dokl. Akad. Nauk SSSR 233 (1977) 1130–1133

[58] B.V. Novozhilov, The theory of surface spin combustion, Pure and Applied Chemistry 65 (1993) 309-316.

The repeated combustion is related to the kinetics of the reactions, especially in solid-gas reactions. The first combustion wave is relatively fast and localized along the exterior surface, while the second wave is slower and the combustion zone is much broader. The limiting parameter in this case is the diffusion of one of the reactants into the interior of the reactant mixture. After studying the relationship between the adiabatic steady-state velocity, V_{ad}, and the velocity prior to quenching out, V_m, the following relation was found:

Eq. 24 $$\mathbf{V_m = \frac{V_{ad}}{1.65}}$$

where V_m is the critical velocity at which the combustion process is on the verge of being quenched out. This relationship was proved to be valid for solid-state combustion.[59] [60] [61]

The importance of the kinetics of energy transport is also shown by the fact that the first theoretical approach to the SHS method is entirely based on these aspects [62]. In their approach, these authors used Fourier's analysis of heat transfer with a heat source, as in:

Eq. 25 $$\mathbf{\rho c \frac{\partial T}{\partial t} = \lambda \frac{\partial^2 T}{\partial x^2} + Q R_r(T, \eta)}$$

Eq. 26 $$\mathbf{\Phi(T, \eta) = \frac{\delta \eta}{\delta t}}$$

where x is the spatial coordinate, Q is the thermal effect of the reaction, and R_r is the reaction rate.

An analytical solution of the problem has been obtained assuming the kinetic law

Eq. 27 $$\mathbf{\Phi = \frac{\delta \eta}{\delta t} = K_0 \exp\left(-\frac{E_a}{RT}\right)(1-\eta)^n}$$

where E is an activation energy and k_0 is a pre-exponential term. Finally, Khaikin and Merzhanov[63] derived the following expression for the velocity (V) of the steady combustion wave

---

59 M. Eslamloo-Grami, Z. A. Munir, The mechanism of combustion synthesis of titanium carbonitride, Journal of Materials Research 9 (1994) 431-435.

60 J.J. Moore, H. J. Feng, Combustion synthesis of advanced materials: Part I. Reaction parameters, Progress Mater. Sci. 39 (1995) 243-273

61 R. Rosa, Microwaves as Ignition Source in the Combustion Synthesis of High Performances Materials, Doctor of Philosophy "High Mechanics and Automotive Design and Technology" at the University of Modena and Reggio Emilia (2010)

62 A.G. Merzhanov, Theory of gasless combustion, Arch. Procesow Spalania, 5 (1974) 17–39

63 B.I. Khaikin, A.G. Merzhanov, Theory of thermal propagation of a chemical reaction front, Combustion, Explosion and Shock Waves 2 (1966) 22-27

Eq. 28 $$V^2 = f(n)\frac{c\rho k}{Q}\frac{RT_c^2}{E}k_0 exp\left(-\frac{E_a}{RT_c}\right)$$

where $f(n_r)$ is a function of the reaction order. Using different reagent dilutions with inert materials or products, it is possible to experimentally achieve different combustion temperatures (T_c). Then, the experimental determination of the combustion speed at different T_c can be used accordingly to obtain the activation energy of the rate determining step of the process from the slope of a $\ln(u/T_c)$ vs $1/T_c$ plot. This approach is important not only because it provides an analytical solution but also because it makes possible the determination of a kinetic parameter (E_a) from coupled measurements of combustion temperature and wave speed. Insight is gained into the reaction mechanism through comparison of the experimental E_a with the activation energy of assumed mechanisms. As a matter of fact, multistep mechanisms[64] are clearly suggested by experimental results. A simple and flexible method was implemented for combining the heat balance equation with the relevant chemistry. The method is devised to include in some way all the sparse indications coming from experiments, to predict the nature of the combustion process, and to provide temperature profiles allowing comparison of results with experiments. In particular, it can include many kinetic models to describe the different chemical and physical steps, in agreement with the current knowledge about the chemical reactivity in heterogeneous systems. Finally, the method can give insight for further experiments to test the importance and features of each step of the model.

Thus Eq. 29 [65]is a relationship that predict the propagating combustion reaction front speed, V, and it is derived Arrhenius kinetics from different chemical kinetics providing that the combustion process is stable and no phase transformation takes place during the combustion reaction, but there is also another relationship that takes into account diffusion-controlled kinetics:

Eq. 29 $$V^2 = \frac{2K}{2r^2 c\rho\eta_s}D_0 exp\left(-\frac{E_a}{RT_c}\right)$$

where K are constants, η_s is the stoichiometric ratio of the reactants, r is the particle size and D_0 is the pre-exponential diffusion coefficient. These relationships Eq. 29 and Eq. 28 can be used to estimate an activation energy for a simple CS reaction and to determine a possible mechanism which is operative during the reaction. The major limitation of this model is that it cannot explain the stability of an SHS reaction, that is largely controlled by parameters other than heat conductivity. The transition from

[64] M. Arimondi et al., Chemical Mechanism of the Zr + O2 → ZrO2 Combustion Synthesis Reaction, J Phys. Chem. B, 101 (1997) 8059–8068

[65] J.J. Moore, H. J. Feng, Combustion synthesis of advanced materials: Part II. Classification, applications and modelling, Progress Mater. Sci. 39 (1995) 275-316

steady-state combustion to unsteady-state combustion is usually the result of an imbalance between heat generation and heat dissipation. A change in either reaction thermodynamics and/or kinetics of the CS reaction could result in different combustion modes.

A cylindrical rod[66] of an uniform composition of the powdered reactant mixture has been set to model CS reaction (as shown in Figure 2.1–3). The powder was ignited at the end (A) and a reaction zone (O) propagated along the rod with uniform velocity V dividing the material into reacted (R) and unreacted (U) zone at temperature T_1 and T_2, that is the same way of self-propagating exothermic reactions in solid reaction systems.

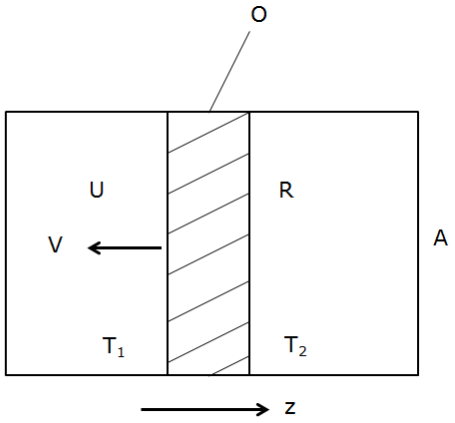

Figure 2.1–3: Model scheme of layer to layer theory[67]

The one dimensional model neglected any heat transfer due to radiation, or the effect of diffusion of the material, and heat losses from the side of the rod. The thermal conductivity, heat capacity and overall density of the powder materials were assumed to be constant over the temperature range of interest. The kinetics of the reaction at each point in the powder compact was presented similarly in the form:

Eq. 30 $$\frac{d\eta}{dt} = \phi(P, \eta, T)$$

where η denotes the fraction of the reducing agent oxidized at any point and P is a parameter denoting the relevant physical factors (e.g. the state of subdivision of the reacting particles etc) which influence the function ϕ. The form of the function ϕ was usually experimentally determined. The value of η in the unreacted zone is zero while, in the reacted zone, it can vary from 0 to 1 depending on the relative amounts of oxidizing

[66] F. Booth, The theory of self-propagating exothermic reactions in solid systems, Trans. Faraday Soc., 49 (1953) 272-281

[67] Ibidem

and reducing agents in the reactant species. Once a steady-state has been attained, the coordinate system can be replaced by:

Eq. 31 $u = x + Vt$

in which u is the new coordinate and V is the velocity of the reaction front in the direction of x which is negative on account of decreasing x as the reaction proceeds under these conditions. Therefore, T and q are a function of u only, and Eq. 8 under the new coordinate system, becomes:

Eq. 32 $$\rho V c \frac{dT}{du} = \lambda \frac{d^2T}{du^2} + QV \frac{d\eta}{du}$$

In order to find the velocity of the combustion front, V, the form of the function $\frac{\partial \eta}{\partial t}$ needs to be found. In an CS reaction involving powders in which all factors except the radius of the reactant powders, r, are kept unchanged, it was found $\frac{\partial \eta}{\partial t} \propto r^{-2}$

This is in agreement with a consideration that the reaction between spherical particles has to overcome any product layer formed and hence results in a parabolic law for the reaction rate.

Another success of this model is its ability to predict V as a function of composition. In some cases special mathematical techniques were employed to solve the equation. For example, introducing dimensionless variables and parameters has been an effective way to solve the problem. However, a complete solution for the equation requires knowledge of the specific CS reaction system. The simplest reaction system, i.e. an elemental solid reaction system, was initially studied by Merzhanov *et al*.[68] In their study, dimensionless, variable parameters were used $\beta = \frac{RT^*}{E}$ and $\gamma = \frac{cRT^{*2}}{QE}$ where T* is a reference temperature which could be the combustion temperature T_c. Assuming the Arrhenius relationship:

Eq. 33 $$\phi = \frac{\partial \eta}{\partial t} \rho K_0 \exp\left(-\frac{E_a}{RT}\right)(1-\eta)$$

Substituting Eq. 25 into Eq. 8 gives a similar relationship as that presented in Eq. 21 where the order of reaction, n_r, is 1. A numerical calculation was employed to solve the equation and the results showed that the reaction front propagation exhibited two regimes: stable and oscillatory, which was dependent on the values of β_c and γ_c (c denotes the values at the combustion temperature). The authors introduced a parameter, Θ, as a function of β_c and γ_c, which characterizes the stability of the reaction, such that:

[68] K.G. Shkadinswi, B.I. Khaikin, A.G. Merzhanov, Propagation of a pulsating exothermic reaction front in the condensed phase, Combust. Explos. Shock Waves 7 (1971) 15-22

Eq. 34 $$\Theta(\beta_c, \gamma_c) = 9.1\gamma_c - 2.5\beta_c$$

If Θ>1, the combustion is stable, but if Θ < 1, the combustion is in the oscillatory mode. Physically, it has been expected that when a layer of the reactant mixture undergoes the CS reaction, heat generated will increase temperature value of an adjacent layer which is still below the ignition temperature. If the thermal conductivity is low, a longer time is needed to bring the adjacent layer to the ignition temperature, thereby, a pulsating mode of reaction result could be resulted. As consequence a critical intervals of both space and time should be found for a real solution. The same model has been analyzed mathematically by Matkowsky *et al*.[69] The purpose of their work was to describe both the existence and stability of the solutions so as to predict the stability of the combustion reactions and their dependence on various reaction parameters.

The parameter that they introduced as a criteria for the stability of the combustion reaction was:

Eq. 35 $$\Theta = \frac{E_a(T_c - T_0)}{2RT_c^2}$$

They found that if $\Theta > \Theta_0$ where Θ_0=2 +√5, the solution is unstable while, for the condition $\Theta < \Theta_0$ is a stable solution. These solutions correspond to the stability of the combustion reaction front.

Hardt and Phung [70] developed a model where time, which the reactant atoms in adjacent particles require to diffuse through the product which formed between them, is the rate of the reaction.

Hardt and Phung proposed a model in which the reactants are assumed to have a layered geometry with the relative thickness of the components depending on the stoichiometry of the desired phase and on the densities of the reacting metals. Hardt and Phung[71] [72] instead of using the homogeneous reactant mixture model, used a layered-reactant mixture model, as schematically represented in Figure 2.1–4.

---

[69] A. Bayliss, B.J. Matkowsky, Modeling and numerical computation of a nonsteady SHS process, Combust. Plasma Synth. High-Temp. Mater., Conference 1990, 61-72

[70] A.P. Hardt, P.V. Phung, Propagation of gasless reactions in solids. Analytical study of exothermic intermetallic reaction rates, Combustion and Flame, 21 (1973) 77-89

[71] Ibidem

[72] Z.A. Munir, U. Anselmi-Tamburini, The synthesis of high -temperature materials by combustion, Division of Materials Science and Engineering, College of Engineering, University of California, Davis, CA 95616, USA (1988)

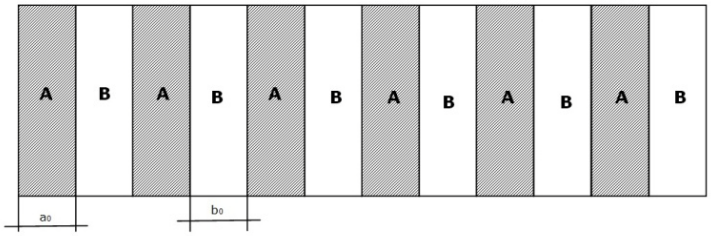

Figure 2.1–4: Layered-reactant mixture of element A and element B

The model considers the reactants as a one dimensional array of cells which are initially at room temperature. The reaction is initiated by setting the first two cells of the array to the combustion temperature to imitate rapid heating by an external heat source. Two cells are used as initiators because cooling of the first cell by convection and radiation is considered. If only the first cell is used to initiate the reaction it is possible for the cell to cool before it initiates an SHS wave. After the first two cells are set at the combustion temperature, heat flow between the cells begins to heat up the reactants in the third cell. Once the reactants in the third cell reach the ignition temperature, i.e. the temperature at which the reaction begins to propagate, it is instantaneously converted to products at the combustion temperature. The fourth cell begins to eat up and the process continues so that a combustion wave travels along the model cells. The model therefore assumes that the rate of reaction is limited by heat transfer only and that reaction kinetics and transport by diffusion play a limited role. [73]

However, owing to the design of this reactant system, the kinetics of the reaction, ∂n/∂t, would be different from those predicted by the Arrhenius relationship in Eq. 10 The diffusion of the species should be the controlling step in this case. Using this reaction model (Figure 3) the following relationship was determined:

Eq. 36
$$\frac{\partial \eta}{\partial t} = \frac{D}{w a_0^2 (1-f)}$$

where D is the diffusion coefficient and w is the ratio of the thicknesses of the alternating layers of elements A and B. By substituting this equation into Eq. 8, the solutions were numerically determined. Using the same reaction system and assumptions, the rate of the propagation wave, V, was also derived:

Eq. 37
$$V = \frac{\lambda}{w a_0 c \rho} \frac{(T_{ad}-T_0)}{(T_{ig}-T_0)}$$

[73] C.R. Bowen, B.Derby, Finite-difference modelling of self-propagating high-temperature syntheses of materials, Acta metall. mater., 43 (1995) 3903-3913

Some of the values of V, calculated by this equation, were in fairly good agreement with those measured from experiments. Modification of this model took into account the melting of one of the reactants and extended the model to two dimensions. The final products were still assumed to be solid. The melting of one of the components can result in a significant increase in heat of the reaction, e.g. from Q to Q + L, where L is the latent heat of fusion. In addition to the latent heat associated with melting, the reaction rate, which was assumed to have the Arrhenius form, is also subjected to a sudden increase by a given factor, a, which is a result of the increased surface contact area between the reactants created by melting of one of the reactants. Based on these consideration, Eq. 7 can be modified to Figure 2.1–5:

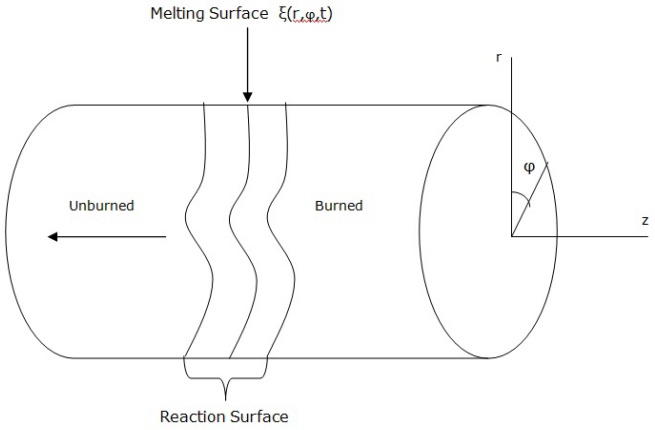

Figure 2.1–5: The propagation of a two-phase (liquid + solid) combustion front in a long cylindrical reaction channel

when $z<\xi(r,\varphi,t)$ **Eq. 30**	when $z\geq\xi(r,\varphi,t)$ **Eq. 31**
$c\rho = \frac{\partial T}{\partial t} = \lambda\nabla^2 T + Q\rho(1-\eta)K_0 exp\left(-\frac{E_a}{RT}\right)$	$c\rho\frac{\partial T}{\partial t} = \lambda\nabla^2 T + \alpha(Q+L)(1-\eta)\rho K_0 exp\left(-\frac{E_a}{RT}\right)$
$\phi = -\frac{\partial\eta}{\partial T} = -\rho(1-\eta)K_0 exp\left(-\frac{E_a}{RT}\right)$	$\phi = \frac{\partial T}{\partial t} = -\alpha(1-\eta)\rho K_0 exp\left(-\frac{E_a}{RT}\right)$

where ∇^2 is a Laplacian operator, $\xi(r,\varphi,t)$ is the location of the isotherm surface where $T = T_m$ in the combustion front, T_m is the melting point of the deficient component in the reactant mixture, and $\xi(r,\varphi,t)$ represents the melting surface which will be determined, as schematically presented in Figure 2.1–5. The solution of the equation has been solved using an analytical plus numerical route. Two important parameters have been used to predict the bifurcation of a pulsating and spinning reaction front or a stable combustion front. One is called the melting parameter, M, in which:

Eq. 38 $$\mathbf{M = \left(1 - \frac{1+L/Q}{\alpha}\right) exp\left[E_a \frac{(T-T_{ad})}{RT_{ad}^2}\right]}$$

The second is the parameter Θ, related to the stability of the reaction, where $\Theta = \frac{\Delta}{2(1-M)}$, with $\Delta = E_a(Tad - Tc)/RT_{ad}^2$

It was found that the boundary between steady planar combustion and non-steady, non-planar combustion depends only on the ratio of Δ to (1 - M). Therefore, if melting occurs at the combustion front, M - 0 and, hence, a smaller value of Δ is needed to achieve steady planar combustion. This means that if every parameter is kept unchanged except M, the melting of a component in the reaction system may result in transition from steady planar combustion to non-steady non-planar combustion.

Although melting was considered in Eq. 37 this model does not include the effect of porosity, pore size and general phase transformations. It could be used a temperature enthalpy approach to model a general process of CS reactions. Since ΔH = cΔT, the heat balance equation in a general condition becomes:

Eq. 39 $$\mathbf{\rho \frac{\partial H}{\partial t} = \frac{\partial}{\partial x}\left(\lambda \frac{\partial T}{\partial x}\right) + Q\phi(\eta, T)}$$

where

Eq. 40 $$\mathbf{\phi(\eta, T) = \rho(1 - V_f)K_0 exp\left(-\frac{E_a}{RT}\right)\varphi(\eta)}$$

in which V_f is the volume fraction of a non-reactive phase, e.g. diluent or reinforcing agent, and ρ is the average density of the compact. When the kinetics of a reaction is first-order, $\varphi(\eta) = c_0(1-\eta)$, where c_0 is the initial concentration of the reactive phase. The enthalpy in Eq. 39 may be different depending on the phase regions in which the reaction system operates. For example: $H = C_sT$ in a solid phase region, $H = C_sT + \Delta H_{sL}$ in a liquid region, where ΔH_{SL} is the latent heat of formation of the liquid phase. A similar expression can be written when a general phase transformation occurs. However, the parameters k and ρ are not constants since they are dependent on the porosity in the compact. The density, ρ, at a level of porosity, p is given as: $\rho=\rho_s(1-p)$, where ρ_s is the average density of the solid phases in the compact. The effective thermal conductivity, λ_e in a porous medium has been derived from a model of solid and isolated regular arrays of closed pores, as illustrated in Figure 5, and given as:

Eq. 41 $$\mathbf{\frac{\lambda_e}{\lambda_s} = \frac{x + \Gamma\left(1 + \frac{1}{\delta}\right) + 1}{x + \frac{\frac{\Gamma}{\delta(1+\Gamma)}}{\Omega T_p^3/T_{ad}^3} + \frac{\lambda_p}{\mu k_s}}}$$

where

Eq. 42 $$\delta = \frac{V}{l} = \frac{\rho^{1/3}}{1-\rho^{1/3}}$$

Eq. 43 $$x = (1+\delta)\left[\frac{2+\delta}{1+\delta}\ln(1+\delta)+1\right]/[\delta \ln(1+\delta)]$$

Eq. 44 $$\Gamma = 1 + \frac{1}{\ln\left(1+\frac{1}{\delta}\right)}$$

Eq. 45 $$\Omega = 4\varepsilon\nu h_p T_{ad}^3/\lambda_s$$

in which λ_s is the average thermal conductivity of the unreacted powders and k_p is the thermal conductivity of the fluid in the pores, ε and h_p are the emissivity of the pore surface and Plank's constant respectively, T_p, and T_{ad} are the adiabatic temperatures at the density of ρ and at zero porosity respectively. The meaning of L and ν are shown in Figure 2.1–6:

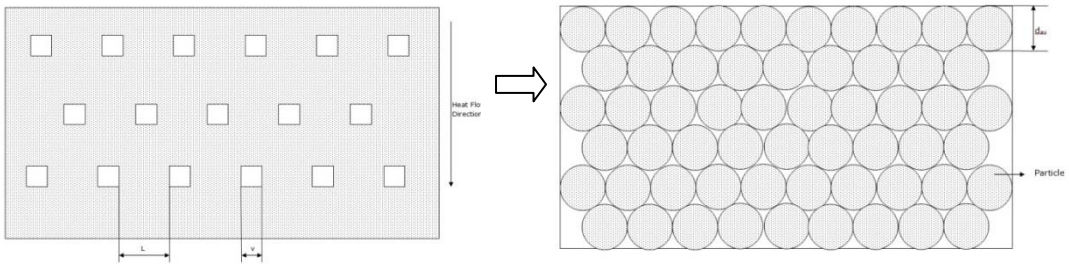

Figure 2.1–6: Schematic representation of the model incorporating a distribution of pores

Combustion front propagation rate shows a minimum for small pore sizes and continuously increases if the pore sizes are large. This is due to radiation effect inside the pores. At a high level of porosity, the predictive capability of this model is limited by the lack of experimental data since such compacts are difficult to make and measure accurately. The results seem to contradict the experimental data in which a loose reactant mixture displayed an unstable combustion mode and in which the combustion reaction was extinguished after it was ignited.

Another approach used to study the mechanism of CS reactions was based on the analysis of temperature profiles which were measured experimentally. Mathematically, there are two different approaches for the temperature profile analysis (TPA): one was provided by Boddington *et al.* and another was by Zenin *et al*. The purpose of this method (TPA) is to find the relationship between the conversion of an SHS reaction and the temperature profile-related parameters so as to calculate the activation energy of the

reaction process. The heat balance equation used by Boddington *et al.* is given as follows:

Eq. 46 $$\frac{\lambda}{V^2}\frac{\partial^2 T}{\partial t^2} - \rho c\frac{\partial T}{\partial t} - \rho\phi - h(T - T_0) = 0$$

where h is a quantity related to the lateral heat transfer coefficient. Substituting T = T_0 - Ξ into Eq. 46 and dividing by cρ the equation can be simplified as:

Eq. 47 $$t^*\frac{\partial^2 \Xi}{\partial t^2} - \frac{\partial \Xi}{\partial t} + G - R\frac{\Xi}{t} = 0$$

where Ξ is the new coordinate variable, t* = mV^{-2} (m = λ/ρc is the effective thermal conductivity), G = ϕ/ ρc, nd r = ρc /h which is the thermal relaxation time related to the lateral heat conduction. The simplest solution for Eq. 35 can be obtained from a one-dimensional wave model. Under adiabatic conditions, h–›0 and, hence, τ–›∞. If there is no thermal effect, i.e. G = 0, which is true for the regions far ahead or behind the combustion front, Eq. 47 becomes:

Eq. 48 $$t^*\frac{\partial^2 \Xi}{\partial t^2} - \frac{\partial \Xi}{\partial t} = 0$$

And its solution is:

Eq. 49 $$\ln\Xi = \frac{t}{t^*} + K$$

where K is a constant. The more general case is when h≠ 0 but it is very small, and the solution of Eq. 48 for the regions remote from the combustion front can be expressed as Ξ= $Ae^{\beta t}$, in which A and β are the constants to be determined from the equation and boundary conditions. There exist two values of β, i.e. β_1 = t, and β_2 = t_d, which satisfy Eq. 48 and correspond, respectively, to the rise time, t_t, in the region ahead of the combustion front and the decay time, t_d in the region behind the combustion front. The plots of lnΞ-t in these two regions can be used to calculate t_t and t_d, and furthermore, t* can be calculated from the relationship.

Eq. 50 $$\frac{t^*}{\tau} = \frac{t_\tau/t_d}{(1-t_\tau/t_d)^2}$$

The mathematical approach for the TPA used by Zenin *et al*. was based on Eq. 7 When the movement of the combustion front becomes stable, x = Vt. Thus, dt = dx/V, and substituting this relationship into Eq. 7 and integrating:

Eq. 51 $$k\frac{\partial T}{\partial x} - c_p\rho V(T - T_0) + Q\rho V\eta = 0$$

the boundary conditions are:

Eq. 52 $$\mathbf{T = T_0, \eta = 0, \frac{\partial T}{\partial x} = 0 \ at \ x = -\infty}$$

Eq. 53 $$\mathbf{T = T_c, \eta = 1, \frac{\partial T}{\partial x} = 0 \ at \ x = +\infty}$$

When the relationship between the thermal conductivity, λ, and the degree of conversion, η is assumed to be

Eq. 54 $$\boldsymbol{\lambda} = \eta(\boldsymbol{\lambda}_r - \boldsymbol{\lambda}_p) + \boldsymbol{\lambda}_r$$

where λ_r and λ_p are the thermal conductivity of the reactants and products respectively, Eq. 51 becomes:

Eq. 55 $$\boldsymbol{\eta = c_p \rho V(T - T_0) - \lambda_r \frac{\partial T}{\partial x} (\lambda_p - \lambda_r) \frac{\partial T}{\partial t} + Q \rho V}$$

Hence, if the temperature profiles T(x) and $\frac{\partial T(x)}{\partial x}$ together with other parameters in Eq. 55 are known, the degree of conversion can be calculated. The kinetic information of the SHS reaction can also be obtained if the function for η is assumed. For example, Zenin *et al*. assumed the function for y as follows

Eq. 56 $$\mathbf{\frac{\partial \eta}{\partial t} = K_0 \eta^{-n} e^{-E_a/RT}}$$

Thus, the activation energy can be determined from the knowledge of the temperature profiles. The TPA approach has been recently discussed and applied to some SHS reaction systems by Dunmead and Munir.

Another method considers unidirectional steady-state mathematical model[74] based on heat transfer and chemical kinetics was formulated.

For the purpose of mathematical modeling sample, it is assumed as ignition way the SHS mode. During SHS temperature change with respect to time or space. The sample is ignited at one end of the pellet, and the combustion front propagates through the pellet to the other end. Thus, for the purpose of mathematical modeling, it is reasonable to assume unidirectional reaction. Assumptions made in using this model are [75] :

1. the reaction proceeds in one direction;

---

[74] H.Y. Sohn, X. Wang, 3288 Mathematical and experimental investigation of the self-propagating high-temperature synthesis (SHS) of $TiAl_3$ and Nia_3Al intermetallic compounds, Journal of Materials Science, 31 (1996) 3281-3288.

[75] W.I. Frankhouser *et al.*, Gasless Combustion Synthesis of Refractory Compounds, Noyes Publications, Park Ridge, New Jersey (1985) 5-60

2. the sample is treated as a homogeneous continuum, the physical properties are isotropic;
3. the effects of temperature on the thermal properties are small. As a consequence averaged values of parameters are used;
4. the physical properties do not change significantly upon reaction, and the same property values can be used for the product(s) and the reactants;
5. heat loss to the surrounds is negligible. It is difficult to obtain the physical properties of the product intermetallic compounds due to the lack of information.

Other model could be described by equation which shown exothermic solid-solid non catalytic heterogeneous reaction systems. An assumption is made that a heterogeneous reaction occurs between two solid materials, S and M,

Eq. 57 $$\mathbf{S_S + M_M \rightarrow P_P}$$

and that the reaction rate can be described by integer power law kinetics

Eq. 58 $$\mathbf{r_R} = kC_s^n C_m^m$$

To develop the model, the following physical assumptions have been made:

- an heterogeneous mixture of solid powders, S and M, behaves as an isotropic homogeneous system;
- temperature dependence of the reaction rate constant can be expressed in the Arrhenius form;
- heat conduction in the solid phase can be described in terms of the Fourier law;
- mass diffusion of the solid reactants or products does not occur;
- all physical properties (density, heat capacity, and effective thermal conductivity) are assumed constant;
- reaction is not accompanied by melting effects;
- radiation effects inside the porous layer do not play an important role. Heat loss from the system can be described by an effective linear driving force;
- the reactant, M, is in excess so that the reaction process can be considered of the first order with respect to S material.

Gas-solid non-catalytic reactions of the type S(s) + A(g) - P(s) can be handled in a similar way if diffusion effects are unimportant. This is satisfied for high-pressure systems and thin layers of S.[76]

2.1.2. Intermetallic Combustion Synthesis

A large variety of materials can be produced by CS technique with several advantages over more conventional preparation strategies.[77]

Some of these SHS-produced materials are listed below:

1. Abrasives, cutting tools and polishing powders, e.g. TIC, cemented carbides.
2. Resistive heating elements, e.g. $MoSi_2$
3. Shape memory alloys (SMA), e.g. TiNi.
4. High temperature intermetallic compounds, e.g. nickel aluminides.
5. Steel processing additives, e.g. nitrided ferroalloys.
6. Electrodes for electrolysis of corrosive media, e.g. TIN, TiB_2.
7. Coatings for containment of liquid metals and corrosive media, e.g. products of aluminium and iron oxide thermite reactions.
8. Powders for further ceramic processing, e.g. Si_3N_4.
9. Thin films and coatings, e.g. $MoSi_2$, TiB_2.
10. Functionally-graded materials (FGM), e.g. TiC + Ni.
11. Composite materials, e.g. TiC + Al_2O_3, TiC + Al_2O_3 + Al.
12. Materials with specific magnetic, electrical or physical properties, e.g. $BaTiO_3$, $YBa_2Cu_3O_3$

The CS method makes it possible to solve other, more complicated problems: the direct synthesis of materials with additional requirements to their structure and the direct synthesis (however, to a lesser extent) of items with certain shapes, sizes, and assumed properties. In the former case, the item obtained is the direct combustion product, i.e., chemical bonds and the structure of the material, and the shape formation, mechanical and other properties of an item are formed in a single CS process. For the solution of these problems, more than 30 technological varieties of SHS were developed, which were united in six main technological types[78], which are: chemical synthesis, SHS sintering,

[76] J. Puszynski, J. Degreve, V. Hlavacek, Modeling of Exothermic Solid-Solid Noncatalytic Reactions, Industrial & Engineering Chemistry Research, 26 (1987) 1424-1434

[77] K. Morsi, Review: reaction synthesis processing of Ni-Al intermetallic materials, Mater. Sci. Eng. A 299 (2001) 1-15

[78] A.G. Merzhanov, Reviews: Fundamentals, achievements, and perspectives for development of solid-flame combustion, Russian Chemical Bulletin 46 (1997) 1-27.

forced SHS compaction, SHS metallurgy (technology of high-temperature SHS melts), SHS welding, gas-transport SHS technology. The generalized scheme of SHS technologies (Figure 2.1–7) includes three traditional parts: preparation of the raw material, synthesis, and reprocessing of the product. All six technological constructed consider that the main stage is carried out in the SHS mode. The SHS technologies differ in types of initial raw material, structure of charges, types of chemical reactions and processes, internal actions, morphology of products and methods of their treatment (reprocessing), and design of the final products.

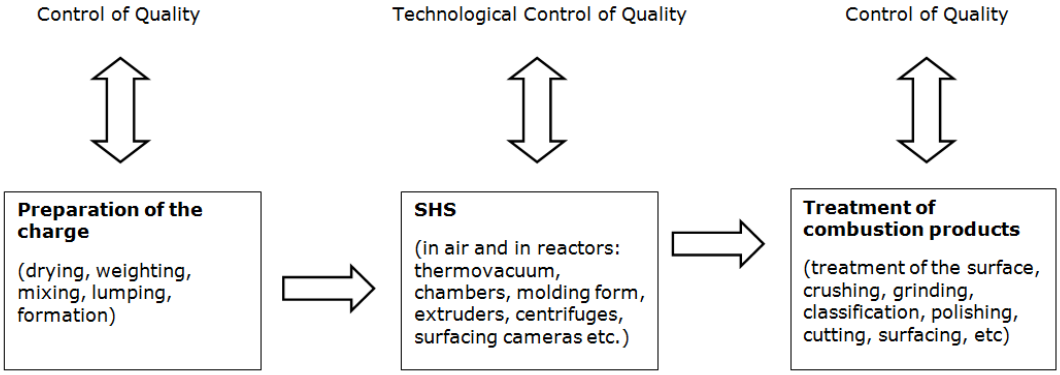

Figure 2.1–7: Generalized scheme SHS technology

Combustion Synthesis (CS) is a process used to form ceramics, intermetallics and their composites at operating temperatures which can also be much lower than their melting points and in very short-processing times[79]. Exothermic reaction processing outstrips difficulties associated with energy-intensive sinter processing conventional methods and so it is being extensively studied for the synthesis of intermetallic compounds. [80]

The selection of the reactant powders is fundamental for the CS reaction and interfacial bond-formation, but the choices are very limited. On one hand thermodynamics limitation is reaction enthalpy, on the other hand kinetic limitations are reaction rate and the effective thermal conductivity. These limitations, if not properly accounted for, could dismiss preparation by self propagating high-temperature synthesis of many important ceramics (e.g SiC, B_4C and WSi_2), most intermetallics (e.g. $TiAl_3$, Fe_3Al) and many composite and solid solution system, without additional activation. In

[79] O. Ozdemir *et al.*, Tribological properties of NiAl produced by pressure-assisted combustion synthesis, Wear 265 (2008) 979–985

[80] H.P. Li, An investigation of the ignition manner effects on combustion synthesis, Material chemistry and Physics 80 (2003) 758-767

most cases, only the simultaneous imposition of the voltage and the activation of the ignition source can initiate self-sustaining reactions. [81]

In the field of inorganic chemistry, the intermetallic compounds and intermetallic phases represent an important group of substances, for which CS can be considered one of the most convenient manufacturing process for the well recognized advantages[82]. Intermetallics are extremely promising materials to improve the performance of engines, pumps, heat exchangers, furnace components, tools and dies parts.[83] These properties make them suitable for high temperature structural and coating applications.[84] In many binary alloy systems, intermetallic compounds appear as stable phases.[85]

Among intermetallic compounds, aluminides, are regarded as promising candidates for the next generation of high temperature, high performance structural and coating materials. It emerges as materials with very attractive properties for applications at high temperatures and/or severe oxidation and/or corrosion condition. It becomes serious candidates for super alloys replacing in structural components, where friction and wear resistance is involved and in high-performance turbine engine applications. Among them, NiAl, is of a high interest due to its favourable property/cost ratio[86], but applications are still limited, among others, due to high brightness and low ductility exhibited at ambient temperature, determined by the high order and low symmetry of its crystal lattice.[87] NiAl compound appeared in a phase diagram (Figure 2.1–8) study published in 1908, where the unusually high melting temperature of this phase was noted. It is well known that phase diagrams must be considered roadmaps not only for the description of these substances and of their reactions, but also for their processing and for research and development planning. Many thermodynamic variables may be used and plotted on phase diagrams, which are equilibrium diagrams thus they describe the final state (stable state) which can be reached in a reaction of the substances involved, in quasi-static

---

81 A. Feng, O.A. Graeve, Z.A. Munir, Modeling Solution for Electric Field-Activated Combustion Synthesis, Computational Materials Science, 12 (1998) 137-155

82 R. Rosa, Microwaves as Ignition Source in the Combustion Synthesis of High Performances Materials, Doctor of Philosophy “High Mechanics and Automotive Design and Technology” at the University of Modena and Reggio Emilia (2010)

83 P. Veronesi *et al.*, Microwave assisted combustion synthesis of non-equilibrium intermetallic compounds, JMPEE, Journal of Microwave Power and Electromagnetic Energy 44 (2010) 45-56

84 S. Dong *et al.*, Synthesis of intermetallic NiAl by SHS reaction using coarse-grained nickel and ultrafine-grained aluminum produced by wire electrical explosion, Intermetallics 10 (2002) 217-223

85 M. Kajihara, Analysis of kinetics of reactive diffusion in a hypothetical binary system, Acta Materialia 52 (2004) 1193–1200

86 G. K. Day, Physical metallurgy of nickel aluminides, Sadhama, 28 (2003) 247–262

87 R.L. Orban, M. Lucaci, Powder Metallurgy Impact on the Nanocrystalline NiAl Processing, Rom. Journ. Phys., 49 (2004) 885–892

conditions. In material science and metallurgy disciplines the diagrams based on plots of temperature vs. composition (atomic per cent) are commonly used.[88]

The Ni-Al phase diagram (Figure 2.1–8) contains five intermetallic compounds (Al_3Ni, Al_3Ni_2, Al_3Ni_5, NiAl, Ni_3Al. Among these, NiAl and Ni_3Al have received an increasing scientific attention and NiAl is one of the most attractive. NiAl as an ordered intermetallic material which revealed several attractive properties including low density (5.91 $g \cdot cm^{-3}$), high melting point (1911 K) and excellent oxidation resistance up to 1573 K, as well as good thermal conductivity (75 $W \cdot (mK)^{-1}$). NiAl is a suitable material for a wide range of engineering applications, including electronic metallization in advanced semiconductor, high temperature environmental coatings, surface catalysts and high-current vacuum circuit breakers. As disadvantages polycrystalline NiAl exhibits a brittle-to-ductile transition at temperature range, depending on stoichiometry, impurity content and grain size from 573 to 873 K which is significantly lower than in other intermetallic compounds. At room temperatures, suffers from low ductility and low fracture toughness and at elevated temperature poor creep resistance and low strength. [89,90,91,92,93]

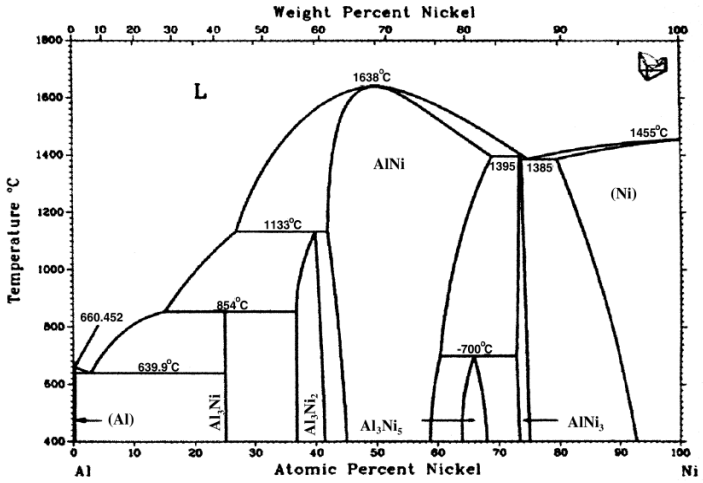

Figure 2.1–8: Phase Diagram Ni-Al[94]

88 R. Rosa, Microwaves as Ignition Source in the Combustion Synthesis of High Performances Materials, Doctor of Philosophy "High Mechanics and Automotive Design and Technology" at the University of Modena and Reggio Emilia (2010)

89 S. Dong *et al.*, Synthesis of intermetallic NiAl by SHS reaction using coarse-grained nickel and ultrafine-grained aluminum produced by wire electrical explosion, Intermetallics 10 (2002) 217-223

90 M. Lieblich, J.L.González-Carrasco, G. Caruana, Thermal stability of an Al/Ni_3Al composite processed by powder metallurgy, Intermetallics 5 (1997) 515-524

91 Ibidem

92 J.M. Yang, The Mechanical Behavior of in-situ NiAl-Refractory Metal Composites, JOM 49 (1997) 40-43

93 T. Czeppe, S. Wierzbinski, Structure and mechanical properties of NiAl and Ni_3Al-based alloys, International Journal of Mechanical Sciences, 42 (2000) 1499-1518

94 K. Morsi, Review: reaction synthesis processing of Ni-Al intermetallic materials, Mater. Sci. Eng. A 299 (2001) 1-15

As highlighted in previous discussion, heat production and dissipation play a central role in CS. Methods to directly monitor the kinetics of the process are almost restricted to the determination of the combustion wave speed by video recording and of the temperature profile of the external surface of the sample as a function of time, with supplementary information given by the analysis of the product at the end of the CS, or after a thermal quenching. Although the synthesis of transition metal has been extensively investigated, most of the available literature is qualitative in nature, with only few cases where the influence of reaction parameters on the propagation characteristics was investigated systematically and quantitatively. The effect of stoichiometry of the reactant mixture and the degree of dilution has been by far the most investigated aspect of these reactions. The dependence of combustion on other parameters, for example particle size, is virtually absent in the majority of the systems investigated. From a chemical point of view, the major criticism of the commonly accepted approach is its oversimplified account of the chemical kinetics. Assuming a single reaction step with a homogeneous-phase kinetic law does not provide a realistic basis for modeling SHS processes and hence for providing a clear understanding. Indeed, since these reactions involve heterogeneous reactants, an extremely wide range of temperatures and thermal gradients, and a wide range of chemical potentials. It is reasonable to expect that the nature of the most relevant chemical step changes when these variables change. Possible chemical steps include gas-phase, gas/solid, or gas/liquid reactions.

For this purpose, it has been developed a flexible and general numerical method that is able to include several reaction steps, possibly with different kinetic laws for each of them, and models the relevant chemical kinetics at the level of the grains of the component powders. Generally speaking, the relevant mechanisms of process can be identified with solid-state diffusion of and gas-phase transport toward the external surface of the metal particle.

Simulation focus the chemical aspect of the intermetallic compound formation on the aspects related to the heterogeneity of the process and to the need of considering many different reaction steps[95].

In case of SHS of transition metal aluminides different assumptions are done:

a) melting of the aluminium reactant;
b) diffusion-controlled dissolution of the remaining reactant (for instance solid nickel) into the molten pool;
c) (possible) melting of the remaining reactant phases;

[95] S. Gennari et al., A new approach to the modeling of SHS reactions: Combustion synthesis of transition metal aluminides, Acta Materialia 54 (2006) 2343–2351

d) precipitation and (eventual) melting of the intermetallic compound;

Melting of pure solid aluminium (a) and possible melting of nickel (c) are considered only in terms of thermal balance without kinetics (enthalpy balance only), while the dissolution of the high-melting metal into the molten pool is governed by an explicit kinetic law. The assumption is that the kinetics of these steps is controlled only by energy transport, which is accounted for at the macro level, these processes are treated "without kinetics", at the microkinetic level. [96]

In this case, simulation approach is built to focus on the heterogeneous aspects of a SHS process. The method is based on the uncoupling between micro and macrokinetic aspects. The microkinetic treatment describes the behaviour of the system at the level of the grains of the solid phases involved in the various phase transformations and chemical reactions. The macrokinetic treatment deals with the Fourier heat balance equation. The microkinetic variables (temperature and conversion degrees of the various chemical steps, which are only functions of time in the microkinetic treatment) are now taken as continuous functions of both time and space variables and inserted into the Fourier equation, which is solved by a FD (finite differences) algorithm.

The microkinetic treatment assumes a spherical shape for the metal particles. The kinetics can be described by different laws, and the choice of these laws depends on current knowledge about simple mechanisms that control the rate and on particular experimental information. To discuss the combustion process of the whole sample (the macrokinetic aspect), the microkinetic variables are replaced with corresponding macrokinetic variables. These are assumed to be continuous variables of time and position within the sample. In particular, for the amount of each chemical component in each phase, we can define a set of variables (which we tentatively refer to as concentrations) to indicate the corresponding molar quantities per unit volume. These variables are related to each other by the stoichiometry of the various reaction steps (which also describes the corresponding heat balance). The heterogeneous system could be described at the macrokinetic level as a homogeneous system, an approximation justified by the fact that the specific aspects of each heterogeneous reaction are already taken into account by the microkinetic laws. Assumptions regarding the sample microstructure are required but do not represent strong limitations on the characteristics that can be investigated by this approach.[97]

---

[96] S. Gennari et al., A new approach to the modeling of SHS reactions: Combustion synthesis of transition metal aluminides, Acta Materialia 54 (2006) 2343–2351

[97] M. Arimondi et al., Chemical Mechanism of the Zr + O2 → ZrO2 Combustion Synthesis Reaction, J Phys. Chem. B, 101 (1997) 8059–8068

On account of previous theory, formulated by Merzhanov, Novozhilov[98,99,100] and Gennari *et al.*,[101,102] in this work aluminides intermetallic combustion synthesis has been studied from model point of view.

To supplement the experimental approach, the computer simulation method is specifically oriented for understanding reaction mechanisms. The method couples the heat transport equation with a detailed kinetic and thermodynamic description of the reaction steps involved.[103] In both cases, the numerical approach gives a great deal of information on various aspects of system dynamics, such as the existence of several unsteady propagation modes in addition to steady propagation, and of the routes to extinction when some SHS specific parameter is changed.

It has been studied the propagation dynamics of the SHS of an intermetallic compound as a function of the heat released by the various reaction steps and to investigate the relation between the rate of these steps and the chemical reaction path actually followed by the system.

To simplify model two assumptions are done at the thermodynamic level:

- a single binary compound is considered;
- heat capacities of the pure phases are taken as temperature independent, whereas mixture proper ties of the liquid phase are modelled by directly using accurate experimental calorimetric determinations.

As assumptions at kinetic level:

- melting of pure aluminium (and possibly pure nickel),
- eutectic crystallization,
- compound deposition under equilibrium conditions are computed only in terms of energy balance, so that their kinetics is controlled indirectly only by energy transport.

An explicit kinetic law is assumed only for the out-of equilibrium dissolution of nickel in molten aluminium, which is described by a diffusion controlled mechanism. Kinetic laws

---

98 M. Arimondi et al., Chemical Mechanism of the Zr + O2 → ZrO2 Combustion Synthesis Reaction, J Phys. Chem. B, 101 (1997) 8059–8068

99 A.G. Merzhanov, Theory of gasless combustion, Arch. Procesow Spalania, 5 (1974) 17–39

100 B.I. Khaikin, A. G. Merzhanov, Theory of thermal propagation of a chemical reaction front, Combustion, Explosion and Shock Waves 2 (1966) 22-27

101 S. Gennari *et al.*, A new approach to the modeling of SHS reactions: Combustion synthesis of transition metal aluminides, Acta Materialia 54 (2006) 2343–2351

102 S. Gennari *et al.*, Combustion Modes and Reaction Paths of the Self-Sustained High-Temperature Synthesis of Intermetallic Compounds: A Computer Simulation Study of the Effect of Exothermicity, J. Phys. Chem. B, 108 (2004) 19550–19556

103 S. Gennari *et al.*, SHS of $NbSi_2$: A Comparison Between Experiments and Simulations, Monatshefte für Chemie - Chemical Monthly 136 (2005) 1871–1875

for nucleation or growth of solid phases, however, can be easily added to the chemical model if required.[104]

SHS it has been shown that the reaction propagates under nearly steady conditions and with a wave velocity close to experimentally reported values, if a suitable thermal conductivity of the green compact is used. Now, intermetallic systems are well-known in the SHS community as a particular case characterized by “low exothermicity” of the process, so that the amount of heat available to sustain the SHS emerges as a very significant parameter to be explored, and this exploration can be most naturally done with computer simulations.

The model here discussed from Gennari *et al.* is then restricted to the simplest case. In its simplified version, the equilibrium phase diagram then shows only three biphasic areas in the composition range $0<x_{Ni}<0.5$ (x = mole fraction) are pure solid Al + liquid, pure compound + liquid, and pure solid Al + pure compound.

In this study is assumed that, when the melting temperature of the low melting metal (i.e., aluminium) is reached, this element melts and only after complete melting does the high melting metal (i.e., nickel) start to diffuse. This changes the composition of the liquid phase and moves the representative point of the system toward the biphasic (compound+ liquid) region of the phase diagram. When the system crosses the AlNi/liquidus curve, the solid compound starts precipitating as required by the phase diagram.

The reaction enthalpy sustaining the SHS process actually comes from two different sources: one heat of formation of the solid compound from the pure elements (the enthalpy of the compound is here modelled as $H= H_0 + C_pT$), the other liquid phase mixing enthalpy.

The method chosen basically uncouples the solution of heat transport (solved for the whole sample and hence referred to as macrokinetics) from the solution of the chemical steps, each being solved at the level of a single particle and referred to as microkinetics. As previous discuss, the microkinetic aspect models the chemical and phase transformations at the level of the grains of the reacting mixture, and the macrokinetics concerns the Fourier equation of energy transport. Technically, at each time step a chemical routine takes care of the irreversible processes at each space step and adjusts the amount and composition of the pertinent phases according to the phase diagram.

The physicochemical model has been implemented in two different ways according to the dimensionality of the problem (1D or 3D). In 1D approach the simulation method basically faces the parabolic system of partial differential equations (PDE):

---

[104] S. Gennari et al., Self-Propagating High-Temperature Synthesis of Intermetallic Compounds: A Computer Simulation Approach to the Chemical Mechanisms, J. Phys. Chem. B 107 (2003) 732-738

The simulation of an SHS process is based on the solution of a parabolic system of partial differential equations:

Eq. 59

$$\begin{cases} \mathbf{c}\frac{\partial \mathbf{T}}{\partial \mathbf{t}} = \boldsymbol{\nabla}\left(\boldsymbol{\lambda}\boldsymbol{\nabla}\mathbf{T} + \frac{2\sigma\epsilon\left(\mathbf{T}^4 - \mathbf{T}_a^4\right)}{\mathbf{R}}\right) + \sum_i \mathbf{q}_{\mathbf{chem}}^{\mathbf{i}} \\ \dot{\mathbf{q}}_{\mathbf{chem}}^{\mathbf{i}} = \mathbf{f}(\mathbf{x}, \mathbf{y}, \mathbf{z}, \mathbf{T}, \mathbf{t}) \end{cases}$$

Two equation: a Fourier's law for heat transport and a kinetic equations. The latter ones describe, at the level of the grains of solid phases, the explicit kinetics of the assumed microscopic chemical mechanism or phase transformations and, hence, the rate of heat evolution. This second equation includes as many chemical steps as required, taking into explicit account the heterogeneous aspects of the process. c_v is the heat capacity per unit volume, σ the Stefan-Boltzmann constant, and ε the emissivity (here ε = 0.99), T_a the room temperature (typically 298 K). The Fourier equation has been written for a cylindrical sample of radius R_0 and length L, and only one spatial coordinate is considered (the coordinate corresponding to the cylindrical axis).

The above system is solved for temperature, and hence initial and boundary conditions are given for T also. Typically the initial conditions are expressed as:

Eq. 60

$$\begin{cases} \mathbf{T}(\mathbf{x}, \mathbf{t} = \mathbf{0}) = \mathbf{T_a} \quad \forall\, \mathbf{x} \in \{\mathbf{0}, \mathbf{L}\} \\ \mathbf{T}(\mathbf{0}, \mathbf{t}) = \mathbf{f_1}(\mathbf{t}) \\ \mathbf{T}(\mathbf{L}, \mathbf{t}) = \mathbf{f_2}(\mathbf{t}) \end{cases}$$

where f_2 is a function for heat input and output due to conduction, chemical reaction and phase transformation, radiation to the surroundings, and f_1 being an ignition function that represents the energy pulse obtained from the igniter. The latter is normally given as:

Eq. 61

$$\mathbf{f_1}(\mathbf{t}) = \mathbf{T_a} + \left(\mathbf{T_p} - \mathbf{T_a}\right)\mathbf{exp}\left[-\frac{(\mathbf{t} - \mathbf{t_{ign}})^2}{2\sigma^2}\right]$$

With T_a room temperature and T_p the maximum temperature reached by igniter, σ the time range and t_{ign} the time lag of ignition.

The Fourier equation describing the heat transfer on the macroscopic scale is solved using the finite difference Crank–Nicolson algorithm. At each time step of solution the amount of transition metal dissolved in the liquid (the irreversible steps) is calculated and the amount and composition of the relevant phases according to the phase diagram are calculated. The amount of heat associated with these processes is then passed back to the Fourier equation, which is then solved for temperature of the next time step.

The 3D approach was implemented by linking a series of user routines to a commercial engine for the solution of PDE systems based on a finite volumes (FV) scheme that directly solves a continuity equation for enthalpy. Boundary conditions and the geometrical model are the same as those for 1D (the ignition function is applied on the front face of the cylinder, while the back face and lateral surfaces are kept at room temperature). The accuracy of the results was controlled with shorter runs with different (finer) discretization steps in space and time. Tests were made in particular to be sure that the oscillations here obtained are real and not an artefact of the numerical algorithm. As mentioned above, processes taken into account in chemical routines are Al reactant melting and diffusion-controlled dissolution of solid nickel into the molten pool. This process is governed by an appropriate kinetic law and we use the invariant field approximation for the solution of the underlying diffusion equation in a semi-infinite pool following:

Eq. 62 $$\mathbf{r^2 = r_0^2 - kDt}$$

Here r is the radius of the particle at a given time, r_0 is its initial value, k depends on liquid composition at the particle liquid interface and bulk liquid composition, and D is the diffusion coefficient.

Eq. 63 $$\mathbf{k = 2\frac{C_1 - C_m}{C_s - C_m}}$$

C_i is the liquid composition at the precipitate-matrix interface, C_m if the far-field composition of the liquid alloy and C_s is the reciprocal molar volume of solid Ni. For the diffusion coefficient an Arrhenius form is used:

Eq. 64 $$\mathbf{D = D_0 exp\left(\frac{-E_a}{RT}\right)}$$

where E_a=76 kJmol^{-1} (activation energy) and D_0=10^{-4} m^{2}s^{-1} (pre-exponential term) were obtained from experimental measurements in isothermal conditions

The simplified kinetic law used here comes from the invariant-field approximation of the underlying diffusion equation (also known as the Laplace approximation)

The step is algorithmically treated at each time interval by first accounting for diffusion and then adjusting (if and when the phase boundary is eventually reached) the liquid composition and amounts of phases according to the equilibrium composition of the liquid phase at the temperature of the time interval. In either case (with or without compound precipitation), the appropriate heat release ($\dot{q}^i_{chem}$) is evaluated and inserted into the FD coefficients of the Fourier equation for the next time integration step.

For the 3D case, explorative simulations were run while the radius of the cylinder was varied. Temperature is just below the melting point of the compound (1800 K). This

situation will be taken as starting point from which all parameters taken into consideration will be changed.

The chemical routine fully encloses the microkinetic aspects of a particular SHS reaction. This is the part of the program that needs to be changed when investigating a novel SHS process, whereas the FD macrokinetic "engine" is left unmodified. On the other side, the organization of the software makes possible to change various aspects of the FD algorithm, leaving unmodified the chemical routine.

Biswas *et al.*[105] describe aluminides combustion synthesis model. The model is divided into two part: the first deal with the formation of the intermediate phase before melting of the Al-rich eutectic through solid state reactive diffusion, the second part approaches the problem of chemical conversion of Ni particles once they are engulfed in liquid Al or Al-rich eutectic.

A sphere of Ni embedded in an Al matrix and a compound layer of Al_3Ni grows at the interface. This is assumed since the average particle sizes of the coarse Ni powders are 2.5–3 times higher than Al powder and Al is the more ductile phase. For a steady rate of diffusion across the compound layer:

Eq. 65
$$\frac{dc}{dt} = \frac{1}{r^2}\frac{d}{dr}\left[Dr^2\frac{dc}{dr}\right] = 0$$

Which boundary condition given by: $c(r=r_{\alpha\beta})=c_{\beta\alpha}$ $c(r=r_{\beta\gamma})=c_{\beta\gamma}$

Eq. 66
$$r^2 = \frac{dc}{dr} = \frac{r_{\alpha\beta}r_{\beta\gamma}}{r_{\alpha\beta}-r_{\beta\gamma}}(c_{\beta\alpha} - r_{\beta\gamma})$$

The case of a compound layer $A_\beta B$ of thickness r_β growing between two saturated phases $A_\alpha B$ and $A_\gamma B$ where $\alpha>\beta>\gamma$, is examined. When $\alpha=\infty$ and $\gamma=0$, $A_\alpha B$ and $A_\gamma B$ represent the pure phases A and B. A similar analysis has been carried out here for a spherical particle.

[105] A. Biswas *et al.*, A study of selfpropagating high-temperature synthesis of NiAl in thermal explosion mode, Acta Materialia 50 (2002) 757-773

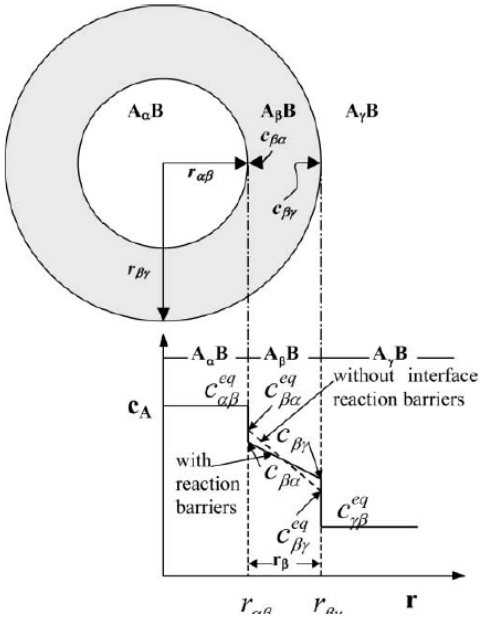

Figure 2.1–9: Schematic representation of the reaction–diffusion model along with the concentration profile of A atoms across an $A_\alpha B/A_\beta B/A_\gamma B$ diffusion couple with or without interfacial barrier. The phases are assumed to be saturated ($\alpha>\beta>\gamma$).

Figure 2.1–9 shows the concentration profile of the component A in the absence of interfacial reaction barriers indicated by a dashed line. The concentrations of A at the interfaces are given by its corresponding equilibrium values $c^{eq}_{\beta\alpha}$ and $c^{eq}_{\beta\gamma}$. In the presence of interfacial reaction barriers, the concentration gradient across the $A_\beta B$ layer is smaller and the actual concentrations at the interfaces are values $c_{\beta\alpha} < c^{eq}_{\beta\alpha}$ and $c_{\beta\gamma} > c^{eq}_{\beta\gamma}$. The chemical interdiffusion coefficient of $A_\beta B$ phase $\widetilde{D}_\beta$ is assumed to be constant. The steady state flow rate $\dot{r}^A_\beta$ of A atoms in the $A_\beta B$ phase will be as follows, from diffusion:

Eq. 67
$$\dot{\mathbf{r}}^{\mathbf{A}}_{\boldsymbol{\beta}} = 4\pi\widetilde{\mathbf{D}}_{\boldsymbol{\beta}}\mathbf{r}^2_{\boldsymbol{\alpha\beta}}\left(\frac{\mathbf{dc}^{\mathbf{A}}_{\boldsymbol{\beta}}}{\mathbf{dr}}\right)_{\boldsymbol{\beta\alpha}} = -4\pi\widetilde{\mathbf{D}}_{\boldsymbol{\beta}}\mathbf{r}^2_{\boldsymbol{\beta\gamma}}\left(\frac{\mathbf{dc}^{\mathbf{A}}_{\boldsymbol{\beta}}}{\mathbf{dr}}\right)_{\boldsymbol{\beta\gamma}} = 4\pi\widetilde{\mathbf{D}}_{\boldsymbol{\beta}}\frac{\mathbf{r}_{\boldsymbol{\alpha\beta}}\mathbf{r}_{\boldsymbol{\beta\gamma}}}{\mathbf{r}_{\boldsymbol{\beta\gamma}}-\mathbf{r}_{\boldsymbol{\alpha\beta}}}\left(\mathbf{c}_{\boldsymbol{\beta\alpha}}-\mathbf{c}_{\boldsymbol{\beta\gamma}}\right)$$

From interfacial reaction

Eq. 68
$$\mathbf{i}^{\mathbf{A}}_{\boldsymbol{\beta}} = 4\pi^2_{\boldsymbol{\alpha\beta}}\mathbf{k}_{\boldsymbol{\beta\alpha}}\left(\mathbf{c}^{\mathbf{eq}}_{\boldsymbol{\beta\alpha}}-\mathbf{c}_{\boldsymbol{\beta\alpha}}\right) = 4\pi^2_{\boldsymbol{\beta\gamma}}\mathbf{k}_{\boldsymbol{\beta\gamma}}\left(\mathbf{c}_{\boldsymbol{\beta\gamma}}-\mathbf{c}^{\mathbf{eq}}_{\boldsymbol{\beta\gamma}}\right)$$

Where $k_{\beta\alpha}$ and $k_{\beta\gamma}$ are the two reaction constants. In this case the flux will not be constant because $r_{\alpha\beta}$ and $r_{\beta\gamma}$ are not equal. So we obtain

Eq. 69
$$\mathbf{c}^{\mathbf{eq}}_{\boldsymbol{\beta\alpha}}-\mathbf{c}_{\boldsymbol{\beta\alpha}} = \widetilde{\mathbf{D}}_{\boldsymbol{\beta}}\frac{\mathbf{1r}_{\boldsymbol{\beta\gamma}}\mathbf{1}}{\mathbf{k}_{\boldsymbol{\beta\alpha}}\mathbf{r}_{\boldsymbol{\alpha\beta}}\mathbf{r}_{\boldsymbol{\beta}}}\left(\mathbf{c}_{\boldsymbol{\beta\alpha}}-\mathbf{c}_{\boldsymbol{\beta\gamma}}\right)$$

Eq. 70
$$\mathbf{c}_{\boldsymbol{\beta\gamma}}-\mathbf{c}^{\mathbf{eq}}_{\boldsymbol{\beta\gamma}} = \widetilde{\mathbf{D}}_{\boldsymbol{\beta}}\frac{\mathbf{1r}_{\boldsymbol{\alpha\beta}}\mathbf{1}}{\mathbf{k}_{\boldsymbol{\beta\gamma}}\mathbf{r}_{\boldsymbol{\beta\gamma}}\mathbf{r}_{\boldsymbol{\beta}}}\left(\mathbf{c}_{\boldsymbol{\beta\alpha}}-\mathbf{c}_{\boldsymbol{\beta\gamma}}\right)$$

Eq. 71 $$\mathbf{c^{eq}_{\beta\alpha} - c^{eq}_{\beta\gamma} -= \left[1 + \widetilde{D}_\beta \frac{1}{r_\beta}\left(\frac{1 r_{\beta\gamma}}{k_{\beta\alpha} r_{\alpha\beta}} + \frac{1 r_{\alpha\beta}}{k_{\beta\gamma} r_{\beta\gamma}}\right)\right](c_{\beta\alpha} - c_{\beta\gamma})}$$

Where $r_\beta = r_{\beta\gamma} - r_{\alpha\beta}$ and $\frac{1}{k_\beta^{eff}} = \frac{1 r_{\beta\gamma}}{k_{\beta\alpha} r_{\alpha\beta}} + \frac{1 r_{\alpha\beta}}{k_{\beta\gamma} r_{\beta\gamma}}$

Combining the above, the expression for flow rate is obtained

Eq. 72 $$\mathbf{i^A_\beta = 4\pi \widetilde{D}_\beta \frac{r_{\beta\gamma} r_{\alpha\beta}}{r_\beta}\left[\left[1 + \widetilde{D}_\beta \frac{1}{r_\beta}\left(\frac{1}{k_\beta^{eff}}\right)\right]\right]^{-1}\left(c^{eq}_{\beta\alpha} - c^{eq}_{\beta\gamma}\right)}$$

Now the position change of the two interface $r_{\alpha\beta}$ and $r_{\beta\gamma}$ with the time t will be:

Eq. 73 $$\mathbf{(c^{eq}_{\alpha\beta} - c_{\beta\alpha})\frac{dr_{\alpha\beta}}{dt} = \widetilde{D}\left(\frac{dc^A_\beta}{dr}\right)_{\beta\alpha}}$$

Eq. 74 $$\mathbf{(c_{\beta\gamma} - c^{eq}_{\gamma\beta})\frac{dr_{\beta\gamma}}{dt} = \widetilde{D}\left(\frac{dc^A_\beta}{dr}\right)_{\beta\gamma}}$$

So the change of layer thickness $r_\beta = (r_{\beta\gamma} - r_{\alpha\beta})$ with time is given by

Eq. 75 $$\mathbf{\frac{dr_\beta}{dt} = i^A_\beta\left(\frac{1}{r^2_{\beta\gamma} c_{\beta\gamma} - c^{eq}_{\gamma\beta}} + \frac{1}{r^2_{\alpha\beta} c^{eq}_{\alpha\beta} - c_{\beta\alpha}}\right)}$$

From equation above it follow that the growth kinetics are different below and above the critical thickness $r^*_\beta = \frac{\widetilde{D}_\beta}{k^{eff}_\beta}$ as shown below:

$r_\beta \propto t$ for $r_\beta \ll r^*_\beta$ interface-controlled

$r_\beta \propto \frac{1}{t2}$ for $r_\beta \gg r^*_\beta$ diffusion-controlled

In the second part of the model, it is assumed that as soon as 640 °C is reached as temperature the Al-rich eutectic melts and engulfs the Ni spheres and an intermediate complex layer of a composition of NiAl forms around it instantaneously. From experimental point of view sample remained unchanged till the temperature reasche approximately 640 °C, when a liquid phase formed and exuded and covered all surface rapidly. Further diffusion across this complex leads to the formation of NiAl by precipitation from the saturated liquid whereas the thickness of the layer remains constant as the rate of growth at the complex–Ni interface is equal to rate of dissolution at the Al–complex interface.

Under steady-state condition, the rate of Al diffusion is equal to the rate of Ni particle consumption if the interfacial reaction barriers are ignored and this will lead to the following equation:

Eq. 76

$$-\frac{M_{Ni}D_0}{\rho_{Ni}r_0^2}\exp\left[-\frac{E}{RT(t)}\right]dt=\frac{\left[\frac{M_{Al}}{\rho_{Al}}r^3+\frac{M_{NiAl}}{\rho_{NiAl}}(r_0^3-r^3)-\frac{M_{Ni}}{\rho_{Ni}}(3r^2\delta)\right]}{r_0^2r^2}\left(\frac{\delta}{r+\delta}\right)dr$$

if the radius of Ni particle is r_0 at time t=0 and r at time t=t (where t>0) and the thickness of the complex layer is δ. Here 4.8 × 10-^{6} m^2/s is used as the value for D_0, E_a is the activation energy for combustion synthesis of NiAl which was experimentally determined to be 170.99 kJ/mole. The above equation is then solved numerically using the experimentally obtained time–temperature profile from 640 °C onward. The diameters of the unreacted Ni particles after being heated to 640 °C were calculated in the first stage of the model and the same were used as the starting diameters here.

Experimental temperature profile are shown in Figure 2.1–10. It depicts (Figure 2.1–10 (a)) the time–temperature profiles of compacts containing Ni_1 and Ni_2 at the linear heating rate of 25 °C/min (where Ni_1 and Ni_2 are different Ni powder). This profile showed a plateau followed by initiation of ignition and a sharp rise to the peak of combustion (T_c) and a second arrest at the crystallization point of the product (T_{cr}) in case the T_c surpassed it. The temperature profiles of combustion for the different Ni powders changed with the variation in heating rate as well. This was especially the case of coarse Ni (Ni_2 and Ni_3) powders and Figure 2.1–10 (b) depicts this effect. The temperature of appearance of initial liquid shifted from close to 640 to 675 °C when the rate of heating was higher than 15 °C/min. T_{ig} and T_c followed a similar trend and Figure 2.1–10(c) shows the effect of the rate of heating on Tig. When the rate was more than 35 °C/min, T_c surpassed the melting point of the product.

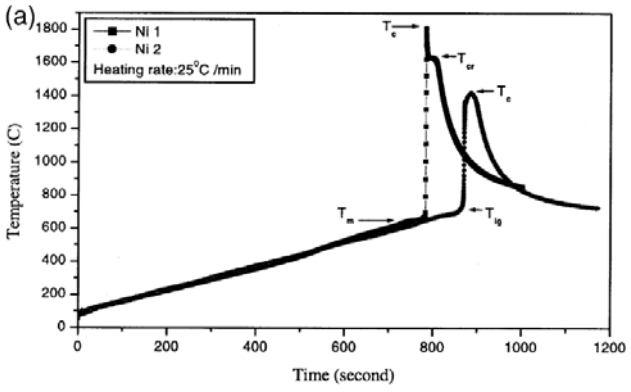

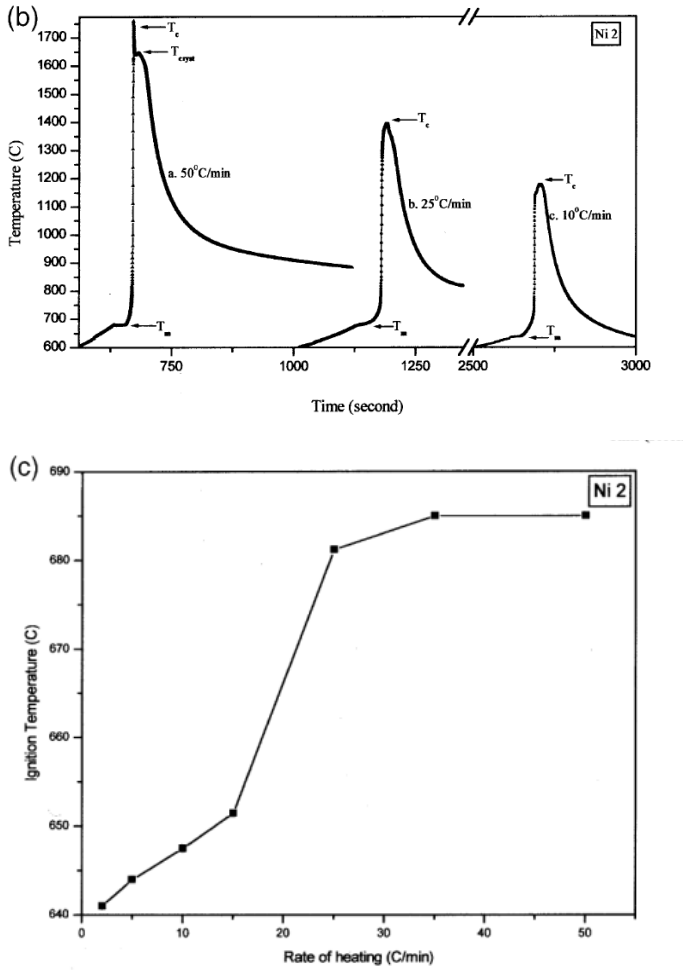

Figure 2.1–10: (a) The time–temperature profiles of thermal explosion of compacts of Ni 1 and Ni 2 at a constant rate of heating (25 °C/min) showing the effect of Ni particle size. (b) Plot showing the effect of heating rate on the temperature profiles of coarse Ni powders. Tm, Tc and Tcryst are the temperature of pre-ignition melting, combustion temperature and the solidification point of the product respectively. (c) Plot showing the effect of rate of heating on Tig.

In general, from experimental[106] point of view the temperature profile is obtained at one point on the sample, using a thermocouple or an optical pyrometer. Temperature profile shape is strongly dependent on the details of the microscopic reaction mechanism. Figure 2.1–11 shows typical SHS temperature profile of NiAl, which is similar for other transition metal aluminides. As previously reported, it is characterized by a very sharp first peak, which is usually followed by a much broader second peak or by a plateau. Although this profile is quite common and has been reported in the literature, no quantitative explanation has been presented for the presence of the two maxima. Figure 2.1–12 (a) shows the calculated temperature profile as a function of time for the SHS of

[106] S. Gennari *et al.*, A new approach to the modeling of SHS reactions: Combustion synthesis of transition metal aluminides, Acta Materialia 54 (2006) 2343–2351

NiAl with x_{Ni} = 0.49, a particle radius r_0=50 µm and a thermal conductivity $\chi = \chi_{bulk}/10$. The temperature profile reproduces reasonably well the shape of the experimental curve of Figure 2.1–11, showing an initial sharp peak followed by the much broader second peak. However, the timescale in this simulation is an order of magnitude lower than the experimental data of Figure 2.1–11. This is due to the high value of thermal conductivity used for this simulation compared to the conductivity values typical of powder compact.

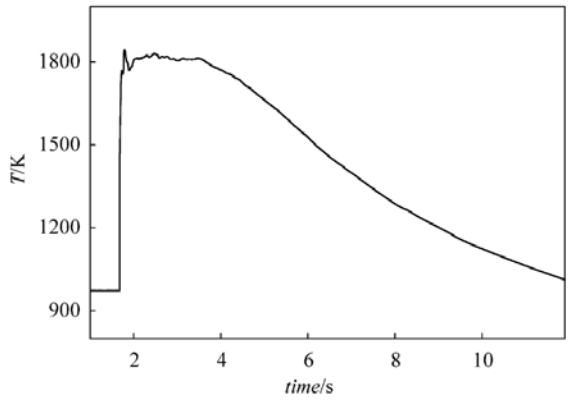

Figure 2.1–11: Experimental profile of temperature for the SHS of NiAl, Ni grain size <10 µm.

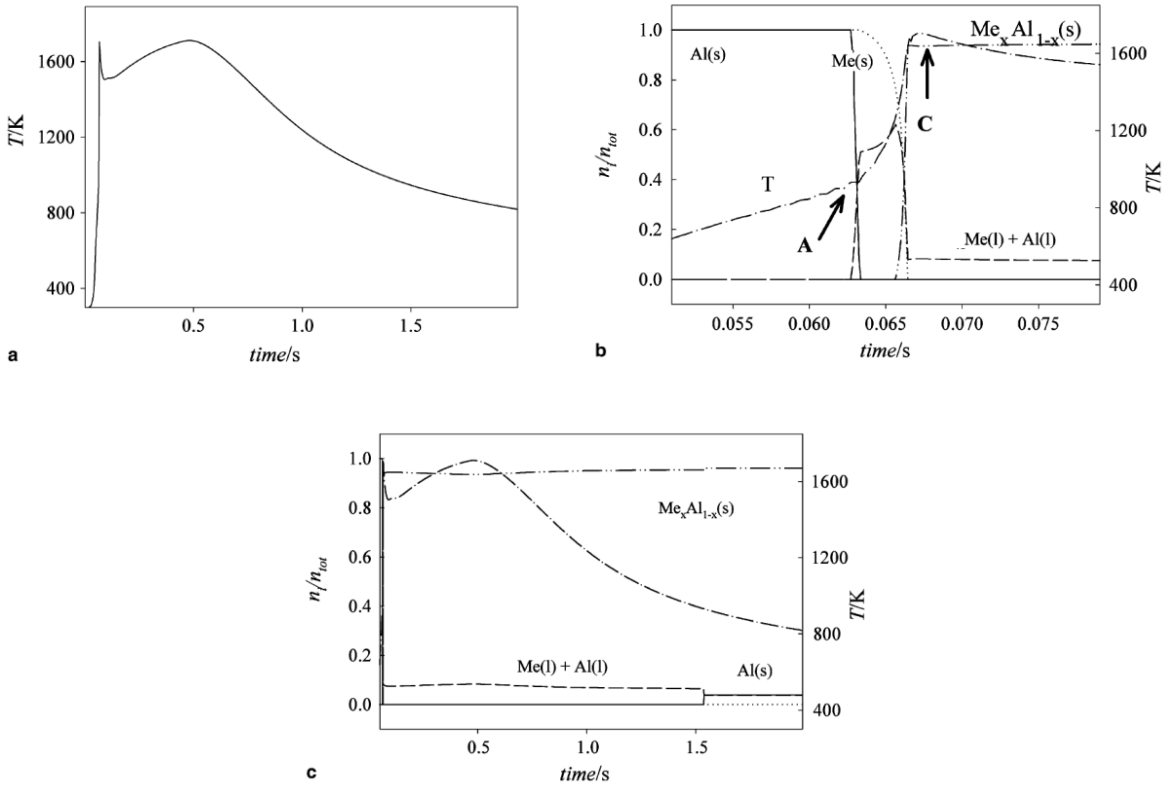

Figure 2.1–12: Simulated temperature profile for the SHS of NiAl, with x_{Ni}=0.49, r_0=50 l_m and v= v_{bulk}/10, and enlargement of the temperature spike region for solid aluminum (continuous line, left axis), solid Ni (dotted line, left axis), solid compound (dash-dot-dot line, left axis), total amount of liquid (dashed line, left axis) and temperature (dash-dot line, right axis).η_i represents the moles per unit volume of a component in a certain phase. For simplicity reasons, η_i is normalized on the total number of moles available ntot of the same component in the actual simulation run.

Some aspects of the temperature profile can be related to the chemical changes accompanying the process. Figure 2.1–12 (b) depicts the phase evolution in the small region across the combustion front. These results are obtained using a simulation made with the same parameters as used in Figure 2.1–12(a). In Figure 2.1–12 (b) the front propagates from right to left. When the temperature reaches the melting point of Al (point A in the figure) the solid transition metal (dotted line, left axis) begins to dissolve in the liquid leading to an increase in the amount of liquid phase (dashed line, left axis) until it reaches a maximum value, after which the solid intermetallic compound (dash-dot line, left axis) begins to precipitate. The large amount of heat released by the precipitation of the compound is responsible for the first, sharp temperature spike in the temperature profile (point C in Figure 2.1–12). However, no further chemical reaction or phase transformation takes place outside this region, as shown on a larger scale in Figure 2.1–12(c) where the amount of all phases is seen to remain constant after the first sharp reaction front. This implies that the second broad peak that is observed in Figure 2.1–11 and Figure 2.1–12(a) cannot be related to any heat release/absorption due to phase transformations and/or to a chemical process. An alternative explanation, however, can be found in the complex mechanism that causes propagation instabilities in this family of reactions.

2.1.3. Microwave Ignited Combustion Synthesis

All combustion syntheses ignited by means of conventional heating techniques usually show an inversion of heat flow before and after the exothermic reaction. Indeed, at the beginning step of CS, the reactive species, usually powders, are exposed to a pre-heated or heating environment to reach the ignition temperature and so the heat flow is directed towards the powders themselves. As soon as the powders reach the ignition temperature, the heat released during the reaction tends to rapidly raise the temperature of the reactants undergoing the CS reaction, and subsequently the heat flow is directed from the reaction zone towards the surrounding environment. Thus, as soon as the reaction occurs, it is no longer possible to continue to transfer heat from an external conventional heating source to the reaction zone. On the contrary, the use of microwaves heating in the ignition of CS reactions is expected to lead not only to a more rapid temperature increase of the whole reaction zone, but also to a continuous energy transfer to the reactants and products during and after the ignition, with consequent heat generation. This can control the cooling stage after CS, extending the time permanence at high temperature.

Microwave heating and sintering of various high dielectric loss materials such as oxide and carbides has been applied in different industrial applications. Microwave heating is

fundamentally different from conventional heating because all the energy is directed at the workpiece, in the case of laser processing, but with a much more penetrating capability deriving form the lower frequency of the EM field. In microwave processes, the heat is generated internally through material microwave interaction instead of coming from an external heating source. This internal volumetric heating results in an energy diffusion form the material under processing to the surrounding environment, that is reverse to the direction of the one observed in conventional heating[107]. Compared with conventional furnaces the use of electromagnetic energy provides a more rapid and efficient heating and sintering methodology. Furthermore, a rapid heating limits grain growth during sintering and thus helps to improve microstructure and mechanical proprieties of the sintered products.[108]

MWs energy possesses selective and volumetric characteristics (according to the dielectric and magnetic properties of the material to be treated) which can be proficiently exploited in the ignition and eventually in the sustaining of CS reactions for joining applications. Microwave heating occurs by energy transfer from the electromagnetic field to the material and subsequent heat generation due to polarization, rather than relying on heat transfer, according to the dielectric and magnetic properties of the material to be heated.[109] Microwave heating selectivity applied to CS of multi-phase systems, like coating-metal substrate, allows maintaining the bulk of the substrate metallic materials to a much lower temperature, compared to combustion synthesis in conventionally heated furnaces. This selectivity of microwave heating, i.e. microwaves are not directly absorbed by the bulk metallic substrate, helps minimizing substrate modification thus maintaining its original microstructure and properties, as previous demonstrated by Veronesi *et a*l.[110]

The use of microwave electromagnetic radiation as means of heating materials is well known from time-saving appliance, so microwave heating could be at heart for welding, as well as brazing and soldering. Microwave welding process achieves coupling between microwave energy and material. Different materials absorb microwave (MW) energy differently. This depends on the materials characteristic (whether it is composed of ions or polar molecules, and which ones), the frequency of the MW energy (due to loss factor effects) and the temperature of the material being irradiated (with absorption usually

---

107 S. Gedevanishvili, D. Agrawal, R. Roy, Microwave combustion synthesis and sintering of intermetallics and alloys, J. Mater. Sci. Letters 18 (1999) 665-668.

108 G. Poli, R. Sola, P. Veronesi, Microwave-assisted combustion synthesis of NiAl intermetallics in a single mode applicator: Modeling and optimisation, Mater. Sci. Eng. A 441 (2006) 149-156

109 P. Veronesi *et al*., Microwave assisted combustion synthesis of non-equilibrium intermetallic compounds, JMPEE, Journal of Microwave Power and Electromagnetic Energy 44 (2010) 45-56.

110 Ibidem

increasing with increasing temperature, for most ceramics and metals). Actually microwave welding is at embryonic state, except for plastics welding. Specially the process has huge potential for hard-to-weld ceramics[111].

The combined application of microwave energy in the ignition and eventually in the sustaining of combustion synthesis reactions allows, as previously mentioned, several advantages, such as the selective and volumetric heating,[112] advantage in terms of time and energy saving and minimization of heat affected zones.

Microwaves permits the generation of a keyhole that effectively concentrates the energy input into a small area, and there is good potential to join dissimilar materials since the microstructural changes are confined to the weld region and a narrow heat affected zone, which has been reported to conserve welding mechanical and chemical properties. This selectivity of microwave heating when joining conductive parts i.e. microwaves are not directly absorbed by the bulk metallic substrate, helps minimizing substrate modification thus maintaining its original microstructure and properties, as previous demonstrated by Veronesi *et al*. in several works. [113,114,115,116]

2.1.3.1. Basics of microwave heating of metal powders

The relevant properties of a material able to describe its interaction with an incident electromagnetic field are its complex permittivity ε^* and permeability μ^*, the first accounting for electric field related interactions, and including also in its general formulation the conductivity, the latter accounting for the magnetic field interactions.. In earlier microwave heating studies, mainly focused on dielectric materials, the heating effect has been attributed to the interaction of electric field with the material, while the magnetic field is usually ignored. Heating arises due to the ability of the electric field to polarize the charges in material and the ability of the polarization to keep up with the rapid changing electric field.[117] Complex permittivity (ε^*) is introduced to macroscopically describe the response of a material to an externally applied sinusoidal field, and to

111 R.W. Messler, Principle of Welding Processes: Physics, Chemistry and Metallurgy, Wiley-VHC, Verlag GmbH & Co. KGaA, 2004 DOI: 10.1002/9783527617487

112 R. Rosa, Microwaves as Ignition Source in the Combustion Synthesis of High Performances Materials, Doctor of Philosophy "High Mechanics and Automotive Design and Technology" at the University of Modena and Reggio Emilia (2010)

113 R. Rosa *et al.*, Microwave Ignited Combustion Synthesis as a Joining Technique for Dissimilar Materials, Journal of Materials Engineering and Performance, 21 (2012) 725-732

114 P. Veroensi *et al*., Microwave assisted combustion synthesis of non-equilibrium intermetallic compounds, JMPEE, Journal of Microwave Power and Electromagnetic Energy 44 (2010) 45-56

115 R. Rosa *et al.*, Ni-Al-Ti Coatings Obtained by Microwave Assisted Combustion Synthesis, Surface Engineering, 28 (2012) 91-95

116 I. Boromei *et al*., Oxidation behavior resistance of a duplex NiAl/Ti-Ni-Al coating by microwave assisted SHS on Ti substrate, EURO PM2009 Proceedings, EPMA, Copenhagen, Denmark, 3 (2009) 161-166

117 A.C. Metaxas, R.J. Meredith, Industrial Microwave Heating, Peter Peregrinus, London (1993) 97-102

account for energy storage and losses. Hence, it is a measure of the ability of a dielectric to absorb and store potential energy. It could be expressed by the following equation (Eq. 77):

Eq. 77 $$\boldsymbol{\varepsilon^* = \varepsilon' - j\varepsilon'' = \varepsilon_0 \varepsilon_r' - j\varepsilon''}$$

The real part of the complex permittivity, ε' also known as dielectric constant, represents the ability of the material to store energy in a reversible way, while ε'', also called loss factor, represents the ability of the material to dissipate energy from the electromagnetic field, i.e. generating heat[118]. Moreover, in Eq. 77 ε_0 is the empty space permittivity of free space (8.86 x 10^{-12} F/m) $\boldsymbol{\varepsilon_r'}$ relative permittivity.

The loss tangent, tanδ, represents the efficiency of the material to convert absorbed energy into heat and it is also commonly used to describe the dielectric response. The loss tangent is expressed by the following equation (Eq. 78):

Eq. 78 $$\boldsymbol{\tan\delta = \frac{\varepsilon''}{\varepsilon'}}$$

The angle δ is the phase difference between the oscillating electric field and the polarization of the material.

Complex permeability, that is response of a material to an applied sinusoidal magnetic field can be described by the complex permeability, which is expressed by the following equation (Eq. 79).

Eq. 79 $$\boldsymbol{\mu^* = \mu' - j\mu'' = \mu_0 \mu_r' - j\mu''}$$

The imaginary part, μ'' represents the magnetic loss factor which accounts for relaxations and resonance processes under the influence of an alternating magnetic field. μ_0 is permeability of free space ($4\pi x10^{-7}$ H/m), and μ_r' relative permeability.

The possibility of conveying energy into a material, according to its dielectric, electric, and magnetic properties can be summarized by the equation of the power density distribution (Eq 80), which describes the power dissipated per unit volume into the material by the conversion of the electromagnetic energy into heat [119]:

Eq. 80 $$\boldsymbol{P_{d(x,y,z)} = \omega \varepsilon_0 \varepsilon_{eff}'' E_{rms}^2 + \omega \mu_0 \mu_{eff}'' H_{rms}^2}$$

where P_d is the power density in the material, expressed in W/m^3, at the position (x,y,z) in space. In Eq. 80, $\omega = 2\pi f$, where f indicates the frequency of the incident

[118] M. Gupta, W.W.L. Eugene, Microwaves and metals, John Wiley and Sons, Singapore, 2007
[119] Ibidem

microwaves, in Hz. The dielectric and magnetic properties of the material are taken into account by ε''_{eff}, which is the effective loss factor, including conductivity losses and by μ''_{eff}, which is the imaginary part of the effective magnetic permeability. The electromagnetic field configuration enters Eq. 80 in terms of the root mean square of its local intensity, and precisely as E_{rms} (local (x,y,z) electric field intensity, in V/m) and H_{rms} (local (x,y,z) magnetic field intensity, in A/m).

In order to quantify how deep the power from the electromagnetic field will penetrate into the material, until a given attenuation is achieved, the power penetration depth must be considered.

In case of dielectric materials, the power penetration depth is a function of the complex permittivity according to (Eq. 81):

Eq. 81 $$\mathbf{D_p = \frac{\lambda_0 \sqrt{\varepsilon'_r}}{2\pi \varepsilon''_r}}$$

When λ_0 is the wavelength of the incident MWs, ε''_r is the relative loss factor

In case of conductive materials, electrical conductivity and permeability control the penetration depth: the higher the permeability, the less the electromagnetic wave will penetrate into materials. Penetration depth in this case is commonly addressed as “skin depth” and it is a measure of the depth of electromagnetic field or power penetration in a conductive material. Penetration depth of the field is defined as the distance from the surface of the materials at which the magnitude of the field strength is reduced to 1/e (= 0.368) of its value at the surface. The penetration depth is inversely proportional to the frequency of the electromagnetic field. In case of good conductors, like metals, this conversion of the electromagnetic field energy into heat occurs only in a very thin layer, hence the term “skin depth”, because total reflection of microwave is not possible due to limited resistance in the materials due to the presence of defects. For most of metals the skin depth can be estimated by (Eq. 82):

Eq. 82 $$\mathbf{d = \frac{1}{\alpha} = \sqrt{\frac{\rho}{\pi f \mu_0 \mu'}}}$$

Where ρ is the electric resistivity of the material.

Table 2.1-2: Skin depth value at 300 K, as temperature, and 2.45 GHz, as frequency.

	T (K)	f (GHz)	δ_s (μm)
Ag	300	2.45	1.26
AISI 304	300	2.45	8.83
Al	300	2.45	1.77
Au	300	2.45	1.60
Bronze	300	2.45	3.29
Cu	300	2.45	1.36
Inconel	300	2.45	11.82
Mo	300	2.45	2.37
Ni	300	2.45	3.21
Brass	300	2.45	2.63
Pt	300	2.45	3.39
Sn	300	2.45	3.47
Ti	300	2.45	6.75
Zn	300	2.45	25.92

Hence, bulk metals are considered reflecting materials at the MW frequencies. At 2.45 GHz, as MW frequency, most metals shows a skin depth values of a few micrometers, which leads to the possibility to directly heat micrometric metallic powders by means of MW energy, but also to negligibly heat bulk metal parts. The powder compact tends to preferentially absorb MW energy and thus it preferentially heats up and then it is softens or melts. Thus, to weld two different types and/or composition pieces, the interface is often packed with a mixture of powders. Porous metal powder compacts heat up when they are subjected to microwaves irradiation. According to the previous equations, the factors relevant to describe the heating of porous metal compacts, besides the thermal ones, in microwave are: effective electrical conductivity, effective permittivity and effective permeability. [120]

However, MW interaction with metal powders is still debated and the possible involved mechanisms could rely on induction of eddy currents due to the H field [121], on the

[120] J. Ma *et al*., Single Mode Microwave Heating of copper Powder Metal Compacts, Proceedings of the COMSOL User Conference 2006 Boston

[121] J. Cheng, R. Roy, D. Agrawal, Experimental Proof of Major Role of Magnetic Field Losses in Microwave Heating of Metal and Metallic Composites, J. Mater. Sci. Lett., 20 (2001) 1561–1563

presence of a thin dielectric oxide layer surrounding each metal particle [122] or on localized breakdown phenomena.[123]

2.1.3.2. Microwave systems

A microwave system is characterized by two main components: a microwave source to generate MWs and an applicator or cavity with the aim to deliver power to the material; further components can be the control system, to monitor and regulate power to material.

As generator, the most common type is magnetron. The magnetron cavity consists of a tungsten thoriated cathode at the center of cavity and a circulator metal anode. Cathode emits electrons when heated, which are accelerated towards the anode by a high voltage of about 4 kV. A magnetic field is applied axially forces the electrons to spiral around the cathode. The circular motion of electrons induces alternating currents in the anode cavities. The cavities are equivalent to tuned circuits and he cavity size determinates the resonant source frequency. The energy is then injected, through a waveguide, into the applicator containing a load. When the load changes significantly, oscillation may jump to another mode.

Recently, the advent of high power solid state generators (up to 200W) opened a completely new era for microwave sources, due to the longer life and possibility of frequency control offered by this new family of generators. Their use in industry, however, is still limited due to the small power and high cost.

Microwave source and applicator are usually connected by a transmission line, which can be a waveguide or a coaxial cable, the latter usually for low power applications. The most popular[124] applicators can be categorized into three classes, namely single mode, multi-mode and slotted feed cavities, as shown in Figure 2.1–13.

---

[122] K.I. Rybakov *et al.*, Microwave Heating of Conductive Powder Materials, J. Appl. Phys., 99 (2006) 023506-1 023506-9

[123] C. Leonelli e*t al.*, Microwave Assisted Sintering of Green Metal Parts, J. Mater. Process. Technol., (205) 2008 489–496

[124] T.V. Chow, H.C. Reader Understanding Microwave Heating Cavities, Artech House Microwave Library (2000) ISB: 1-58053-094-X

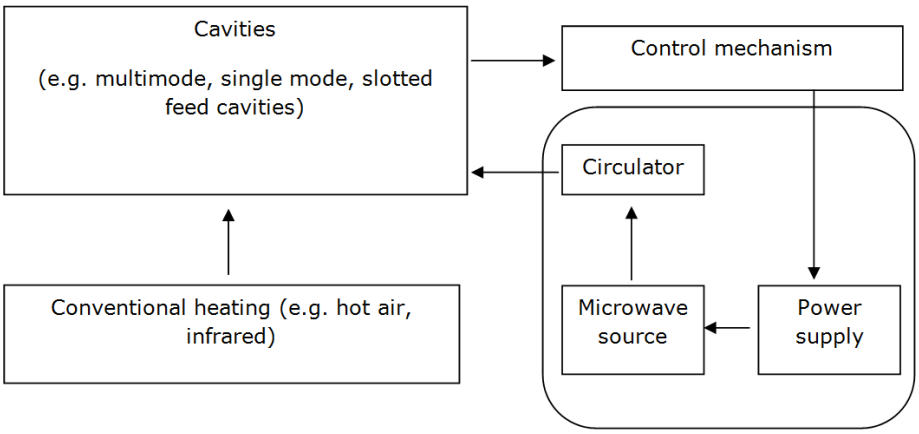

Figure 2.1–13: Typical block diagram of microwave systems.

Depending on the electromagnetic field distribution in the applicator, this means that in the first case only one mode (or pattern) of distribution of the EM field will be present, while in the second case, a superimposition of a plurality of modes will determine the overall EM field distribution. Slotted feed cavities or radiat applicators are used instead when the EM field is no longer confined by the applicator walls, but it radiates towards the external parts, which can be open air or a second applicator or enclosure.

A single-mode sustain only one mode, which is the field pattern that exists in the cavity, and it usually has dimensions comparable to the microwave wavelength, hence it is suitable for small loads. Multimode cavity sustains many modes and is used for bulkier items and for batch or continuous processes.[125] The material heating is controlled by variations in the power and duration of microwaves radiation on the materials.

Depending on the applicator used, the EM field distributions inside the cavity can be manipulated. In a multimode cavity, multiple modes are excited within the cavity, hence it is not possible to isolate the electric and magnetic field with tuning.

The single-mode cavity solves multimode problem[126]. It supports only one mode at the source frequency. Its attraction is that the field pattern is well defined in the space. For this type of mode, the area of high intensity electric field is restricted and the material to be processed needs careful placement for optimum heating. The disadvantage is the relative small sized object could be treated.[127]

The simplest single mode cavity is a rectangular piece of waveguide closed at both ends with metal plates.

---

125 Ibidem

126 T.V. Chow, Howard C. Reader Understanding Microwave Heating Cavities, Artech House Microwave Library (2000) ISB: 1-58053-094-X

127 Ibidem

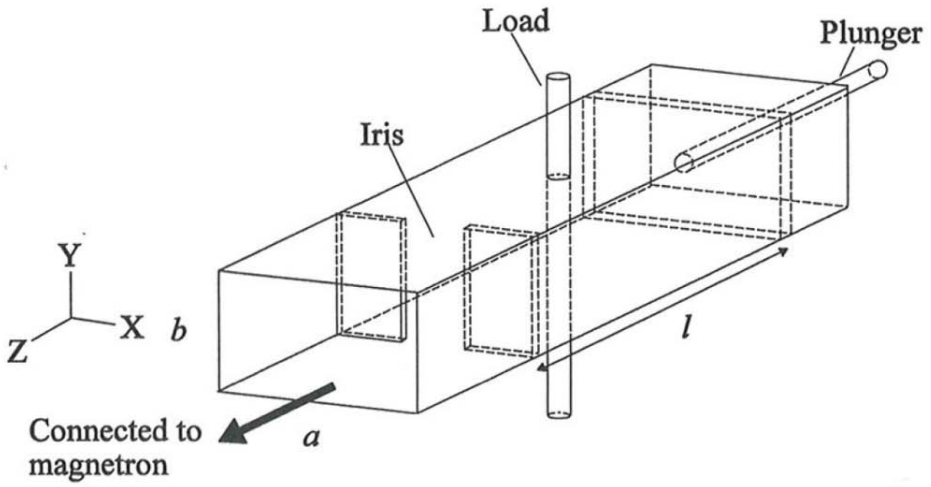

Figure 2.1–14: Rectangular single-mode cavity with centrally located cylindrical sample. Iris and plunger are for impedance matching and for tuning cavity, respectively.

Figure 2.1–14 shows a schematic diagram of the cavity with a cylindrical load centrally located in the broad wall. A coupling iris separates the source from the load and is used for impedance matching purposes, i.e. to reduce reflected power and increase efficiency. The size of the aperture determines the impedance matching from the source thus determining the transfer of power into cavity. Instead of closing the other end of the waveguide, a variable short circuit plunger is moved to restore the original mode when the load is introduced. This makes the cavity suitable to heat a variety of materials.

Because of boundary condition (metal walls), the wave that propagates inside a homogeneously filled waveguide are different from TEM waves and are known as transverse electric (TE or H) waves and transverse magnetic (TM or E_x) waves. TE waves have $E_z=0$ while TM waves has Hz=0. For TE waves there is a component of H along the direction of propagation while for TM waves it is the E_x component that exists in the same direction. In both case, energy is carried by the electric and magnetic fields associated with the wave. The wave forms a field pattern inside the waveguide known as a mode. Inside the waveguide it is possible to have several modes of propagation, which correspond to solution of Maxwell's equation. The mode that has the lowest frequency in a particular waveguide is known as the dominant mode.

Assuming a rectangular coordinate system, Figure 2.1–15 shows a plane wave with sinusoidal electric and magnetic field variation in the z-direction. The wave has only E_x and H_y components that are transverse to the direction of propagation.

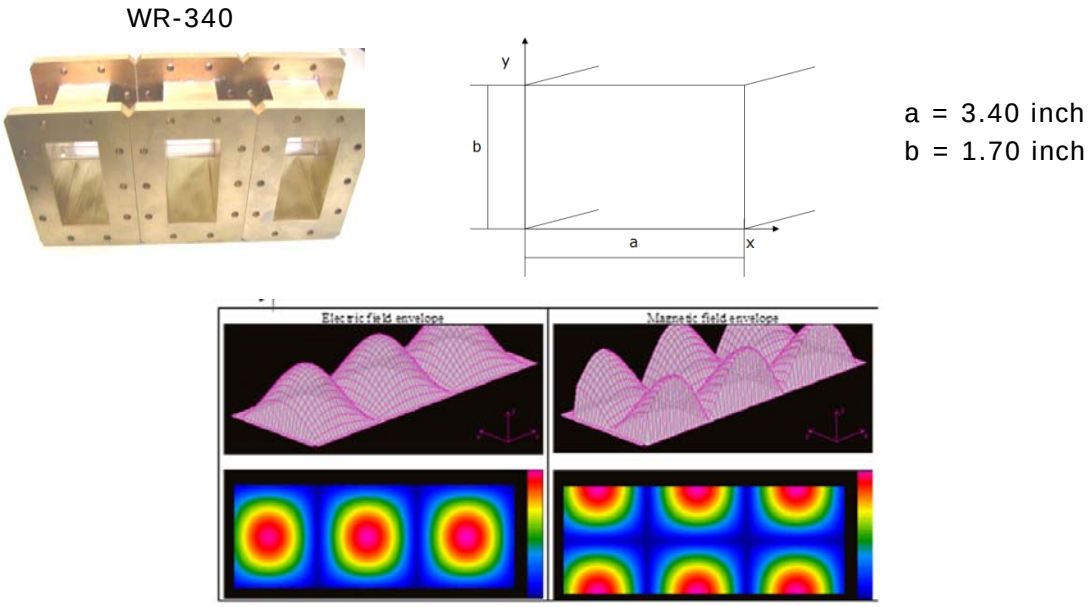

Figure 2.1–15: Electric and Magnetic field envelope in WR-340 wave guide

2.1.4. Microwave ignition and sustaining of CS

Several strategies exist to activate combustion synthesis. These include the application of thermal, mechanical, or electromagnetic energy. Pre-heating, or thermally activated combustion synthesis (TACS), is one of the simplest and more widely used strategies for activation of CS reactions. TACS processes have been shown to be highly sensitive to heating rate. This is a drawback as most furnaces are limited to relatively low heating and cooling rates determined by the furnace cycle, which leaves sample time for diffusion and formation of undesirable phases during processing.

Electromagnetic activation via microwave has some interesting consequences due to the manner in which the energy is absorbed. Microwave energy is absorbed volumetrically, resulting in volumetric heating. The heated area is limited to the sample volume and the susceptor (if one is used). This inverts the temperature profile, with the surface of the sample being cooler than the interior. Heat generation at the sample and the inverted temperature profile allow for very rapid heating and cooling rates. Once the reaction begins, the hot reaction usually zone becomes the most strongly absorbing area in the system. This is due to the rise in dielectric loss factor that occurs as the temperature is raised, and it applies for most ceramics, polymers and metals. Above a certain threshold, the absorption of microwaves by the sample rises very rapidly. This condition, generally referred to as thermal run away, is a unique effect of microwave activated processing. This effect also aids in CS processing of high-density green bodies,

which is difficult by other methods. In addition, microwave energy has been shown to reduce the apparent activation energy of a reaction. This still debated phenomenon has been documented in catalyzed reactions, and in terms of enhanced diffusion during sintering.[128]

Electromagnetic activation could be obtained in two different ways: one is the “Field Activated Combustion Synthesis (FACS)” process, the other is “Microwave Activated Combustion Synthesis” MACS . The processes differ in the application method of the electric field and the mechanism by which activation occurs. FACS exploits a mechanism of joule heating due to electrical resistance, while MACS relies on microwave absorption. In FACS, an appropriately shaped sample is placed between two electrodes and a voltage is applied. A tungsten coil is used to initiate the reaction. The electric field provides energy to the propagating reaction.

In MACS, direct or indirect ignition can occur, depending on the reactants properties. Direct ignition occurs by conversion of the energy of the EM field into heat within the reactants. Indirect heating occurs when an external absorber (susceptor) is used or when locally the dielectric strength of the reaction media are surpassed, triggering breakdown phenomena (plasma, arching).

The most controllable way to ignite a CS by microwaves is the use of a susceptor (e.g. silicon carbide), which preferentially absorbs part of the incident microwaves, providing ignition and activating combustion reactions.

Once temperature high enough are reached, the microwave absorption can become predominant on the reacting species, rather than in the susceptor, or the susceptor can continue to present the higher power density. In both cases, microwave heating occurs throughout the materials (reactants or susceptors), determined by the dielectric loss factor of the materials involved. The volumetric heating inverts the typical temperature profile, so the sample is hottest at the centre and cooler near the surface as heat radiates to the surroundings. The point of ignition for microwave activated combustion synthesis can, therefore, be within the bulk of the material.

The combustion process itself is also affected by microwave heating. In a combustion process, the hottest region occurs where the reaction is taking place, hence further favouring heat generation by direct microwave absorption in such zone. The same occurs when cooling laser and microwave processing.[129]

---

[128] J.R. Jokisaari, S. Bhaduri, S.B. Bhaduri Microwave activated combustion synthesis of bulk cobalt silicides, Journal of Alloys and Compounds 394 (2005) 160–167

[129] M. Willert-Porada *et al*., Microwave Sintering of High-Performance Ceramics: Material and Technological Aspects, CFI Ceramic Forum International, 75 (1998) 19-25

Microwave activated combustion synthesis was successfully utilized in activating reactions in various mixtures of Ti and Al in order to form intermetallics of nominal compositions of TiAl and Ti_3Al. A higher reaction temperature was recorded in MACS as compared to TACS samples. This may be attributable to several characteristics of microwave activation including high heating rates and the preferential absorption of microwave energy at the reaction zone. [130]

Microwave energy has been used in triggering various combustion reactions. There are numerous experimental studies of microwave heating of metallic powders.[131]

Dalton *et al.* for the first time[132] recognized that microwave energy may be helpful in triggering combustion reactions in Ti and C as well as in a mixture of TiO_2, Al, and C[133]. The authors investigated the following mixtures, Ti + C, Si + C, 4B + C, Ti + 2B, Mo + 2Si, 5Ti + 3Si, 2Al + N_2, 2Ti + N_2 and $3TiO_2$ + 4Al + 3C. In those experiments 700 W and 6.4 kW microwave powers were used, at the frequency of 2.45 GHz

Ma *et al.* study microwave heating of copper powder compacts in either a magnetic or an electric field in a single mode (TE102) cavity has been studied together with measurements of magnetic and electric properties of metal compacts. The dependence of the conductivity of the sample as a function of heating time is also measured giving insight into the mechanisms of pre-sintering stage with characteristic high heating rates. In the work by Luo *et al.* the heating rate of nickel– iron alloy powders is related to the theoretically derived formula of power absorbed by the compact. Rybakov *et al.* describe the absorption mechanism of microwaves in metallic powders with a thin oxide layer using the effective-medium approximation. Mingos and Baghurst synthesized several borides utilizing a modified home microwave and elemental powders of Fe, Cr, Zr, and B. Vaidhyanathan and Rao reported the synthesis of several disilicides in a home microwave oven using amorphous C as a susceptor. They showed that metallic powders could be heated by microwaves. However, combustion issues were not addressed. Gedevanishvili *et al.* published results on combustion synthesis of single phase CoAl from a stoichiometric composition of reactants. Jokisaari *et al.* [134] have successfully applied the MACS process in the synthesis of Mo_5Si_3.

---

130 J.R. Jokisaari, S. Bhaduri, S.B. Bhaduri Microwave activated combustion synthesis of bulk cobalt silicides, Journal of Alloys and Compounds 394 (2005) 160–167

131 T Galek *et al.*, Extraction of effective permittivity and permeability of metallic powders in the microwave range, Modelling Simul. Mater. Sci. Eng. 18 (2010) 025015-1/025015-13

132 R. Rosa, Microwaves as Ignition Source in the Combustion Synthesis of High Performances Materials, Doctor of Philosophy “High Mechanics and Automotive Design and Technology” at the University of Modena and Reggio Emilia (2010)

133 J.R. Jokisaari, S. Bhaduri, S.B. Bhaduri Microwave activated combustion synthesis of bulk cobalt silicides, Journal of Alloys and Compounds 394 (2005) 160–167

134 J.R. Jokisaari, S. Bhaduri, S.B. Bhaduri Microwave activated combustion synthesis of bulk cobalt silicides, Journal of Alloys and Compounds 394 (2005) 160–167

However, in many cases reactions are not exothermic enough to be self-sustaining. In these systems the propagation of reaction fronts is erratic and non-uniform. This leads to non-uniform microstructures and properties. Many reactions belong in this category, including cobalt silicides.

MACS process is used to synthesize $CoSi_2$ and CoSi. While CoSi behaved much the same in synthesis by MACS, conventional CS, and TACS methods, combustion synthesis of $CoSi_2$ proceeded differently. In terms of activation, these results compare well with predictions based on the thermodynamic calculations and literature. Conventional CS occurred in low-energy spin-mode propagation. The result was a banded microstructure and incomplete conversion into product. In TACS, the reaction product was an approximate 50:50 mixture of CoSi and CoSi2, and failed to consolidate. The reaction most likely occurred in thermal explosion mode. This is suggested by the poor consolidation of the product. With MACS, the reaction propagated in a planar manner producing a uniformly porous product of single-phase $CoSi_2$.[135]

MACS [136] is exploit to activate a CS reaction in metallic reactants to synthesize an intermetallic compound (e.g. Mo_5Si_3). It was shown that the MACS process successfully activated and allowed for stable propagation of combustion fronts in elemental mixtures of Mo and Si. These metallic constituents couple microwaves and with some pre-heating, a propagating combustion reaction ensues. The present results compare well with previous the Si being present as spherical droplets and the Mo appearing as bright regions within the Mo_5Si_3 grains. MACS samples show a nearly pure-phase product with only a small amount of Mo as an impurity, but with no $MoSi_2$ present. MACS sample shows a more uniform microstructure that its TACS counterpart. Unreacted particles are found throughout the microstructure; the presence of both elemental Si and Mo indicates that the reaction is incomplete, after 2 h at 1200 °C microwaves add sufficient energy to allow the reaction to be self-propagating. Conventional CS and TACS were also attempted, and the results compared with the MACS process. Under CS, stable combustion could not be maintained. The combustion front and correspondingly the product was non-uniform and contained large quantities of $MoSi_2$, Mo, and Si. The TACS process allowed combustion to occur, but the product was not of the same quality as that achieved through the MACS process. Specifically significant amounts of unreacted

[135] Ibidem

[136] J.R. Jokisaari *et al*., Processing of single phase Mo5Si3 by microwave activated combustion synthesis, Materials Science and Engineering A, 323 (2002) 478–483

constituents (e.g. Mo, Si) as well as secondary phases such as $MoSi_2$ were found interspersed throughout the microstructure along with the primary Mo_5Si_3 phase.[137]

The main reason why the microwave process yields better mechanical properties is two-fold, especially in the case of powdered metals: it produces finer grain size, and the shape of the porosity (if any) is different from that generated during conventional heating. In microwave-processed powdered-metal samples we observed round-edged porosities, producing higher ductility and toughness.

Rosa *et al.* [138] reported a scheme, Figure 2.1–16, of MWs absorption selectivity by reactive and micrometric metal powders mixture if bulk metallic substrates reflect or absorb MWs.

In the first case substrates temperature is almost unaltered, leading to advantage in terms of time and energy saving as well as minimization of heat-affected zones. If substrate absorbs MWs it involves in converting electromagnetic field energy into heat. Moreover sometimes the product formed can absorb MWs continuing to heat the system after CS reaction occurred. This is expected to enhance chemical bonding and inter-diffusion. However, the highest temperature manifested during the whole process is coincident with the combustion temperature reached in the joining material, thus the heat-affected regions of the substrates are usually very thin. [139]

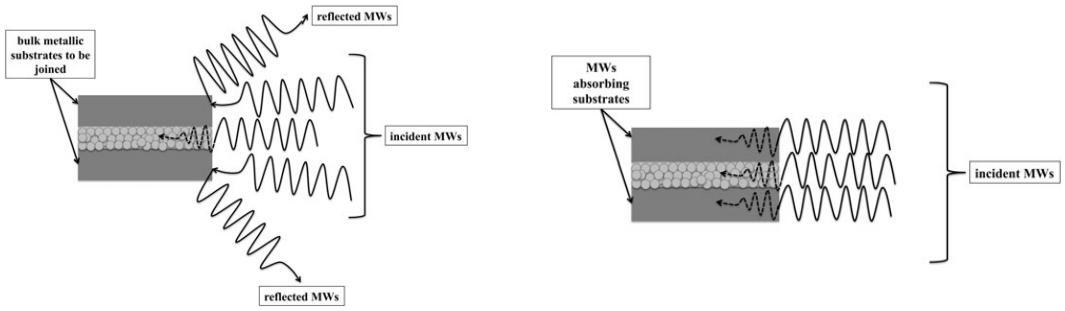

(a) (b)

Figure 2.1–16: (a) Substrate reflects MWs, (b) Substrate absorbs MWs

[137] J.R. Jokisaari *et al.*, Processing of single phase Mo5Si3 by microwave activated combustion synthesis, Materials Science and Engineering A, 323 (2002) 478–483

[138] R. Rosa *et al.*, Microwave Ignited Combustion Synthesis as a Joining Technique for Dissimilar Materials, Journal of Materials Engineering and Performance, 21 (2012) 725-732

[139] R. Rosa, Microwaves as Ignition Source in the Combustion Synthesis of High Performances Materials, Doctor of Philosophy "High Mechanics and Automotive Design and Technology" at the University of Modena and Reggio Emilia (2010)

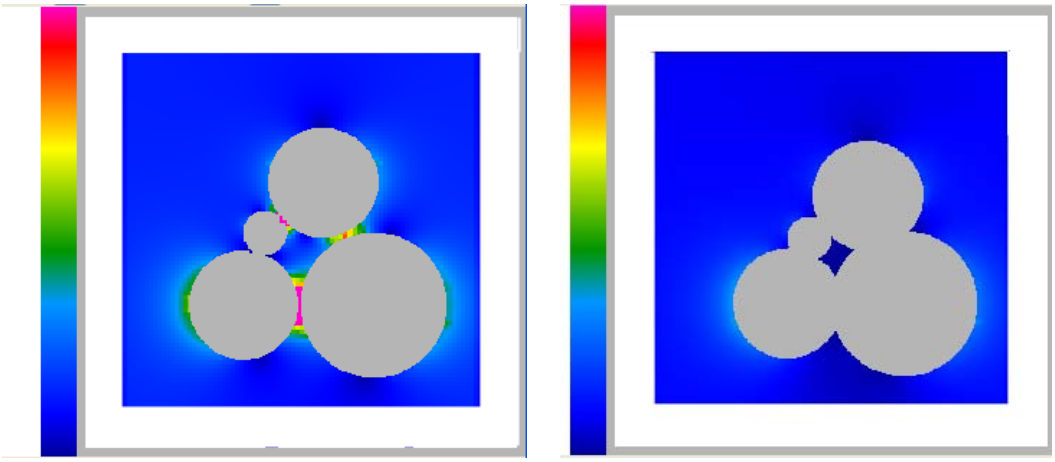

(a) (b)

Figure 2.1–17: Electric field envelope in the mid-section of the 4-spheres aggregate: a) before particles necking; b) after particles necking. Scale: minimum 0 V/m; maximum= $3 \cdot 10^6$ V/m.

Veronesi *et al.* [140] studied neck formation during MWs sintering of metal powder coupling experimental results to numerical simulation. A 3D system portion is studied thanks to software Concerto 4.0 (Vector fields, U.K.). Two different scales (macro – micro) are used to simulate microwave heating. Macro-scale calculates Specific Absorption Rate (SAR, W/kg) value of sample, which is represented by an equivalent load, whereas micro-scale is able to identify variation of electric field distribution. Electromagnetic field distribution is simulated by four spherical particles characterized by electric and magnetic properties of brass and steel (diameter 20 μm, P-CuZn20) or steel (diameter 15 and 6 μm, AISI 304). Simulation is conducted using two different condition to represent two different steps: electrical properties at room temperature to simulate sintering beginning and electrical properties at 600 °C to simulate step after neck formation; as assumptions: particles are external at powder compound, they are prone to 400 W, as power, and at 2.45 GHz, as frequency. Before neck formation a high electric field concentration is shown among particles (Figure 2.1–17 a). Intensity field value could exceed the air dielectric strength ($3 \cdot 10^6$ V/m), leading to arch formation or air ionization nearness neck particles. Both mechanisms could cause a local overheating, which lead to liquid phase formation among particles or other transport mechanisms by evaporation condensation. After neck formation (Figure 2.1–17 b) simulation results show that maximum electric field not only is not present among particles but also it does not reached the highest previous value. The configuration reduces possibility to form arches,

[140] C. Leonelli, G. Poli, P. Veronesi, Simulazione numerica ed evidenza sperimentale della accelerata formazione di colli durante le fasi iniziali della sinterizzazione assistita da microonde di polveri metalliche, Metallurgia Italiana, 4 (2007) 27-34

so metal powder compound is heated thanks to both direct microwaves heating and heating coming from nearby regions.

A similar analysis is done in case of millimetric powder size. Indeed increase powder size could lead to reduce ratio between treated material volume and microwaves directly heated volume which corresponds to spherical shell characterized by skin depth, at microwaves frequency, as thickness value. The supporting materials play an important role as well: for instance, literature results show the difference in processing powder metals in two different crucibles: SiC and mullite. Changing crucible materials change electric field distribution, as shown in Figure 13. In case of SiC crucibles the maximum intensity is between particles but the value is like of value in external crucible zone, about 50 V/m. In case of mullite crucible maximum electric field value is still among particles, about 700 V/m, that is two order of magnitude higher than external electric field value. Moreover electric field value of mullite crucibles is about two order of magnitude higher than SiC crucible to support that SiC softens microwaves. So results show two different way to sinter powder. The mullite crucibles lead to arch formation so metal particles absorb directly microwave and consequently neck formation is due to electromagnetic field between particles. The SiC crucible leads to an indirect absorption by metal particles: microwaves are absorbed by crucible, which heats up and it transfer part of such heat to the neighbouring particles.

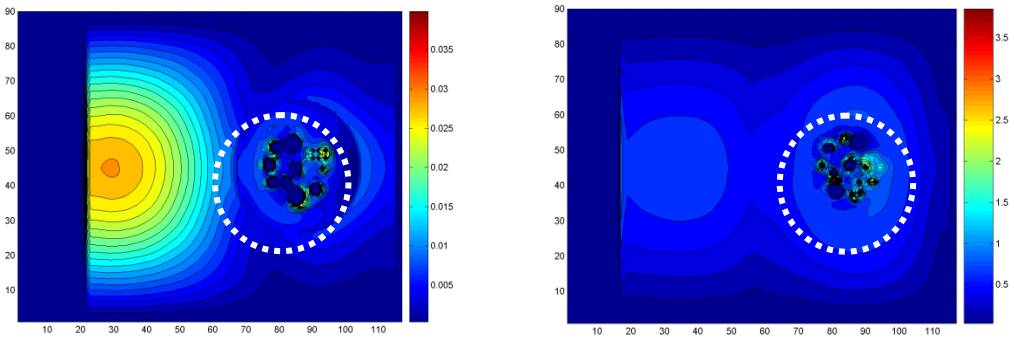

(a) (b)

Figure 2.1–18: Calculated electric field intensity (colour scale: 1= 2000V/m) in case of: a) SiC crucible; b) mullite crucible

Figure 2.1–19 (a) and (b) show a brass and a copper sample. They are sintered into mullite (direct absorption) and SiC (indirect absorption) respectively.

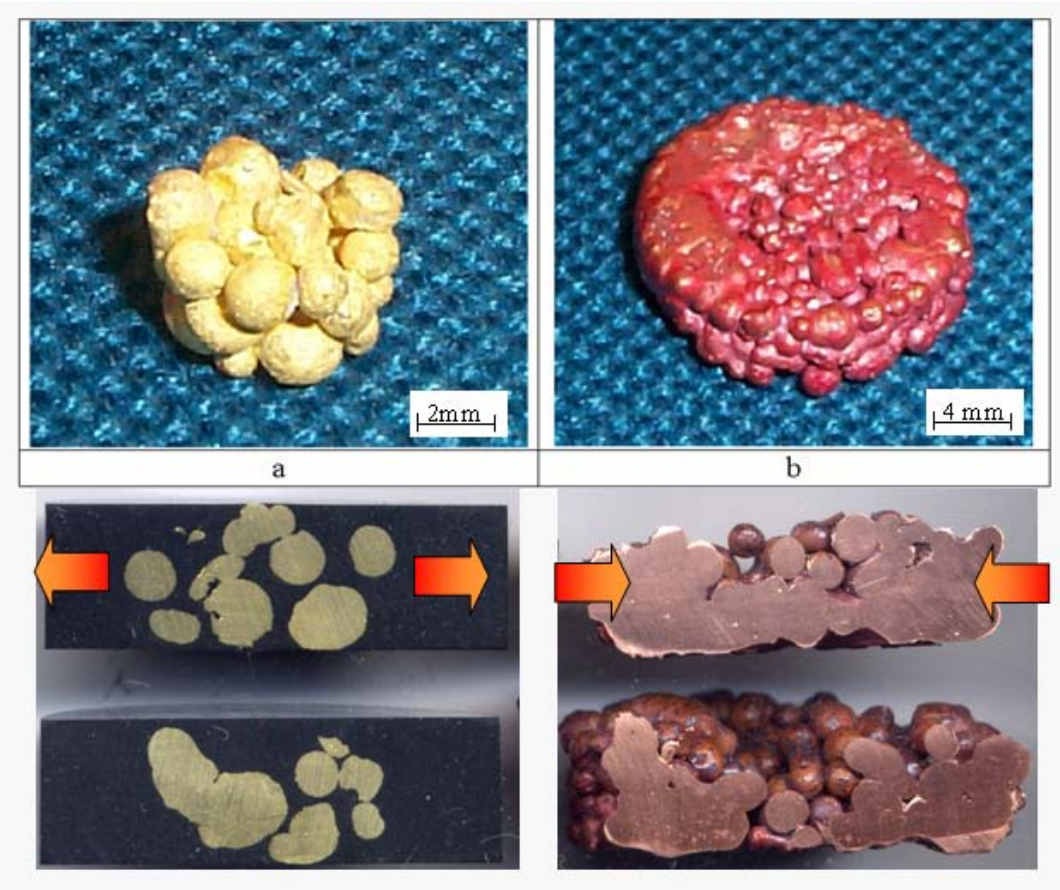

Figure 2.1–19: Microwave sintered samples of: (a) brass spheres in mullite crucible, (b) copper spheres in SiC crucible. In the sections, the arrows indicate the temperature spatial distribution which can be inferred by the microstructure: (a) higher temperature in the inner regions; (b) higher temperature in the outer regions.

Sample sintered in mullite crucible confirms that the microwaves absorption is direct because all neck are formed inside sample and spheres get in touch with crucible are not melted. Otherwise sample in SiC crucible shows melting of external spheres and neck formation is less clear than mullite crucible, because they are formed only by means of heat conduction.

From microwaves simulation point of view, Veronesi *et al.* used Concerto 4.0 (Vector Fields, U.K.) software to numerically simulate the heating behavior of a metallic powder compact in a microwave single mode applicator, based on the WR340 waveguide geometry. Thanks to simulation the most suitable refractory support is chosen. As a matter of fact, the refractory deeply influences the heating behaviour and the energy efficiency of the whole process, since it can absorb or reflect microwaves, as well as modify the electromagnetic field distribution around the sample.[141] The presence of a

[141] G. Poli, R. Sola, P. Veronesi, Microwave-assisted combustion synthesis of NiAl intermetallics in a single mode applicator: Modeling and optimisation, Mater. Sci. Eng. A 441 (2006) 149-156

different support material (base disc) will affect the heating behaviour of a load positioned on substrate.[142]

In this study microwave energy will be exploited to ignite the combustion synthesis to obtain different joints between metal and silicon carbide materials. In details this work is focussed on modeling approach to combustion synthesis, to optimize conditions leading to homogenous joints, with minimum extension of heat affected zones.

[142] C. Leonelli, G. Poli, P. Veronesi, Optimisation of the microwave assisted SHS of intermetallics in single mode applicators

2.2. Methods and Results

2.2.1 Hybrid Structures: an Overview

Joining between dissimilar material is mostly exploited both as a repairing technique and to obtain hybrid structures. Such hybrid structures combine dissimilar metals and metallic alloys in order to reach higher performances than the ones which could be attained from individual metallic components.

Among metallic materials, in this study will be exploited nickel based super alloy and titanium.

Heat resistant nickel-based superalloys are high temperature materials used to manufacture hot sections components of aero and land-based gas turbine engines due to their reliable high temperature mechanical properties, hot corrosion resistance and oxidation resistance at elevated temperatures[143]. These excellent hot corrosion behavior is due to simultaneous presence of chromium, aluminum, and molybdenum in the alloys composition[144], so they are broadly applied in reducing and oxidizing environment. Chromium content provides resistance to many corrosive media and high temperature environments, oxidation resistance is further enhanced by aluminum content. Among these Inconel 601 is a face centered cubic solid solution nickel chromium alloy for applications that require resistance to heat and corrosion. It shows excellent resistance to high temperature oxidation, a good resistance to carburizing, nitriding in dissociated ammonia and aqueous corrosion but it should not be used in atmospheres containing sulphur, especially reducing sulphur. Inconel 601 has good strength, ductility and toughness, and can be used at cryogenic temperatures. It is suitable for thermal and chemical process, pollution control, aerospace and power generation. In industrial furnaces, the alloy is used for radiant tubes, muffles, retorts, flame shields, strand-annealing tubes, woven-wire conveyor belts, chain curtains, burner nozzles, and electrical resistance heating elements. Chemical-processing applications include process heaters, condenser tubes in sour-water strippers and insulating cans in ammonia reformers. The alloy is also used for combustor components and catalyst grid supports in equipment for nitric acid production. In petrochemical processing, the alloy is used for catalyst regenerators and air preheaters in the manufacture of high-density polyethylene. In pollution-control applications, it is used for thermal reactors in exhaust systems of gasoline engines and for combustion chambers in solid waste incinerators. In the power-

[143] H.C. Chen, A.J. Pinkerton, L. Li Int J Adv Manuf Technol, 52 (9-12) (2010) 977-987

[144] H. Shah Hosseini ,M. Shamanian, M., A. Kermanpur, Characterization of Microstructures and Mechanical Properties of Inconel 617/310 Stainless Steel Dissimilar Welds, Mater. Character., 62 (2011) 425–431.

generation field, it is used for superheater tube supports, grid barriers, and ash handling systems. The alloy is also used for jet-engine igniters and for combustion-can liners, diffuser assembles, and containment rings in gas turbines for aircraft, industrial, and vehicular applications. [145] [146] [147]

Inconel 718 is an age-hardenable material, which has been used in a wide range of applications such as space shuttle main engine, power plants gas turbines, aircraft engines and nuclear plants because of its good mechanical properties at high temperatures. Inconel 718 exhibits a good weldability, thanks to its resistance to strain-aged cracking during post-weld heat treatment, but it shows Boron/Niobium segregation. Niobium is the key alloy element of Inconel 718 and, when the grain boundaries are rich in it, their melting temperature decreases. Interaction between grain boundary and stress during cooling cause microfessures; also the grain size has a great influence on microfissuring; fine-grain materials are less prone to microfissuring. The Nb-rich phases at the grain boundaries are related to one of the metallurgical reasons for microfissuring, which are different if the alloy is in a wrought or cast state. [148,149]

To create several new structural materials titanium and its alloy are holding one of the leading roles in the 20th century. Titanium and its alloys are characterized by low density, high tensile strength and toughness (even at high temperatures), extraordinary corrosion resistance, ability to withstand extreme temperatures, [150] fracture resistant, non-magnetic properties and exceptional corrosion resistance.[151] [152] [153] [154] For example, titanium shows useful performances at temperatures up to about 600ºC with a density about 60% of engineering steels and almost half that of nickel alloys. If the operation temperature exceeds 130 °C, titanium alloys can be used as replacements for aluminium-based materials to achieve improvement in mechanical properties at elevated

---

145 Austral Wright Metals, 2002

146 Special Metals Corporation, Publication Number SMC-028, 2005

147 E.O. Ezugwu, Z.M. Wang, A.R. Machado, The machinability of nickel-based alloys: a review, Journal of Materials Processing Technology 86 (1999) 1–16

148 S. Gobbi *et al.*, High powder CO_2 and Nd-YAG laser welding of wrought Inconel 718, Journal of Materials Processing Technology 56 (1996) 333-345

149 J.K. Hong *et al*., Microstructures and mechanical properties of Inconel 718 welds by CO_2 laser welding journal of materials, Journal of Materials Processing Technology, 201 (2008) 515-520

150 Lütjering, G., Influence of Processing on Microstructure and Mechanical Properties of (α+β)Titanium Alloys, Mater. Sci. Eng. A, 243 (1998) 32–45.

151 P.J. Bridges, B. Magnus, Cost Effective Application of Titanium Alloys in Military Platforms, (2001) ISBN: 92-837-0026-0

152 E.O. Ezugwu , Z.M. Wang, Titanium alloys and their machinability-a review, Journal of Materials Processing Technology 68 (1997) 262-274

153 E. Akman *et al.*, Laser welding of Ti_6Al_4V titanium alloys, Journal of Materials Processing Technology, 209 (2009) 3705-3713

154 Y.C. Chen, , K. Nakata, Microstructural characterization and mechanical properties in friction stir welding of aluminum and titanium dissimilar alloys, Materials & Design, 30 (2009) 469-474

temperatures for applications such as the external shells of turbines, the power units for avionics and the landing gear structural components in airplane. Since titanium exhibits very low corrosion rates in human body fluids, it shows a relevant role in medical industry, where it could be exploited as prosthetic devices, such as artificial heart pumps, pacemakers, heart valve parts, and load bearing bone, for hip bone replacement.[155] Despite the increasing use and production of titanium and its alloys, high cost of raw materials, extraction process complexity and machining confine their use to military applications, aircraft, spacecraft, medical devices, automotive, petrochemical, nuclear, power generation industries and, connecting rods in expensive sports cars, as well as in some premium sports equipment and consumer electronics.

Although the welding procedures and equipment used for austenitic stainless steel and aluminum alloys can be applied in order to join commercially pure titanium and Ti-based alloys, their increased reactivity with atmospheric elements at high temperatures needs additional precautions.[156]

Joining titanium alloy with aluminum alloy could have a major application in the field of aerospace and automobile industry where high strength and low density are desirable. However, joining between titanium and aluminum exhibit inferior mechanical properties due to the formation of brittle intermetallic phases in weld. Other solid-state welding methods for joining these two materials such as pressure welding, diffusion bonding and friction welding processes have been reported. Selected mechanical testing results of joints showed that diffusion bonding is a suitable process for high strength applications.[157]

Another material applied in semiconductor industries, nuclear and high temperature power plants, parts of engines and aerospace vehicles is silicon carbide (SiC). It is a very important engineering ceramic due to excellent properties at high temperatures, such as high strength, high chemical stability and high wear and corrosion resistance. [158] Silicon carbide matrix composites show a greater resistance to high temperature and aggressive environments than other conventional engineering materials. Thermal shock resistance, radiation stability and low neutron-induced activation, together with its high thermal conductivity, low thermal expansion, high thermal shock resistance and high-temperature abrasion resistance, make this material suitable candidate for nuclear

---

155 E. Akman *et al.*, Laser welding of Ti_6Al_4V titanium alloys, Journal of Materials Processing Technology, 209 (2009) 3705-3713

156 E. Akman *et al.*, Laser welding of Ti6Al4V titanium alloys, Journal of Materials Processing Technology, 209 (2009) 3705-3713

157 Y.C. Chen, , K. Nakata, Microstructural characterization and mechanical properties in friction stir welding of aluminum and titanium dissimilar alloys, Materials & Design, 30 (2009) 469-474

158 S. Somiya, Y. Inomata, Silicon Carbide Ceramics - 1 Fundamental and Solid Reaction, Elsevier Applied Science, New York, 1991.

applications, like for fusion blanket structures and flow channel inserts and also in various advanced fission systems. [159,160] However, engineering design of silicon carbide based components for different applications usually requires complex shapes and/or large dimensions, which, due to the nature of SiC ceramics, are difficult to manufacture in one step and substantially increase the preparation costs. Hence, assembling by joining simpler or smaller SiC components to build-up complex-shaped or large-dimensions ones can be an effective method to overcome manufacturing difficulties.

Welding and brazing techniques offer particular advantages for joining in term of processing variety and structural efficiency, however different materials differ in their welding or brazing abilities. [161]

Traditional fusion weld does not adapt to join materials characterized by mismatched properties [162], but today the so called “dissimilar welding process” is increasingly attracting more attention in industry, since it can reduce the material costs and improve the design flexibility [163]. Some of the greatest challenges in the welding or brazing of materials occurs with intermetallics, both as monolithic and as reinforced composite forms [164]. The ability to join both classes of material to metals would be extremely beneficial for high performance hybrid structures.[165,166]

It is well known that combining powder metallurgy and combustion synthesis techniques, the manufacture could benefit from the fast kinetics involved, allowing to create non-equilibrium structures or leading to products less prone to homogenization, thus preserving the gradient structure imparted during the forming step.[167] Among the wide number of ignition techniques, microwave (MW) energy possess selective and volumetric characteristics ([168]) (according to the dielectric and magnetic properties of the

---

159 M. Ferraris *et al.*, Joining of SiC-based materials for nuclear energy applications, Journal of Nuclear Materials 417 (2011) 379-382.

160 L.L. Snead *et al.*, Silicon carbide composites as fusion power reactor structural materials, Journal of Nuclear Materials 417 (2011) 330-339

161 R.W. Messler *et al.*, Welding with Self Propagating High Temperature Synthesis, Welding J., 74 (1995) 37–44

162 R.W. Messler *et al.*, Welding with Self Propagating High Temperature Synthesis, Welding J., 74 (1995) 37–44

163 H.C. Chen, A.J. Pinkerton, L. Li Int J Adv Manuf Technol, 52 (9-12) (2010) 977-987

164 R.W. Messler *et al.*, Welding with SelfPropagating HighTemperature Synthesis, Welding J., 74 (1995) 37–44

165 R.W. Messler, Joining Advanced Materials, Adv. Mater. Process., 2 (1995) 47–49

166 C. Pascal, R.M. Marin-Avral, J.C. Tedenac, Joining of nickel monoaluminide to a superalloy substrate by high pressure self-propagating high-temperature synthesis, J. Alloys and Compounds 337 (2002) 221-225

167 R. Rosa, P. Veronesi, Functionally Graded Materials Obtained by Combustion Synthesis Techniques: A Review, Chap. 2, Functionally Graded Materials, Nathan J. Reynolds Ed., Nova Science Publishers Inc., New York, 2011, pp. 93–122, ISBN 978-1-61209-616-2

168 R. Rosa, Microwaves as Ignition Source in the Combustion Synthesis of High Performances Materials, Doctor of Philosophy “High Mechanics and Automotive Design and Technology” at the University of Modena and Reggio Emilia (2010)

material to be treated) which can be proficiently exploited in the ignition and eventually in the sustaining of combustion synthesis reactions for joining applications.

Microwave heating and sintering of various high dielectric loss materials such as oxides and carbides has been applied in different industrial fields. Compared with conventional furnaces, the use of electromagnetic energy provides a more rapid and efficient heating and sintering. Furthermore, rapid heating limits grain growth during sintering and thus helps to improve microstructure and mechanical proprieties of the sintered products[169].

MW heating is based on energy transfer from the electromagnetic field directly into the joining material and subsequent heat generation due to polarization, conductive and magnetic losses.

Among materials, porous metal powder compacts have both effective dielectric and effective magnetic losses corresponding to effective permittivity and effective permeability of the porous metal compacts. Together with the effective electrical conductivity, these three factors account for the heating of these porous metal compacts in microwave fields[170].

The investigations of CS were motivated by the need to understand the various aspects (mechanisms and kinetics) of combustion synthesis, which becomes important to be able to control process parameters and products. The available theories cannot properly describe the gasless combustion due to a lack of extensive understanding of the microscopic mechanisms involved. The mechanistic is difficult to study due to high rate of the combustion reaction, high temperature at which the reaction takes place and lack of direct experimental methods. Most existing ideas about the mechanism of the combustion synthesis are based on the results from indirect experimental observations.[171]

The aim of the present part of the work is to numerically simulate and experimentally study the microwave ignited combustion synthesis of intermetallic based materials as an innovative technique to join dissimilar materials.

---

169 G. Poli, R. Sola, P. Veronesi, Microwave-assisted combustion synthesis of NiAl intermetallics in a single mode applicator: Modeling and optimisation, Mater. Sci. Eng. A, 441 (2006) 149-156

170 J. Ma *et al*., Single Mode Microwave Heating of copper Powder Metal Compacts, Proceedings of the COMSOL User Conference 2006 Boston

171 Ping Zhu , J.C.M. Li, C.T. Liu, Reaction mechanism of combustion synthesis of NiAl Materials Science and Engineering A, 329-331 (2002) 57–68

2.2.2. The Multiphysic Models

2.2.2.1. Generic Model: Joints between NiAl and Metallic Substrates

At the research beginning, a simplified multi-physics model of Ni and Al metal powders reaction to form the NiAl intermetallic between metal substrates by means of microwave-assisted combustion synthesis has been realized and validated[172]. Numerical simulation, thus, is used to estimate the heating and cooling rates in each portion of the reactants and products volume, as well as of the surrounding substrates and supporting materials.

In this work, numerical simulation of the microwave assisted CS was performed using the commercial software Comsol Multiphisics. Validation of the modeling results has been performed in a single mode applicator operating at 2.45 GHz.

To make the problem tractable during modeling, and to partially account for the lack of reliable data on high temperature properties of the reacting species, the following assumptions were made:

- the permittivity of the reacting powders and the surface emissivity are temperature independent;
- no dimensional changes of the specimen, or its density, occurred during and after reaction;
- no reaction occurs between NiAl powders and metallic substrates.

These assumptions are generally not true. However, as a first approximation it can be considered true if the volume of the reaction layer between the reacting species and the metallic substrate is small, then the heat of reaction involved is negligible compared to the heat generated by the main reaction between the pressed powders.

The numerical simulation of the microwave assisted CS requires to couple an electro-thermal model (electroheat, considering microwave power generation and heat transfer) with a chemical model, the latter necessary to study the exothermic reaction between powders and account for a further heat generation term. In this way it is possible to obtain a simplified model to study compositional and temperature variations, as well as reaction kinetics during the CS.

This allows to couple thermal and radio-frequency aspects of the problem, to estimate the average power density in the load, which is used to compute the temperature distribution in the materials, because, in turn, it affects their electrical and dielectric properties.

---

[172] E. Colombini *et al.*, Microwave ignited combustion synthesis of intermetallic compounds, modelling and experimental results, Metallurgia Italiana, 4 (2011) 29-34

The electromagnetic part of the model (RF module) is based on a prismatic microwave applicator, based on the WR-340 waveguide. It reproduces the experimental setup used experimentally. The generally used model geometry and dimensions are sketched in Figure 2.2–1.

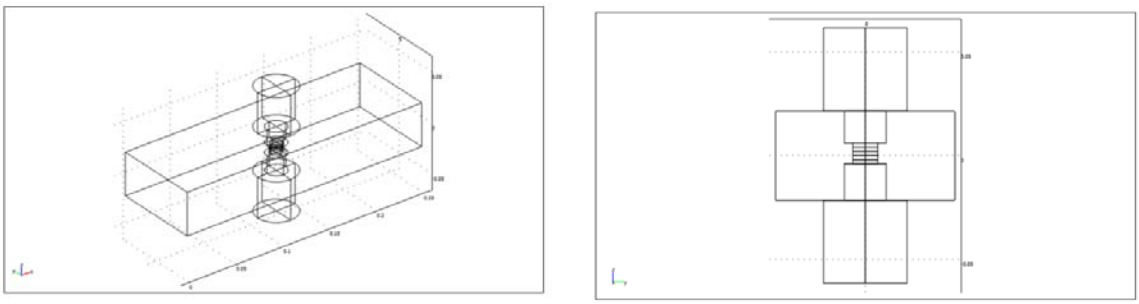

(a) (b)

Figure 2.2–1:(a) model based on WR340 waveguide (b) front view

The sample (pressed disc mixture of Ni+Al powders) is placed, in both cases, in the region characterized by maximum of electric field. This configuration allows attaining rapidly the ignition conditions in comparison with maximum magnetic field configuration, as demonstrated by the Rosa *et al.* in a previous work [173]. The work is based on CS ignition of Fe+Al, Co+Al and Ni+Al powder mixture in predominant magnetic field (H) without help of any MWs co-absorber but maintaining a good control and reproducibility of the process. In detail FeAl and CoAl intermetallic compound show the same behavior. Combustion synthesis was rapidly reached in both experimental configuration, in the maximum of electric (E) and magnetic (H) field, though ignition temperature was reached in a relative longer and more scattered time compared to ignition time necessary in H field maximum. Indeed in combustion of single phase NiAl intermetallic compound the ignition temperature for NiAl combustion synthesis was not reached in predominant magnetic field, despite of ferromagnetic nature of Ni powders. This is probably due to ignition temperature for NiAl combustion synthesis, which lies above 600 °C, that is higher than Ni Curie temperature (358 °C).

The subdomain equation used by the RF application modes is (Eq 1):

Eq 1
$$\nabla \times (\mu_r^{-1} \nabla \times \mathbf{E}) - \left(k_0^2 - j\frac{\sigma}{\omega \varepsilon_0}\right)\mathbf{E} = 0$$

[173] R. Rosa *et al.*, Microwave (MW)-assisted combustion synthesis of micrometric metallic powders for the preparation of intermetallic based materials, PM2010 World Congress and Exhibition, Florence, Italy 10-14 October 2010, Proceedings Vol. 2, pp. 217-223, ISBN 978 1 899072 11 8

Perfect electric conductor boundary condition was chosen for the external walls of the waveguide, (Eq 2), while as microwave input is chosen microwave inlet port, where a sinusoidal 2.45 GHz excitation in the TE10 mode is set (Eq 3).

Eq 2 $$\mathbf{n} \times \mathbf{E} = \mathbf{0}$$

Eq 3 $$\mathbf{S} = \frac{\int (\mathbf{E} \cdot \mathbf{E_1}) \cdot \mathbf{E_1}}{\int \mathbf{E_1} \cdot \mathbf{E_1}}$$

Heat developed by microwaves is used as input value to activate CS of Nickel and Aluminum powders. All combustion syntheses described in this work have been modeled using the pre-defined Comsol Reaction Engineering Laboratory module. Two different ways to form NiAl have been taken into account: one considers three intermediate reactions (Eq 4), the other one is based on one step reaction (Eq 5) The reaction engineering module requires kinetic parameters such as Arrhenius pre-exponential factors, A, and activation energy, E, as well as thermodynamic factors (e.g. entropy, enthalpy and specific heat) and physical data specific to the model geometry and synthesis conditions (concentration, density and molecular weight). Table 2.2-1 and Table 2.2-2 show used data and, when available, references used, both in case of intermediate reactions to lead to NiAl formation and in case of considering only one reaction.

The intermediate reactions considers the following steps [174]:

Eq 4
$$\begin{cases} \mathbf{Ni + 3Al \rightarrow NiAl_3} \\ \mathbf{NiAl_3 + Ni \rightarrow Ni_2Al_3} \\ \mathbf{Ni_2Al_3 + Ni \rightarrow 3NiAl} \end{cases}$$

The one step reaction to form intermetallic with the aim to simplify the model is reported in Eq 5:

Eq 5 $$\mathbf{Ni + Al \rightarrow NiAl}$$ [175]

The parameters used during simulation are reported Table 2.2-1 and Table 2.2-2.

[174] O.B. Kovalev, V.A. Neronov, Metallochemical Analysis of the Reaction in a Mixture of Nickel and Aluminum Powders, Combustion, Explosion, and Shock Waves, 40 (2004) 172–179

[175] S. Gennari *et al.*, SHS (Self-sustained high-temperature synthesis) of intermetallic compounds: effect of process parameters by computer simulation, Intermetallics 11 (2003) 1355-1359

Table 2.2-1: Kinetic and thermodynamic parameters

Reaction	A [176][177]	E [kJ·mol^{-1}] [178]	H [kJ·mol^{-1}] [179]	S [J·mol^{-1}·K^{-1}] [180]
1) Ni+3Al => $NiAl_3$	8.4	135	-151	-110.7
2) $NiAl_3$ + Ni=> Ni_2Al_3	4.06	119	-131.8	25.7
3) Ni_2Al_3 + Ni => 3NiAl	0.07	76	-164	-82.2
Ni+Al => NiAl	4.587	76	-118	-4.1

The pre exponential factor A is obtained from literature data. [181,182] It is based on the following assumptions:

- the effects of phase changes and heat losses (conductive, convective, and radiative) are neglected;
- atomic diffusion is represented with a single binary diffusion coefficient, D;
- physical properties such as thermal conductivity, density, and heat capacity are independent of composition;
- the reaction occurs in a fast, diffusion-limited regime;
- temperature variations across the layers y direction are ignored because thermal diffusivity is several orders of magnitude larger than atomic diffusivity and the bilayer period is small.

Under these assumptions, the governing equations describing combustion of the reactants are:

Eq 6
$$\frac{\partial C}{\partial t} = \nabla \cdot (D \nabla C)$$

Eq 7
$$\rho c \frac{\partial T}{\partial t} = k \frac{\partial^2 T}{\partial x^2} + \frac{\partial Q(C)}{\partial t}$$

where C(x,y,t) is the conserved Shvab-Zeldovich variable.

---

176 V.H. Garcia, P.M. Mors C. Scherer, Modeling of the self-propagating reactions of nickel and aluminum multilayered foils Acta mater. 48 (2000) 1201-1206

177 I.E. Gunduz *et al.*, Investigations on the self-propagating reactions of nickel and aluminum multilayered foils, Applied Physics Letters 93 (2008) 134101/1-134101/3

178 O. Kubaschewski, C.B. Alcock, P.J. Spencer., Materials Thermochemistry, 6th Edition, Oxford; New York: Pergamon Press, 1993, p.299

179 O. Kubaschewski, C.B. Alcock, P.J. Spencer., Materials Thermochemistry, 6th Edition, Oxford; New York: Pergamon Press, 1993, p.299

180 O. Kubaschewski, C.B. Alcock, P.J. Spencer., Materials Thermochemistry, 6th Edition, Oxford; New York: Pergamon Press, 1993, p.299

181 Jayaraman et al., Numerical predictions of oscillatory combustion in reactive multilayers, J. Appl. Phys., 86 (1999) 800-809

182 A.B. Mann *et al.*, Modeling and characterizing the propagation velocity of exothermic reactions in multilayer foils, J. Appl. Phys., 82 (1997) 1178-1188

The atomic diffusivity D is assumed to be composition-independent and to follow an Arrhenius dependence on temperature given by

Eq 8 $$\mathbf{D = D_0 \exp\left(-\frac{E}{RT}\right)}$$

where D_0 is the Arrhenius pre-exponent, and R is the gas constant.

The thermal diffusivity ($\alpha=\lambda/c\rho$) [$m^2 \cdot s^{-1}$] on the other hand, is assumed to be constant.

Accordingly, the ratio of the atomic diffusion coefficient and the thermal diffusivity α:

Eq 9 $$\mathbf{\frac{D}{\alpha} = A\exp\left(\frac{E}{RT}\right)}$$

In the models developed in this work equation Eq 8 is substituted by Eq 9, thus:

Eq 10 $$\mathbf{A = \frac{D_0}{\alpha} = \frac{D_0}{k}\rho c_p}$$

Concentration is calculated by stoichiometry, according to real geometric dimension obtained measuring a powder compact produced in laboratory according to experimental procedures.

Table 2.2-2: C_p and concentration values

Element	C_p [$J\cdot mol^{-1}\cdot K^{-1}$] [7] [11]	C_0 [$mol\cdot m^{-3}$]
Ni	$[11.17+(37.78\cdot10^{-3}\cdot T)-(3.18\cdot10^{5}\cdot T^{-2})\cdot(T<631)]+$ $[20.54+(10.08\cdot10^{-3}\cdot T)-(15.40\cdot10^{5}\cdot T^{-2})\cdot(T>631)]$	49347.85
Al	$[31.38-(16.4\cdot10^{-3}\cdot T)-(3.6\cdot10^{5}\cdot T^{-2})+(20.75\cdot10^{-6}\cdot T^{2})]$	49347.85
$NiAl_3$	53.49	0
Ni_2Al_3	75.95	0
NiAl	$(41.925+(13.6e\text{-}3\cdot T)-(0.033e5\cdot T^{-2})+(0.1e\text{-}6\cdot T^{2}))$	0

An average porosity, about 30%, is considered. This value is applied to specific heat (Eq 11), density (Eq 12) and thermal conductivity (Eq 13), according to equations[183]:

Eq 11 $$\mathbf{C_{real} = C_{theoretic}\cdot(1-\%porosity)}$$

Eq 12 $$\mathbf{\rho_{real} = \rho_{theoretic}\cdot(1-\%porosity)}$$

Eq 13 $$\mathbf{k_{real} = k_{theoretic}\cdot[(1-\%porosity)/(1+(\%porosity/2))]}$$

[183] O. Biceroglu, Thermal conductivity of sintered metal powders at room temperature Letters in Heat and Mass Transfer, 3 (1976) 183-191

Reaction Engineering Laboratory was run distinctly as regards the other modules. Then RF module runs in stationary mode and results obtained from the previous one have been used as input in heat transfer and diffusion modules. This implies that the thermal and RF modules are decoupled (i.e. no permittivity variation with temperature), which is a strong simplification.

From the Chemical module two values have been exported: reaction rate and entalphy of reaction. The former is used into diffusion module to describe diffusion reaction to form products from reagents, the latter represents heat developed during CS, employed into heat transfer module.

Results obtained by solving separately the reaction engineering laboratory module (chemical model) simulation are shown in Figure 2.2–2. Figure 2.2–2 (a) and (b) show the temperature and concentration variation in case of three reaction steps, Figure 2.2–2 (c) and (d) in case of one step reaction. In both cases (Figure 2.2–2 (a) and (c)) it is possible to notice the rapid temperature increase due to CS ignition, occurring when the microwave power generated in the load increases the temperature up to the ignition temperature. It is not evident any cooling after reaction occurred, because in the chemical part of the model no heat loss is implemented. Figure 2.2–2 (b) and (d) show the time-dependent concentration of the reacting species and products, demonstrating that, according to experimental and literature[184] results, NiAl is the only product at the end of the reactions 1-3.

[184] O.B. Kovalev, V.A. Neronov, Metallochemical Analysis of the Reaction in a Mixture of Nickel and Aluminum Powders, Combustion, Explosion, and Shock Waves, 40 (2004) 172–179

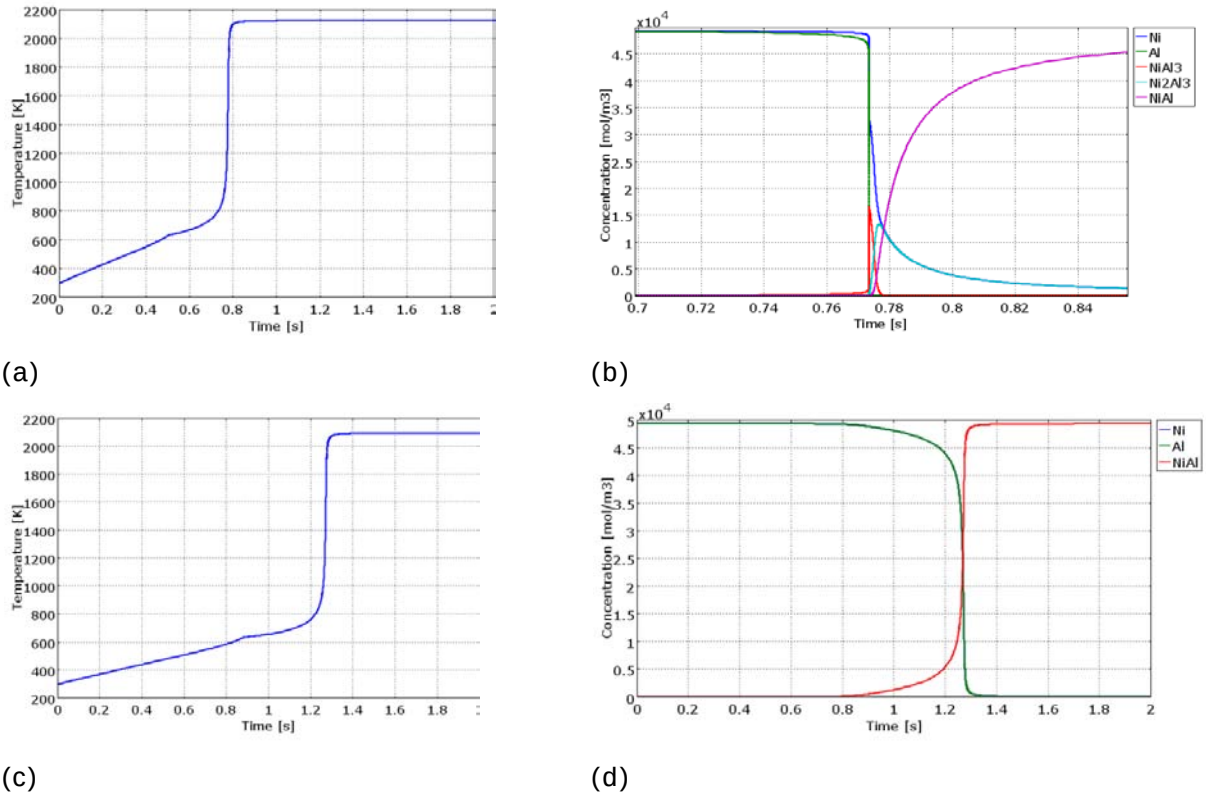

Figure 2.2–2: Reaction Engineering Lab results: (a) and (d) Temperature [K] vs time [s] plot, (c) and (d) species concentration variation during CS in case of 3 reactions and one reaction (respectively)

The subdomain equations used by the heat transfer and diffusion application modes are respectively (Eq 14) and (Eq 15). As boundary condition are used respectively equations (Eq 16) and (Eq 17). The first (Eq 16) constitutes insulation symmetry in diffusion mode, the second (Eq 17) is boundary heat condition, that is room temperature on applicator walls.

Eq 14 $$\frac{\delta_{ts}\rho c_p \partial T}{\partial t} - \nabla(k\nabla T) = Q$$

Eq 15 $$\frac{\delta_{ts}\partial c}{\partial t} - \nabla(D\nabla c) = R$$

Eq 16 $$n \cdot (-D\nabla c) = 0$$

Eq 17 $$T = T_0$$

NiAl between Titanium Discs

To validate the theorethical method, a simple experimental study was performed. A NiAl intermetallic between metal substrate has been combustion-synthetized from Ni and Al metal powder.

Nickel (≈ 3 µm, 99,7% purity) and Aluminium (≈ 200 mesh, 99% purity) powders were provided by Aldrich Milan, Italy. The powders have been mixed in Al_2O_3 agate jar for 30 minutes under vacuum, with ratio 1:1 at%. Disc-shaped compacts have been prepared by inserting the powder mixtures into a 20 mm diameter mould and applying 140 MPa of uniaxial pressure. In this way, a series of compacts with diameter of 20 mm and weight of 3-5 g are prepared for further microwave processing, between two grade 2 titanium discs. The objective is to achieve a reactive synthesis with the titanium support, as described in a previous work.[185]

Heating was carried out in a single mode applicator (Figure 2.2–3) , which is constituted by a magnetron generator (with an output power level ranging from 300 to 3000 W) connected to a three-ports circulator and to a three-stubs tuner, both based on the WR-340 rectangular waveguide geometry (86 x 43 mm section). During the synthesis a pressure of 0.8 MPa is applied to reduce product porosity. The pressure is obtained by application of two low-loss (i.e. not generating heat when exposed to microwaves) refractory cylinders during combustion synthesis, inserted trough two circular ports (circular waveguides under cut-off condition, so as to microwaves does not propagate to the surrounding environment) placed at upper and lower side of cavity. This configuration allows both to minimize perturbation of the electromagnetic field distribution and to apply the load on the upper side of powder compact [186]. Two different fixed microwave power (600 W and 1200 W) were directed towards the pressed sample, which is placed at cavity centre, where the electric field is predominant, as a result of TE10(n) mode in the cavity. Simulation results were validated by means of a Mikron M680 Infraducer connected to a MW-transparent sapphire fiber (temperature range ~ 873-1973 K), which was inserted into the single mode cavity from a side hole under cut-off conditions, and was placed into direct contact with the joining couple.

[185] R. Rosa *et al.*, Microwave assisted combustion synthesis of intermetallics based functionally graded materials: numerical simulation and experimental results, *Int. J. SHS* 18 (3), 2009, 163-172

[186] P. Veronesi *et al.*, Enhanced reactive NiAl coatings by microwave-assisted SHS, Compel: The International Journal for Computation and Mathematics in Electrical and Electronic Engineering, 24 (2008) 491-499

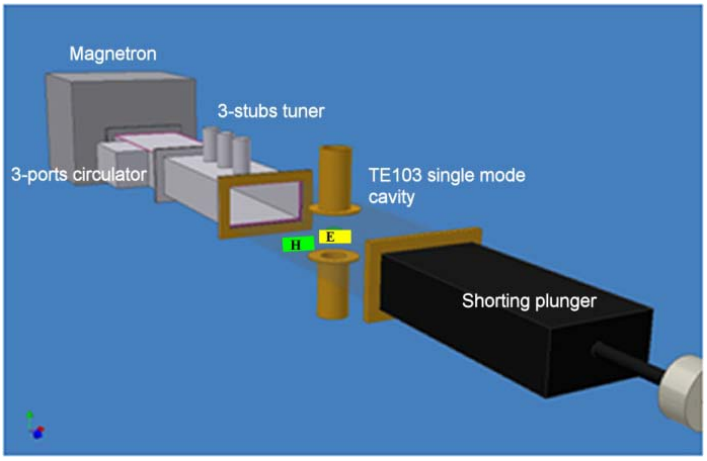

Figure 2.2–3: Microwave single mode applicator components. The yellow rectangle (E) represents the sample positioned in predominant E field while the green one (H) represents the sample positioned in predominant H field.

Synthesized sample have been cut in order to investigate microstructure and chemical composition by optical microscopy as well as by ESEM (Quanta-200 Fei, Oxford Instruments).

The optical microscope images shown in Figure 2.2–4 and Figure 2.2–5 show the cross sections of NiAl (left part of the micrographs) obtained by power application of 600 W and 1200 W, respectively, in the case of titanium substrate (right part of the micrograph).

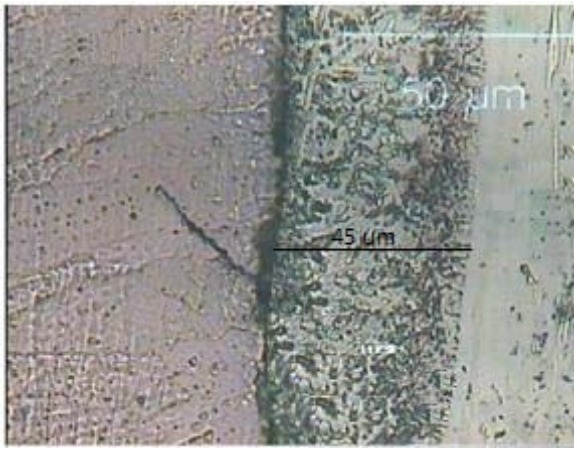

Figure 2.2–4: Sample treated at 600 W

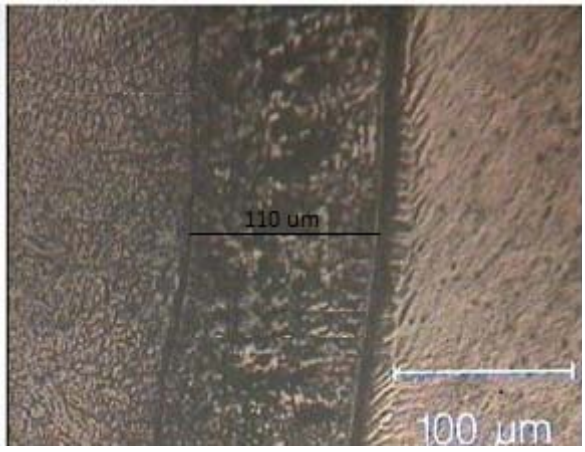

Figure 2.2–5: Sample treated at1200 W

In both cases, chemical etching with glyceregia for 10 s evidenced the presence of a dendritic intermediate layer (dark regions of Figure 2.2–4 and Figure 2.2–5) with presence also of eutectic microstructures, as shown in a previous work [187,188]. The ESEM-

[187] P. Veronesi *et al.*, Enhanced reactive NiAl coatings by microwave-assisted SHS, Compel: The International Journal for Computation and Mathematics in Electrical and Electronic Engineering, 24 (2008) 491-499

EDS analyses showed the presence of Ni, Al and Ti in this intermediate layer, suggesting that during CS, reactions between the substrate and the reactants occurred. The zones presenting only NiAl formation (left part of Figure 2.2–4 and Figure 2.2–5) exhibit a typical solidification structure, with equiaxial grains growth, confirming the achievement of temperature, during synthesis, in excess of the melting temperature of NiAl. Thus, at the very end of CS, the newly formed phases are in the liquid state and this can favour the rapid reaction between the molten NiAl and the Ti substrates, leading to the generation of the intermediate layer, where formation of eutectics in the Ni-Al-Ti system occurs. In particular, in the Ni-Al-Ti system, the liquid phase can exist down to 905°C. [189]

The intermediate layer thickness shown in Figure 2.2–4 and Figure 2.2–5 results higher in case of 1200 W microwave power applied, thus suggesting a direct interaction of such layer with the microwave field, with possible heat generation occurring selectively in this layer (the titanium substrate can be considered microwave reflective). Hence, the measured thickness difference of the intermediate layer can be ascribed to a different reaction time between the newly formed intermetallics and the Ti substrate. The reaction time is affected by existence time of the liquid phase, which depends on the microwave power generation in this layer.

To highlight the importance of numerical simulation, the experiment has been performed varying input power in order to understand the dependence of the intermediate layer thickness on the microwave applied power. Results, shown in Table 2.2-3 and in Figure 2.2–6 (a) and (b), demonstrate that the increase of power, as expected, leads to a proportional increase of resistive heating (time averaged) and of the square root of electric field maximum value.

Table 2.2-3: Power density (time average) in the load and electric field maximum value at different power levels in the coaxial applicator

Input Power [W]	Power Density [$W \cdot m^{-3}$]	Electric Field [$V \cdot m^{-1}$]
600	2.307e7	7.812e4
1000	3.846e7	9.271e4
1200	4.614e7	1.016e5

[188] G.P. Cammarota *et al.*, Ni–Al–Ti coatings obtained by microwave assisted SHS: Effect of annealing on microstructural and mechanical properties, Surface & Coating Technology 203 (2009) 1429-1437

[189] R.W. Messler, Joining Advanced Materials, Adv. Mater. Process., 2 (1995) 47–49

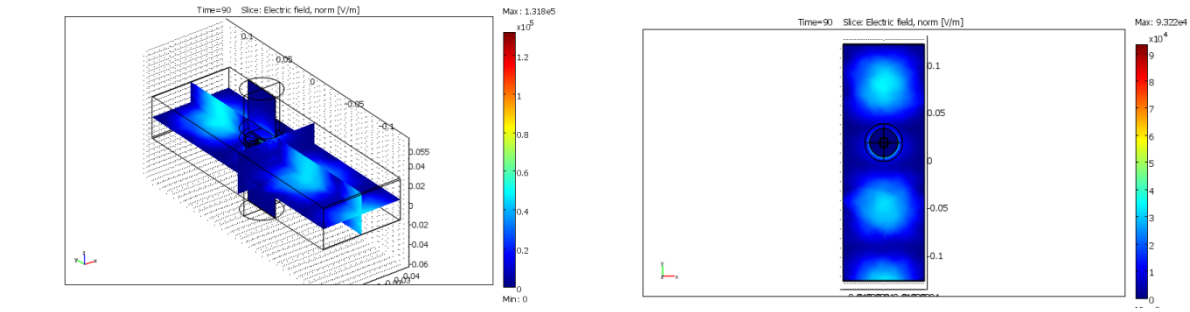

Figure 2.2–6: (a) Electric field distribution [Vm^{-1}], at 600 W, in the WR340 based applicator (b) Particular to show the sample position on maximum of Electric field distribution [$V \cdot m^{-1}$]

Figure 2.2–6 (b) shows that the zone with higher electric field intensity effectively corresponds to the position of the sample. In these conditions, the extremely high electric field values can lead to arcing, with uncontrollable and localised ignition of the CS. In order to avoid such occurrence, maximum microwave emitted power before CS must be carefully controlled.

Figure 2.2–7 (a) and (b) show calculated heating and cooling curves in the centre of the sample (black line) and in the centre of titanium support (blue line) at 600 W and 1200 W, respectively. Results clearly demonstrated the microwave selectivity, which is one of the peculiarity of this type of heat source. Indeed Titanium substrate reaches lower temperature than the neighbouring intermetallic materials, increasing the cooling rate after combustion synthesis completion. In the simulation, microwaves are stopped 5 second after CS occurred.

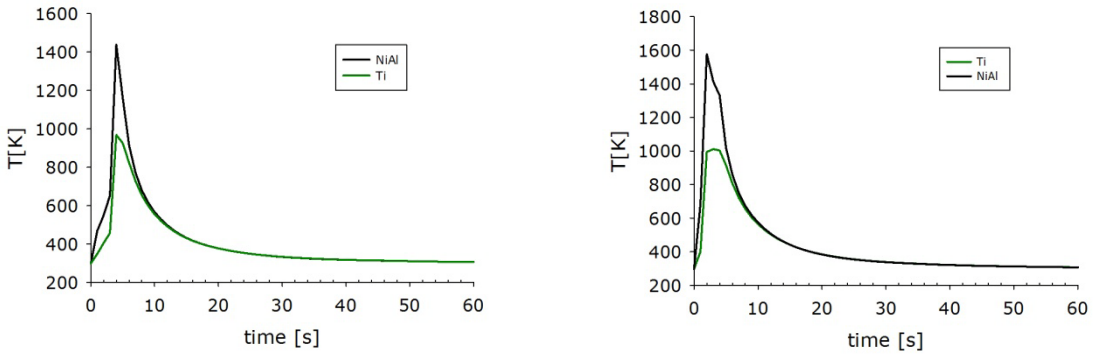

Figure 2.2–7: CS curve of the centre of NiAl (black line) and of the center of Ti support (green line) (a) at 600 W, and (b) at 1200 W

Increasing microwave power decreases the ignition time of CS, which occurs approximately after 85 seconds at 600 W and after 40 seconds at 1200 W. However the

maximum temperature reached is affected by the different ignition power, indicating a predominant role of combustion synthesis in this stage. Also, cooling rate depends on microwave forward power, with sample exposed to 600 W reaching 905 °C (the minimum eutectic temperature in the ternary Ti-Ni-Al phase diagram) after only 1 second after CS completion, while in case of 1200 W power, this temperature is reached 20 seconds after CS completion, as shown in Figure 2.2–8. This is because a short ignition time leads surrounding metals to be cooler, so heat losses are higher, and a quick cooling occurs. Thus power decreasing leads to increase time at which system is subjected to microwave energy, increasing surrounding metal temperature.

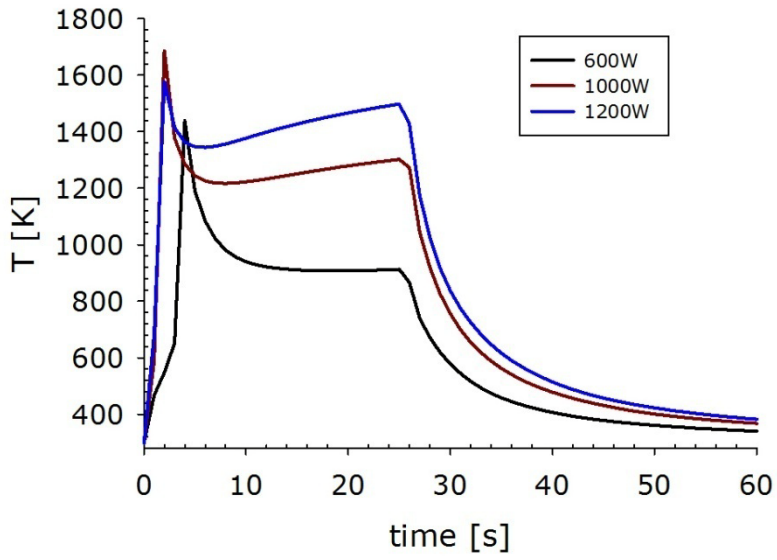

Figure 2.2–8: Different CS curve in case of increasing power value (black line at 600 W, red line at 1000 W and blue line at 1200 W). In this case, microwave power is turned off at 5 second after CS occurred

Figure 2.2–9 shows different CS plot in case of same power applied but different time at which MWs are switched off, i.e the microwave generator is kept on even after CS completion. Increasing exposure MW time leads to promote interaction between intermetallic and substrate, thanks to the extended existing time of liquid phase, due to more permanence at temperatures in excess of 905°C.

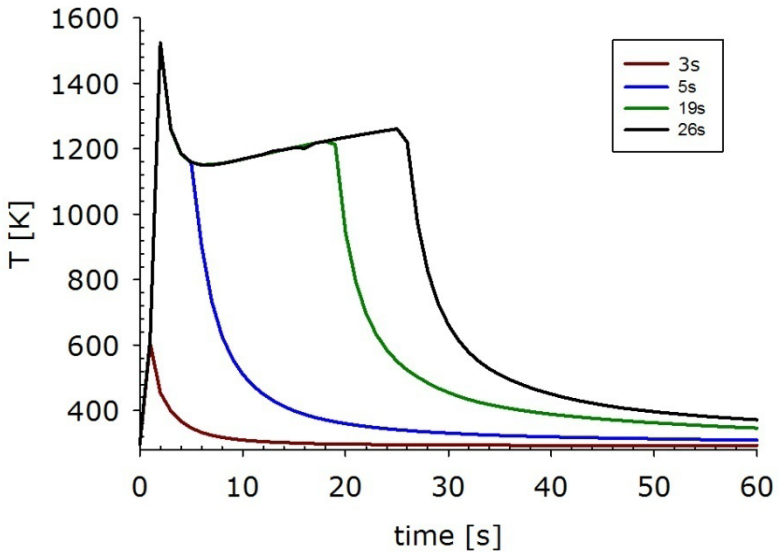

Figure 2.2–9: Same microwave power applied, different time exposition.

The latter aspect is a distinctive feature of microwave heating, where volumetric heating generation on sample allows to slow down the cooling. In the case of reactive support (titanium) a slow cooling leads to longer time of existence of liquid phase, which affects the interface thickness (Ni-Al-Ti).

Thus, by varying the microwave power applied during CS, the ternary layer thickness can be controlled directly during intermetallic synthesis.

Ti-Steel Joining

A further model was developed to study NiAl intermetallic as joining between Ti and steel substrates.

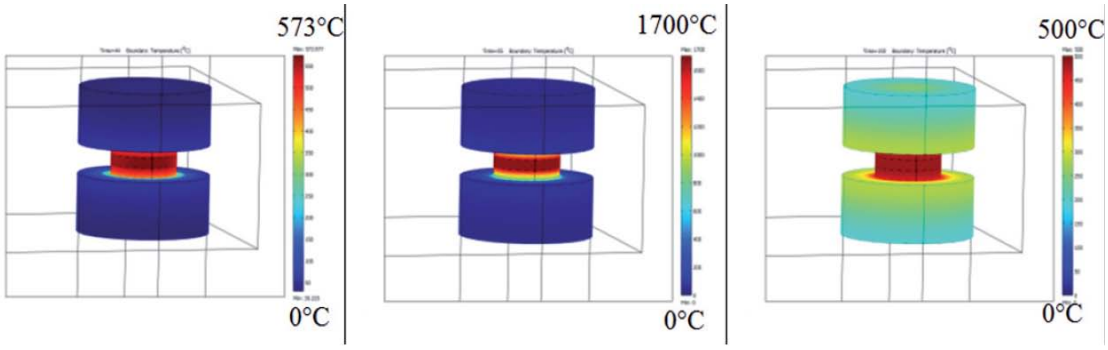

Figure 2.2–10: Boundary temperature plot distribution of sample 3-3-3 exposed for 8 s to 1800 W of microwave power after: (a) 44 s (heating), (b) 55 s (CS ignition and propagation); (c) 150 s (cooling, microwave off)

Simulation results[190] (Figure 2.2–10) show the boundary plots referred to three different simulation times, before, during and after CS. The plot of Figure 2.2–10 b shows that during CS the reactants reach temperature higher than the melting temperature of NiAl (1638°C). The result is in agreement with the literature results[191] and the presence of the liquid phase implies that the resulting solidification microstructure (dendritic or equiaxed) will depend on the experienced cooling rate and on the direction of the heat flux. It is important to notice also that during microwave heating, the two metallic substrates remain substantially colder than the pressed powders, and equilibrium is reached only during cooling. A series of virtual temperature sensors have been inserted in the model in the pressed Ni+Al powders region, in order to acquire heating and cooling curves as a function of the model parameters (microwave forward power, time stop of ignition, substrates and pressed powders thickness). Figure 2.2–11 shows the temperature vs. time curves in case of microwave (MW) or conventional heating (CONV), with a forward power of 600 and 1800 W (P6, P18), on a specimen made “s” mm thick of Ti or steel substrates and “p” mm thick pressed powders (_s-ps_), exposed to microwaves for _tx seconds. In case of conventional heating, furnace set temperature is indicated in K (T). Results show that microwave energy application allows to form a new intermetallic, by reason of the extension of residence time at high temperature. This phenomenon is expected to further promote reactions between the intermetallic and the surrounding substrate, in case that a liquid phase exists at the intermetallic-substrate interface. This has been shown to happen in Ni-Al binary systems, where the reaction temperature is slightly higher than the NiAl equilibrium melting point[192]. However, if the newly formed NiAl cannot remain in the liquid state for a time long enough to react with the Ti substrate, no ternary eutectics with Ti are formed and the resulting microstructure will belong to the binary Ni-Al system, this impression the steel side on the couple. Moreover, in the Ni-Al-Ti system, a large number of eutectics exists, some of them being in the liquid state at temperature as low as 950°C.[193] Thus, the cooling rate will affect the final microstructure in case a significant reaction with the Ti.

---

190 P. Veronesi et al., Microwave assisted combustion synthesis of non-equilibrium intermetallic compounds, JMPEE, Journal of Microwave Power and Electromagnetic Energy 44 (2010) 45-56

191 S. Gennari, et al., Simulation Study of Wave Propagation Instabilities for the Combustion Synthesis of Transition Metals Aluminides, J. Phys. Chem. B 110 (2006) 7144-7152

192 K. Morsi, Review: reaction synthesis processing of Ni–Al intermetallic materials”, Materials Science and Engineering A 299 (2001) 1–15

193 B. Huneau *et al.*, The ternary system Al-Ni-Ti Part I: Isothermal section at 900°C; Experimental investigation and thermodynamic calculation”, Intermetallics, 7 (1999) 1337-1345

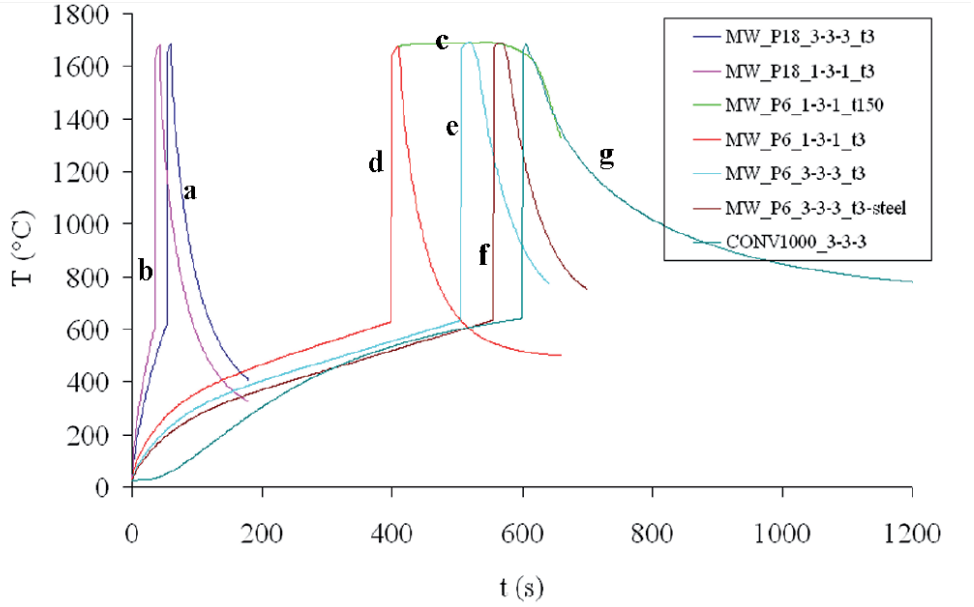

Figure 2.2–11: Temperature vs. time curves in case of CS of NiAl between two Ti discs: a) MW_P18_3-3-3_t3, b) MW_P18_1-3-1_t3, c) MW_P18_1-3-1_t150, d) MW_P6_1-3-1_t3, e) MW_P6_3-3-3_t3. Microwave assisted CS between two steel discs f) W_P6_3-3-3_t3. Conventional CS in furnace at 1000 K: g) CONV1000_3-3-3.

Modeling results (samples b and c) show that by increasing the exposure time at microwaves it is possible to maintain the reactants at temperatures in excess of the NiAl melting point; higher microwave forward power result in a reduced ignition time, but in this case the materials surrounding the reacting species remain colder. This implies that as soon as microwaves are turned off, the samples will experience a rapid heat loss, and thus will be subjected to high cooling rates. Reducing the microwave power to one third, instead, requires longer time to reach the ignition temperature, but then the subsequent cooling occurs more slowly (samples a and e; b and d). This can be ascribed to the larger amount of energy transferred to the system before ignition occurs (applying one third of forward power increases the ignition time by more than 3-fold, thus the energy conveyed to the whole system, equal to the product of the power by time, is also higher). This energy, converted into heat in the pressed powders disc, raises the temperature of the surrounding materials, and the subsequent cooling occurs therefore slower in a hotter environment. In this case, a higher substrate temperature is also expected before and after CS. Comparing the two different substrates (samples e and f), the higher thermal conductivity of steel is responsible for higher heat losses, and consequently for the increase of the ignition time (heat is lost in the surrounding air) and the reduction of the residence time at high temperatures (the steel substrate acts like a heat sink). Conventional heating (sample g) by placing the samples in a furnace heated at 1000 K, requires longer ignition times compared to the simulated microwave assisted cases, and the residence time at high temperature amounts to 13 seconds. Moreover, the long time

exposure to high temperature tends to overheat the surrounding metal substrate, as shown in Figure 2.2–6, where the calculated heating and cooling curves are reported for the case MW_P18_3-3-3 and CONV_T1000_3- 3-3, in the intermetallic formation zone and in the substrate material. It is evident, in case of microwave heating, that the substrate temperatures are much lower than in case of conventional heating: 160°C lower at the beginning of CS and 370°C at CS completion. This expected result can be ascribed to the heating selectivity of microwaves, which tend to generate heat only in the pressed Ni+Al powders sample and not in the metallic substrate. On the contrary, conventional heating heats the substrate and the reacting species at the same temperature, before CS occurs. This phenomenon is expected to lead to the formation of a thinner heat affected zone in the substrate when microwave assisted CS is performed, also due to the shorter ignition times.

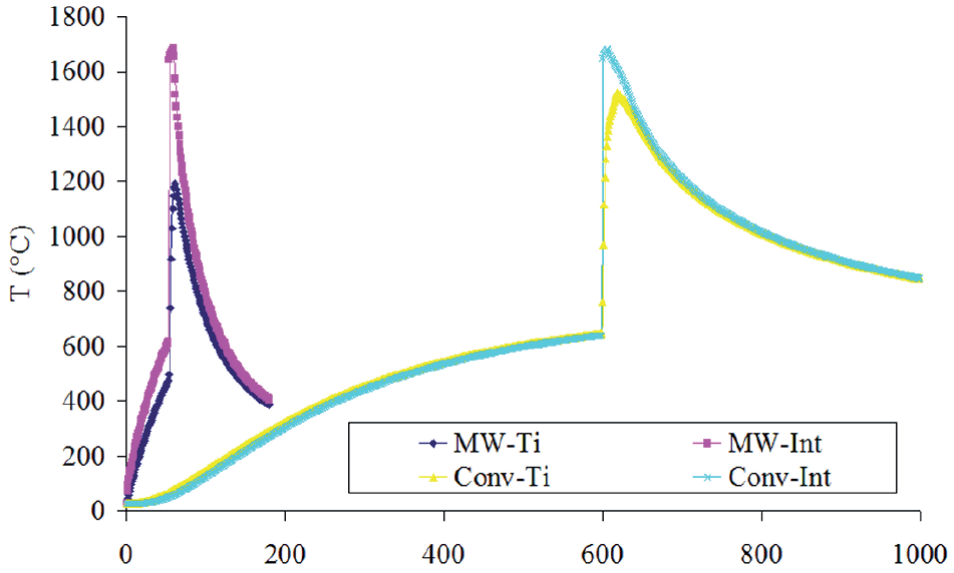

Figure 2.2–12: Temperature vs time curves for the MW_18_3-3-3 and CONV1000_3-3-3_t3 case, in different regions of sample (Ti=titanium substrate, mid section; Int=intermetallic layer, at the TI interface)

The measured temperature vs. time curve acquired during CS is shown in Figure 2.2–13, together with the numerical simulation prediction. The numerical simulation results are in satisfactorily good agreement with the experimental data, considering the assumptions made. The main discrepancies lie in the heating curve before CS occurs.

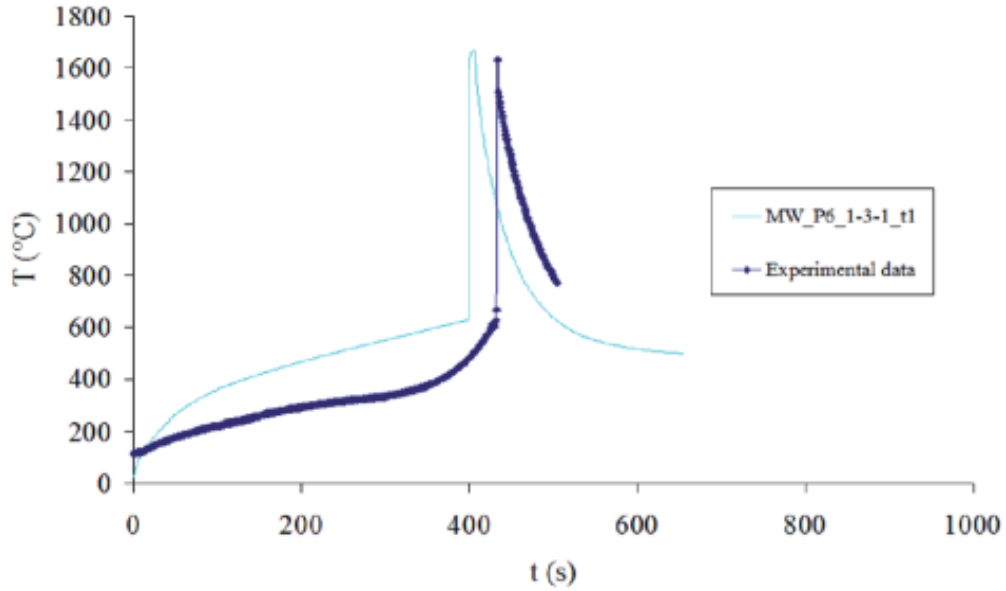

Figure 2.2–13: Experimental data vs. simulation plot result.

The previous proofs demonstrated the validation of theoretical model thanks to experimental results. At the beginning, the model is exploited to understand NiAl behavior as joint between different metal substrate, then it will be developed to study hybrid systems.

Ti-Inconel Joining

For this purpose, in this study three different nickel superalloys (Inconel 601, 625 and 718) have been used. Their different composition reflects the differences in the mechanical properties, as reported in Table 2.2-4.[194]

Table 2.2-4: Inconel alloys properties

Alloy	601	625	718
Density [g·cc^{-1}]	8.11	8.44	8.19
Heat Capacity at constant pressure [J·g^{-1}·°C^{-1}]	0.448	0.41	0.435
Heat Conductivity [W·m^{-1}·K^{-1}]	11.2	12.8	11.4
Tensile Strenght Ultimate [MPa]	760	880	1375
Tensile Strenght Yeld [MPa]	450	460	1100
Elongation at break [%]	42	50	25

Inconel (type 601, 625 and 718) and Titanium (grade 2) substrates were provided by Akrapovič (Ivancna Gorica, Slovenia). Nickel (≈ 3 µm, 99,7% purity), Aluminum (≈ 200

194 ASM Aerospace Specification Metals, Inc, Metal Distributor Dealer Supplier

mesh, 99% purity) and Titanium (-325 mesh, 99.8% purity) powders were provided by Sigma Aldrich (Milan, Italy).

General experimental procedure to prepare reactive joining material is the same previously used[195]. Ni + Al (50:50 at.%) powders have been mixed and molded to obtain a series of cylindrical compacts with diameter of 20 mm and 2-3 mm height, put between Titanium grade 2 and Inconel discs. Experimental microwave setup [196] too is the same applied in the previous works: a single mode applicator WR-340 with sample in the maximum of electric field and a pressure of 0.8 MPa applied during reaction to reduce porosity.

The model geometry is sketched in Figure 2.2–14(a). It shows the experimental set-up of the specimens in the single mode applicator. It has been developed with 3D model, considering only one step reaction to form intermetallic with the aim to simplify the model.

As previous quoted (Paragraph 2.2.2.1), the parameters using during simulation are reported in Table 2.2-1 and Table 2.2-2.

In Figure 2.2–14 (a) and (b) the blue discs represent the substrate to be joined (Inconel and Ti respectively) while the red one constitutes the joining material to be ignited (Ni+Al compacted powders).

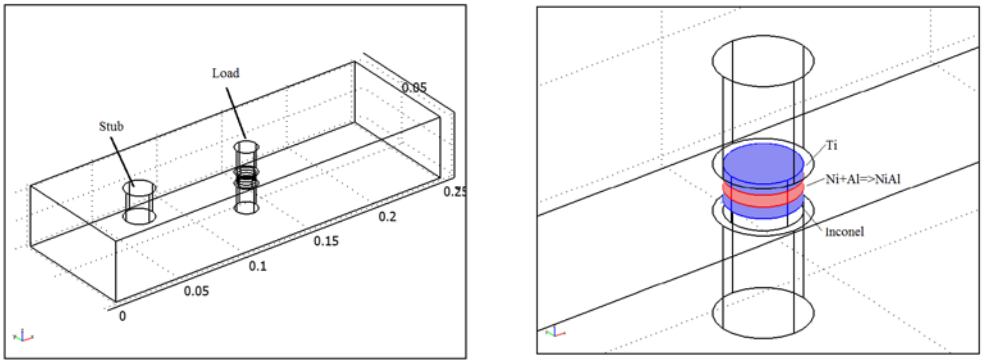

Figure 2.2–14: (a) geometry model, (b) load detail

[195] E. Colombini *et al.*, Microwave ignited combustion synthesis of intermetallic compounds, modelling and experimental results, Metallurgia Italiana, 4 (2011) 29-34

[196] R. Rosa, P. Veronesi, C. Leonelli, A. B. Corradi, Microwave (MW)-assisted combustion synthesis of micrometric metallic powders for the preparation of intermetallic based materials, PM2010 World Congress and Exhibition, Florence, Italy 10-14 October 2010, Proceedings Vol. 2, pp. 217-223, ISBN 978 1 899072 11 8.

As in previous works, [197,198] from the chemical module two values have been exported: reaction rate and enthalpy of reaction. Then RF module has been added to the model. Because of lack of time dependent electromagnetic data, RF modules has been solved, in stationary condition, separately from the other two modules, which are time dependent. Due to the lack of reliable high temperature data on magnetic and dielectric properties of reactants and products at 2.45 GHz, the electromagnetic part of the model has been solved independently on the thermal one, in stationary conditions, to calculate the power density generated in the load, by microwave heating, which has been subsequently used as source term in the heat transfer equation. Afterwards, thermal and diffusion modules have been run. The RF model shows the presence of a stub tuner (Figure 2.2–14) which has been used in order to reach a low S_{11} (reflection coefficient) value. Results obtained by RF module have been reported in Figure 2.2–15 (a) and (b).

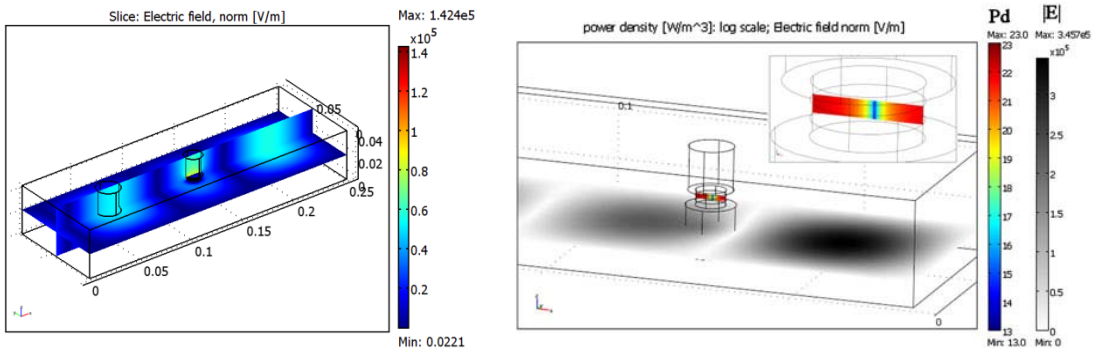

Figure 2.2–15: (a) Electric field distribution [V·m^{-1}], (b) Electric field (E) distribution (reported in gray scale) along the single mode applicator and MWs power density (Pd) distribution (reported in rainbow-like colored scale) in the joining couple, in the case of reflecting substrates. In the inset, an enlarged view of Pd distribution is reported

In particular, Figure 2.2–15 (b) shows the electric field distribution along the applicator and the MWs power density distribution in the joining couple positioned in the center of the single mode cavity, at room temperature

As reported in the zoomed view in Figure 2.2–15(b), at the very beginning step of the joining process, the only MWs absorbing component in the whole load results the Ni + Al (50:50 at.%) compacted powders mixture, thus clearly confirming the selective nature of MWs heating technique in the particular application field of CS ignition. MW-assisted CS of β-NiAl intermetallic phase has already proved to be an interesting route to form NiAl protective coatings on Ti, leading to a NiAl outer layer and an inner hypoeutectoid Ni-Al-

197 P. Veronesi *et al.*, Microwave assisted combustion synthesis of non-equilibrium intermetallic compounds, JMPEE, Journal of Microwave Power and Electromagnetic Energy 44 (2010) 45-56

198 E. Colombini *et al.*, Microwave ignited combustion synthesis of intermetallic compounds, modelling and experimental results, Metallurgia Italiana, 4 (2011) 29-34

Ti ternary layer.[199,200,201] CS of β-NiAl intermetallic (starting from a 50:50 at.% mixture of Ni and Al) phase has been ignited by means of MW energy in order to join Ti components and Ti to Inconel alloy (type 601).

Diffusion module has only one subdomain activated, i.e. the compacted powder disc, where reaction rate, as mentioned above obtained by reaction laboratory, calculated. The heat transfer module takes thermal conductivity, k, heat capacity, cp, density, ρ, and heat source, Q, into account for each disc. The heat source value, in case of NiAl, is made up of two terms: the combustion synthesis heat (exported from Reaction Engineering Laboratory) and microwave heat source, for all other components the heat is zero and only heat transfer accounts for their temperature raise

Results obtained by means of simulation are reported in Figure 2.2–16.

Figure 2.2–16 (a) shows CS referred to different kind of Inconel supports. Inconel 601 has higher heat capacity value so it employees more time to reach the ignition temperature. Different reaction rates, estimated by different concentration variation during CS (as shown in Figure 2.2–16 (c)) support this theory. Titanium has an higher value of both c_p and k, so it reaches the same temperature slower than Inconel, but maximum temperature is approximately the same (Figure 2.2–16 (d) Figure 2.2–16 and (e))

[199] G.P Cammarota et al., Ni–Al–Ti coatings obtained by microwave assisted SHS: Effect of annealing on microstructural and mechanical properties, Surface & Coating Technology 203 (2009) 1429-1437

[200] R. Rosa *et al.*, Ni-Al-Ti Coatings Obtained by Microwave Assisted Combustion Synthesis, Surface Engineering, 28 (2012) 91-95

[201] I. Boromei *et al.*, Ni-Al-Ti Coatings Obtained by Microwave Assisted SHS: Oxidation Behaviour in the 750-900 C Range, Surf. Coat. Technol., 204 (2010) 1793–1799

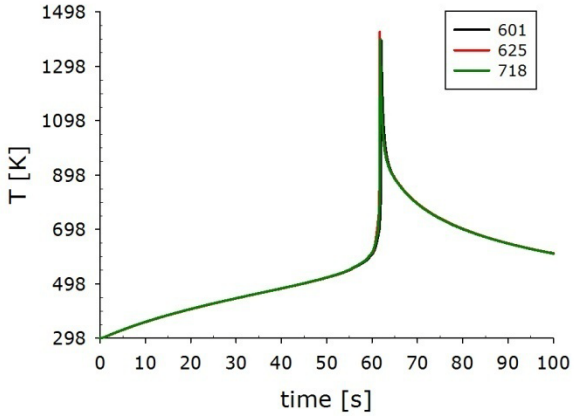

(a) CS curves for different Inconel type

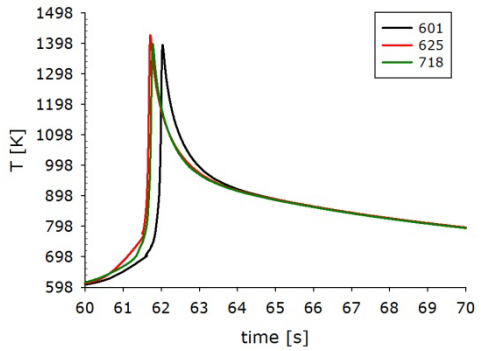

(b) Details, at ignition time, for different Inconel supports

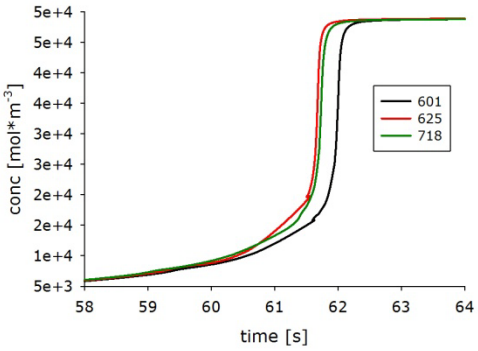

(c) Concentration variation for different Inconel type

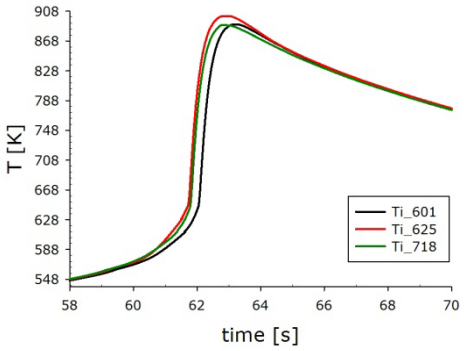

(d)Distribution temperature on Titanium substrates

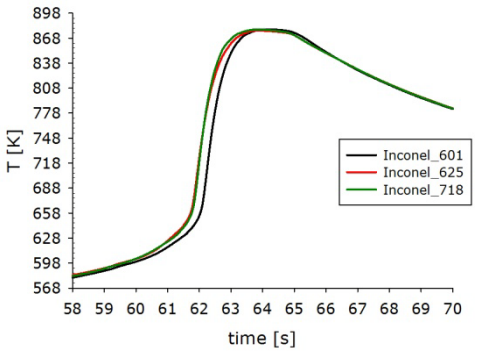

(e) Inconel substrates temperature distribution

Figure 2.2–16: Simulation results

By means of simulation it is possible to study system temperature distribution and thus calculating, by means of image analysis, the heat affected zones (HAZ).

Ignition time is the same (about 61 s after microwave switching on), Inconel 625 shows an higher HAZ than other Inconel alloys; this is due to a higher k value and higher

heat capacity. The combustion synthesis maximum temperature value is reached in model where Inconel 718 is used.

Table 2.2-5: HAZ, T_{max} and time to reach T_{max} of different models

Inconel	HAZ_Inconel [%]	HAZ_Ti [%]	T_{max} [K]	$t_{\_Tmax}$ [s]
601	0.85	21.96	1440	62.0
625	1.31	23.29	1478	61.7
718	1.24	13.42	1506	61.5

2.2.2.2. CS exploiting SiC

Joints between Titaniun and Inconel

Starting from the study of joining between Titanium, NiAl and different type of Inconel, Inconel 601 has been chosen as a substrate in a model which can be used to understand the effect of Silicon carbide during combustion synthesis.

Silicon carbide (SiC)-based materials are known to be good MWs absorbers and they are often used in MW processing of materials as ‘‘susceptors’’ or co-absorbers in order to obtain more uniform temperature distributions and better electromagnetic field homogenization, decreasing at the same time electric arcs occurrence inside the MW cavity. The differences from the previous case (Figure 2.2–15), since the substrate is microwave-absorbing, can be pointed out in Figure 2.2–17. It shows the electric field distribution and power density into the single mode cavity. The load is still placed in the maximum of electric field, but the resistive heating time average, demonstrates how it is possible to selectively microwave heat both SiC and Ni+Al portions of the load by means of microwave-matter interaction.

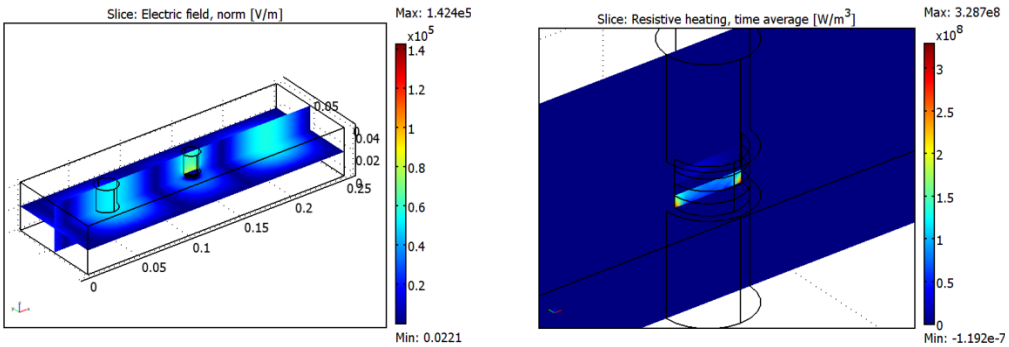

Figure 2.2–17: Electric field distribution [$V \cdot m^{-1}$] and power density distribution [Wm^{-3}]

Plot shown in Figure 2.2–18 has been obtained by simulation using. Ti and Inconel 601 as base metal and NiAl as joining material, with or without SiC susceptor. If SiC is

present CS is formerly activate and an higher maximum temperature is reached, (Figure 2.2–18 (d)), as proof that SiC leads to more uniform temperature distributions and better electromagnetic field homogenization, decreasing at the same time electric arcs occurrence inside the MW cavity, as previously demonstrated by some researches.[202]

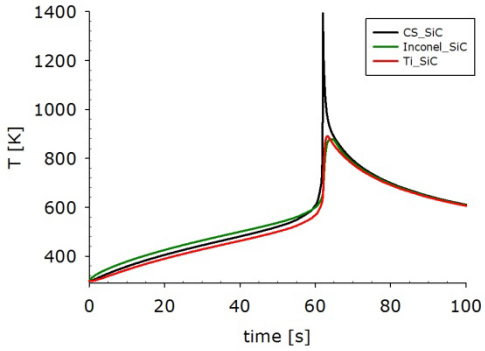

(a)Distribution temperature Inconel 601 with SiC

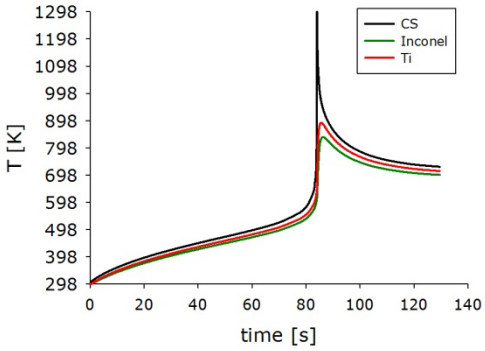

(b) Distribution temperature Inconel 601 without SiC

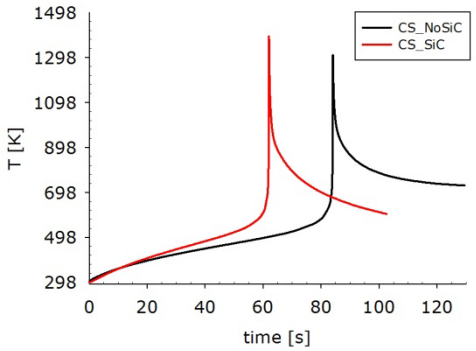

(c) Details, NiAl distribution temperature, with and without SiC

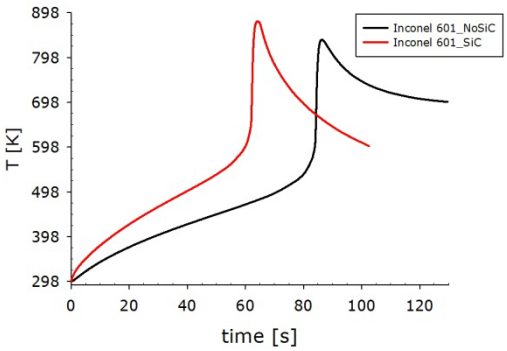

(d) Details, Inconel distribution temperature, with and without SiC

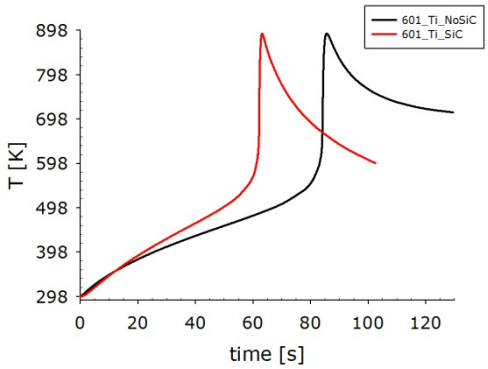

(e)Details, Ti distribution temperature, with and without SiC

Figure 2.2–18: Simulation results.

[202] R. Rosa *et al.*, Microwave Ignited Combustion Synthesis as a Joining Technique for Dissimilar Materials, Journal of Materials Engineering and Performance, 21 (2012) 725-732

As in previous case of Ti and different type of Inconel joining without SiC support, the heat affected zone is estimated (Table 2.2-6)

Table 2.2-6: HAZ, T_{max} and ignition time of two different models

Inconel 601	HAZ_ Inconel [%]	HAZ_Ti [%]	t_{ing} [s]	T_{max} [K]
without SiC	73.25	40.5	84.0	1309
with SiC	39.35	30.82	61.5	1393

HAZ is smaller in case of SiC support, probably because it is required less time to reach ignition time; the different ignition time of two models is about 20 s. Maximum combustion synthesis temperature is higher with SiC support (surrounding materials are hot, instead of cold).

The SiC presence allows both to have less time before the CS trigger and to reach higher temperature by the side of NiAl and substrates. Without SiC the system stays between 400-600 K for 20 s more than with SiC.

From the experimental point of view, the characterization of samples obtained has been performed to understand the microstructure and mechanical properties of the joint, in detail on the cross section of the joint XRD, SEM and Vickers Hardness Test have been carried out. XRD analysis (Figure 2.2–19) confirmed the achievement of β-NiAl phase as the main product, with the presence of a small amount of Ni_3Al as secondary phase.

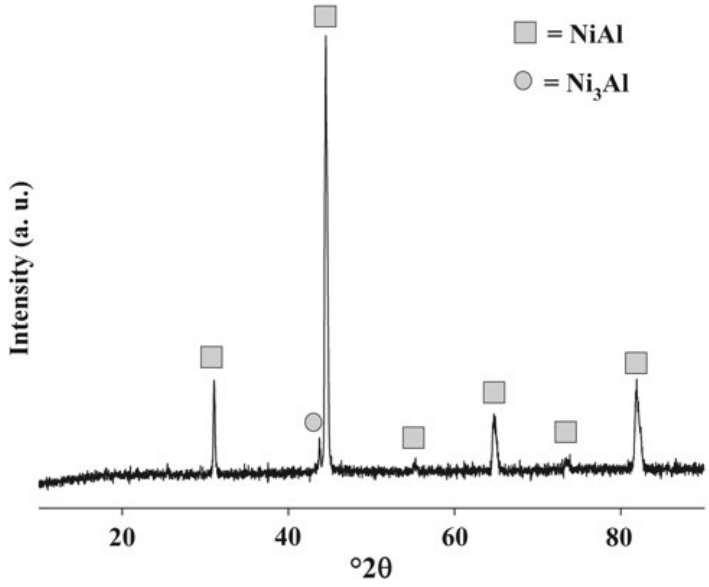

Figure 2.2–19: XRD pattern of the combustion synthesized b-NiAl based joining material used for MWs reflecting substrates

The ESEM-EDS analyses showed the presence of Ni, Al and Ti in this intermediate layer, suggesting that during CS, reactions between the substrate and the reactants occurred, as previously demonstrated (paragraph 2.2.2.1) and the formation of intermediate layer between NiAl and Ti occurs. Interfaces between the newly combustion synthesized β-NiAl phase and Inconel and Ti substrates are reported in Figure 2.2–20 (a) and (b), respectively. Aluminum diffuses from the NiAl phase towards the Ni-based superalloy substrate[203], as shown from the slightly darker middle layer (labeled in Figure 2.2–20 (a)) and from the EDS line scan of Al, superimposed to Figure 2.2–20(a). NiAl-Ti interface (Figure 2.2–20 (b)) is characterized by a thickness range of 50 to 100 μm and the microstructure shows typically mixed dendritic and eutectic features, which came from the reactions between liquid NiAl and the Ti substrate.[204,205,206]

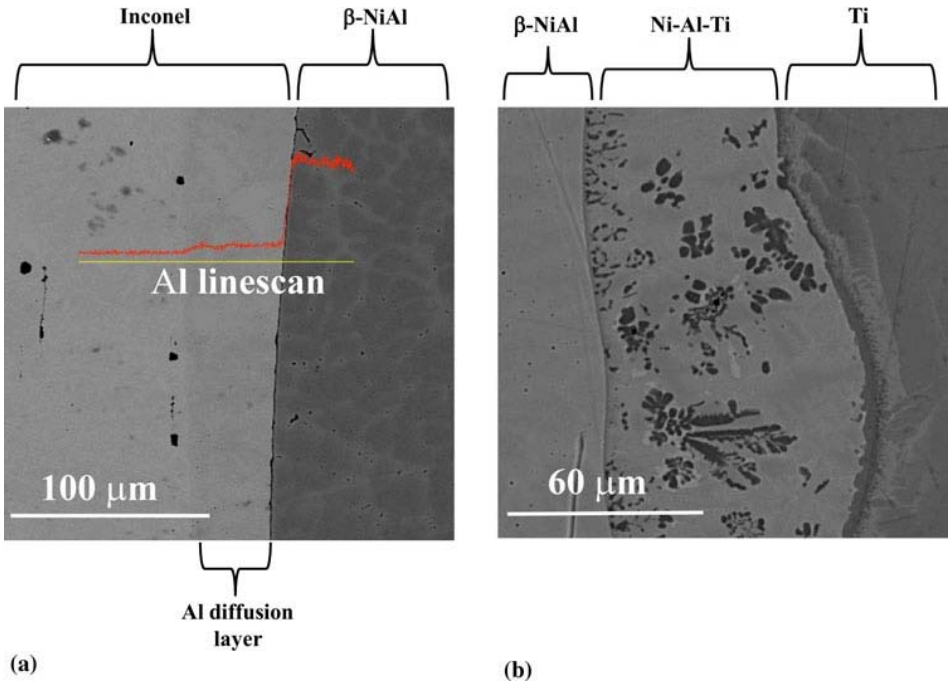

Figure 2.2–20: Interface between CS β-NiAl and Inconel substrate; EDS Al line scan across the cross section shows Al diffusion from the intermetallic phase toward the Ni-based superalloy substrate. (b) Ni-Al-Ti reaction layer formed after joining at the interface between titanium component and MWs combustion synthesized b-NiAl phase

[203] R. Rosa *et al.*, Energy Transfer in Microwave Assisted Combustion Synthesis of Inorganic Compounds, Proceedings of 13th International Conference on Microwave and RF Power Applications, AMPERE 13th, Toulouse, France, (2011) 169–172, ISSN 0832-7823

[204] G.P Cammarota et al., Ni–Al–Ti coatings obtained by microwave assisted SHS: Effect of annealing on microstructural and mechanical properties, Surface & Coating Technology 203 (2009) 1429-1437

[205] R. Rosa et al., Ni-Al-Ti Coatings Obtained by Microwave Assisted Combustion Synthesis, Surface Engineering, 28 (2012) 91-95

[206] I. Boromei et al., Ni-Al-Ti Coatings Obtained by Microwave Assisted SHS: Oxidation Behaviour in the 750-900 C Range, Surf. Coat. Technol., 204 (2010) 1793–1799

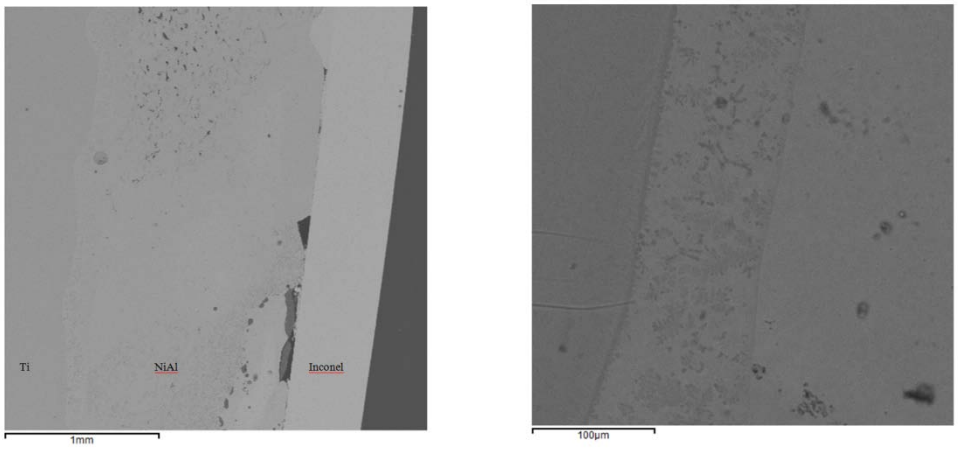

(a) (b)

Figure 2.2–21: (a) SEM images of joint, (b) interface detail of interaction between NiAl and Ti,

SiC as susceptor leads to enhance adhesion and possible reactions between the substrates and the joining material, as reported in Figure 2.2–22 (c) and (d). Using SiC, typical solidification structure, with equiaxial grains growth, is highlighted to confirm the temperature exceeding NiAl melting point, during synthesis. The newly formed phases in the liquid state lead to the rapid reaction between the molten NiAl and the Ti substrates, generating the intermediate layer, where formation of eutectics in the Ni-Al-Ti system occurs.[207]

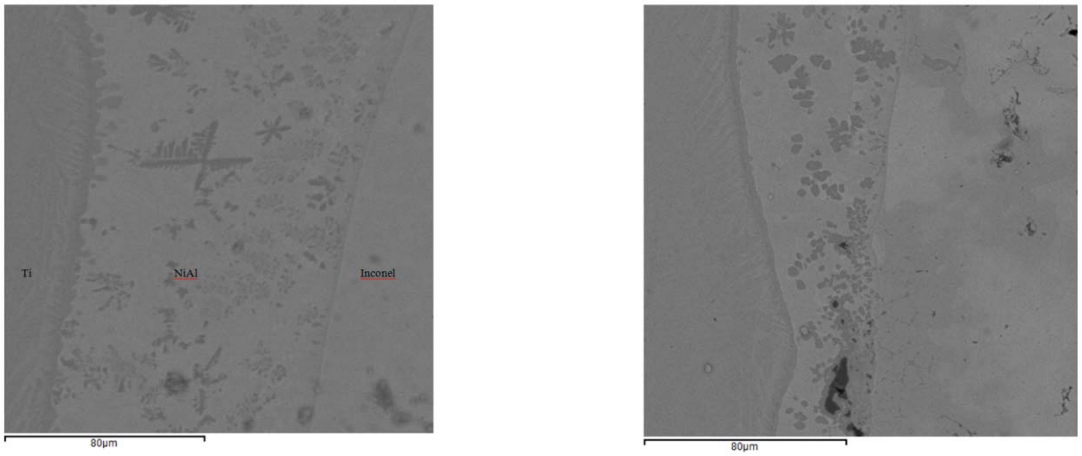

(c) (d)

Figure 2.2–22: Joint detail (SEM images) (c) microstructure in case of SiC substrate, (d) microstructure without SiC substrate.

Microhardness measurements have been performed by 402 MVD Vickers and Knoop Testers Wolpert Wilson® Instruments at 500 g as load (HV 05). The range of results are shown in Table 2.2-7

[207] A.G. Merzhanov, The chemistry of self-propagating high-temperature synthesis, J.Mater.Chem., 14 (2004) 1779-1786

Table 2.2-7: Hardness value

Materials	HV 05
NiAl	260-360
Inconel	140-160
Ti	160-180

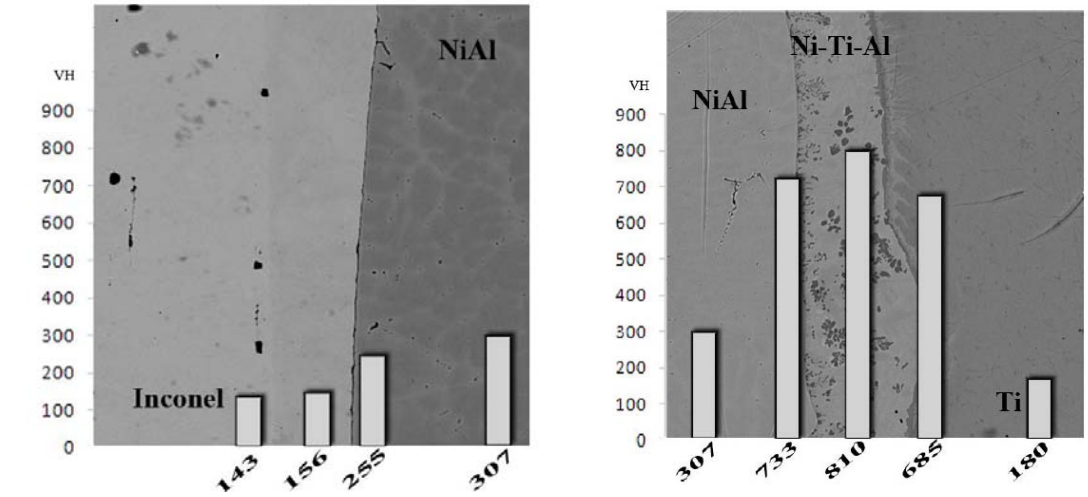

Figure 2.2–23: Vickers microhardness: (a) on NiAl-Inconel interface and (b) NiAl-Ti interface

Porosity caused both a decrease of hardness material value and it does not lead to a correct evaluation. Hardness on interface is an average value between two pure phases hardness values. NiAl interface shows an hardness value of 307 HV, 810 HV is the value on Ni-Ti-Al; the value between NiAl and Ni-Ti-Al interface is 730 HV, which is an intermediate value between the previous ones, but slightly higher than average (558 HV). This data support the high hardness of new phases and also show cross properties formation into joints.

When MWs ignited CS technique was exploited to join MWs absorbing components, like SiC-based materials, it has been shown the competition in MWs absorption between the substrates and the reactive powders. Although somehow this hides the selective nature of dielectric heating, it can enhance conversion degree of the starting reactants, adhesion, interdiffusion, and chemical bonding between the CS products and the substrates. These two aspects can be instead proficiently combined in realizing mixed joints between MWs reflecting (like metals) and MWs absorbing (some ceramics or composites) components.

NiAl between SiC

A more accurate 3D numerical simulation of the joining process between CVD SiC ceramic substrates, exploiting the combustion synthesis of NiAl intermetallic phase, was possible due to the simpler nature of the system involved and the E field axial symmetry in the region of the applicator hosting the load.

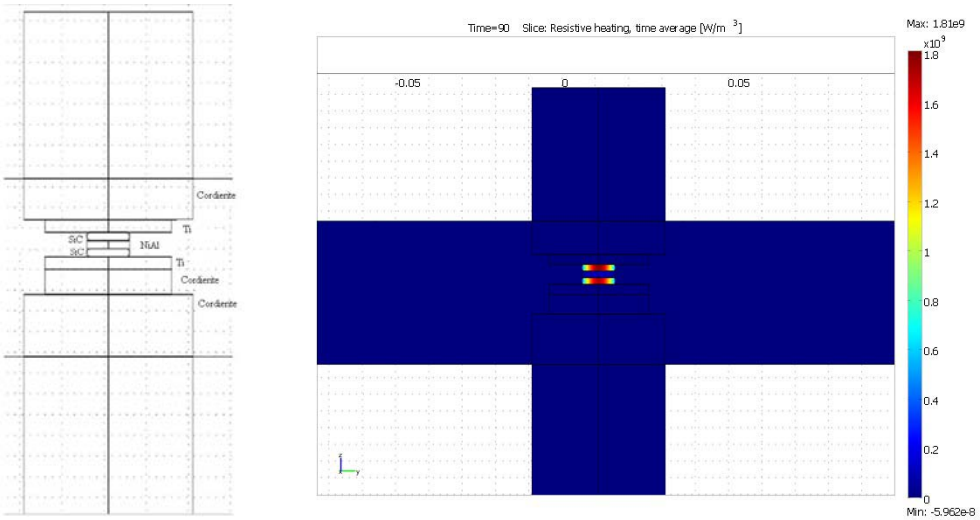

Figure 2.2–24: Load configuration (a) and power density developed in the load during joining process (b)

In order to, further and more clearly, separately analyze the temperature evolution in the different components of the load, time development of temperature are reported in Figure 2.2–26. It shows plot in the middle of cordierite refractory basement, Ti separator, CVD SiC substrate and Ni-Al joining material. Figure 2.2–27 shows simulation results, in terms of temperature distribution in the load, after 2 and 90 seconds from the turning on of microwave generator. Together with plots reported in Figure 2.2–26 results confirm the fact that combustion synthesis, as joining technique, allows to limit the heat-affected zone of the whole pieces to be joined, due to the rapid and highly localized heat generation typical of CS processes. Moreover a further peculiarity comes from the use of microwave energy ignition source. Its selective nature, indeed, avoids the overheating (up to ignition temperature for instance) of the components not directly involved in the joining process.

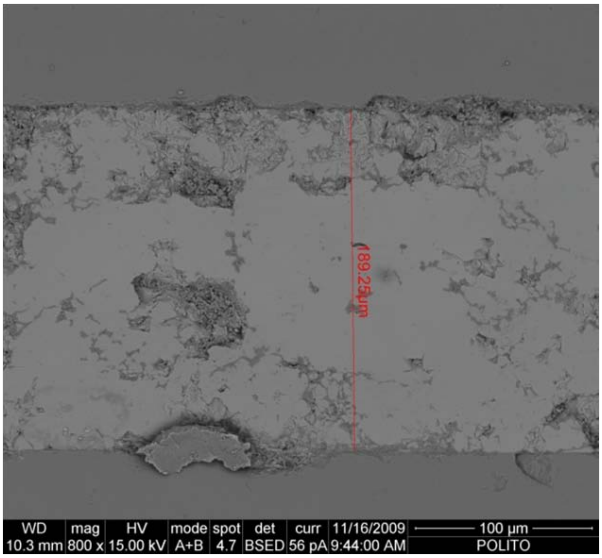

Figure 2.2–25: Homogeneous joint between NiAl and SiC**.**

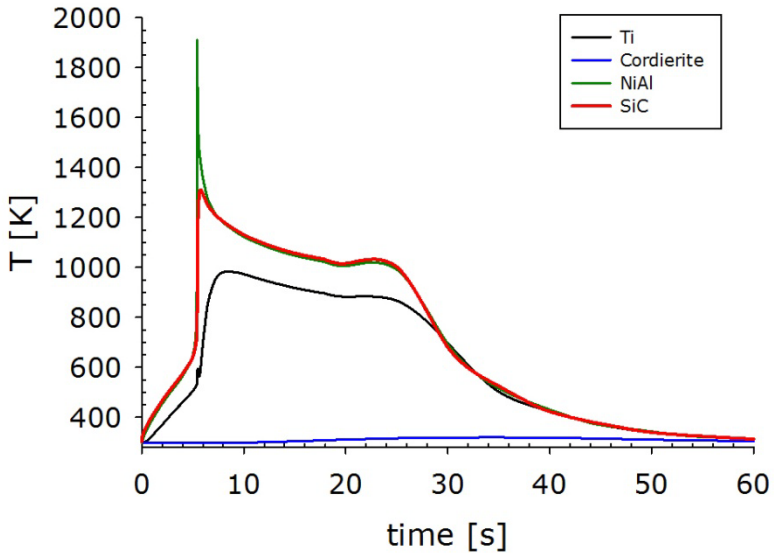

Figure 2.2–26: Temperature plot of different load component during CS synthesis

Figure 2.2–25 shows joint between NiAl and SiC, characterized by an average thickness of 200 mm. Since SiC is a co-absorber ignition point increase leading to rapid cooling that cause a decreasing of grain size.

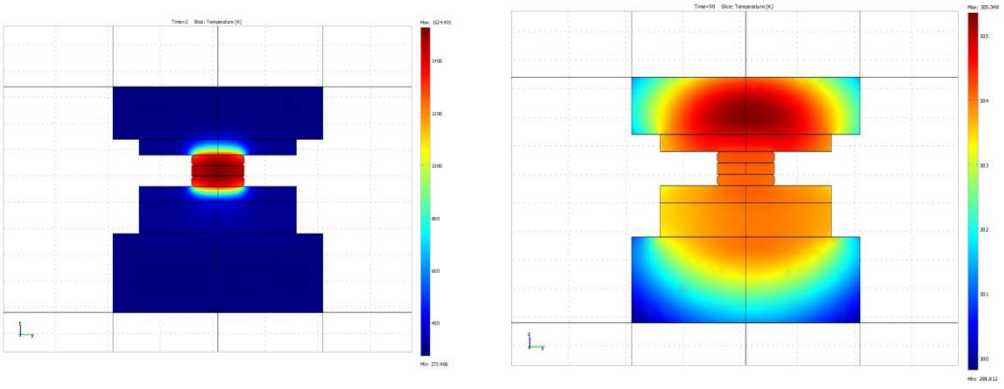

Figure 2.2–27: Temperature distribution in the whole load after 2 s (a) and 90 s (b) after microwaves generation was turned on.

2.2.2.3. Microwave silicon carbide assisted combustion synthesis

Both experimental and numerical literature results [208] demonstrate that joining of SiC can be rapidly obtained by microwave ignition of the combustion synthesis in the ternary system Ti-Si-C, with local overheating of the reactive joining material and reduction of the extension of heat affected zone in the SiC substrates.

Ti, Si and C are considered suitable elements for joining silicon carbide fibres reinforced silicon carbide matrix (SiC_f/SiC) composites, which can be used in several fission system and nuclear application. [209,210] CS approach [211,212] could be exploited to directly in situ synthesise refractory phases with high chemical compatibility with the substrate constituents, such as SiC[213] itself and TiC[214], and different kind of silicides. [215,216]

---

208 R. Rosa *et al.*, Microwave assisted combustion synthesis in the system Ti-Si-C for the joining of SiC: Numerical simulation and experimental results Elsevier Editorial System(tm) for Journal of the European Ceramic Society, Submitted.

209 M. Ferraris et al., Joining of machined SiC/SiC composites for thermonuclear fusion reactors, J. Nucl. Mater. 375 (2008) 410-415.

210 Y. Katoh *et al.*, Current status and critical issues for development of SiC composites for fusion applications, J. Nucl. Mater 367-370 (2007) 659-671.

211 M. Ferraris *et al.*, Joining of machined SiC/SiC composites for thermonuclear fusion reactors, J. Nucl. Mater. 375 (2008) 410-415.

212 B. Riccardi *et al.*,Issues of low activation brazing of SiCf/SiC composites by using alloys without free silicon, J. Nucl. Mater. 329-333 (2004) 562-566.

213 J. Peng, J. Binner, S. Bradshaw, Microwave initiated self-propagating high-temperature synthesis of SiC, J. Mater. Synth. Proc. 9 (2001) 363-368.

214 G. Golkar, S.M. Zebarjad, J.V. Khaki, Optimizing the ignition behavior of microwave-combustion synthesized Al2O3/TiC composite using Taguchi robust design method, J. Alloys. Compd. 487 (2009) 751-757.

215 J.R. Jokisaari, S. Bhaduri, S.B. Bhaduri, Processing of single phase Mo_5Si_3 by microwave activated combustion synthesis, Mater. Sci. Eng. A 323 (2002) 478-483.

To join SiC, it is not possible to use only Si and C powder because of low mechanical properties[217]. It is due to adiabatic temperature, which is not high enough to originate a liquid phase able to wet substrates in the limited time of joining process.

As a consequence, the addition of Ti to the Si and C mixture was determinated in order to exploit more exothermic reactions, set by the formation of titanium carbide starting from elemental Ti and C (ΔH_0^f= -92.9 ± 8.9 kJ/mol,[218]), and the formation of titanium silicides, starting from elemental Ti and Si (Ti_5Si_3: ΔH_0^f= -579.5 ± 58.6 kJ/mol; $TiSi_2$: ΔH_0^f = -133.9 ± 20.9 kJ/mol [219]).

The generic model here described was adapted. In the model one reaction has been exploited to simulate the Ti-Si-C system synthesis. X-ray diffraction analysis[220] highlighted the presence of two mainly phase TiC and $TiSi_2$. (among TiC, Ti_5Si_3 and $TiSi_2$). Among those, the formation reaction of $TiSi_2$ is the more exothermic one, so it has been chosen as the main newly synthesised phase and it has been simulated according to:

Eq 18 $$\mathbf{Ti + 2Si \rightarrow TiSi_2 + 133.9\ kJ \cdot mol^{-1}}$$

The reaction kinetic parameters such as the Arrhenius pre-exponential factor (A) and the activation energy (E), as well as thermodynamic (entropy, enthalpy and specific heat) and chemical-physical (concentration, density and molecular weight) properties for all of the species involved in the reaction are reported in Table 2.2-8.

---

216 J.R. Jokisaari, S. Bhaduri, S.B. Bhaduri, Microwave activated combustion synthesis of bulk cobalt silicides, J. Alloys Compd., 394 (2005) 160-167.

217 Han S., Joining of Ceramics and Ceramic Matrix Composites for Nuclear Applications, Polytechnic of Turin, Turin, Italy, Ph.D. Thesis, 2012.

218 O. Kubaschewski, C.B. Alcock, P.J. Spencer., Materials Thermochemistry, 6th Edition, Oxford; New York: Pergamon Press, 1993 pag.315

219 O. Kubaschewski, C.B. Alcock, P.J. Spencer., Materials Thermochemistry, 6th Edition, Oxford; New York: Pergamon Press, 1993 pag.315

220 R. Rosa *et al.*, Microwave assisted combustion synthesis in the system Ti-Si-C for the joining of SiC: Numerical simulation and experimental results, Journal of the European Ceramic Society, Submitted

Table 2.2-8: Kinetic and thermodynamic parameters for the main reaction and the chemical species involved

Reaction	A	E (kJ·mol^{-1})	H (kJ·mol^{-1})	S [J·mol^{-1}·K^{-1}]
$Ti + 2Si \rightarrow TiSi_2$	4.587	155 [221]	-133.9 [222]	-7.2 [223]

Species	C (J·mol^{-1}·K^{-1}) [224]	c_0 (mol·m^{-3})
Ti	$[24.94+(6.75\text{-}3\cdot T)\text{-}(1.63\cdot10^{5}\cdot T^{-2})+(1.34\cdot10^{-6}\cdot T^{2})]\cdot[T<1155] + [30.84\text{-}(8.87\text{-}3\cdot T)+(6.64\cdot10^{-6}\cdot T^{2})]\cdot[T\geq1155]$	$0.63\cdot10^{5}$
Si	$[(23.93+(2.2\cdot10^{-3}\cdot T)\text{-}(4.14\cdot10^{5}\cdot T^{-2}))\cdot(T<1658)] + [(27.20\cdot(T>1658)]$	$1.26\cdot10^{5}$
$TiSi_2$	$[70.42+(17.57\cdot10^{-3}\cdot T)\text{-}(9.04\cdot10^{5}\cdot T^{-2})]$	0

Starting concentration (c_0) was calculated on the basis of the stoichiometry of the reaction.

An average porosity of 30% was considered, and the real specific heat, density (ρ) and thermal conductivity (k) were corrected accordingly to Eq 11, Eq 12 and Eq 13.[225]

The model geometry is sketched in Figure 2.2–28 together with an expanded view of the load position inside the microwave cavity (Figure 2.2–28 b). Compacted powders disc used as joining material (red disc in Figure 2.2–28 (b)) between two titanium discs, placed between a couple of cordierite cylinders. The compacted powders disc thickness in the model was varied over an order of magnitude, from 0.2 to 2 mm. To investigate the effect of the reactive powders on the maximum achievable temperature. Microwave input port is placed on the left and a matching iris is placed along the WR-340 waveguide, as well as a metallic stub, used for impedance matching purposes, i.e. to minimize microwave reflected power at the operating frequency of 2.45GHz.

A two way coupling between the thermal and RF application mode, has been implemented, taking into account the variation of thermal and electrical properties of the materials as heating proceeds. In the simplified model, permittivity of the reacting powders was maintained constant due to the lack of reliable high temperature data and to the unpredictable volume variation of the pressed powders as CS proceeds, under the application of an external moderate pressure. SiC discs properties are considered constant instead of T-dependent.

---

221 C.L. Yeh, W.H. Chen, C.C. Hsu, Formation of titanium silicides Ti_5Si_3 and $TiSi_2$ by self-propagating combustion synthesis, J. Alloys Compds. ,432 (2007) 90-95

222 O. Kubaschewski, C.B. Alcock, P.J. Spencer., Materials Thermochemistry, 6th Edition, Oxford; New York: Pergamon Press, 1993 pag.315

223 O. Kubaschewski, C.B. Alcock, P.J. Spencer., Materials Thermochemistry, 6th Edition, Oxford; New York: Pergamon Press, 1993 pag.315

224 O. Kubaschewski, C.B. Alcock, P.J. Spencer., Materials Thermochemistry, 6th Edition, Oxford; New York: Pergamon Press, 1993 pag.315

225 O. Biceroglu, Thermal conductivity of sintered metal powders at room temperature Letters in Heat and Mass Transfer, 3 (1976) 183-191

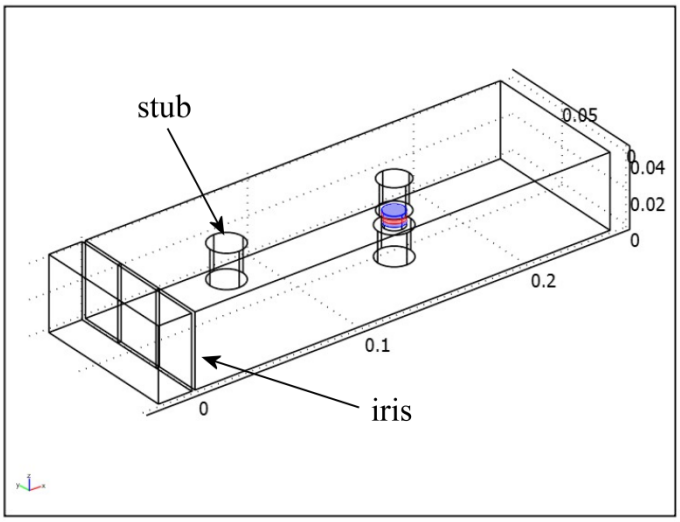

a

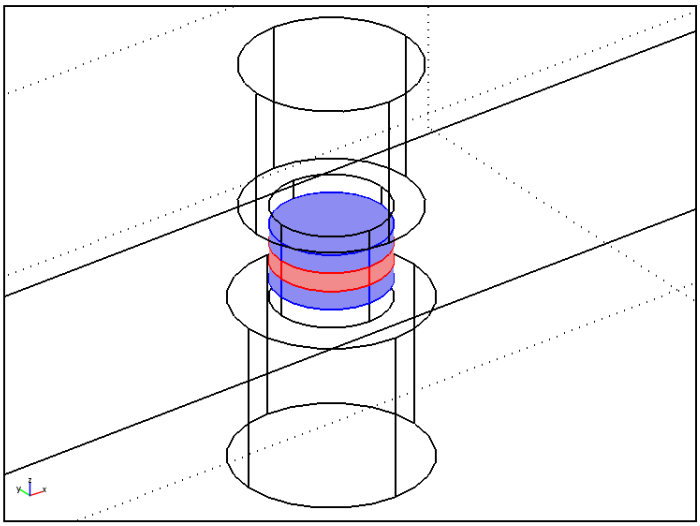

b

Figure 2.2–28: Model geometry (a) in which dimensions are expressed in meters and the expanded view of the load disposition into the single mode cavity (b), composed, by a symmetrical arrangement, from the outside to the inside, of 2 cylindrical cordierite elements, 2 supporting titanium discs, 2SiC discs to be joined and pressed powder joining material (centre)

The final model was meshed using triangular advancing front elements (normal refined mesh), with the compacted powders disc (representing the joining material, in which the CS reaction will occur) meshed with the same kind of elements but of 0.01 mm maximum dimensions and further adaptive refinement. The model consisted of 87184 elements, corresponding to 467376 degrees of freedom; the PARADISO transient direct solver was used to numerically simulate the CS of titanium disilicide ignited by MW heating.

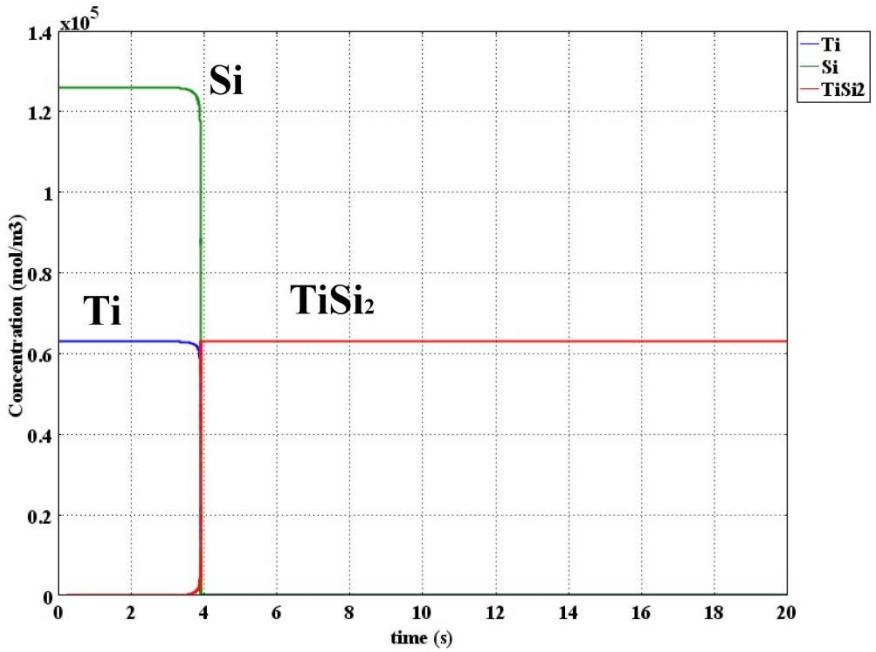

Figure 2.2–29: Ti (blue curve), Si (green curve) and TiSi2 (red curve) concentration variations during combustion synthesis**.**

As previously done, in case of metallic and NiAl powder mixtures, due to the lack of reliable temperature dependent data on magnetic and dielectric properties of reactants and product at 2.45 GHz, the electromagnetic part of the model was solved in stationary conditions, i.e. independently on the thermal one, in order to obtain the average power density generated into the load. Heat Transfer and Diffusion mode was solved in 2D axial symmetry.

Multiphysics numerical simulation results in terms of temperature in the middle of the different components constituting the load are shown in Figure 2.2–30 (a) and (b) (referred to compacted powders discs of 2 mm and 0.2 mm thickness respectively), in case of 1.2 kW MW forward power. The longer ignition time, in comparison to what observed from Figure 2.2–29, can be ascribed to the presence of the materials to be joined and to the supporting materials. The latter subtracts heat from the reaction zone by means of heat transfer. In case of SiC substrates, SiC competes together with the reacting powders in absorbing microwaves. The differences in the ignition time, reaction rate and maximum combustion temperature (1967 K for the 2 mm thick reactive disc and 922 K for the 0.2 mm thick one) are due to the different heat contributions generated by such different reactive masses.

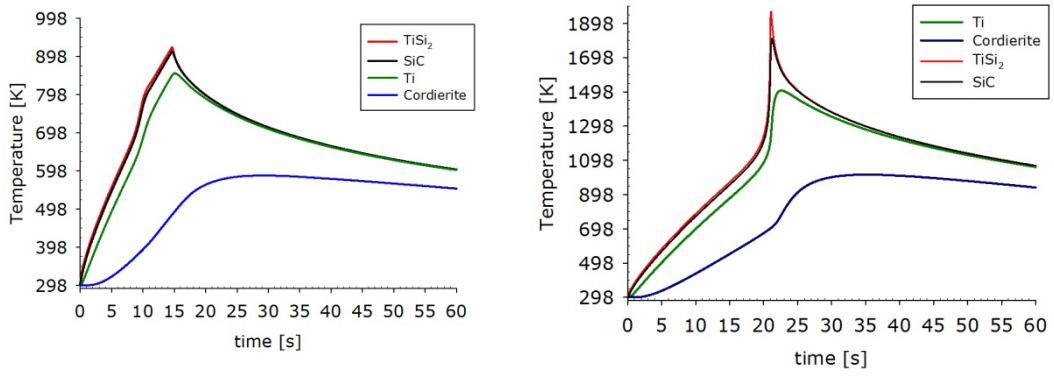

Figure 2.2–30: Temperature evolution in the middle of the different components constituting the load, referred to a compacted powders disc of 2 mm thickness (a) and 0.2 mm thickness (b).

Results clearly highlight that combustion synthesis technique is a heat-localized joining methodology. Indeed, the highest temperature was reached only in the joining material, during the formation of $TiSi_2$. The maximum combustion temperature of 922 K in the 0.2 mm thick compacted powders disc is significantly lower than in the case of 2 mm thick reactive sample (1967 K), due to the lower heat contribution generated by such small mass. As heating proceeds, the Si-C-Ti powders mixture is ignited but exposed to a much hotter environment with respect to the case of MW reflective substrates. Moreover, the CS products of the Si-C-Ti system are still good MW absorbers, and heat generation continues in the joining region, even after CS, until MW power is switched off [226]

Relating to the temperature distribution during synthesis, Figure 2.2–31 shows a further possible use of the numerical model developed. By numerical simulation it is possible to quantify the extent of the joining couple areas subjected to temperatures higher than a certain threshold value, and the time of permanence at such temperature. This value was considered to be 1873 K, since it roughly corresponds to the higher operative temperature at which CVD SiC can be discontinuously used in nuclear environments[227].

This threshold temperature of 1873 K was reached in the two CVD SiC substrates only when 2 mm thickness reactive disc was used as joining material.

In detail, Figure 2.2–31 shows the percentage of the two CVD SiC substrate cross sections exceeding 1873 K, computed every 0.01 s time step during the occurrence of CS reaction in the joining material.

---

[226] P. Veronesi *et al.*, Microwave assisted combustion synthesis of non-equilibrium intermetallic compounds, JMPEE, Journal of Microwave Power and Electromagnetic Energy 44 (2010) 45-56

[227] K. Dawi *et al.*, F. High temperature oxidation of SiC under helium with low-pressure oxygen. Part 3: beta-SiC-SiC/PyC/SiC, J Eur Ceram Soc, 32 (2012) 485-494

From the numerical simulation results it was possible to calculate that during CS reaction in the joining material of 2 mm thickness, the maximum volume percentage of the two SiC substrates exposed to temperatures higher than 1873 K was ca. 22.5 %. As well evident from Figure 2.2–31, this percentage rapidly decreases to zero in less than 0.3 s.

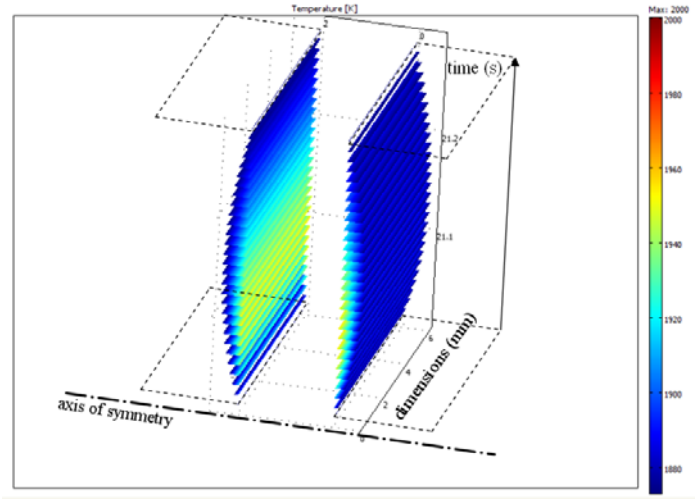

Figure 2.2–31: Percentage of the 2 CVD SiC substrate cross sections exceeding 1873 K, computed every 0.01 s time step during CS of TiSi2. The axis of symmetry around which the 2D axial symmetry was considered is reported as well. The dashed lines indicate the original shape of the SiC substrates cross sections.

Results show that the threshold temperature value was not reached in the entire CVD SiC substrates volume. Repeating the calculations for the joining materials, instead, the threshold was reached in approximately one third of the volume, and maintained for less than 1.5 seconds

Numerical simulation results obtained regarding joining materials size and sample arrangement were exploited in order to experimentally obtain the joining of SiC components by performing combustion synthesis reactions in the system Ti-Si-C ignited by means of microwave energy.

MWs absorption by both SiC substrates and joining powders helped the rapid reaching of the ignition temperature of the powders, leading to the formation of a complex mixture of phases in the joined area. The typical microstructure of the joined samples cross sections referred respectively to joints obtained by using loose powders and compacted pellets is shown in Figure 2.2–32

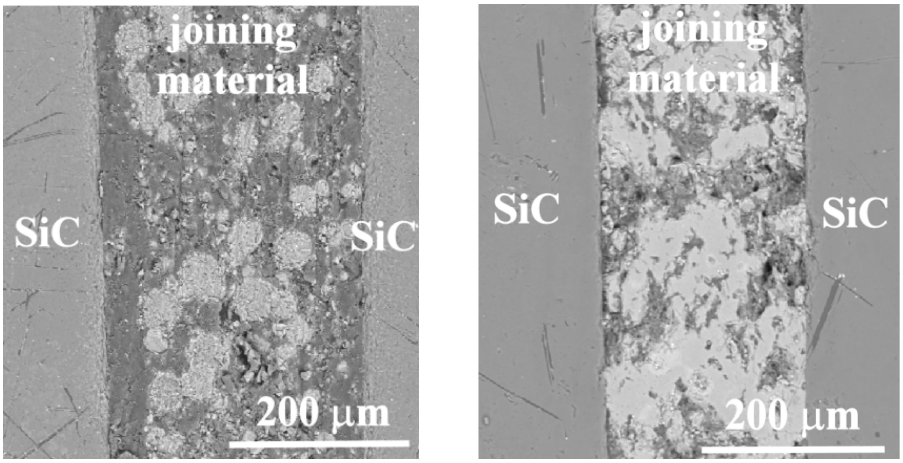

(a) (b)

Figure 2.2–32: Scanning electron micrograph of the cross section of SiC substrates joined with Ti-Si-C loose powders mixture

Furthermore it is also clear the presence of unreacted graphite and oxidized titanium respectively. The latter could be ascribed to a not perfectly inert atmosphere during synthesis. The white region in joining material is a partially unreacted Ti particle. As expected, the use of loose powders led to a thicker joint, approximately 250-280 micrometers, compared to the 200 micrometers achieved by using compacted powders. It is also evident that the use of discs (or pellets) led to a lower porosity and better joint homogeneity.

Microwave assisted combustion synthesis was successfully employed to join CVD SiC samples, using the exothermic reaction of titanium, silicon and graphite powders, mixed in 1:1:1 atomic ratio. Results have demonstrated that a 0.2 mm thick joining material disc would lead to lower temperatures in the reaction zone, minimizing the heat affected regions of the substrate to be joined.

From the inset in Figure 2.2–33 (a) and (b) it clearly appears that in case of MWs ignited CS joining of SiC-based components, MWs are absorbed both by the reactive powders and by the substrates, but to a different extent. In particular, due to the different room temperature dielectric properties of the substrates and of the powders mixture, modeling results show that the power density, and hence heat generation, is much higher in the two outer SiC discs at room temperature.

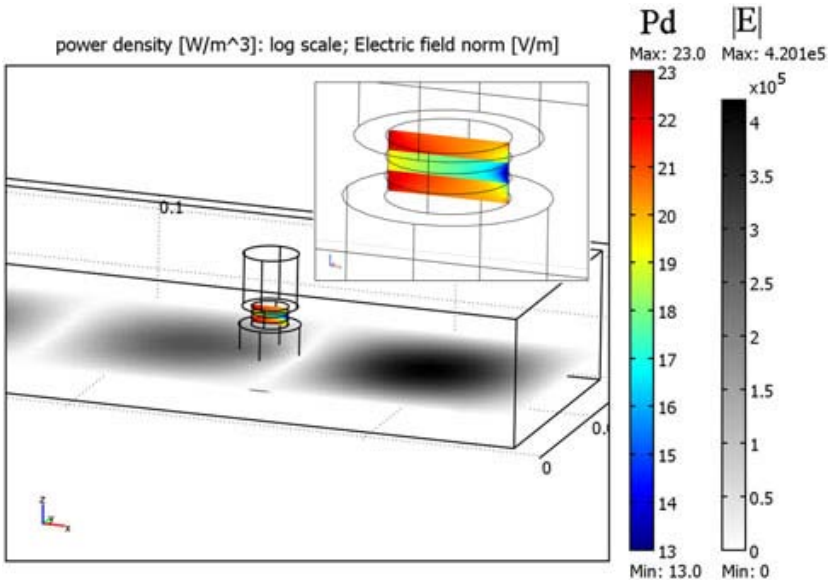

Figure 2.2–33: Power density (Pd) distribution (reported in rainbow-like colored scale) and electric field (reported in gray scale) in case of SiC along the single mode applicator in the joining couple.

Interfacial microstructure observation confirms this expectation, as shown in Figure 2.2–34, in which the porous SiC substrate exhibits good adhesion with the CS obtained joining material in the ternary Si-C-Ti system. The main phases constituting the joining material after CS resulted $TiSi_2$ and TiC as detailed elsewhere.[228,229,230]

Experimental tests show that the joining of SiC substrates by the CS among loose powders mixture presented a maximum apparent shear strength value of 9.9 MPa, while ignition of the CS reactions in compacted powders discs allowed reaching a maximum apparent shear strength value of 45.1 MPa.[231] The difference could be ascribed to the larger amount of un-reacted Si and C in loose powders than in compacted powder. The decreased residual Si amount led to a more interpenetrating and continuous network, which can be considered responsible for higher shear strength values.

---

228 R. Rosa *et al.*,, Microwave Activated Combustion Synthesis and Compaction in Separate E and H Fields: Numerical Simulation and Experimental Results, Proceedings of CIMTEC 2010, 12th International Ceramics Congress, June 6-11, 2010, Montecatini Terme, Italy, Adv. Sci Technol. 63 (2010) 197–202

229 P. Veronesi *et al.*, Microwave Activated SHS for the Joining of SiCf/ SiC Composites to Themselves and to SiC matrix, Proceedings of the Global Congress on Microwave Energy Applications GCMEA 2008 MAJIC 1st, August 4-8, 2008, Otsu Prince Hotel, Lake Biwa, Otsu, Japan, pp 713–716

230 R. Rosa *et al.*,, Microwave Assisted Combustion Synthesis in the Ti-Si-C System for the Joining of SiC: Numerical Simulation and Experimental Results, Journal of Materials Chemistry, Submitted for publication

231 R. Rosa *et al.*, Microwave Assisted Combustion Synthesis in the Ti-Si-C System for the Joining of SiC: Numerical Simulation and Experimental Results, Journal of Materials Chemistry, Submitted for publication

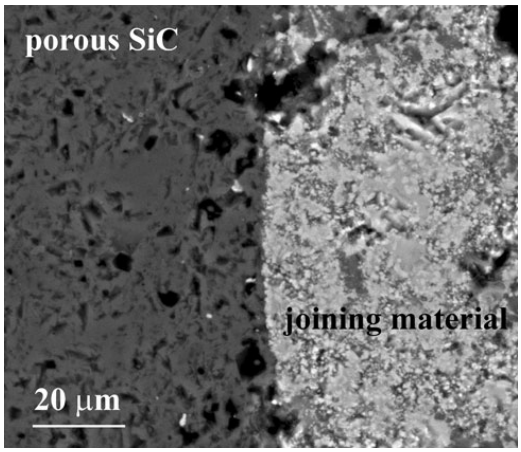

Figure 2.2–34: SEM micrograph of the interface between porous SiC substrate and the products obtained by MWs ignited CS of Si-C-Ti powders mixture

2.3. Conclusions

In this part of the work, joints between dissimilar materials to obtain hybrid structures have been numerically simulated and experimentally investigated. Combustion synthesis is a well known joining technique characterized by the great advantage of rapid and highly localized heat generation easy, higher products purity, time and energy saving process. As ignition method microwaves have been chosen thanks to their property to transfer energy instead of heat as well as due to their peculiar characteristic, , i.e. selectivity, volumetrically, faster heating rates, inversion of classical heating profile. Numerical simulation and experimental results demonstrated the advantage to combine combustion synthesis with the microwaves heating to obtain hybrid materials for high temperature applications. Indeed it is difficult to perform experimental measurements during combustion reactions, due to reaction speed and in addition the use of microwave interferes with equipments used to measure the reacting system characteristics. Thus, numerical simulation resulted a powerful tool to overcome difficulties concerning high temperature measurements and rapid kinetics, leading to understand variable effects, such as sample dimension and load arrangement inside the MW applicator.

The multiphysics model developed to simulate the microwave assisted combustion synthesis is in good agreement with experimental results, despite it is simplified both due to the lack of reliable temperature dependent materials properties data (permittivity and permeability) and to reduce computational costs. It couples electro-thermal application modes and local heat generation by exothermic reactions in order to obtain temperature distributions of all components involved in the joining process. Numerical simulation was used to estimate the heating and cooling rates in each portion of the reactants, as well as

of the surrounding substrates. Moreover it is also possible to calculate electromagnetic field distribution, concentration variation with time of the species and the volume of heat affected zone (based on a threshold temperature value) depending on joining materials. Thanks to microwave heating selectivity a lower substrate temperature is obtained when joining metals, compared to conventional joining techniques. Indeed microwaves are selectively absorbed by micrometric metallic particles mixtures leading to the ignition of the combustion reaction without exposing the overall bulk metallic joining couple to very high temperatures. This suppresses possible unwanted transformations of the substrates, phase change and microstructural alterations. Alternatively, the use of microwaves, if applied after CS ignition, leads to an extension of the holding time at the maximum reaction temperature. This promotes reactions of the newly formed products with the surrounding substrate, leading to the formation of a complex intermediate layer belonging to ternary systems, as demonstrated. Intermediate layer thickness and microstructure could be modified altering synthesis conditions, such as microwave forward power, time of microwave switching off, dimensions of the substrates or pressed powders discs dimensions.

The model is however under refinement, especially as far as the microwave and chemical modules are concerned, due to the lack of temperature dependent materials properties data and difficult to measure pre exponential factor that is one of the most important values used in chemical mode. Experimentally, quite well adhered joints between different substrates for structural high temperature applications by means of a microwave activated combustion synthesis have been achieved.

Chapter 3

C/C/CNT: Carbon Nanotube on Carbon-Matrix Carbon-Fiber Composite

3.1. Background

Nanotechnology manipulates matter on an atomic and molecular scale. It is considered the technology of the future and it has been called “extreme technology”, because it reaches the theoretical limit of accuracy which is the size of a molecule or atom. Nanotechnology deals with materials and systems having the following key properties[232]:

- at least one of their dimension is lower than 100 nm;
- they are designed through processes that exhibit fundamental control over the physical and chemical attributes of molecular-scale structures;
- they can be combined to form larger structure

Nanostructured materials are able to access to new ranges of electronic, magnetic, mechanical or optical properties. For example polycrystalline materials with grain sizes less than a few nanometres exhibit different properties because they are relatively highly affected by the grain boundaries.[233]

Since nanotechnology exploits nanoparticles, problems can actually arise from the exposure to these particles from people who are handling these, due to their small size. Moreover, nanotechnologies are very expensive, indeed they are usually characterized by expensive raw materials and manufacturing processes. As advantages, the technology can actually revolutionize electronic products, procedures, and applications. In this field, the areas that benefit from nanotechnology development are electronic products including nano-transistors, nano-diodes, organic light-emitting diode (OLED), plasma displays and quantum computers. Nanotechnology can also benefit the energy sector, such as energy-producing, energy-absorbing and energy storage products, like batteries, fuel cells, and solar cells, which could be built smaller and made to be more effective thanks to this technology. Another industrial field that can benefit from nanotechnology

[232] A.G. Mamalis *et al.*, Nanotechnology and nanostructured materials: trends in carbon nanotubes. Precision Engineering 28 (2004) 16–30

[233] Ibidem

is the manufacturing sector that will need materials like nanotubes, aerogels, nanoparticles, and other similar items to produce their high performances products with. These materials are often stronger, more durable, and lighter than those that are not produced with the aid of nanotechnology. Nanotechnology in medicine is now focusing on areas like tissue regeneration, bone repair, immunity and even cures for such ailments like cancer, diabetes, and other life threatening diseases.[234, 235]

In this work, advanced composites utilizing aligned carbon nanotubes (CNTs) in various morphologies are being developed for enhancing laminate-level multifunctional properties. Since their identification, CNTs have been envisioned as a constituent in various applications due to their numerous and attractive multifunctional properties, both mechanical and non-mechanical. Many of CNTs mechanical properties are unrivaled by any other material, especially when the properties are normalized to density. This, together with their small scale and possibly defect-free structure makes them an attractive material for aerospace applications. The most common approach to exploit the attractive properties of CNTs is the combination of CNTs with polymers to create polymer nanocomposites (PNCs). Some produced nanocomposites take full advantage of CNT properties at engineering-relevant length scales due to synthesis and fabrication issues.[236]

3.1.1. Carbon and Carbon Nanotubes

Carbon is one of the most versatile elements on the periodic table thanks to number of compounds, which it might form, that are virtually an infinite number. It depends on both bond types, and the number of different elements which it could bond to. Carbon forms single, double or triple bonds. It assumes many structural forms because a carbon atom can form several distinct types of valence bonds, where the chemical bonds refer to the hybridization of orbitals. Thus, carbon-based materials clusters and molecules are found in variety of forms such as graphite, diamond, carbon fibers, fullerenes, and carbon nanotubes.[237]

Hybridization lies in mixing two or more pure atomic orbitals of an atom with almost same energy to form same number of identical and degenerate hybrid orbitals, which are suitable for the qualitative description of atomic bonding properties.[238] The new orbitals

---

234 http://en.wikipedia.org/wiki/Nanotechnology

235 http://nanogloss.com

236 E.J. Garcia *et al.*, Fabrication and Multifunctional Properties of High Volume Fraction Aligned Carbon Nanotube Thermoset Composites, Journal of Nano System and Technology 1 (2009) 1-11.

237 R Saito *et al.*, Physical Properties of Carbon Nanotube, Imperial College Press, London (1998) ISBN 978-1860942235

238 http://en.wikipedia.org/wiki/Orbital_hybridisation

formed are also known as hybrid orbitals. Hybridization is a transformation of some orbitals during formation of covalent bonds enabling more effective overlapping of orbitals. [239] Valence shell electron pair repulsion (VSEPR) rules are a model in chemistry used to predict the shape of individual molecules based upon the extent of electron-pair electrostatic repulsion[240]. In this model, atoms and pairs of electrons will be arranged to minimize the repulsion of these atoms and pairs of electrons. The introduction of hybridization theory is a consequence of good results, which have been obtained to forecast molecule geometry of this theory. Hybridization was introduced by Linus Pauling to improve valence bond theory, which was proposed by Heitler and London to explain the formation of covalent bond quantitatively using quantum mechanics. [241] Valence bond theory describes a chemical bond as the overlap of atomic orbitals. Attraction increases as the distance between the atoms gets closer but nuclear-nuclear repulsion becomes important if the atoms approach too close. The hybridization of atomic orbitals is a mathematical concept based on quantum mechanics. During this process, the wave functions, Ψ, of atomic orbitals of same atom are combined to give new wave functions corresponding to hybrid orbitals.

Each carbon atom has six electrons which occupy $1s^2$, $2s^2$, and $2p^2$ atomic orbitals. The $1s^2$ orbital contains two strongly bound electrons, and they are called core electrons. Four electrons occupy the $2s^2$ and $2p^2$ orbitals, and these more weakly bound electrons are called valence electrons. Carbon has been characterized by three hybridizations: sp, sp^2 and sp^3; other group IV elements such as Si, Ge exhibit primarily sp^3 hybridization. Carbon differs from Si and Ge insofar as carbon does not have inner atomic orbitals except for the spherical 1s orbital, and the absence of nearby inner orbital facilitates hybridizations involving only valence s and p orbitals for carbon[242]. In the crystalline phase the valence electrons give rise to 2s, $2p_x$, $2p_y$ and $2p_z$ orbitals which are important for forming covalent bonds in carbon materials. Since the energy difference between the upper 2p energy levels and the lower 2s level in carbon is small compared with the binding energy of the chemical bonds, the electronic wave functions for these four electrons can readily mix with each other, thereby changing the occupation of the 2s and three 2p atomic orbitals so as to enhance the binding energy of the C atom with its neighbouring atoms. The sp^n hybridization is necessary for determining the dimensionality of not only carbon-based molecules, but also carbon-based solids. Carbon

239 school-sector.relarn.ru/nsm/chemistry//Enu/Data
240 http://en.wikipedia.org/wiki/VSEPR_theory
241 http://en.wikipedia.org/wiki/Valence_bond_theory
242 R. Saito *et al*., Physical Properties of Carbon Nanotube, Imperial College Press, London (1998) ISBN 978-1860942235

is the only element in the periodic table that has isomers from 0 dimensions (OD) to 3 dimensions (3D).[243]

In sp^n hybridization, (n + 1) σ bonds per carbon atom are formed, these σ bonds making a skeleton for the local structure of the n-dimensional structure. In sp hybridization, two σ bonds make only a one-dimensional chain structure, which is known as a 'carbyne' (i.e. a monovalent carbon radical species consisting of an electrically neutral univalent carbon atom with three non-bonded electrons[244]). A three-dimensional solid is formed by gathering these carbyne chains. In sp^3 hybridization, four σ bonds defining a regular tetrahedron are enough to form a three-dimensional structure known as the diamond structure. It is interesting that sp^2 hybridization which forms a planar structure in two-dimensional graphite also forms a planar local structure in the closed polyhedra (0-dimensional) of the fullerene family and in the cylinders (1-dimensional) called carbon nanotubes. Closely related to carbon nanotubes are carbon fibers which are macroscopic one-dimensional materials, because of their characteristic high length to diameter ratio. A carbon fiber, however, consists of many graphitic planes and microscopically exhibits electronic properties that are predominantly two-dimensional.

Amorphous carbon is a disordered, three-dimensional material in which sp^2 and sp^3 hybridization are both present, randomly. Amorphous graphite, which consists mainly of sp^2 hybridization, is a graphite with random stacking of graphitic layer segments. Because of the weak interplanar interaction between two graphitic planes, these planes can move easily relative to each other, thereby forming a solid lubricant. In this sense, amorphous graphite can behave like a two-dimensional material. Under ambient conditions and in bulk form, the graphite phase with strong in-plane trigonal bonding is the stable phase, as indicated by the phase diagram of Figure 3.1–1. Under the application of high pressure and high temperature (both of which are somewhat reduced when catalyst particles like iron or nickel are used), transformation to the diamond structure takes place. Once the pressure is released, diamond remains essentially stable under ambient conditions although, in principle, it will very slowly transform back to the thermodynamically stable form of solid carbon, which is graphite. When exposed to various perturbations, such as irradiation and heat, diamond will quickly transform back to the equilibrium graphite phase.[245]

---

243 R. Saito *et al.*, Physical Properties of Carbon Nanotube, Imperial College Press, London (1998) ISBN 978-1860942235

244 http://en.wikipedia.org/wiki/Carbyne

245 R. Saito *et al.*, Physical Properties of Carbon Nanotube, Imperial College Press, London (1998) ISBN 978-1860942235

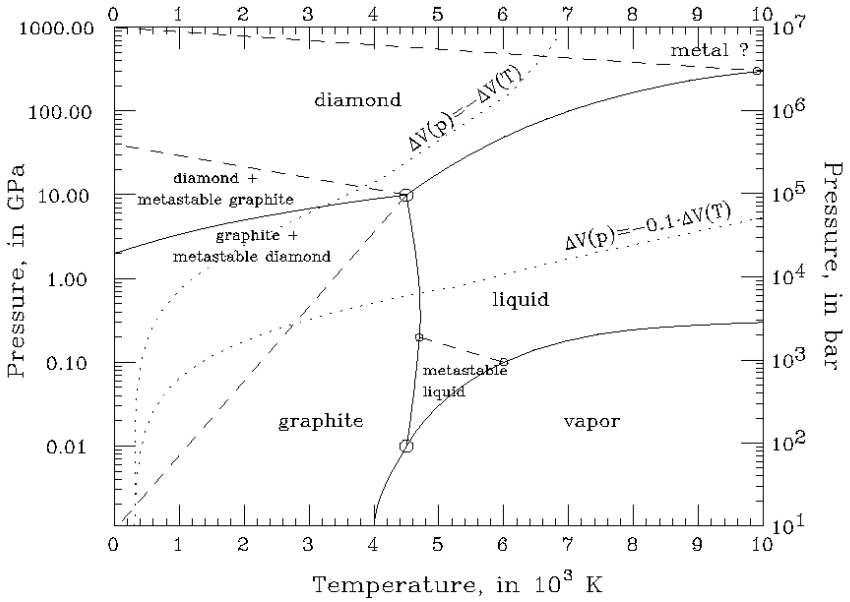

Figure 3.1–1: Carbon phase diagram[246]

In 1952, scientists discovered and described unusual carbon structures, known today as carbon nanotubes (CNTs).[247] Nanotubes belong to a promising group of nanostructured materials. Although other nanotubes based on boron nitride and molybdenum have been reported, currently carbon nanotubes are by far the most important group. These tubes contain one or several concentric graphite-like layers with diameters in the range of 0.4 nm up to tens of nanometres.[248]

Although carbon nanotubes (CNTs) were first observed at least 60 years ago, Iijima's report in 1991 triggered enormous world-wide interest in these archetypical nanomaterials.[249] Carbon nanotubes have received an increasing scientific interest due to their exceptional mechanical, thermal, electrical and various physical and chemical properties. [250,251,252] These properties exceed those of any previously existing materials.[253]

---

246 J.M. Zazula, On Graphite Transformations at High Temperature and Pressure Induced by Absorption of the LHC Beam, LHC Project Note 78 / 97 January 18, 1997

247 A.R. Boccaccini *et al.*, Electrophoretic deposition of carbon nanotubes, Carbon 44 (2006) 3149–3160

248 A.G. Mamalis *et al.*, Nanotechnology and nanostructured materials: trends in carbon nanotubes. Precision Engineering 28 (2004) 16–30

249 A.R. Boccaccini *et al.*, Electrophoretic deposition of carbon nanotubes, Carbon 44 (2006) 3149–3160

250 L.H. Chen *et al.*, Growth of aligned carbon nanotubes on carbon microfibers by dc plasma-enhanced chemical vapor deposition, Applied Physics Letters 88 (2006) 033103-1-3

251 K. Tanaka, T. Yamabe, Fukui K. The Science and Technology of Carbon Nanotubes, Chapter 2 M. YUMURA Synthesis and Purification of Multi-Walled and Single-Walled Carbon Nanotubes, Elsevier, 1999 ISBN: 0080426964

252 M. Houlle *et al.*, Mechanical enhancement of C/C composites via the formation of a machinable carbon nanofiber interphase, Carbon 46 (2008) 76 –83

253 A.R. Boccaccini *et al*. Electrophoretic deposition of carbon nanotube Carbon 44 (2006) 3149–3160

3.1.1.1. Carbon Nanotube properties and characteristics

CNTs can be described as rolled-up sheets of graphite, with the carbon atoms arranged in a honeycomb-like hexagonal structure. These hollow graphene cylinders can be open-ended or closed with a hemispherical structure, such as fullerene. [254] Nanotubes are long, slender fullerenes where the walls of the tubes are hexagonal carbon (graphite structure) and often capped at each end. These cage-like forms of carbon have been shown to exhibit exceptional material properties that are a consequence of their symmetric structure.[255] Carbon nanotubes have been shown to possess exceptional stiffness and strength, extraordinary resilience, remarkable thermal and electrical properties, and low density[256]. The properties of nanotubes depend on the helicity (the orientation between the graphitic hexagons and the nanotube axis), the diameter and length of the tubes, and the crystalline quality. Many of the remarkable properties of CNTs are now well established and their exploitation in a wide range of applications forms a major part of current research and development efforts.[257]

Carbon nanotubes are classified as single-wall (SWCNTs) or multi-wall (MWCNTs) carbon nanotube (Figure 3.1–2), it depends on the number of graphene sheets which constitute them.[258]

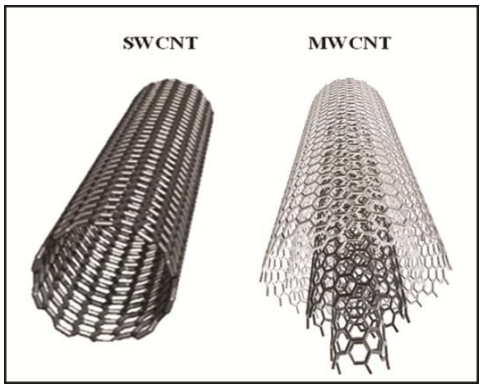

Figure 3.1–2: SWCNT and MWCNT [259]

[254] V.I. Alexiadis *et al.,* Influence of the composition of Fe_2O_3/Al_2O_3 catalysts on the rate of production and quality of carbon nanotubes, Materials Chemistry and Physics 128 (2011) 96–108

[255] E.T. Thostenson, Zhifeng Ren, Tsu-Wei Chou, Composites Science and Technology 61 (2001) 1899–1912

[256] E.T Thostenson *et al.*,Carbon Nanotube carbon fiber hybrid multiscale composites, Journal of Applied Physics 91 (2002) 6034-6037

[257] A.R. Boccaccini *et al*., Electrophoretic deposition of carbon nanotubes, Carbon 44 (2006) 3149–3160

[258] V.I. Alexiadis *et al.,* Influence of the composition of Fe_2O_3/Al_2O_3 catalysts on the rate of production and quality of carbon nanotubes, Materials Chemistry and Physics 128 (2011) 96–108

[259] V. Choudhary, A. Gupta, Carbon Nanotubes - Polymer Nanocomposites, Chapter Polymer/Carbon Nanotube Nanocomposites Centre for Polymer Science and Engineering Indian Institute of Technology Delhi, India ISBN: 978-953-307-498-6

A single-wall carbon nanotube (SWCNTs) can be described as layer of the hexagonal graphite lattice rolled into a cylindrical shape so that the structure is one-dimensional with axial symmetry, and in general exhibiting a spiral conformation, called chirality, which is given by a single vector called the chiral vector[260]. As synthesized, CNTs are capped at their ends by half of a fullerene-like structure. A single-wall nanotube is defined by a cylindrical graphene sheet with a diameter of lower than 2 nm. If we neglect the two ends of a carbon nanotube and focus on the large aspect ratio of the cylinder, for example length/diameter ratio valuated as large as 10^4-10^5, these nanotubes can be considered as one-dimensional nanostructures.[261] A concentric arrangement of a number of graphitic cylinders (2 to 30) is termed a multi-walled carbon nanotube (MWCNT) (Figure 3.1–2) and diameters can reach from 10 to 50 nm and length of more than 10 μm. These concentric tubes are held together by Van der Waals bonding between the layers, which are separated by approximately 0.34 nm. As the diameter increases, at some point the perfect cylindrical structure is lost and the structure becomes more similar to a vapour-grown carbon fiber. On the other hand, SWCNT is much thinner with the diameters from 1.0 to 1.4 nm.[262] Figure 3.1–3 shows the terminations of three different nanotubes. The terminations are often called caps or end caps and consist of a “hemisphere” of a fullerene. Each cap contains six pentagons and an appropriate number and placement of hexagons that are selected to fit perfectly to the long cylindrical section. From Figure 3.1–3 it can be seen that the orientation of the six-member ring in the honeycomb lattice relative to the axis of the nanotube can be taken almost arbitrarily.

260 R Saito *et al.*, Physical Properties of Carbon Nanotube, Imperial College Press, London (1998) ISBN 978-1860942235

261 L. Qu, Y. Zhao, L. Dai, Carbon microfibers sheathed with aligned carbon nanotubes: Towards multidimensional, multicomponent, and multifunctional nanomaterials, Small 2 (2006) 1052–1059

262 K. Tanaka, T. Yamabe, K. Fukui, The Science and Technology of Carbon Nanotubes, Chapter 2 M. YUMURA Synthesis and Purification of Multi-Walled and Single-Walled Carbon Nanotubes, Elsevier, 1999 ISBN: 0080426964

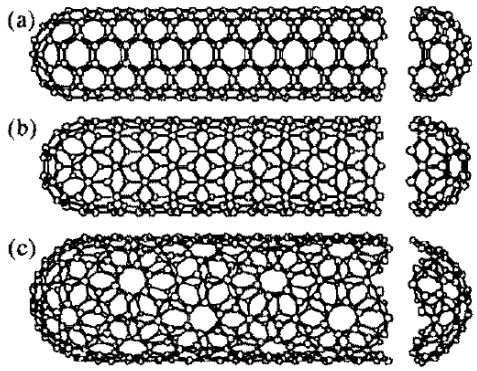

Figure 3.1–3: Classification of carbon nanotubes: (a) armchair, (b) zigzag, and (c) chiral nanotubes. [263]

The elongated shape and nanoscale dimension combined with extraordinary mechanical, electrical and thermal properties enable to design novel nano-devices and nano-composite materials. The extraordinary properties of CNTs have been described in several papers. [264,265,266,267,268,269,270,271]

Theoretical and experimental results show extremely high elastic modulus, greater than 1 TPa, reported strengths 10–100 times higher than the strongest steel at a fraction of the weight but their density is six-times lower. [272,273] The stiffness of CNTs was first determined by observing the amplitude of thermal vibrations in transmission electron microscopy (TEM) and the average stiffness values of 1.8 TPa and 1.25 TPa were reported for MWCNTs and SWCNTs, respectively. The in-situ tensile tests on individual MWCNTs and ropes of SWCNTs was performed by carrying out a stress-strain

---

263 M. Mir, A. Hosseini, G.H. Majzoob, A numerical study of vibrational properties of single-walled carbon nanotubes, Computational Materials Science 43 (2008) 540–548

264 K.L. Kepple *et al.*, Improved fracture toughness of carbon fiber composite functionalized with multi walled carbon nanotubes, Carbon 46 (2008) 2026 –2033

265 E.T. Thostenson, Z. Ren, T.W. Chou, Composites Science and Technology 61 (2001) 1899–1912

266 V. Choudhary, A. Gupta, Carbon Nanotubes - Polymer Nanocomposites, Chapter Polymer/Carbon Nanotube Nanocomposites Centre for Polymer Science and Engineering Indian Institute of Technology Delhi, India ISBN: 978-953-307-498-6

267 K.L. Kepple *et al.*, Improved fracture toughness of carbon fiber composite functionalized with multi walled carbon nanotubes, Carbon 46 (2008) 2026 –2033

268 E.J. Garcıa *et al.*, Fabrication of composite microstructures by capillarity-driven wetting of aligned carbon nanotubes with polymers." Nanotechnology, 18 (2007) 165602-165612

269 V. Choudhary, A. Gupta, Carbon Nanotubes - Polymer Nanocomposites, Chapter Polymer/Carbon Nanotube Nanocomposites Centre for Polymer Science and Engineering Indian Institute of Technology Delhi, India ISBN: 978-953-307-498-6

270 E.T. Thostenson, Zhifeng Ren, Tsu-Wei Chou, Composites Science and Technology 61 (2001) 1899–1912

271 V. Choudhary, A. Gupta, Carbon Nanotubes - Polymer Nanocomposites, Chapter Polymer/Carbon Nanotube Nanocomposites Centre for Polymer Science and Engineering Indian Institute of Technology Delhi, India ISBN: 978-953-307-498-6

272 K.L. Kepple *et al.*, Improved fracture toughness of carbon fiber composite functionalized with multi walled carbon nanotubes, Carbon 46 (2008) 2026 –2033

273 E.T. Thostenson, Zhifeng Ren, Tsu-Wei Chou, Composites Science and Technology 61 (2001) 1899–1912

measurement using a nanostressing stage operating inside a scanning electron microscope (SEM). Strength of MWCNT outer shell ranged from 11 to 63 GPa at fracture strains of up to 12% and modulus values varied from 270 to 950 GPa. It was observed that strength of nanotubes depends on the number of defects, as well as interlayer interactions in MWCNTs and bundles of SWCNTs. Structural defects as well as bends or twists significantly affect mechanical strength of CNTs.[274] Although reported mechanical properties [275,276] are accurate, carbon nanotubes may result in an entire new class of advanced materials, thanks to the ability to possess a very high aspect ratio while maintaining extraordinary strength and stiffness. Indeed carbon nanotube due to exceptional high aspect ratio, length can exceed 1 mm and tube diameter is on nanometre scale. This, combined with specific stiffness and strength, makes them ideal as composite reinforcement. [277]

CNTs present high thermal conductivity of approximately 6000 W/mK, that is about twice than diamond and implying that only a small amount of CNTs is required to significantly alter the materials thermal properties. [278]

Theoretical studies of the electronic properties of SWCNTs, suggest that nanotube shells can be either metallic or semiconducting, depending critically on helicity.[279] The room temperature electrical conductivity of metallic SWCNT was found to be 10^5 to 10^6 S/m and for semiconducting tubes about 10 S/m. The conductivity of SWCNT is close to the in-plane conductivity of graphite (10^5 to 10^6 S/m). Conductivities of individual MWCNTs have been reported in the range of 10^7 to 10^8 S/m, depending on the helicities of the outermost shells or the presence of defects. The axial thermal conductivity of individual, perfect CNTs is reported to be as high as 3300 W/mK[280]. CNTs are thermally stable up to 2800 °C in vacuum while maintaining their electrical conductivity about 1000

274 V. Choudhary, A. Gupta, Carbon Nanotubes - Polymer Nanocomposites, Chapter Polymer/Carbon Nanotube Nanocomposites Centre for Polymer Science and Engineering Indian Institute of Technology Delhi, India ISBN: 978-953-307-498-6

275 K.L. Kepple *et al.*, Improved fracture toughness of carbon fiber composite functionalized with multi walled carbon nanotubes, Carbon 46 (2008) 2026 –2033

276 E.T. Thostenson, Zhifeng Ren, Tsu-Wei Chou, Composites Science and Technology 61 (2001) 1899–1912

277 E.T. Thostenson *et al.*,Carbon Nanotube/carbon fiber hybrid multiscale composites, Journal of Applied Physics, 91 (2002) 6034-6037

278 K.L. Kepple *et al.*, Improved fracture toughness of carbon fiber composite functionalized with multi walled carbon nanotubes, Carbon 46 (2008) 2026 –2033

279 V. Choudhary, A. Gupta, Carbon Nanotubes - Polymer Nanocomposites, Chapter Polymer/Carbon Nanotube Nanocomposites Centre for Polymer Science and Engineering Indian Institute of Technology Delhi, India ISBN: 978-953-307-498-6

280 Ibidem

times than copper wires[281] and they show an high capacity for carrying electrical current.[282,283]

With the recent developments in nanoscience and nanotechnology, a large variety of single-component nanomaterials (e.g., carbon nanotubes, nanoparticle quantum dots) and devices have been reported. Owing to their unique one-dimensional electronic structure, carbon nanotubes (CNTs) offer particular advantages as molecular wires for the development of nanotube nano-devices, including nanotube sensors and other optoelectronic systems.[284]

The exceptional properties of carbon nanotube [285,286] have been investigated for devices such as field-emission displays[287], nanoelectronic devices, catalyst supports, storage materials for hydrogen and other gases and probe tips for atomic force microscope AFM scanning probe microscopy tips. While there are a very large number of publications on nanotube growth and their applications, engineering the shape of CNTs is an important issue for successful applications of nanotubes.[288,289] Thanks to their excellent electrical properties, high specific surface area and chemical inertness, carbon nanotubes have been exploited to improve properties, such as high electric-field concentration and where a large surface area is desirable as in catalytic reactions, such as fuel cell or battery applications (such as Li ion batteries), of electrode materials in a variety of application, such as fuel cells and biosensors.[290,291] field emission devices, supercapacitors, and biosensors[292]

Carbon nanotubes (CNTs) are also thought to be promising candidates for selective reinforcement of matrix-rich interlaminar regions of composites due to their nanoscale diameter, high aspect ratios and desirable mechanical, electrical, and thermal properties. These same attributes are also useful for the modification of interfacial properties. When

---

281 E.T. Thostenson, Zhifeng Ren, Tsu-Wei Chou, Composites Science and Technology 61 (2001) 1899–1912

282 K.L. Kepple *et al.*, Improved fracture toughness of carbon fiber composite functionalized with multi walled carbon nanotubes, Carbon 46 (2008) 2026 –2033

283 E.J. Garcıa *et al.*, Fabrication of composite microstructures by capillarity-driven wetting of aligned carbon nanotubes with polymers. Nanotechnology, 18 (2007) 165602-165612

284 L. Qu, Y. Zhao, L. Dai, Carbon microfibers sheathed with aligned carbon nanotubes: Towards multidimensional, multicomponent, and multifunctional nanomaterials, Small 2 (2006) 1052–1059

285 E.T. Thostenson, Zhifeng Ren, Tsu-Wei Chou, Composites Science and Technology 61 (2001) 1899–1912

286 Y. Luo et al., Fabrication of high-quality carbon nanotube fibers for optoelectronic applications Solar Energy Materials & Solar Cells 97 (2012) 78–82

287 E.T. Thostenson, Zhifeng Ren, Tsu-Wei Chou, Composites Science and Technology 61 (2001) 1899–1912

288 Ibidem

289 L.H. Chen *et al.*, Growth of aligned carbon nanotubes on carbon microfibers by dc plasma-enhanced chemical vapor deposition, Applied Physics Letters 88 (2006) 033103-033106

290 Ibidem

291 H.S. Kim *et al.*, Synthesis of Aligned Few-Walled Carbon Nanotubes on Conductive Substrates, J. Phys. Chem. C, Letters 113 (2009) 17983–17988

292 A. Magrez *et al.*, Striking Influence of the Catalyst Support and Its Acid–Base Properties: New Insight into the Growth Mechanism of Carbon Nanotubes, *ACS* Nano, 5 (2011) 3428–3437

properly designed, carbon nanotubes have the potential to work with carbon fiber to make multifunctional, lightweight structural composites with superior strength. Growth of CNTs at the surface of carbon fibers to create hierarchical carbon structures is a promising approach for improving mechanical, electrical and thermal properties of a structural composite (traditionally, these systems have excellent in-plane two dimensional (2D) properties but poor interlaminar properties.[293]

The scientific interest of carbon nanotube was also focalized on their homologue, carbon nanofibers, according to their similarities. Moreover, if CNTs were combined with other materials to form composites, it is generally important to develop processing methods that disperses the CNTs homogeneously in the appropriate polymer, ceramic or metallic matrix.[294]

Thanks to these unique properties, both multi walled CNTs (MWCNT) and single walled CNTs (SWCNT) could be exploited to create a composite. One area of interest is CNT as reinforcement of woven carbon fiber (CF) laminar composite systems. CF is an optimal substrate for CNT reinforcement because it is strong, low density, and can withstand the extreme temperatures used in growing CNTs. These characteristics make these two materials excellent for lightweight reinforcement for numerous applications ranging from aerospace to high performance automotive.[295] Recently, attention has been paid also to biomedical applications of functionalized CNTs, which have shown real promise as highly accurate vehicles for delivering antitumor agents into malignant cells. Cells have been shown to grow on carbon nanotubes, thus they appear to have no toxic effect. The cells do not adhere to the carbon nanotubes, potentially giving rise to applications such as coatings for prosthetics and anti-fouling coatings for ships. The ability to chemically modify the sidewalls of carbon nanotubes also lead to biomedical applications such as vascular stents, as well as neuron growth and regeneration.[296]

3.1.2. Polymer Nano Composites

The unique structure of CNTs and the resulting exceptional electrical, thermal and mechanical properties have made them ideal reinforcement materials for the next generation of multifunctional high performance nanocomposites. Efforts are focused on

---

293 K.L. Kepple, G.P. Sanborn, P.A. Lacasse, K.M. Gruenberg, W.J. Readyd, CARBON 46 (2008) 2026 –203

294 A.R. Boccaccini *et al.*, Electrophoretic deposition of carbon nanotubes, Carbon 44 (2006) 3149–3160

295 K.L. Kepple *et al.*, Improved fracture toughness of carbon fiber composite functionalized with multi walled carbon nanotubes, Carbon 46 (2008) 2026 –2033

296 V.I. Alexiadis *et al.,* Influence of the composition of Fe_2O_3/Al_2O_3 catalysts on the rate of production and quality of carbon nanotubes, Materials Chemistry and Physics 128 (2011) 96–108

using CNTs as improved carbon fiber replacements, where enhancement in mechanical properties of the composite can be achieved with exceptionally low loadings. [297]

In order to exploit CNTs and their extraordinary properties in real-world applications, CNT/polymer nanocomposites were developed.

Currently, polymer composite is the biggest application area for CNTs. These nanocomposites are being utilized in different fields including transportation, automotive, aerospace, defense, sporting goods, energy and infrastructure sectors. Such wide range applications of these materials are due to their high durability, high strength, low density, design and process flexibility. CNT/polymer nanocomposites are also used as electrostatic discharge (ESD) and electromagnetic interference (EMI) shielding material because of their high electrical conductivity. However, the effective application of CNTs for fabricating nanocomposites strongly depends on the homogeneous dispersion of CNTs throughout the matrix without destroying their integrity. Furthermore, good interfacial bonding is also required to achieve significant load transfer across the CNT–matrix interface, a necessary condition for improving the mechanical properties of composites. So it is very important to achieve high degree of CNT dispersion during processing without affecting its property. In the following section we will discuss about the different processing techniques and properties of CNT/polymer nanocomposite. [298]

Polymer nanocomposites (PNC) are polymers (thermoplastics, thermosets or elastomers) that have been reinforced with small quantities (less than 5% by weight) of nano-sized particles having high aspect ratios (L/h > 300). PNCs represent a radical alternative to conventional filled polymers or polymer blends – a staple of the modern plastics industry. In contrast to conventional composites, where the reinforcement is on the order of microns, PNCs are exemplified by discrete constituents on the order of a few nanometers. PNC technology has several peculiarity as mechanical enhancement of the neat resin, the direct replacement of current filler, the capability to provide value-added properties not present in the neat resin, without sacrificing the resin's inherent, nor adding excessive weight. As a matter of facts, PNCs contain substantially less filler and thus enable greater retention of the inherent ability of the neat resin to be processed, as well as its toughness. [299]

Today, nanocomposites are really nanofilled plastics, where the total internal interfacial area becomes the critical characteristic rather than simply the relative volume

---

297 K.S. Coleman, Nanotubes, Annu. Rep. Prog. Chem., Sect. A: Inorg. Chem., 104 (2008) 379-393

298 V. Choudhary, A. Gupta, Carbon Nanotubes - Polymer Nanocomposites, Chapter Polymer/Carbon Nanotube Nanocomposites Centre for Polymer Science and Engineering Indian Institute of Technology Delhi, India ISBN: 978-953-307-498-6

299 W. Gacitua E., A. Ballerini A., J. Zhang, Polymer Nanocomposites: Synthetic and Natural Fillers: a Review, Maderas.Ciencia y tecnologia, 7 (2005) 159-178

fraction of constituents. The use of the moniker nano-'composites' invokes parallels to traditional fiber-reinforced composite technology and the ability to spatially 'engineer, design, and tailor' materials performance for a given application. Currently, the realization of 'compositing' PNCs is over the horizon. For the vast majority of investigations, the challenge is still to achieve single-particle dispersions and the subsequent PNCs are treated much as an isotropic, filled polymer. [300]

Development of PNCs, as with any multicomponent material, must simultaneously balance four interdependent areas: constituent selection, cost-effective processing, fabrication and performance.[301]

Figure 3.1–4 shows a schematic comparison between macro and micro composite, the former containing 1 µm x 25 µm (x L) fibers in an amorphous matrix, the latter containing 1 nm x 25 nm fibers at the same volume fraction of filler. Scanning electron micrograph in the figure shows E-glass reinforced polyolefin (15 µm fiber) and transmission electron micrograph shows montmorillonite-epoxy nanocomposite (1 nm thick layers).

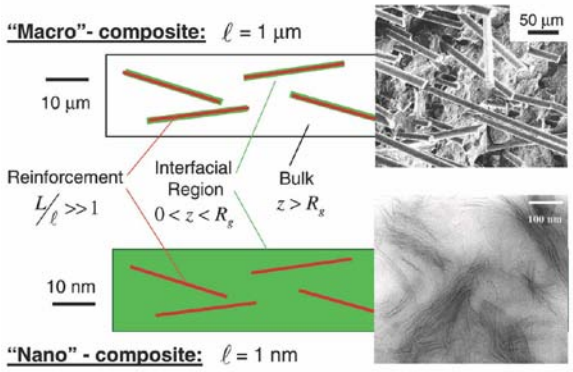

Figure 3.1–4: Schematic comparison of a 'macro'-composite and 'nano'-composite at the same volume fraction of filler, but containing 1 nm x 25 nm fibers. There are three main material constituents in any composite: the matrix (white), the reinforcement (fiber, red), and the so-called interfacial region (green), which extends (z) into the matrix on the order of Rg, the radius of gyration of the polymer.[302]

[300] E.J. Garcia *et al.*, Fabrication and multifunctional properties of a hybrid laminate with aligned carbon nanotubes grown In Situ, Composites Science and Technology 68 (2008) 2034–2041

[301] R.A. Vaia, H.D. Wagner, Framework for nanocomposites, Materials Today (Oxford, United Kingdom) 7 (2004) 32-37

[302] R.A. Vaia, H.D. Wagner, Framework for nanocomposites, Materials Today (Oxford, United Kingdom) 7 (2004) 32-37

3.1.2.1. Polymer-based nanocomposites reinforced with CNTs

Polymer-based nanocomposites have been pursued in recent years to harness the attractive properties of carbon nanotubes (CNTs). Hybrid advanced composite material system exhibits enhanced multifunctional laminate-level engineering properties. The hybrid system (Figure 3.1–5) is comprised of three parts: advanced fibers (diameter of order microns) organized in tows and woven, a thermoset polymer resin, and dense aligned CNTs (diameter of order nanometres) organized within the polymeric matrix. [303]

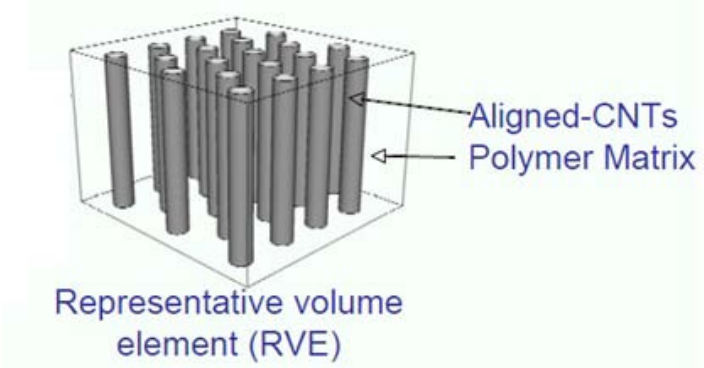

Figure 3.1–5: CNT alignment and spacing in the RVE (Representative Volume Element) are idealized [304]

In this case, the aligned-CNT polymeric nanocomposite is part of a larger microstructural description of the hybrid nano-engineered composite laminate. Similar to existing advanced composites, the ideal PNC has high volume fraction (V_f) of aligned, continuous, high-quality CNTs homogeneously dispersed in a surrounding matrix with no voids (i.e. the composite is simply aligned-CNTs and matrix). In advanced composite materials (e.g. carbon fiber reinforced plastics, CFRP), high fiber volume fraction allows the properties of the advanced fibers to dominate the composite properties, while the matrix provides support (e.g. from buckling under shear or compression), protection, and a path for load-sharing between the fibers. The ideal nanocomposite morphology likely looks similar, with the CNTs replacing the micron-diameter fibers as the reinforcement. The effect of CNT alignment on nanocomposite mechanical properties is significant (220% vs. <100% Young's Module increasing)[305]. Hence, most of the work on CNT-based composites presented in the literature to date focuses on using CNTs as a reinforcement, or as a filler, in a polymeric matrix by dispersing and perhaps subsequently aligning

[303] E.J. Garcia *et al.*, Fabrication and multifunctional properties of a hybrid laminate with aligned carbon nanotubes grown In Situ, Composites Science and Technology 68 (2008) 2034–2041

[304] E.J. Garcia *et al.*, Fabrication and Multifunctional Properties of High Volume Fraction Aligned Carbon Nanotube Thermoset Composites, Journal of Nano Systems & Technology, 1 (2009) 1-11

[305] E.J. García *et al.*, Fabrication and Nanocompression Testing of Aligned Carbon-Nanotube–Polymer Nanocomposites, Adv. Mater., 19 (2007) 2151–2156

single- or multi-walled CNTs in the matrix.[306] Typical fraction volume for CNTs dispersed in polymers are only a few percent and dispersion of the CNTs is difficult to achieve. [307] Hybrid composite developed by Wardle's group [308] shows CNTs organized (Figure 3.1–6) radially around the existing micron-size fibers, and the polymeric matrix binds all the filaments, advanced fibers and CNTs together. The alignment and dispersion of CNTs within the dense array of woven tows and fibers in the cloth material is achieved by radial in situ growth of CNTs from the surface of the woven fibers. The CNTs reinforce the polymer matrix in the space between the advanced fibers, so as to provide enhanced strength and toughness as well as an electrically conductive pathway. The resulting laminated structure is described as a hybrid advanced composite laminate, rather than as a nanocomposite, but it is perhaps best described as a radially aligned CNT fiber reinforced plastic (ACNT-FRPs), or more succinctly 'fuzzy' fiber reinforced plastic (FFRP). Alignment, dispersion, and adhesion of CNTs in polymer matrices are critical for structural composite applications. To disperse CNTs in polymers show difficulties when CNT-modified matrices are introduced into typical aligned-fiber advanced composites, where the CNT containing matrix must effectively impregnate a high volume fraction (V_f) of advanced fibers. Due to issues such as agglomeration and poor dispersion, only marginal mechanical property improvements are observed for both nanocomposites and hybrid composites when CNTs are introduced into the bulk matrix. More success has been achieved with nanoscale modification of the interface between composite plies, by growing CNTs on the surface of cloth or placing unaligned CNTs at low Vf on fibers (including at the ply interface). The hybrid architecture above described uses a dry form of woven cloth with in situ grown aligned CNTs that are subsequently impregnated with a thermoset resin. Due to the CNT alignment and organization around the fibers, the CNTs offer both interlaminar and intralaminar modification of the composite performance. Aligned CNTs readily draw up such polymers through capillary action, and that adhesion between the CNTs and the thermosets creates an effective composite.[309] It is now well known that tangled CNTs are difficult to disperse and wet with polymers, even with improvements brought about by solvent-modified polymers and functionalized CNTs. Thus, due to the in situ growth of aligned CNTs on the fibers, the uncured polymer is drawn into the CNT-fiber dry form to create a well-consolidated composite.[310]

---

306 E.J. Garcıa *et al.*, Fabrication of composite microstructures by capillarity-driven wetting of aligned carbon nanotubes with polymers. Nanotechnology, 18 (2007) 165602-165612

307 E.J. Garcia *et al.*, Fabrication and Multifunctional Properties of High Volume Fraction Aligned Carbon Nanotube Thermoset Composites, Journal of Nano Systems & Technology, 1 (2009) 1-11

308 Ibidem

309 E.J. Garcia *et al.*, Fabrication and multifunctional properties of a hybrid laminate with aligned carbon nanotubes grown In Situ, Composites Science and Technology 68 (2008) 2034–2041

310 Ibidem

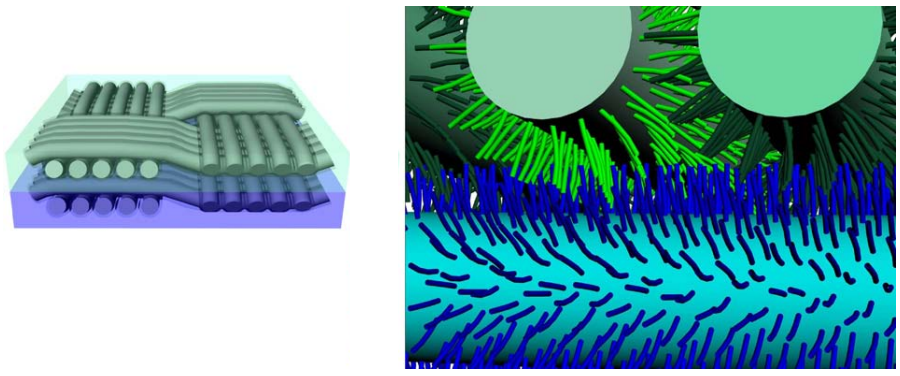

(a) (b)

Figure 3.1–6: Illustration of the hybrid composite developed by Garcia *et al.* [311]: (b) Schematic illustration of the architecture composed of a cloth containing fiber tows, covered by CNTs, in a polymer matrix. The two different plies are shown in two different colours; (b) Closer view of the interface cross-section between the two composite plies. The CNTs grown on the surface of each individual fiber interact with the CNTs of the fibers nearby, achieving reinforcement inter-tow (as in the case of the two fibers from the upper ply) and interlaminar (as in the case of CNTs from the upper and lower plies).

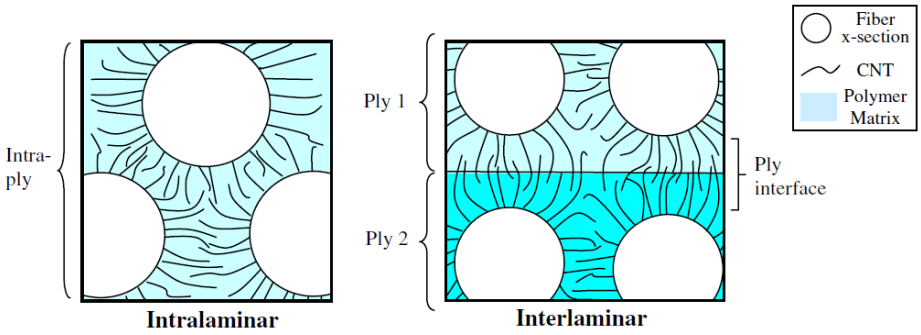

Figure 3.1–7: Illustration of intralaminar and interlaminar reinforcement from the CNTs in the hybrid composite. All dimensions approximately to scale except CNT diameter and volume fraction.[312]

Incorporation of CNT in polymer matrix resulted in a significant change in mechanical, electrical and thermal properties of polymer matrices. [313] Various factors that influence property modification are processing techniques, type of CNT, aspect ratio and CNT content. It is generally observed that a particular processing method which is good for one property may not be good for another. One such example is surface modification of

311 E E.J. Garcia *et al.*, Fabrication and multifunctional properties of a hybrid laminate with aligned carbon nanotubes grown In Situ, Composites Science and Technology 68 (2008) 2034–2041

312 Ibidem

313 V. Choudhary, A. Gupta, Carbon Nanotubes - Polymer Nanocomposites, Chapter Polymer/Carbon Nanotube Nanocomposites Centre for Polymer Science and Engineering Indian Institute of Technology Delhi, India ISBN: 978-953-307-498-6

CNT which generally enhances the mechanical properties but deteriorates the electronic properties. So it is very important to optimize the various conditions to obtain the nanocomposite with desired properties. [314]

The four most influential processing factors for the mechanical properties of the hybrid composite were identified by Thostenson *et al.*[315]: CNT length, matrix–CNT adhesion, particularly alignment and dispersion of the CNTs within the matrix. Especially alignment and dispersion are critical factors that are difficult to control experimentally using oft-repeated mixing methods. Moreover CNT quality, such as defect density, wall structure, is another important factor.[316]

Controlled growth of carbon nanotubes, both with regard to their length and diameter and alignment, is important either for potential applications or for detailed characterization of their properties. It may be a new technique to directly produce aligned and isolated CNTs by thermal decomposition of hydrocarbon gas.[317]

3.1.2.2. C/C nanocomposites reinforced with CNTs

Among the different existing hybrid composites, carbon fiber reinforced carbon matrix (C/C) composites have been widely used in many fields in the past 30 years for their excellent properties especially at high temperatures.

Carbon fibers represent an important basic material for synthesizing lightweight composite for high-performance materials. [318,319] Depending on the application fields of the material, the filling of the composite varies from polymeric to inorganic matrixes. Carbon/carbon (C/C) composites belong to the second group and consist of a fibrous carbon substrate embedded in a carbonaceous matrix. Even though the same element forms the phases and it also is a constituent, a C matrix of a C/C composite comes from two different ways both based on the carbonization of an organic solid or liquid precursor and the infiltration and densification of gaseous hydrocarbons (CH_4, C_2H_4, C_2H_2, etc.) into textured carbon support[320], but one consist of the direct infiltration of the carbon preform by a liquid precursor followed by a carbonization process, the other of the direct

[314] V. Choudhary, A. Gupta, Carbon Nanotubes - Polymer Nanocomposites, Chapter Polymer/Carbon Nanotube Nanocomposites Centre for Polymer Science and Engineering Indian Institute of Technology Delhi, India ISBN: 978-953-307-498-6

[315] E.T. Thostenson, Zhifeng Ren, Tsu-Wei Chou, Composites Science and Technology 61 (2001) 1899–1912

[316] E.J. Garcıa *et al.*, Fabrication of composite microstructures by capillarity-driven wetting of aligned carbon nanotubes with polymers. Nanotechnology, 18 (2007) 165602-165612

[317] S. Xie *et al.*, Carbon nanotubes arrays, Materials Science and Engineering A286 (2000) 11–15

[318] F. Cesano *et al.*, Connecting carbon fiber by means of catalytically grown carbon nanofilaments: formation of carbon- carbon composites, Chem. Mater. 17, (2005) 5119-5123

[319] M. Houlle *et al.*, Mechanical enhancement of C/C composites via the formation of a machinable carbon nanofiber interphase, Carbon 46 (2008) 76 –83

[320] F. Cesano *et al.*, Connecting carbon fiber by means of catalytically grown carbon nanofilaments: formation of carbon- carbon composites, Chem. Mater. 17, (2005) 5119-5123

deposition of the carbon matrix through the decomposition of gaseous hydrocarbons. The two processes generally require a high temperature treatment to generate a strong bonding between the two carbon phases. In general several cycles of treatment are necessary to obtain a dense and stable composite. The micrometric diameter of the traditional carbon fibers also reduces the efficiency of the mechanical reinforcement of the final composites, due to the low contact surface between the two phases.[321] These C/C composites find increasing uses in military and civilian applications owing to their exceptional properties. They exhibit several advantages compared to traditional composites made by powder metallurgy such as low density, high stability and high thermal conductivity. Mechanical, thermal and electrical properties of C/C composites are mainly determined by the microstructure of the pyrocarbon. Pyrocarbon exhibits various morphologies correlated to different microstructures and textures. As a result, correlated terminology that describes the morphology of pyrocarbons has developed since the 1960s.[322] The nature of the interfaces in carbon/carbon (C/C) composites and their influences on properties are extremely complex. The bonds formed between carbon fibers and matrix may be strong or weak chemical links, mechanical interlocking and friction couplings. Strong bond leads to brittle fracture of composites while weak bond would result in inefficient utilization of fiber properties.[323]

Together with carbon nanotubes, changing the reinforcement scale relative to carbon fibers offers opportunity to combine potential benefits of nanoscale reinforcement with well-established fibrous composites to create multiscale hybrid micro/nano composites. By varying the reinforcement scale, it may be possible to tailor the mechanical and physical properties of the composites.

In this work, carbon nanotubes grown on carbon fibers are used to create multiscale hybrid carbon nanotube/carbon fiber composites where individual carbon fibers, which are several microns in diameter, are surrounded by nanotubes. The subsequent inclusion of such composite fibres into a C matrix will lead to the final product, with properties suitable for highly mechanically and thermally loaded components for the automotive and aerospace sector. Hybrid composite architectures combining traditional composite materials with CNTs offer significant potential mechanical and multifunctional performance benefits. However, the properties of microscopic and macroscopic composite

---

321 M. Houlle *et al.*, Mechanical enhancement of C/C composites via the formation of a machinable carbon nanofiber interphase, Carbon 46 (2008) 76 –83

322 Q. Gong *et al.*, The effect of carbon nanotubes on the microstructure and morphology of pyrolytic carbon matrices of C–C composites obtained by CVI, Composites Science and Technology 65 (2005) 1112–1119

323 J. Zhang *et al.*, Effect of isotropic interlayers on the mechanical and thermal properties of carbon/carbon composites, Materials Letters 64 (2010) 1536–1538

structures containing CNTs have not yet approached the properties of individual CNTs, let alone those of existing fiber-reinforced polymeric composites.[324]

3.1.3. Synthesis of CNTs

The detailed mechanisms responsible for nanotube growth are not yet well understood [325]. A system must have three essential components[326] to be suitable to grow carbon nanotube: a source of carbon, a source of heat and the presence of metal catalytic particles. CNTs was firstly synthesized as a by-product in arc-discharge method in synthesis of fullerenes, which include the electric arc-discharge between two graphite electrodes (although these electric arc methods can produce gram quantity of MWCNT and SWCNT, the raw product requires rather tedious purification process[327]), but other techniques can be used, like the laser ablation of a carbon target or the catalytic decomposition of hydrocarbon.[328,329] Figure 3.1–8 shows the outlines of plasma arc discharge, pulsed laser vaporization (PLV), and chemical vapour deposition (CVD) methods experimental setups. Other new methods have been proposed such as electrolysis and solar energy methods and flame synthesis.

---

[324] E.J. Garcıa *et al.*, Fabrication of composite microstructures by capillarity-driven wetting of aligned carbon nanotubes with polymers. Nanotechnology, 18 (2007) 165602-165612

[325] R. Saito *et al.*, Physical Properties of Carbon Nanotube, Imperial College Press, London (1998) ISBN 978-1860942235

[326] W. Merchan *et al*., Combustion synthesis of carbon nanotubes and related nanostructures, Progress in Energy and Combustion Science 36 (2010) 696-727

[327] K. Tanaka, T. Yamabe, K. Fukui, The Science and Technology of Carbon Nanotubes, Chapter 2 M. YUMURA Synthesis and Purification of Multi-Walled and Single-Walled Carbon Nanotubes, Elsevier, 1999 ISBN: 0080426964

[328] Ibidem

[329] V.I. Alexiadis *et al.,* Influence of the composition of Fe_2O_3/Al_2O_3 catalysts on the rate of production and quality of carbon nanotubes, Materials Chemistry and Physics 128 (2011) 96–108

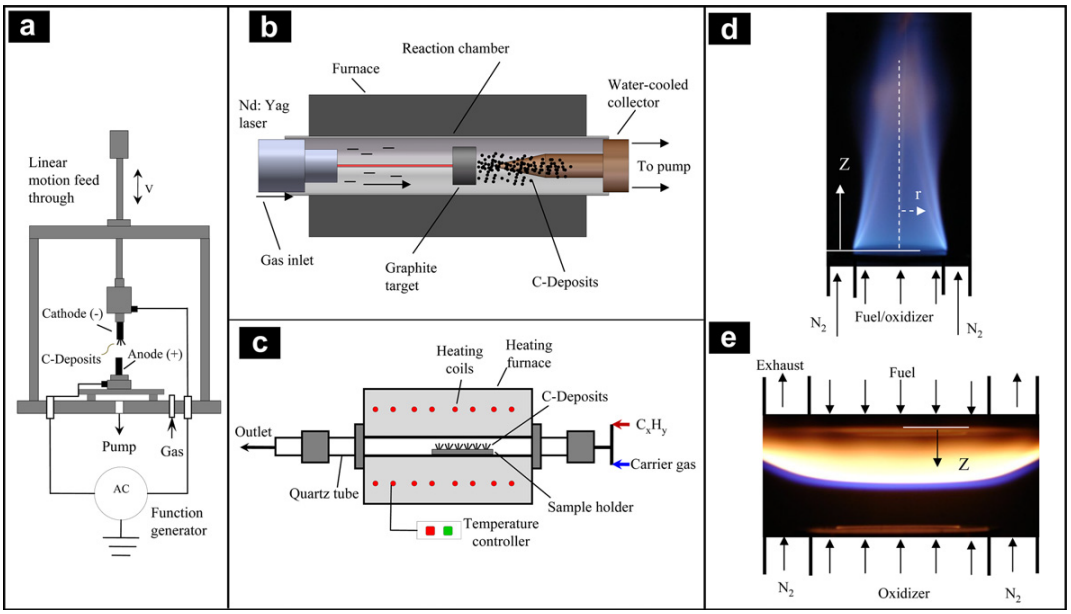

Figure 3.1–8: Methods currently applied for the growth of CNT and related carbon structures: (a) the arc-discharge method; (b) the pulsed laser vaporization method; (c) the chemical vapour deposition method, and (d and e) images of typical co- and counterflow flame methods used for CNT synthesis.[330]

3.1.3.1. Electric arc discharge

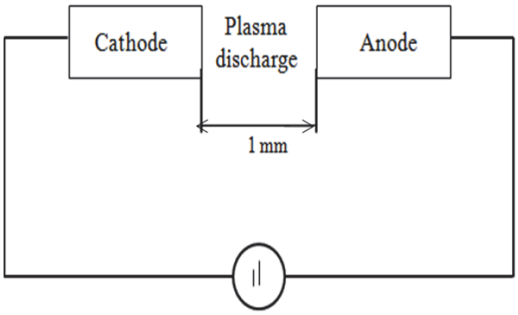

Figure 3.1–9: Arc discharge apparatus scheme [331]

When the arc-discharge is carried on, as shown in Figure 3.1–9, keeping the gap between the carbon electrodes about 1 mm, cylindrical deposit forms on the surface of the cathode. Cathode deposit diameter is the same of the anode stick. Under the conditions that diameter of the anode carbon is 8 mm with the arc-electric current of 80

330 W. Merchan *et al.*, Combustion synthesis of carbon nanotubes and related nanostructures, Progress in Energy and Combustion Science 36 (2010) 696-727

331 J. Zhao *et al.*, Continuous and low-cost synthesis of high-quality multi-walled carbon nanotubes by arc discharge in air, Physica E 44 (2012) 1639–1643

A (voltage is about 23.5 V) and He pressure of 300 Torr, the cathode deposit grows at the rate of about 2-3 mm per min. This cylindrical cathode deposit consists of two portions: an inside black fragile core and an outside hard shell. The inner core has the fabric structure growing along the length of the cathode-deposit cylinder and the inside of which includes nanotubes and polyhedral graphitic nanoparticles. The outer-shell part consists of the crystal of graphite. MWCNT grows only inside the cathode deposit and does not exist in other places in the reactor. Quantity of MWCNT obtained depends on the pressure of He atmosphere in the reactor, that is the most important parameter. The highest quantity of MWCNT is obtained when the pressure of He is about 500 Torr. When this value becomes below 100 Torr, almost no MWCNT grow. This contrasts to the highest quantity of fullerene obtained when the pressure becomes 100 Torr or less. Another important parameter is the electric current for discharge. If the current density is too high, the quantity of the hard shell increases and MWCNT decreases. To keep the arc discharge stable and the electrode cool are effective ways to increase the product quantity of MWCNT. A considerable quantity of graphite is produced in the cathode deposit even under the most suitable condition to the synthesis of MWCNT[332].

High currents in the electric arc discharge [333] method have been shown to increase the rate of production of single-walled carbon nanotubes (SWCNTs), but with lower purity.

The arc-discharge method, using nickel formate dehydrate as a catalyst precursor, has been used to selectively produce double-walled carbon nanotubes (DWCNTs) with high thermal stability[334]. Inexpensive Fe_3O_4 has been used in arc-discharge in an H_2/Ar gas atmosphere to produce SWCNTs.[335] Typically as produced samples of SWCNTs contain both metallic and semiconducting nanotubes. However, it has been suggested that the arc-in-water method under extremely low gravity conditions can be used to increase the amount of semiconducting nanotubes present offering the possibility of chirality control in SWCNT production.[336,337,338]

---

[332] K. Tanaka, T. Yamabe, K. Fukui, The Science and Technology of Carbon Nanotubes, Chapter 2 M. YUMURA Synthesis and Purification of Multi-Walled and Single-Walled Carbon Nanotubes, Elsevier, 1999 ISBN: 0080426964

[333] K.S. Coleman, NNanotube, Annu. Rep. Prog. Chem., Sect. A, 104 (2008) 379–393

[334] K.S. Coleman, NNanotube, Annu. Rep. Prog. Chem., Sect. A, 104 (2008) 379–393

[335] Ibidem

[336] Ibidem

[337] Jean-Christophe Charlier and Sumio Iijima, Growth Mechanisms of Carbon Nanotubes, Carbon Nanotubes, 81 (2001) 55-81

[338] M.S. Dresselhaus, G, Dresselhaus, P. Avouris, Carbon Nanotubes: Synthesis, Structure, Properties, and Applications, Topics Appl. Phys. 80, (2001) ISBN: 3-540-41086-4

3.1.3.2. Laser ablation

This method has also been applied for the CNT synthesis, but length of MWCNT is much shorter than that by arc-discharge method. Therefore, this method does not seem adequate to synthesize MWCNT, but SWCNT has been obtained by laser-ablation method. The laser ablation technique uses two lasers to vaporize a graphite target mixed with a small amount of Co and/or Ni in order to condense the carbon into single-wall tubes[339] Similarly, laser vaporisation, where the carrier gas and reactor chamber pressure is controlled, has been used to synthesise specific SWCNT chiral distributions.[340]

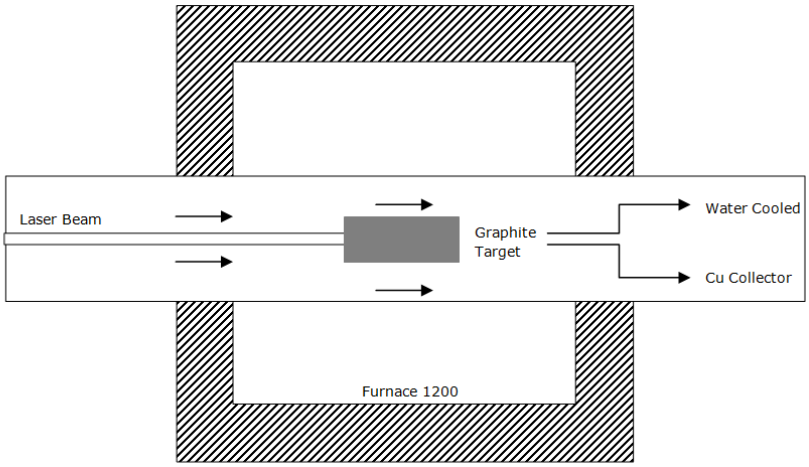

Figure 3.1–10: Laser ablation setup[341]

Both electric arc discharge and laser ablation control the growth conditions and maintain them over for a long time, to achieve a more uniform vaporization. Another technique to growth carbon nanotube is Chemical Vapour Deposition. As compared to arc-discharge and laser-ablation methods, CVD is a simple and economic technique for synthesizing CNTs at low temperature and ambient pressure, thus it is the most suitable candidate technique for CNT synthesis. [342]

339 J.C. Charlier and S. Iijima, Growth Mechanisms of Carbon Nanotubes, Carbon Nanotubes, 81 (2001) 55-81

340 K.S. Coleman, Nanotube, Annu. Rep. Prog. Chem., Sect. A, 104 (2008) 379–393

341 K. Tanaka, T. Yamabe, K. Fukui, The Science and Technology of Carbon Nanotubes, Chapter 2 M. YUMURA Synthesis and Purification of Multi-Walled and Single-Walled Carbon Nanotubes, Elsevier, 1999 ISBN: 0080426964

342 M. Kumar, Y.I Ando, Chemical Vapor Deposition of Carbon Nanotubes: A Review on Growth Mechanism and Mass Production Journal of Nanoscience and Nanotechnology 10 (2010) 3739–3758

3.1.4. Chemical Vapour Deposition

Chemical vapour deposition developed in 1996 is a useful technique for depositing ceramics, such as oxides, onto a target substrate.[343] In a typical CVD process substrate is exposed to one or more organoletic volatile precursors, which react and/or decompose on the substrate to produce the desired deposit. Volatile by-products are frequently produced, but they are removed by gas flow through the reaction chamber.

The first application of CVD for the synthesis of carbon filaments dates back to nineteenth century. In 1890[344], French scientists observed the formation of carbon filaments during experiments involving the passage of cyanogens over red-hot porcelain. In the 1970s extensive works were carried out to synthesize and understand tubular nanofibers of multi-layered carbon. Thus the CVD, that is may probably be the most-ancient technique to grow CNTs in the name of filaments and fibers, is today most popular CNT technique. The process to grow nanotube has two main advantages: CNTs are obtained at much lower temperature, in spite of a lower quality and the catalyst can be deposited on a substrate, which allows the formation of novel structures.[345] In crystallinity, arc- and laser-grown CNTs are superior to the CVD-grown ones (although CVD-grown MWCNTs possess inferior crystallinity, the crystallinity of SWCNTs grown by CVD is close to that grown by arc or laser methods). However, in yield and purity, CVD overcome the arc and laser methods. CVD is versatile because it offers harnessing plenty of hydrocarbons in any state (solid, liquid or gas), enables the use of various substrates, and allows CNT growth in a variety of forms, such as powder, thin or thick films, aligned or entangled, straight or coiled nanotubes, or a desired architecture of nanotubes on predefined sites of a patterned substrate. It also offers better control on the growth parameters [346]

In CVD process nanotubes are formed on the substrate by the decomposition of the mixture of hydrocarbon gas (acetylene, methane or ethylene) and nitrogen at temperatures 700–900 °C and atmospheric pressure[347]. CVD usually allows synthesis of longer CNTs (up to centimetres) but with more defects compared to higher temperature

---

343 E.T. Thostenson *et al*., Carbon Nanotube/carbon fiber hybrid multiscale composites, Journal of Applied Physics, 91 (2002) 6034-6037

344 Guest Editorial, Who should be given the credit for the discovery of carbon nanotubes, Carbon 44 (2006) 1621

345 R. Khare, S. Bose, Carbon Nanotube Based Composites: A Review, Journal of Minerals and Materials Characterization & Engineering, 4 (2005) 31-46

346 J.M. Kumar, Y.i Ando, Chemical Vapor Deposition of Carbon Nanotubes: A Review on Growth Mechanism and Mass Production Journal of Nanoscience and Nanotechnology 10 (2010) 3739–3758

347 V. Choudhary, A. Gupta, Carbon Nanotubes - Polymer Nanocomposites, Chapter Polymer/Carbon Nanotube Nanocomposites Centre for Polymer Science and Engineering Indian Institute of Technology Delhi, India ISBN: 978-953-307-498-6

processes such as laser ablation and gas discharge, although a post-annealing process at temperatures close to 2000 °C may recover the crystalline structure.[348]

A normal CVD [349] process involves complex flow dynamics since gases are flowing into the reactor, reacting, and then by-products are exhausted out of the reactor. The sequence of events during a CVD reaction are shown in Figure 3.1–11 and as follows:

- precursor gases input into the chamber by pressurized gas lines;
- mass transport of precursors from the main flow region to the substrate through the boundary layer (Figure 3.1–11);
- adsorption of precursors on the substrate (normally heated) (Figure 3.1–11b);
- chemical reaction on the surface (Figure 3.1–11c) 5) Atoms diffuse on the surface to growth sites;
- desorption of by-products of the reactions (Figure 3.1–11d);
- mass transport of by-products to the main flow region (Figure 3.1–11e).

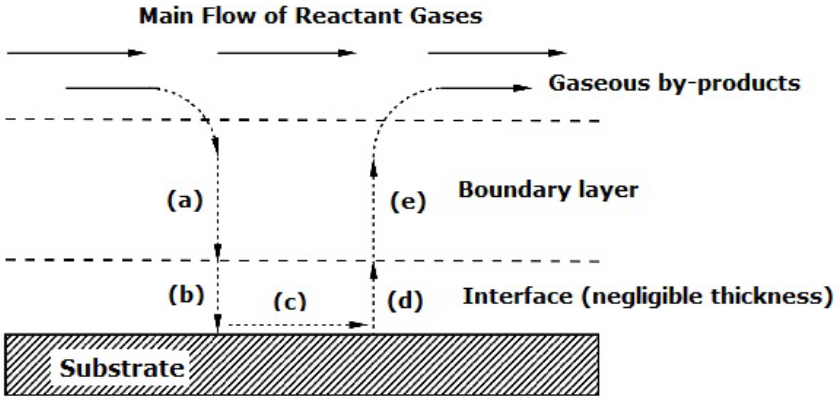

Figure 3.1–11: Sequence of events during CVD: (a) diffusion of reactants through boundary layer, (b) adsorption of reactants on substrate, (c) chemical reaction takes place, (d) desorption of adsorbed species, and (e) diffusion out of by-products through boundary layer.[350]

The CVD process is based on using an energy source (e.g., a furnace with resistive or inductive heater, hot filament, infra-red lamp, etc.) to decompose the precursor gases and to heat the sample to allow CNT nucleation and growth. The activation of the

[348] G.D. Nessim, Properties, synthesis, and growth mechanisms of carbon nanotubes with special focus on thermal chemical vapor deposition, Nanoscale, 2 (2010) 1306–1323

[349] A. Barron, Chemical Vapor Deposition, Connexions Web site. http://cnx.org/content/m25495/1.2/ Jul 13, 2009.

[350] H. O. Pierson, Handbook of Chemical Vapor Deposition, Noyes Publications, Park Ridge, New Jersey, U.S.A., (1992) ISBN: 0-8155-1432-8

molecules or of the nanostructured fragments is achieved using a variety of methods which can be roughly summarized as: plasma CVD and thermal CVD.

In thermal CVD, the heat of the furnace is responsible for the decomposition of the precursor gases in addition to affecting the catalytic function of the substrate. Other CVD systems such as plasma-enhanced CVD (PECVD) use plasma to aid the gas decomposition, which often allows CNT growth at lower temperatures although it produces defects in the nanotube structure [351]

The plasma used to decompose and activate the reactants in the gas phase are usually generated by hot filaments (HF) or by electrical discharges at different frequencies (DC, RF, MW). In general, the diameter and distribution of CNTs synthesized by CVD processing are dependent on the morphology of catalyst particles or layer applied bias voltage, the nature of catalyst and buffer layer deposition as well as the composition of plasma in a dc plasma-enhanced CVD process. The growth direction of the nanotubes can be controlled by the electrical field related to either applied bias or plasma induced bias, which is often perpendicular to the substrate surface [352]. Plasma-enhanced CVD (PECVD) methods can in general be easily scaled-up and offer the great advantage of having the deposited material almost totally located on the substrate from which it can be recovered. Moreover, such techniques are, at present, the only ones that allow one to control alignment and orientation of the CNT bundles, as well as their control on a nanometre scale.[353] An interesting variant is hot-filament CVD, where a hot filament heats the gases to high temperature in close proximity to the sample. [354]

Otherwise the thermal CVD technique makes use of a flow reactor inserted into a furnace for the thermal decomposition of carbon compounds. As reactants, C-rich gases mixed with argon or nitrogen flows are mainly used, but sometimes the starting material can be a liquid that is subsequently vaporized. The catalyst can be either in solid form, supported on a previously coated substrate, or driven into the reactor mixed with the gaseous feeding species. The deposition reactors are typically kept under atmospheric pressure, even if some interesting processes can be carried out under high-pressure conditions. The thermal techniques have the advantage of being remarkably cheap and offer the possibility of being easily scaled-up, but in general do not allow one to control the deposition area or the nanotube organization. Another disadvantage is the presence

---

351 G.D. Nessim, Properties, synthesis, and growth mechanisms of carbon nanotubes with special focus on thermal chemical vapor deposition, Nanoscale, 2 (2010) 1306–1323

352 L.H. Chen *et al.*, Growth of aligned carbon nanotubes on carbon microfibers by dc plasma-enhanced chemical vapor deposition, Applied Physics Letters 88 (2006) 033103-1-3

353 M.L. Terranova, V. Sessa, M. Rossi, The world of carbon nanotubes: an overview of CVD growth methodologies, Chem. Vap. Deposition 12 (2006) 315–325

354 G.D. Nessim, Properties, synthesis, and growth mechanisms of carbon nanotubes with special focus on thermal chemical vapor deposition, Nanoscale, 2 (2010) 1306–1323

in the deposits of a large amount of residual metallic catalysts[355]. By mean of this approach, high-quality SWNT material has been produced from methane using a supported transition metal oxide catalyst. The catalyst was prepared by impregnating fumed alumina nanoparticles with a methanol solution containing $Fe(NO_3)_3$ $9H_2O$. After impregnation the methanol solution was removed, the material heated at 150 °C and a resulting Fe_2O_3/alumina catalyst was obtained. [356] By contrast, in a reactor kept at 800–1000 °C, flowing methane/ethylene mixtures on iron nanoparticles, MWNTs could be obtained. [357]

The superior properties of CNTs offer exciting opportunities for new nanocomposites, but the important limitation for some potential applications of CNTs come from the fact that randomly oriented nanotubes embedded in polymer matrices have exhibited substantially lower electrical and thermal conductivities than expected. Nanotube alignment can be obtained prior or during or after composite fabrication by in-situ polymerization, mechanical stretching, melt fiber spinning, electrospinning and application of magnetic or electric field[358]. Among different techniques described, CVD is able to control growth direction on a substrate, to synthesize a large quantity of nanotubes,[359] to limit required equipment, to produce uniform CNT growth on complex surface and it guarantees an easy scale-up.[360,361] Moreover chemical vapour deposition is able to produce high-purity, high-performance solid materials. The process is often used in the semiconductor industry to produce thin films.[362] Four basic parameters affect CNT growth in a chemical vapour deposition (CVD) system: pressure, temperature, gases, and the metal-support-interface.[363] The CVD techniques tend in general to produce nanotubes with fewer carbonaceous impurities with respect to the other synthesis techniques and the residual particles of the metal catalyst are frequently found at an

355 M.L. Terranova, V. Sessa, M. Rossi, The world of carbon nanotubes: an overview of CVD growth methodologies, Chem. Vap. Deposition 12 (2006) 315–325

356 Ibidem

357 Ibidem

358 V. Choudhary, A. Gupta, Carbon Nanotubes - Polymer Nanocomposites, Chapter Polymer/Carbon Nanotube Nanocomposites Centre for Polymer Science and Engineering Indian Institute of Technology Delhi, India ISBN: 978-953-307-498-6

359 Rupesh Khare, Suryasarathi Bose, Carbon Nanotube Based Composites: A Review, Journal of Minerals & Materials Characterization & Engineering, 4 (2005) 31-46

360 Q. Zhang et al., Hierarchical composites of carbon nanotubes on carbon fiber: Influence of growth condition on fiber tensile properties , Composites Science and Technology 69 (2009) 594–601

361 K.S. Coleman, Nanotubes, Annu. Rep. Prog. Chem., Sect. A, 104 (2008) 379–393

362 http://en.wikipedia.org/wiki/Chemical_vapor_deposition

363 A. Tasha, D. Binh, Supapan Seraphin, Effects of Catalyst Components on Carbon Nanotubes Grown by Chemical Vapor Deposition, Journal of Undergraudate Research in Physics (2012) 1-8

extremity of the nanotubes, making their elimination by post-synthesis chemical processes easier. [364]

CNT growth on carbon substrate by CVD can be achieved via several techniques under a wide range of experimental conditions and combining different methodologies.[365]

For carbon fiber substrates, the high temperature and reactive conditions used during carbon nanotube growth can introduce defects that can significantly degrade mechanical properties. For example, carbon fibers are easily attacked by oxygen at temperatures as low as 400 °C. They could also be degraded by the iron catalyst particles used for CNT nucleation when the temperature is above iron–carbon eutectic temperature of 723 °C . An important challenge for CNT growth is obtaining the desired CNT density, coverage, length, and orientation on carbon fiber while simultaneously the processes must be mitigate because it could compromise the mechanical properties of substrate. The key issue to grow CNTs on carbon composite is to mitigate the processes that can have detrimental effects on the carbon/carbon properties.[366]

Some methods involve the loading of catalyst or catalyst precursor directly onto the fiber surface. These include application of aqueous catalyst ions via incipient wetness techniques, (such as dip-coating, in situ deposition of catalyst nanoparticles during CVD growth of CNTs) via vapour-phase decomposition of organometallic iron complexes (such as a process that employs xylene/ferrocene and e-beam evaporation of catalyst metal onto the fiber surface).[367] CNT morphologies can be varied widely depending on the growth conditions. However, the formation of CNTs on carbon substrates differs from that on quartz substrates due to the temperature limitation of the substrate and to the potential reactions of catalyst or carbon source with the carbon fiber substrate. [368]

Some investigations[369] have been done to prepare carbon nanotube/carbon fiber (CNT/CF) hybrid composites. The growth of CNTs on the carbon surface is a promising approach for improving mechanical, electrical and thermal properties of structural composites. However, there are several problems on growing CNTs on carbon composite substrate such as:

---

364 M.L. Terranova, V. Sessa, M. Rossi, The world of carbon nanotubes: an overview of CVD growth methodologies, Chem. Vap. Deposition 12 (2006) 315–325

365 Ibidem

366 V. Gonzaga de Resende, Growth of carbon nanotube forests on carbon fibers with an amorphous silicon interface, Carbon 48 (2010) 3635-3658

367 Stephen Alan Steiner III, Carbon Nanotube Growth on Challenging Substrates: Applications for Carbon-Fiber Composites, Doctor of Philosophy at the Massachusetts Institure of Technology

368 Q. Zhang et al., Hierarchical composites of carbon nanotubes on carbon fiber: Influence of growth condition on fiber tensile properties , Composites Science and Technology 69 (2009) 594–601

369 V. Gonzaga de Resende, Growth of carbon nanotube forests on carbon fibers with an amorphous silicon interface, Carbon 48 (2010) 3635-3658

- the catalysts of transition metals can easily diffuse into the carbon substrate,
- mixed phases of carbon materials can be formed on the surface of the C/C,
- the CNTs may grow only locally on the surface of the substrate,
- the synthesis conditions used for the CNT growth may cause the introduction of defects that can significantly degrade the carbon/carbon properties.

The substrate and the use of the catalyst deserve special attention, because they determine the structure of the tubes. The nanotube diameter depends on the catalyst particle size, therefore, the catalyst deposition technique, in particular the ability to control the particle size, is critical to develop nanodevices. The nanotubes grow parallel to each other and perpendicular to the substrate surface, because of catalyst–surface interaction and the Van der Waals forces developed between the tube. [370,371]

Catalytic chemical vapour deposition (CVD) is the most promising growth technique for the technological integration of carbon nanotubes (CNTs) because of the ability to control location, direction, and diameter. Optimized CVD recipes can lead to grow dense, vertically aligned, mm-long mats or forests of multi- and single-walled carbon nanotubes. The CNT alignment is caused by their high packing density, which forces vertical growth. Chemical vapour deposition (CVD) through thermal catalytic decomposition of hydrocarbons, alcohols or CO is achieved by means of nanoparticles of the transition metals Fe, Co or Ni over a catalyst.[372]

The common factor in most but not all cases of CNT forest growth is the use of Fe as a catalyst on an Al_2O_3 support layer.[373] This is one of the most promising methods for large scale production of CNTs, because it can produce relatively large amounts of CNTs under mild conditions and with reduced cost[374]. Control over the diameter, length, morphology as well as the growth rate of the CNTs can also be achieved by altering the size of the nanoparticles and the deposition conditions. CVD synthesis of aligned CNT forest or spatially oriented CNTs is a two-step process consisting of a catalyst preparation step followed by the actual synthesis of the nanotubes over the catalyst [375]. Usual catalytic supports comprise zeolites, silica, alumina, clay minerals, graphite and activated carbon

---

370 R. Khare, S. Bose, Carbon Nanotube Based Composites: A Review, Journal of Minerals & Materials Characterization & Engineering, 4 (2005) 31-46

371 Q. Zhang et al., Hierarchical composites of carbon nanotubes on carbon fiber: Influence of growth condition on fiber tensile properties , Composites Science and Technology 69 (2009) 594–601

372 S. Takenaka *et al.*, Formation of carbon nanotubes through ethylene decomposition over supported Pt catalysts and silica-coated Pt catalysts, Carbon 47 (2009) 1251–1257

373 M. Kumar, Y.i Ando, Chemical Vapor Deposition of Carbon Nanotubes: A Review on Growth Mechanism and Mass Production Journal of Nanoscience and Nanotechnology 10 (2010) 3739–3758

374 M. Kumar, Y.i Ando, Chemical Vapor Deposition of Carbon Nanotubes: A Review on Growth Mechanism and Mass Production Journal of Nanoscience and Nanotechnology 10 (2010) 3739–3758

375 M.L. Terranova, V. Sessa, M. Rossi, The world of carbon nanotubes: an overview of CVD growth methodologies, Chem. Vap. Deposition 12 (2006) 315–325

[376] [377]. There has been little exploration of the effects of perpendicular growth of CNT onto woven CF in a layered composite system.[378]

Catalytic decomposition of hydrocarbon[379] in the reactor to growth CNTs has been reported in Figure 3.1–12.

In this way MWCNT shape is not straight more than MWCNT obtained by arc-discharge method. This difference could be ascribed to the structure without pentagons nor heptagons in graphene sheet of the MWCNT synthesized by the catalytic decomposition of hydrocarbon, which would affect its electric conductivity and electron emission. Crucial point is to control the MWCNT production with regard to length, diameter and alignment. To overcome these problems, novel catalyst methods have been developed[380]. Li *et al.*[381] have reported a method for producing aligned CNT (nanotubes brushes) grown on silicates by using Fe particle on meso-porous silica. Terrones *et al*.[382] have developed a controlled production method of aligned-MWCNT bundles by using thin film of Co catalyst patterned on the silica substrate.

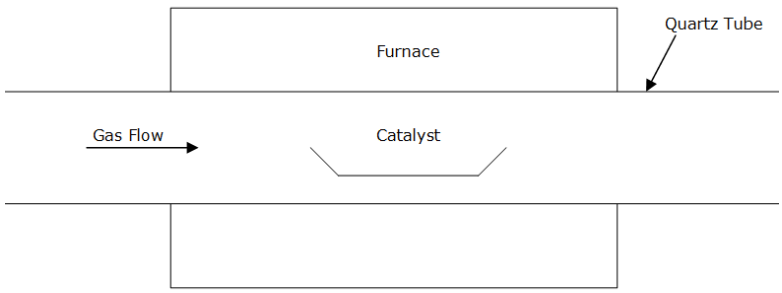

Figure 3.1–12: Schematic drawing of the apparatus used for the catalytic decomposition of hydrocarbon.

Fluidised bed CVD methodology using the common CNT producing metals iron, cobalt, and nickel supported on Al_2O_3 has been used to produce multi-walled carbon nanotubes (MWCNTs) on a scale of 0.5 kg h^{-1} using ethylene as a carbon source.[383] Laser assisted CVD has been used as a rapid method to determine appropriate catalyst and feedstock

[376] V.I. Alexiadis *et al.,* Influence of the composition of Fe_2O_3/Al_2O_3 catalysts on the rate of production and quality of carbon nanotubes, Materials Chemistry and Physics 128 (2011) 96–108

[377] R. Khare, S. Bose, Carbon Nanotube Based Composites: A Review, Journal of Minerals & Materials Characterization & Engineering, 4 (2005) 31-46

[378] C. Mattevi, *et al.*, In-situ X-ray Photoelectron Spectroscopy Study of Catalyst-Support Interactions and Growth of Carbon Nanotube Forests, J. Phys. Chem. C 112 (2008) 12207–12213

[379] Ibidem

[380] K. Tanaka, T. Yamabe, K. Fukui, The Science and Technology of Carbon Nanotubes, Chapter 2 M. YUMURA Synthesis and Purification of Multi-Walled and Single-Walled Carbon Nanotubes, Elsevier, 1999 ISBN: 0080426964

[381] W.Z. Li, *et al*., Large-Scale Synthesis of Aligned Carbon Nanotubes, Science 274 (1996) 1701-1703.

[382] M.Terrones, *et al*., Controlled Production of Aligned-Nanotube Bundles, Nature 388 (1997) 52-55

[383] K.S. Coleman, Nanotubes, Annu. Rep. Prog. Chem., Sect. A, 104 (2008) 379–393

combinations for the bulk synthesis of DWCNTs in conventional thermal CVD systems.[384] NiO catalysts supported on Al_2O_3 afford synthesis of MWCNTs following the catalytic decomposition of methane at 550 °C whereas SiO_2, HZSM-5 and CeO_2 give carbon nanofibres.[385]

MWCNTs have been grown from montmorillonite clay catalysts, in which the intercalated sodium ion was exchanged for cobalt(II) and iron(III) ions, via decomposition of ethylene at 700 °C. Similarly, MWCNTs have been synthesized using Ni_2O_3, NiO, $Ni(OH)_2$ and $NiCO_3$ $2Ni(OH)_2$ as catalysts in the presence of organic-modified montmorillonite by catalytic combustion of polypropylene.

MWCNTs with large diameters have been synthesized over anodic titanium oxide (ATO) template by CVD using acetylene as the carbon source.[386] Dense vertically aligned MWCNTs containing only a few walls have been grown from Fe–V–O nanoparticles by CVD.[387] Decomposition of methane over MgO impregnated with various precious metals such as Fe, Co, Ni, Ru, Rh, Pd, Os, Ir, or Pt led to MWCNTs (with the graphite layers parallel to the tube axis) with Group 8 and 9 metals and carbon nanofibers (CNFs) with herringbone type graphene sheets with Group 10 metals.[388] Iron-based nanoparticles isolated by size using centrifugation, with size variation on the subnanometre order, have been used for the growth of diameter-controlled MWCNTs.[389] Thermal pyrolysis of ferrocene dissolved in xylene, assisted by an ultrasonic evaporator, produces aligned MWCNTs.[390,391] Millimetre long vertically aligned CNTs have been grown by the CVD of ethylene over a silicon substrate surface containing a layer of Al_2O_3 and a nanometre thick layer of Fe.[392] Equimolar amounts of acetylene and CO_2 react to produce MWCNTs in the presence of an Fe/Co catalyst[393]. High-purity nitrogen-doped MWCNTs have been produced in high yield from a methane-hydrogen-ammonia mixture using the catalyst

---

384 A. Bachmatiuk *et al.,* Facilitating the CVD synthesis of seamless double-walled carbon nanotubes Nanotechnology, 18 (2007) 275619 (5pp)

385 S. P. Chai, S. H. S. Zein and A. R. Mohamed, Synthesizing carbon nanotubes and carbon nanofibers over supported-nickel oxide catalysts via catalytic decomposition of methane, Diamond Relat. Mater., 2007, 16, 1656.

386 I. Eswaramoorthi, L.P. Hwang, Synthesis and characterisation of larger diameter multi-walled carbon nanotubes over anodic titanium oxide template, Letters to the Editor Carbon 44 (2006) 2330–2356

387 K.S. Coleman, Nanotubes, Annu. Rep. Prog. Chem., Sect. A, 104 (2008) 379–393

388 I. Eswaramoorthi, L.P. Hwang, Synthesis and characterisation of larger diameter multi-walled carbon nanotubes over anodic titanium oxide template, Letters to the Editor Carbon 44 (2006) 2330–2356

389 T. Inoue *et al.*, Synthesis of diameter-controlled carbon nanotubes using centrifugally classified nanoparticle catalysts, Carbon 45 (2007) 2164–2170

390 J. Prasek *et al.*, Methods for carbon nanotubes synthesis—review, J. Mater. Chem., 21 (2011) 15872-15884

391 A. Suhail Farooqi, Review of Single Step Techniques for Production of ACNT's, International Journal Of Engineering And Computer Science 1 (2012) 23-27

392 K.S. Coleman, Nanotubes, Annu. Rep. Prog. Chem., Sect. A, 104 (2008) 379–393

393 A. Magrez, Catalytic CVD Synthesis of Carbon Nanotubes: Towards High Yield and Low Temperature Growth, Materials 3 (2010) 4871-4891

$Co_xMg_{1-x}MoO_4$[394] Boron doped MWCNTs, usually only accessible by arc-discharge based methods, have been prepared by CVD using $Fe/Ca(BO_3)_2/CaCO_3$ as the catalyst, acetylene as the carbon-source and BF_3/MeOH as the source of boron.[395] MWCNTs with ultrafine inner diameters of only a few nanometres have been synthesised through a simple ethanol flame method.[396]

The CNT properties depends on method of production and experimental parameters, which allow to control type of CNTs synthesised (single-walled vs. multiwalled) and the quality of the material produced (the amount of impurities present).

3.1.4.1. Catalyst in Chemical Vapour Deposition

The catalytic synthesis method is considered to have the best possibility for mass production. CNT can be synthesized by the chemical reaction at relatively low temperature.[397] The role of the catalyst in CNT growth is not completely understood, but it is known that nanoparticles act as dynamic templates dictating the nanotube size distribution. [398]

Catalyst[399] nanoparticles serve as points of chemical activity from which hollow, seamless cylindrical graphitic fibrils emerge upon exposure to certain carbon-containing feedstocks, such as ethylene and acetylene, at elevated temperatures, typically 700-900°C. Early 1990's works show carbon nanofibers (CNFs, nanostructured carbon fibrils with non-parallel graphitic walls) and CNTs (fibrous carbon nanostructures small as 5 nm in diameter) growth on carbon fibers by catalytic CVD from ethylene, employing metal catalysts applied to the surface of fibers and fiber weaves through dip-coating with aqueous solutions of the nitrates of these metals.[400] The most important property[401] of the metals with regard to CNT formation is their ability to catalytically decompose gaseous carbon-containing molecules. To synthesize CNTs, typically, nanometer-size

---

394 X.Y. Tao *et al.*, Large-scale CVD synthesis of nitrogen-doped multi-walled carbon nanotubes with controllable nitrogen content on a $CoxMg_1-xMoO_4$ catalyst, Diamond and Related Materials 16 (2007) 425–430

395 K.S. Coleman, Nanotubes, Annu. Rep. Prog. Chem., Sect. A, 104 (2008) 379–393

396 L. Wang Controllable synthesis of carbon nanotubes with ultrafine inner diameters in ethanol flam Physica B: Condensed Matter 398 (2007) 18–22

397 K. Tanaka, T. Yamabe, K. Fukui, The Science and Technology of Carbon Nanotubes, Chapter 2 M. YUMURA Synthesis and Purification of Multi-Walled and Single-Walled Carbon Nanotubes, Elsevier, 1999 ISBN: 0080426964

398 V.I. Alexiadis *et al.,* Influence of the composition of Fe_2O_3/Al_2O_3 catalysts on the rate of production and quality of carbon nanotubes, Materials Chemistry and Physics 128 (2011) 96–108

399 W. B. Downs and R. T. K. Baker, Modification of the surface properties of carbon fibers via the catalytic growth of carbon nanofibers, J. Mater. Res., 10 (1995) 625-633

400 S. Zhu *et al*., Carbon nanotube growth on carbon fibers Diamond and Related Materials 12 (2003) 1825–1828

401 A. Moisala, A.G. Nasibulin and E.I Kauppinen, The role of metal nanoparticles in the catalytic production of single-walled carbon nanotubes—a review, .J. Phys.: Condens. Matter, 15 (2003) S3011–S3035

metal particles are required to enable hydrocarbon decomposition at a lower temperature [402] than the spontaneous decomposition temperature of the hydrocarbon. Among these nanosized transition metal particles, such as nickel, iron, molybdenum and cobalt, have been widely used in CVD either in oxide or metallic forms or as mixtures [403]. The use of these metals is mainly due to high solubility of carbon in these metals at high temperatures and high carbon diffusion rate in these metals. As metallic catalyst Fe, Co or Ni are crucial in the catalytic decomposition of hydrocarbon. In order to efficiently obtain CNT and to control its shape, it is necessary and indispensable to have enough information on chemical interaction between carbon and these metals. [404] The peculiarity to form ordered carbons is thought to be related to a combination of factors, such as the metals catalytic activity for the decomposition of volatile carbon compounds, their ability to form metastable carbides and the carbon capability to diffuse quickly through and over the metals[405]. If there is significant reaction away from the metal, other undesirable forms of carbon, such as amorphous carbon nanoparticles, will be co-produced. Restriction of the reaction to the surface is controlled through the choice of the carbon precursor, its partial pressure, and the reaction temperature.[406]

Besides that, high melting point and low equilibrium-vapor pressure of these metals offer a wide temperature window of CVD for a wide range of carbon precursors. Recent considerations are that Fe, Co, and Ni have stronger adhesion with the growing CNTs than other transition metals do and hence they are more efficient in forming high-curvature (low-diameter) CNTs.[407]

Over thin metal foils, which in the present context can be considered as bulk metal, carbon dissolves to form a solid solution. On cooling, it precipitates on the surface as a continuous thin film of highly crystalline graphite in which the graphite basal planes are oriented parallel to the substrate[408]. The high degree of crystalline perfection that is obtained in a matter of seconds demonstrates that carbon atoms are extremely mobile and can move easily over and through the metal. When the metal is present as particles

---

402 M. Kumar, Y.I Ando, Chemical Vapor Deposition of Carbon Nanotubes: A Review on Growth Mechanism and Mass Production Journal of Nanoscience and Nanotechnology 10 (2010) 3739–3758

403 A. Moisala, A.G. Nasibulin and E.I Kauppinen, The role of metal nanoparticles in the catalytic production of single-walled carbon nanotubes—a review, .J. Phys.: Condens. Matter, 15 (2003) S3011–S3035

404 K. Tanaka, T. Yamabe, K. Fukui, The Science and Technology of Carbon Nanotubes, Chapter 2 M. YUMURA Synthesis and Purification of Multi-Walled and Single-Walled Carbon Nanotubes, Elsevier, 1999 ISBN: 0080426964

405 K.B.K. Teo e*t al*., Catalytic Synthesis of Carbon Nanotube and Nanofiber, Encyclopedia of Nanoscience and Nanotechnology, Edited by H.S. Nalwa, Volume X, 1-22

406 S.B. Sinnott et al., Model of carbon nanotube growth through chemical vapor deposition Chemical Physics Letters 315 (1999) 25–30

407 M. Kumar, Y.I Ando, Chemical Vapor Deposition of Carbon Nanotubes: A Review on Growth Mechanism and Mass Production Journal of Nanoscience and Nanotechnology 10 (2010) 3739–3758

408 S.B. Sinnott et al., Model of carbon nanotube growth through chemical vapor deposition, Chemical Physics Letters 315 (1999) 25–30

of diameter in the range of tenths of a micron, the carbon is produced as filaments of similar diameter.[409] The catalyst particle size determines the size of the 'filament'. As the particle diameter is reduced, the filament curvature increases, imposing an increasing strain on the basal planes of the crystallites. Eventually, a continuous surface is energetically more favourable and MWNTs are formed. Logically, if the particle size is reduced still further, SWNTs will be formed.[410] The metal particles can be supported on a substrate or introduced as 'floating' particles in a gas stream that flows through the reactor. If the particles are considered to be spherical or pear shaped, the deposition of carbon atoms takes place on one half of the surface on the lower curvature face for pear shapes.[411]

Solid organometallocenes (ferrocene, cobaltocene, nickelocene) are also widely used as a CNT catalyst, because they liberate metal nanoparticles in-situ which catalyze the hydrocarbon decomposition more efficiently. It is a general experience that the catalyst-particle size dictates the tube diameter. Hence, metal nanoparticles of controlled size, pre-synthesized by other reliable techniques, can be used to grow CNTs of controlled diameter. Thin films of catalyst coated on various substrates are also proven good in getting uniform CNT deposits[412] Apart from the previously mentioned transition metals (Fe, Co, Ni), other metals of this group, such as Cu, Au, Ag, Pt, Pd were also found to catalyze various hydrocarbons for CNT growth. On the role of CNT catalysts transition metals have been proven to be efficient catalysts not only in CVD but also in arc-discharge and laser-vaporization methods. Therefore, it is likely that these apparently different methods might inherit a common growth mechanism of CNT, which is not yet clear. Hence this is an open field of research to correlate different CNT techniques in terms of the catalyst's role in entirely different temperature and pressure range. [413] Several mechanistic[414] studies have been conducted to determine the dependence of the CNT diameter on the catalyst particle size. Catalyst particles with predetermined size have been used to prove the connection. For instance, iron nanoparticles with average mean diameters of 3, 9 and 13 nm, yielded CNTs with wall diameters of 3, 7 and 12 nm

409 Ibidem
410 Ibidem
411 S.B. Sinnott et al.r Chemical Physics Letters 315 (1999) 25–30, Model of carbon nanotube growth through chemical vapor deposition
411 K.S. Coleman, Nanotubes, Annu. Rep. Prog. Chem., Sect. A, 104 (2008) 379–393
412 M. Kumar, Carbon Nanotubes - Synthesis, Characterization, Applications, Carbon Nanotube Synthesis and Growth Mechanism, Dr. Siva Yellampalli (Ed.), ISBN: 978-953-307-497-9
413 M. Kumar, Y.I Ando, Chemical Vapor Deposition of Carbon Nanotubes: A Review on Growth Mechanism and Mass Production Journal of Nanoscience and Nanotechnology 10 (2010) 3739–3758
414 A. Moisala, A.G. Nasibulin and E.I Kauppinen, The role of metal nanoparticles in the catalytic production of single-walled carbon nanotubes—a review, .J. Phys.: Condens. Matter, 15 (2003) S3011–S3035

respectively.[415] The CNTs produced with the smallest catalyst particles were primarily SWCNTs with few double-walled carbon nanotubes (DWCNTs). With larger catalyst particles, the number of DWCNTs and thin MWCNTs increased in the product. Precipitation methods generally lead to wide particle size distributions. Therefore, several attempts have been made to control the size distribution and dispersion of catalyst particles. Organic carriers, such as apoferritin[416,417] or polyamidoamine dendrimers[418], have been successfully used to decrease the spread of the nanoparticle size distribution to the 1–3 nm range.[419] Similar results were also obtained with molybdenum oxide-based cage molecules.[420] Good dispersion of narrow size distribution particles on the support surface has been achieved with the use of dispersion agents such as acids and amines.[421]

As previously mentioned the size of the catalyst used in metal catalyzed chemical vapour deposition (CVD) can define the diameter of as-grown carbon nanotubes. This hypothesis has been supported by the observation that catalytic particles at the ends of CVD-grown nanotubes have sizes commensurate with the nanotubes diameters [422]. However, direct growth of different diameter carbon nanotubes from monodisperse catalyst such as Fe/Mo and Co nanoclusters, which could provide much stronger support for this idea, have not yet been reported.[423] In addition, investigations of the CVD growth demonstrate that the supply of carbon reactant is critical for the preparation of large diameter nanotubes from large iron nanoclusters, and that growth temperature is also important for achieving high-quality large diameter nanotubes. [424] Monodisperse iron nanoclusters can be used to define the diameters of carbon nanotubes grown by metal-catalyzed CVD.[425] Investigations of growth conditions demonstrate that the supply of carbon reactant is important to grow large diameter nanotubes from large iron nanoclusters, and that growth temperature is especially important for achieving high-

415 Ibidem

416 Li Y, *et al.*, Growth of single-walled carbon nanotubes from discrete catalytic nanoparticles of various size, J. Phys. Chem. B 105 (2001)11424–11431

417 Y. Zhang *et al.*, Imaging as-grown single-walled carbon nanotubes originated from isolated catalytic nanoparticles, Appl. Phys. A 74 (2002) 325–328

418 H.C. Choi *et al.*, Delivery of Catalytic Metal Species onto Surfaces with Dendrimer Carriers for the Synthesis of Carbon Nanotubes with Narrow Diameter Distribution, J. Phys. Chem. B 106 (2002) 12361–12365

419 A. Moisala, A.G. Nasibulin and E.I Kauppinen, The role of metal nanoparticles in the catalytic production of single-walled carbon nanotubes—a review, .J. Phys.: Condens. Matter, 15 (2003) S3011–S3035

420 L. An *et al.*, Synthesis of nearly uniform single-walled carbon nanotubes using identical metal-containing molecular nanoclusters as catalysts. J. Am. Chem. Soc. 124 (2002) 13688–13689

421 C.L Cheung *et al.*, Diameter-controlled synthesis of carbon nanotubes, J. Phys. Chem. B 106 (2002) 2429–2433

422 Ibidem

423 H. Ago et al., Dispersion of metal nanoparticles for aligned carbon nanotube arrays Appl. Phys. Lett. 77 (2000) 79-81

424 C.L. Cheung *et al.*, Diameter-Controlled Synthesis of Carbon Nanotube, J. Phys. Chem. B 106 (2002) 2429-2433

425 Ibidem

quality large diameter nanotubes. Through the use of, for example, iron oxide nanoparticles of different diameters, multiwall CNTs (MWNTs) of corresponding diameters have been obtained and in this case, the Fe/Mo catalyst is formed in situ on the surface of the Al_2O_3 nanoparticles.[426]

3.1.4.2. Growth Mechanism of Carbon Nanotubes

The formation and growth of nanotubes is an extension of other known processes where over metal have been formed graphitic structures, whose form is closely related to the physical dimensions of the metal catalyst particles.[427]

By CVD techniques, CNTs grow via precipitation of dissolved carbon from a moving catalytic particle surface. When impurities-poisoned catalyst or a stable metal carbide has been formed, growth terminates.[428] In case of multi-wall carbon nanotubes, no catalyst particle or any external agent seem to be involved during growth and the tips of the multishell nanotubes are frequently observed to be closed.[429] Two different assumptions must be considered. The former is that the tube remains closed during growth, thus the longitudinal growth of the tube occurs by the continuous incorporation of small carbon clusters; for instance, the present models fail to explain multilayer tube growth and how the inside shells grow often to a different length compared with the outer ones.[430] The latter assumption regards the ends of nanotubes, which is open during the growth process and carbon atoms are added at their open ends.[431]

---

426 L. Jodin *et al.*, Influence of the Catalyst Type on the Growth of Carbon Nanotubes via Methane Chemical Vapor Deposition, J. Phys. Chem. B 110 (2006) 7328-7333

427 S.B. Sinnott *et al.*, Model of carbon nanotube growth through chemical vapor deposition, Chemical Physics Letters 315 (1999) 25–30

428 P.M. Ajayany, T.W. Ebbesenz, Nanometre-size tubes of carbon, Rep. Prog. Phys., 60 (1997) 1025–1062

429 J.C. Charlier, S. Iijima Growth Mechanisms of Carbon Nanotubes, Nature 354 (1991) 55-81

430 M.Endo, H.W. Kroto, Formation of carbon nanofibers, J. Phys. Chem., 96 (1992) 6941–46944

431 S. Iijima, P.M. Ajayan, T. Ichihashi, Growth model for carbon nanotubes, Phys. Rev. Lett. 69, (1992)3100–3103

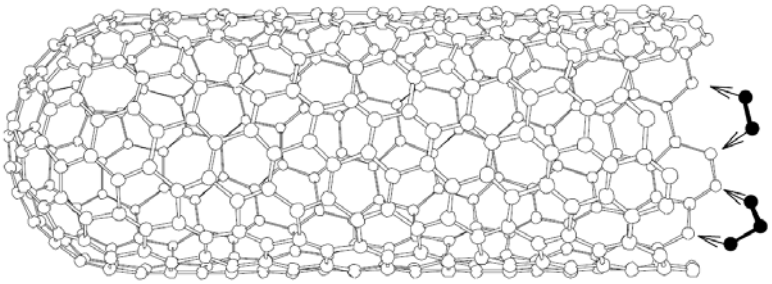

Figure 3.1–13: Growth mechanism of a carbon nanotube at an open end by absorption [432]

The sequential addition of carbon will result in the continuous growth of chiral nanotubes.

Hence the model describes the growth as a open tube where growth is in axial direction thanks to the addition of carbon clusters to the network at the open ends to form hexagonal rings, as shown in Figure 3.1–13. The open-end tube is the starting form nucleus, as shown in Figure 3.1–14(a), where tube ends are open while growing by accumulating carbon atoms. A successive supply of hexagons on the tube periphery results in a longer tube as illustrated in Figure 3.1–14 (b). Enclosure of this tube can be completed by introducing six pentagons to form a polygonal cap Figure 3.1–14 (c). Open circles represent locations of pentagons. Once the tube is enclosed, there will no more growth on that tube. A second tube, however, can be nucleated on the first tube side-wall and eventually cover it, as illustrated in Figure 3.1–14 (d) and Figure 3.1–14 (e) or even over-shoot it, as in Figure 3.1–14 (f). [433]

[432] R. Saito et al., Physical Properties of Carbon Nanotube, Imperial College Press, London (1998) Cap 5, Pg 92, ISBN 978-1860942235

[433] M.S. Dresselhaus, G, Dresselhaus, P. Avouris, Carbon Nanotubes: Synthesis, Structure, Properties, and Applications, Topics Appl. Phys. 80, (2001) ISBN: 3-540-41086-4

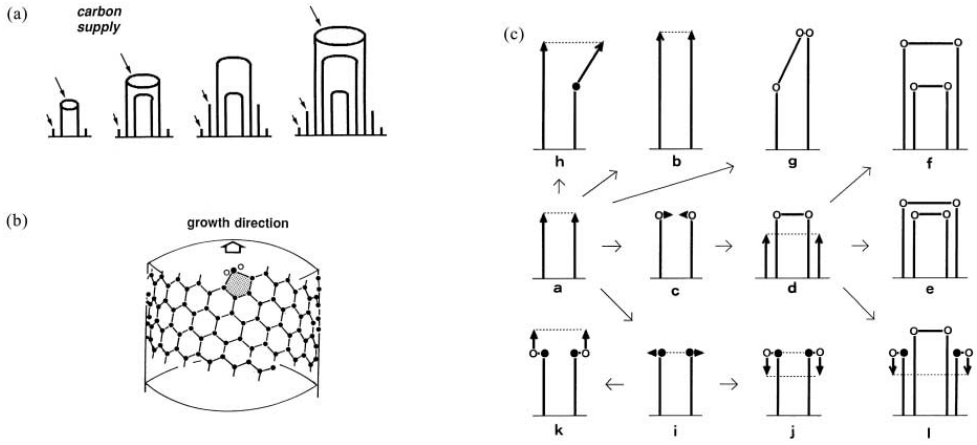

Figure 3.1–14: Model for the open-end growth of the nanotube. Evolution of carbon nanotube terminations based on the open-end tube growth. Arrows represent passes for the evolution. Arrow heads represents terminations of the tubes and also growth directions. Open and solid circles represents locations of pentagons and heptagons, respectively [434]

In case of CNT synthesis by means of catalyst chemical vapor deposition a mechanism to describe the formation of carbon nanotubes has been proposed by several authors.[435,436,437,438,439] All correlate nanotube diameter to metal catalyst particle size and it is widely-accepted that the growth mechanisms for CNTs occurs according to two models: tip-growth and base-growth model, as shown in Figure 3.1–15 (a)-(b). In the "tip growth mode" the catalyst particles can stay at the tips of the growing nanotube during the growth process. In the "base growth mode" catalyst particles remain at the nanotube base, depending on the adhesion between the catalyst particle and the substrate. [440]

[434] J.C. Charlier and S. Iijima , Growth Mechanisms of Carbon, Carbon Nanotubes Topics in Applied Physics Volume 80, (2001) 55–81

[435] S.B. Sinnott *et al.*, Model of carbon nanotube growth through chemical vapor deposition, Chemical Physics Letters 315 (1999) 25–30

[436] V. Choudhary, A. Gupta, Carbon Nanotubes - Polymer Nanocomposites, Chapter Polymer/Carbon Nanotube Nanocomposites Centre for Polymer Science and Engineering Indian Institute of Technology Delhi, India ISBN: 978-953-307-498-6

[437] L. Jodin *et al.*, Growth of CNTs via Methane CVD, J . Phys. Chem. B, 110 (2006) 7328-7333

[438] S. Bai *et al*, Influence of ferrocene/benzene mole ratio on the synthesis of carbon nanostructures Chemical Physics Letters 376 (2003) 83–89.

[439] M. Kumar, Y.i Ando, Chemical Vapor Deposition of Carbon Nanotubes: A Review on Growth Mechanism and Mass Production Journal of Nanoscience and Nanotechnology 10 (2010) 3739–3758

[440] V. Choudhary, A. Gupta, Carbon Nanotubes-Polymer Nanocomposites, Chapter Polymer/Carbon Nanotube Nanocomposites Centre for Polymer Science and Engineering Indian Institute of Technology Delhi, India ISBN: 978-953-307-498-6

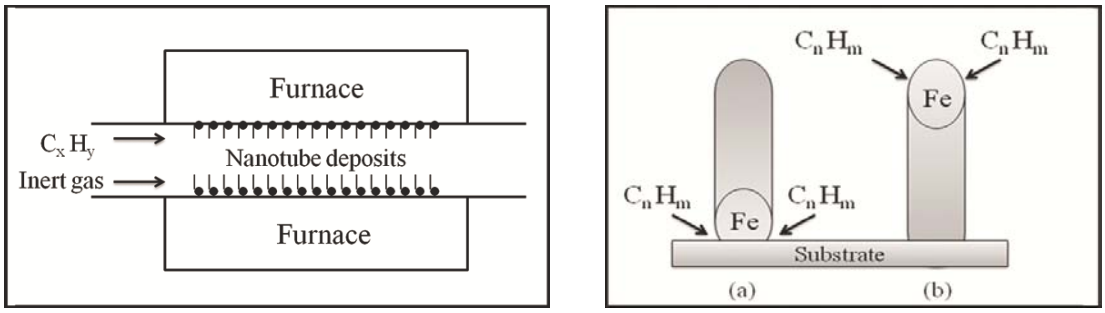

Figure 3.1–15: Chemical vapour deposition setup; b. Growth modes for CVD (a) base growth mode and (b) tip growth mode[441]

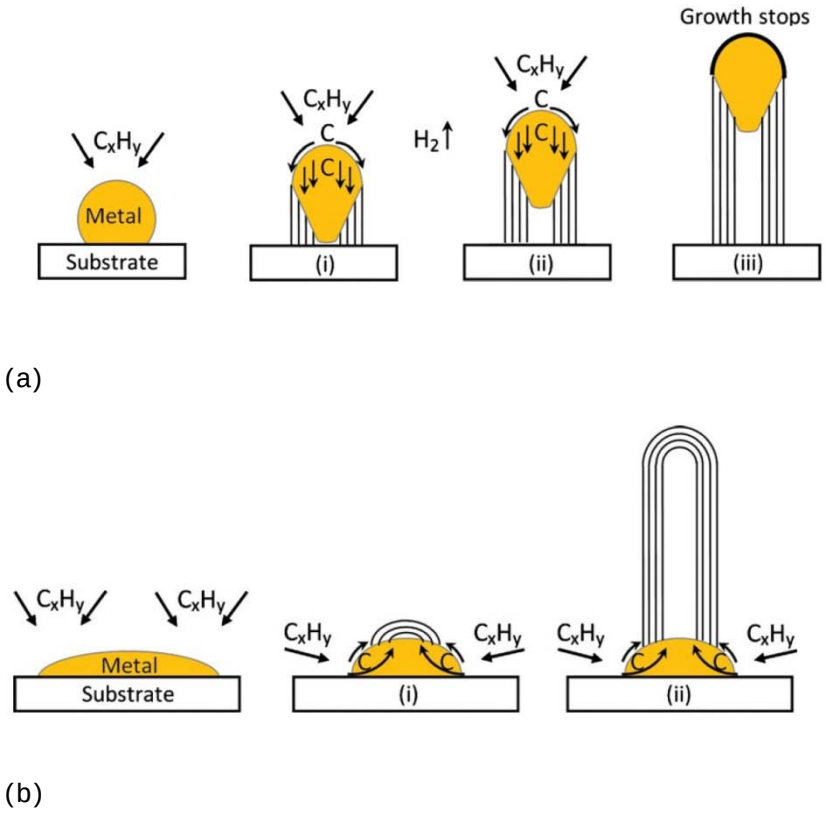

Figure 3.1–16: Widely-accepted growth mechanisms for CNTs: (a) tip-growth model, (b) base-growth model.[442]

In "base growth" mechanism, the catalyst particle remains fixed to the substrate surface, and the tube will grow upwards, open-ended. This allows the accumulation of additional metal catalyst particles along the length of the tube, as shown in Figure 2.1–16 (b). In this model the catalyst–substrate interaction is strong, indeed metal has an

[441] V. Choudhary, A. Gupta, Carbon Nanotubes - Polymer Nanocomposites, Chapter Polymer/Carbon Nanotube Nanocomposites Centre for Polymer Science and Engineering Indian Institute of Technology Delhi, India ISBN: 978-953-307-498-6

[442] M. Kumar, Y.I Ando, Chemical Vapor Deposition of Carbon Nanotubes: A Review on Growth Mechanism and Mass Production Journal of Nanoscience and Nanotechnology 10 (2010) 3739–3758

obtuse contact angle with the substrate, initial hydrocarbon decomposition and carbon diffusion take place similar to that in the tip-growth case, but the CNT precipitation fails to push the metal particle up; so the precipitation is compelled to emerge out from the metal's apex. First, carbon crystallizes out as a hemispherical dome (the most favourable closed-carbon network on a spherical nanoparticle, step (i) in Figure 3.1–16 (b) which then extends up in the form of seamless graphitic. Subsequent hydrocarbon deposition takes place on the lower peripheral surface of the metal, and as dissolved carbon diffuses upward, as reported in step (ii) of Figure 3.1–16 (b). [443,444,445]

In the "tip growth" mechanism metal catalyst particles initially rise with the tube tips as they grow, although friction between the particles and the tube walls eventually causes the particles to become fixed in place. Growth would slowly occur on the open tube tip until another catalyst particle deposited, starting the process again. In this method, as the nanotube lengthens, the metal catalyst particle will be lifted from the substrate surface. Since the exposed end of the nanotube is filled with the catalyst particle, and the opposite end is fixed to the substrate, there is no way for additional metal catalyst particles to get inside of the tube. On the contrary to the previous model, the catalyst–substrate interaction is weak, indeed metal has an acute contact angle with the substrate, thus hydrocarbon decomposes on the top surface of the metal, carbon diffuses down through the metal, and CNT precipitates out, as depicted in Figure 3.1–16 (a) step (i). As long as the metal's top is open for fresh hydrocarbon decomposition (concentration gradient exists in the metal allowing carbon diffusion), CNT continues to grow longer and longer, step (ii) in Figure 3.1–16 a. Once the metal is fully covered with excess carbon, its catalytic activity ceases and the CNT growth is stopped, as shown in step (iii) in Figure 3.1–16 a. This nanotube formation theory is not consistent with the current observations for vapour phase CVD-grown CNTs, where catalyst particles were often found along the length of the carbon nanotubes. Zhang *et al*.[446] suggest that tubes grow by a tip growth model until friction between the catalyst particles and the tube walls prevent the particle from moving. At this point, growth slowly continues open-ended, until another particle could deposit on the nanotube end. Frictional forces between a particle and the tube walls are a function of the contact area, so for a given tube, a larger particle would have greater contact area, and therefore travel a shorter distance at the

[443] C.P. Deck, K. Vecchio, Growth mechanism of vapor phase CVD-grown multi-walled carbon nanotubes, Carbon 43 (2005) 2608–2617

[444] M. Kumar, Y.i Ando, Chemical Vapor Deposition of Carbon Nanotubes: A Review on Growth Mechanism and Mass Production Journal of Nanoscience and Nanotechnology 10 (2010) 3739–3758

[445] C.M. Seah, S.P. Chai, A.R. Mohamed, Synthesis of aligned carbon nanotubes, Carbon 49 (2011) 4613–4635

[446] X. Zhang *et al*., Rapid growth of well-aligned carbon nanotube arrays, Chem Phys Lett 362 (2002) 285–90.

tube tip before being stopped by friction. By the same reason, a smaller particle would be expected to travel a larger distance until it grows large enough for friction to stop its movement. A very small particle might not have a sufficient contact area to be stopped due to friction, suggesting that all particles would need to grow to a minimum size before they could stop and before an additional particle could accumulate on the open tube tip. Authors [447] have also observed catalyst encapsulated in the middle of the tubes. This behaviour could be explained suggesting base growth as mechanism instead of tip growth. Indeed the catalyst particle remains fixed to the substrate surface, and the tube will grow upwards, open-ended; this allows the additional metal catalyst particles storage along the length of the tube, matching. The base growth theory for carbon fiber and nanotube nucleation by Baker *et al*. [448] and Sinnott *et al*. [449] does not explain the mechanisms; on the other hand, the theory of Zhang *et a*l.[450] predicts this elongation occurring as a combination of plastic deformation caused by constraining forces of the nanotube walls and the addition of other catalyst particles to the original particle. As the tube grows past an encased particle, it remains open, as described by the base growth theory. Additional metal atoms could travel down this open channel, and combine with the catalyst cluster. By this method, the encapsulated metal particle could increase in volume beyond its initial size. Constraining forces from the walls of the encapsulating nanotube would confine the catalyst particle to a fixed diameter, so any additional growth would have to be in the axial direction, resulting in a particle with a high aspect ratio. Nanotubes grown by CVD would have at most one particle at each end, but could have multiple particles located along the middle of the tube. Different growth parameters, such as catalyst addition rate and growth reaction time, will determine the number of particles located inside the middle of the nanotubes. Due to process variations, the exact ratio of end-to-middle particle locations cannot be determined, but it is assumed that for a sufficiently long growth period, there will be a larger percentage of particles located in the middle of a tube relative to those located at the tube ends.

Carbon precipitates out with graphitic structure when solubility limit within the metal is reached. Specie formed depends on the size of catalyst particle, graphite, carbon filaments, or carbon nanotubes, in order to decrease particle size and increase particle curvature. As more carbon is deposited on the catalyst, it will either diffuse into or over

---

447 C.P. Deck, K. Vecchio, Growth mechanism of vapor phase CVD-grown multi-walled carbon nanotubes, Carbon 43 (2005) 2608–2617

448 M. Kumar, Y.I Ando, Chemical Vapor Deposition of Carbon Nanotubes: A Review on Growth Mechanism and Mass Production Journal of Nanoscience and Nanotechnology 10 (2010) 3739–3758

449 S.B. Sinnott *et al*., Model of carbon nanotube growth through chemical vapor deposition, Chemical Physics Letters 315 (1999) 25–30,

450 X. Zhang *et al*. Rapid growth of well-aligned carbon nanotube arrays, Chem Phys Lett 362 (2002)285–290

the surface of the particle and become incorporated into the graphitic lattice, increasing the tube length.

In case of CVD, carbon nanotube grows by tip growth method. In case of spray pyrolysis, it initially grows by the base growth mechanism, rather than the tip growth method.[451]

Concerning aligned growth mechanisms, literature reports that alignment of CNTs is simply caused by the van der Waals force.[452,453] The strong interaction of the van der Waals force enables the CNTs bound together to form dense ordered packing. During the initial stage of CVD, the lack of van der Waals forces results in the formation of entangled CNTs. It is assumed the base-growth mode as mechanism. At the beginning of CVD, growing gas molecules are catalytically decomposed on the iron oxide nanoparticles. As supersaturation occurs, a nanotube grows off each of the densely packed catalyst particles and extends to open space along the direction normal to the substrate. As the nanotubes lengthen, their outermost walls interact with those of neighbouring nanotubes via van der Waals forces to form a large bundle with sufficient rigidity. As the catalyst film becomes thicker, the interaction between the nanotube walls induces the growth of CNTs with a straight form that is parallel to the substrate. The van der Waals interactions can be utilized as binding energy between adjacent CNTs and the CNT yarns can be drawn for various application. This rigidity enables nanotubes to keep growing along the original direction. The open end of the tubes containing charged dangling bonds inhibits the closing of the tube end. Another reason why this approach works is that the tip of the tubes possesses a constant orientation of catalytic particles. The polarised catalyst particles and the induced dipole moment align the CNTs parallel to the electric field all the way through the growth of the CNTs.[454]

Large-scale synthesis of aligned carbon nanotubes has been achieved using a method based on chemical vapour deposition catalysed by iron nanoparticles embedded in mesoporous silica. [455,456]

The direct synthesis of CNTs on electrode materials is one of the most promising ways to obtain high quality CNTs. Authors[457] developed a robust method to grow high quality

---

451 C.P. Deck, K. Vecchio, Growth mechanism of vapor phase CVD-grown multi-walled carbon nanotubes, Carbon 43 (2005) 2608–2617

452 S. Fan *et al.*, Self-Oriented Regular Arrays of Carbon Nanotubes and Their Field Emission Properties, Science 283 (1999) 512-514

453 C.M. Seah, S.P. Chai, A.R. Mohamed, Synthesis of aligned carbon nanotubes, Carbon 49 (2011) 4613–4635

454 Ibidem

455 S. Xie *et al.*, Carbon nanotubes arrays, Materials Science and Engineering A 286 (2000) 11-15

456 R. Khare, S. Bose Vol. 4, No.

457 H.S. Kim, *et al.*, Synthesis of Aligned Few-Walled Carbon Nanotubes on Conductive Substrates, J. Phys. Chem. C, 113 (2009) 17983-17988

few-walled CNTs directly on conductive substrates. The difficulty in growing CNTs on conductive substrates is mainly due to the degradation of substrates and catalytic nanoparticles under the reactive CNT growth conditions, such as the hydrogen environment at elevated temperatures. For example, hydride-forming metals, including Ti and Ta, are partially etched by the formation of volatile metal hydrides and become resistive, and metals with a low melting temperature, such as Au, ball up and become discontinuous after CNT growth. Moreover, the catalytic activity of the seed nanoparticles can deteriorate because the catalysts may react with the supporting conductive substrates at high growth temperatures. For example, catalytic iron nanoparticles react with silicon to form $FeSi_2$ or Fe_2SiO_4, or with carbon-based substrates to produce unwanted phases of carbon materials and lose their catalytic activity. Catalyst poisoning caused by amorphous carbon deposition on the nanoparticle surface can also significantly reduce the catalytic activity and lower the efficiency of the synthesis. In addition, the aggregation of nanoparticles at elevated temperatures promotes the growth of multiwalled CNTs instead of few-walled CNTs. Therefore, in order to grow few-walled CNTs directly on conductive substrates, it is essential to employ non-reactive substrates, preserve the catalytic activity, and control the catalytic nanoparticle size during the CVD process.

CNT forests[458] can easily be grown on amorphous Si interface deposited on the surface of CF to obtain a multiphase CNT/Si/CF. In this method, Si acts as a barrier, preventing the Fe catalyst to diffuse into the CF. The time of CNT growth affects the density (coverage) and alignment of the MWCNT. In other words, the density and the degree of alignment increase as the time of CNT synthesis increases.

As previously explained, CNTs growth could be achieved by means of different technique. Among these the use of catalyst or catalyst precursor are commonly employed. Catalyst applies directly on substrate could cause interaction with fiber, due to high temperature involved, such as such as carbide formation or catalytic restructuring of the fiber surface. Coating could be used to prevent fiber from damage, because it could provide an alternative textural and/or chemical surface over the geometry of a fiber without disrupting the chemistry or microstructure of the fiber.

Coating should present several characteristic, such as:

- to promote CNT alignment, to prevent catalyst nanoparticles from interacting with the fiber surface and thus to avoid chemical modification of carbon fiber surface,

[458] V. Gonzaga de Resende, Growth of carbon nanotube forests on carbon fibers with an amorphous silicon interface, Carbon 48 (2010) 3655-3658

- to improve wettability towards ions and depositions mediated by polar intermediates,
- to reduce temperature required for CNT growth,
- to design a process scalable to large scale continuous process.

Towards this target the processing techniques of sol-gel deposition, electrodeposition and chemical vapor deposition were explored by Stephen Alan Steiner III during his PhD[459].

The present work is focus on CNTs growth on carbon carbon surface and it exploits some methods used in Steiner's research. Thanks to the results obtained by previous research, alumina has been chosen as coating to prevent fiber damage and promote CNTs growth. Indeed alumina is widely used as a support for Fe catalysts in the growth of aligned CNT arrays.[460,461,462,463,464]

Alumina avoids particle coarsening of Fe catalyst nanoparticles and it maintains a closely-spaced population of small nanoparticles to facilitate growth of the high area density of CNTs. Alumina could be deposited by several techniques: sol-gel deposition, electrodeposition and chemical vapour deposition. In this thesis sol-gel and CVD has been studied.

3.1.4.3. Substrate Coating for Aligned CNT growth

Chemical Vapour Deposition of Alumina

For deposition of alumina on carbon fibers CVD can be applied. As solid precursor for alumina deposition, in the present work it has been chosen aluminium triisopropoxide (ATI, $Al(OC_3H_7)_3$). To use it, the compound is either sublimed or melted (melting point 128-133°C) to generate a vapour which is then delivered into the deposition chamber by a flow of an inert carrier gas such as Ar. Solid precursors such as ATI are frequently placed directly into a heated reaction chamber in proximity to the deposition target. Liquid precursors, most commonly aluminium tri-secbutoxide (ATSB) are easier to

459 S.A. Steiner III, Carbon Nanotube Growth on Challenging Substrates: Applications for Carbon-Fiber Composites, Doctor of Philosophy at the Massachusetts Institute of Technologies.

460 E.J. Garcıa *et al.*, Fabrication of composite microstructures by capillarity-driven wetting of aligned carbon nanotubes with polymers. Nanotechnology, 18 (2007) 165602-165612

461 C. Mattevi, In-situ X-ray photoelectron spectroscopy study of catalyst-support interactions and growth of carbon nanotube forests, Journal of Physical Chemistry C 112 (2008) 12207-12213.

462 S. Noda, *et al.*, Millimeter-Thick Single-Walled Carbon Nanotube Forests: Hidden Role of Catalyst Support, Japanese Journal of Applied Physics, Part 2: Letters and Express Letters 46 (2007) L399-L401

463 K. Hata *et al.*, Water-Assisted Highly Efficient Synthesis of Impurity-Free Single-Walled Carbon Nanotubes, Science 306 (2004) 1362-1364

464 O.A. Louchev, *et al.*, Growth mechanism of carbon nanotube forests by chemical vapor deposition, Applied Physics Letters 80 (2002) 2752-2754

process than solid precursors. To use them, the precursor, typically located outside of the deposition chamber, is heated to generate a vapour pressure and then it is delivered into the chamber by bubbling a carrier gas through the heated liquid. CVD alumina from solid-phase ATI was the first alumina CVD processed evaluated as it requires no special process equipment beyond what is available in a typical CVD reactor for CNT growth. In the processes investigated, a ceramic crucible is filled with a quantity of solid ATI. The crucible and a target substrate are then placed into a quartz process tube and heated with an electric clamshell furnace under a flow of an inert carrier gas such as He, N_2, or Ar. The ATI is positioned upwind of the substrate in order to have the carrier gas carry ATI vapor to the substrate. It was hypothesized that by setting the temperature profile of the furnace correctly, ATI would generate vapor (either as a liquid or solid), make its way to target substrates positioned throughout the quartz tube, and decompose via a surface-reaction-limited process to yield a conformal coating of alumina over the target, i.e. carbon fibers in this work.

Sol-Gel Deposition

The sol-gel process is a wet-chemical technique applied primarily to prepare gels, glasses, ceramic powder and metal oxides starting from nanoparticles dispersed in a liquid (a colloidal solution, namely sol) that acts as the precursor that extends throughout the liquid to form a continuous three-dimensional network (or gel) of either discrete particles or network polymers. Typical precursors are metal alkoxides and metal salts (such as chlorides, nitrates and acetates), which undergo various forms of hydrolysis and polycondensation reactions. The inertia of the dispersed phase is small enough that it exhibits Brownian motion, a random walk driven by momentum imparted by collision of solid particles in a liquid. [465]

Most sol-gel processes begin with a solution containing reactive monomers appropriate for producing the target material, for instance an organometallic such as an alkoxide. The monomers in this solution are then chemically, thermally, or photolytically invoked to undergo polymerization. The result of this polymerization event is the formation of a plurality of nanostructured particles throughout the liquid. Alternatively, nanostructured particles can be manufactured by another process and then dispersed in a liquid to create a sol. The nanostructures in the solution are then further invoked to agglomerate through sustention of the polymerization event (if applicable), introduction of a chemical, thermal, or photolytic stimulus, and/or allowing mutual attractive forces among the

[465] A.C Pierre, Introduction to sol gel processing, Boston Dordrecht London, Kluwer Academic Publisher (1998) ISBN: 0792381211-9780792381211

nanostructures to cause the nanostructures to adsorb and/or bond to each other. As nanostructures continue to agglomerate together, the viscosity of the solution increases until reaching infinity, at which point a porous, three-dimensional network of interconnected nanostructures spans the volume of the liquid medium. If one molecule reaches macroscopic dimensions so that it extends throughout the solution, the substance became a so called gel. The gel point is the time or degree of reaction at which the last bond is formed that completes this giant molecule. Thus a gel is a substance that contains a solid skeleton enclosing a continuous liquid phase. Gel can also be formed from particulate sols, when attractive dispersion forces cause them to stick together in such a way as to form a network.[466]

Many variations can be brought to sol-gel synthesis. The first step of any sol gel process always consists in selecting a precursor of the wanted materials, which allows to distinguish the types of sol-gel.[467] The colloidal route utilizes fine powder to form multicomponent systems, such as aluminosilicates. The polymeric route employs smaller scale precursors such as alkoxides, which give greater flexibility in the end product than the colloidal route, making it the most commonly used sol-gel route. Sol-gel can produce uniform crystalline particle size powders, which allows greater morphological control leading to greater homogeneity and purity. Sol-gel coatings can be modified with additives to provide functional properties such as adhesion, abrasion and corrosion resistance. [468]

Application of the sol-gel solution to the substrate to obtain a coating is either through spinning, dipping or spraying. Certainly one of the most technologically important aspect of sol-gel process is that, prior to gelation, the fluid sol or solution is ideal to prepare thin film by such common processes as dipping, spinning, or spraying. Sol-gel film formation requires considerably less equipment and is potentially less expensive than CVD. However the most important advantage of sol-gel processing over conventional coating methods is the ability to control precisely the microstructure of the deposited film, such as pore volume, pore size and surface area.[469] Thin films and coatings were the first commercial application of sol-gel processing technology.[470]

---

466 C.J. Brinker, G.W. Scherer, The physics and chemistry of Sol Gel Processing, Academic Press 1990 ISBN: 0-12-134970-5

467 A.C Pierre, Introduction to sol gel processing, Boston Dordrecht London, Kluwer Academic Publisher (1998) ISBN: 0792381211-9780792381211

468 C. Williams and J. Fernie, Novel joining and sealing processes for solid oxide fuel cells, 5th European Solid Oxide Fuel Cell Forum, Lucerne, Switzerland, 1-5th July 2002.

469 C.J. Brinker, G.W. Scherer, The physics and chemistry of Sol Gel Processing, Academic Press 1990 ISBN: 0-12-134970-5.

470 B.Viswanathan, Frontiers in Chemestry, Chapter 5: Synthetic Strategies in chemist-SOL-GEL TECHNIQUES L.H. Kumar, National Centre for Caralysis Research Indian Institute of Technology, Madras, April 2008

Thin films thinner than 1 µm can be deposited by dip-coating or spin-coating using small amounts of raw materials. The samples are dried and fired to remove the organics from the coating. The coating subsequently crystallizes during the firing cycle to produce a uniform and homogeneous structure. In order to improve the mechanical properties of the coating, ceramic particles can be dispersed within the sol-gel matrix to form a composite material, thus thick coatings in the range of 5-200 µm is reached. Cracking of the coating is limited due to the powder particles acting as crack inhibitors. Volume shrinkage is also reduced (due to a reduction in volume of the matrix) producing a strong bond between the particles, the matrix and the substrate. [471]

Large substrates may be accommodated and it is possible to uniformly coat both sides of planar and axially symmetric substrates such as pipes, tubes, rods and fibers. Ceramic coatings are usually deposited on metals for improving their performances in high temperature aggressive environments. Some important applications, include improving resistance against gas, solid, condensed, and molten-phase corrosion, to localized overheating and melting; decreasing fretting and wear; decreasing heat losses and/or reflecting radiations in high temperature systems. [472]

Aluminum hydroxides and oxo-hydroxides is applied as precursors to transition alumina as used as catalyst supports and absorbent as well as α-Al2O3, used commonly as structural ceramic. Hydrolysis and condensation studies of both aqueous and organic aluminum system indicate that the condensation pathway is very sensitive to precise condition of hydrolysis, aging and peptization. [473] Further maturation of the gel network generally continues after the gel point is reached, as reactive materials are still present throughout the pore liquor the volume of liquid within the pore network. The gel network is both nanostructured and substantially nanoporous and presents a high-surface-area chemical functionality over its sponge-like skeleton. If the pore liquor is removed evaporatively, capillary stresses will evolve at the solid-liquid interface as the liquid-vapor interface penetrates into the pore, that is the liquid leaves the gel network. If the modulus of the gel network cannot resist the capillary stresses that result from this phenomenon, the gel network will collapse in on itself and densify into a solid with substantially less porosity than the starting gel. If the surface chemistry of the solid network is self-interactive (such as a hydroxylated surface), the gel network will chemically bond to itself, thus gel network irreversible collapse. Alternatively, if the

---

471 C. Williams and J. Fernie, Novel joining and sealing processes for solid oxide fuel cells, 5th European Solid Oxide Fuel Cell Forum, Lucerne, Switzerland, 1-5th July 2002.

472 B.Viswanathan, Frontiers in Chemestry, Chapter 5: Synthetic Strategies in chemist-SOL-GEL TECHNIQUES L.H. Kumar, National Centre for Caralysis Research Indian Institute of Technology, Madras, April 2008

473 C.J. Brinker, G.W. Scherer, The physics and chemistry of Sol Gel Processing, Academic Press 1990 ISBN: 0-12-134970-5

surface chemistry is substantially non-interactive (such as a trimethylsilylated surface) or has been chemically passivated prior to drying (for example, by reacting surface hydroxyl groups with trimethylchlorosilane), the gel network can recover the majority of its original volume through a process known as spring back.

Sol-gel-derived alumina coatings are both stoichiometrically imperfect, usually presenting hydroxyl-terminated surfaces as-deposited, and generally exhibit high surface areas, arising from their highly porous precursors. These features, in addition to ambient-temperature processing and solution-based deposition, make sol-gel a highly appealing approach to deposit alumina coatings on carbon fibers.[474]

Sol-gel process could be characterized by a series of distinct steps:

1. Formation of the 'sol', for example stable solutions of the alkoxide or solvated metal precursor
2. Gelation resulting from the formation of an oxide- or alcohol-bridged network (the gel) by a polycondensation or polyesterification reaction that results in a dramatic increase in the viscosity of the solution.
3. Aging of the gel, during which the polycondensation reactions continue until the gel transforms into a solid mass, accompanied by contraction of the gel network and expulsion of solvent from the gel pores.
4. Drying of the gel, that is the loss of water, alcohol and other volatile components. It happens first as syneresis expulsion of the liquid as the gel shrinks latter as evaporation of liquid from within the pore structure with associated development of capillary stress which frequently leads to cracking. This also includes super critical drying, in which capillary stress is avoided by the use of supercritical fluids, such as CO_2, in conditions where there are no liquid/vapor densities. Drying process is complicated due to fundamental changes in the structure of the gel. The drying process has itself been broken into four distinct steps: constant rate period, the critical point, the first falling rate period, the second falling rate period.

3.1.4.4. Purification

In many of the synthesis methods that have been reported, carbon nanotubes are found along with other materials, such as amorphous carbon and carbon nanoparticles. For this reason purification generally is necessary to isolate carbon nanotubes from other

[474] S.A. Steiner III, Carbon Nanotube Growth on Challenging Substrates: Applications for Carbon-Fiber Composites, Doctor of Philosophy at the Massachusetts Institute of Technologies

entities[475]. The classical chemical techniques to purify (such as filtering, chromatography, and centrifugation) have been tried, but they are not able to remove carbon nanoparticles, amorphous carbon and other unwanted species. Heating preferentially decreases the amount of disordered carbon relative to carbon nanotubes, and it could be useful to purify, but it causes an increase of nanotube diameter due to the accretion of epitaxial carbon layers from the carbon in the vapor phase resulting from heating [476]. Because of their hydrophobic nature, carbon nanotubes tend to agglomerate hindering their dispersion. The resulting nanotube bundles or aggregates reduce the mechanical performance of the final composite. The surface of the carbon nanotubes can be modified to reduce the hydrophobicity and improve interfacial adhesion to a bulk polymer through chemical attachment.[477] Three basic methods have been used to purify nanotubes: gas phase, liquid phase, and intercalation methods.

The gas phase method removes nanoparticles and amorphous carbon by an oxidation or oxygen-burning process. Much slower layer-by-layer removal of multi-wall cylindrical layers nanotubes occurs because of the greater stability of a perfect graphene layer to oxygen. This method was first used to synthesize a single-wall carbon nanotube.[478] The gas phase purification process also tends to burn off many of the nanotubes. The carbon nanotubes obtained by gas phase purification are generally multi-wall nanotubes with diameters of 20-200 Å and 10 nm- 1 µm as length, since the smaller diameter tubes tend to be oxidized with the nanoparticle.[479] Liquid phase removal of nanoparticles and other unwanted carbons has been carried out with some success using a potassium permanganate $KMn0_4$ treatment method which tends to give higher yields than the gas phase method, but results in nanotubes of shorter length [480]. Finally, the intercalation of unpurified nanotube samples results in intercalation of the nanoparticles and other carbon species. Thus subsequent chemical removal of the intercalated species can be carried out [481]. The first stage is to immerse the crude cathodic deposit in a molten copper chloride and potassium chloride mixture at 400°C and leave it for one week. The product of this treatment, which contains intercalated nanoparticles and graphitic fragments, is then washed in ion exchanged water to remove excess copper chloride and

475 R Saito *et al*., Physical Properties of Carbon Nanotube, Imperial College Press, London (1998) ISBN 978-1860942235

476 Ibidem

477 http://en.wikipedia.org/wiki/Carbon_nanotube_chemistry

478 S. C. Tsang, P. J. F. Harris and M. L. H. Green Thinning and opening of carbon nanotubes by oxidation using carbon dioxide, Nature 362 (1993) 520 - 522

479 T.W. Ebbesen, Carbon Nanotubes, Annu. Rev. Mater. Sci. 24 (1994) 235-264

480 R Saito et al., Physical Properties of Carbon Nanotube, Imperial College Press, London (1998) ISBN 978-1860942235

481 T. W. Ebbesen, In Carbon Nanotubes: Preparation and Properiaes, (1997) Chapter IV page 139, CRC Press, Inc., Boca Raton, Florida, USA

potassium chloride. In order to reduce the intercalated copper chloride-potassium chloride metal, the washed product is slowly heated to 500°C in a mixture of Helium and hydrogen and held at this temperature for 1 hour. Finally, the material is oxidized in flowing air at a rate of 10°C/min to a temperature of 555°C. A disadvantage of this method is that some amount of nanotubes are inevitably lost in the oxidation stage, and the final material may be contaminated with residues of intercalates.[482]

[482] P.J.F. Harris, Carbon Nanotube and Related Structures New Materials for the Twenty-first Century, Cambridge University Press (2010) ISBN: 9780511605819

3.2. Method and Results

3.2.1. Overview of the Study

The aim of the research activity is focused on high-temperature clutch materials improvements, especially to modify a clutch material "blanket" with aligned-CNTs, grown on the working surfaces. Material issues in the clutch pads are similar to those for brakes, and include torque increases due to coefficient of thermal expansion (CTE) of the carbon/carbon (C/C) disc material, and frictional coefficient drift as a function of temperature. Both phenomena lead to overall reduced performance. The aim of the study is to realize a new composite material combining aligned carbon nanotubes (CNTs) with C/C, with improved and tailorable properties.

Different methods have been developed and described in literature to optimize the growing process for aligning carbon nanotubes on carbon fibers in a carbon matrix. Wardle's group from MIT has experience in thermomechanical design, fabrication, and characterization of both advanced ceramic materials [483,484,485,486,487,488] and specifically CNT-enhanced hybrid composites for the aerospace industry.[489,490,491,492]

The surface modification of C/C Clutch Materials by aligned CNTs is expected to lead to:

---

[483] N. Yamamoto, Thermomechanical Testing of Materials and Structures for a Microfabricated Fuel Cell, MIT S.M. Thesis, August 2006

[484] P. Capozzoli, Residual Stress and Electrochemical Properties of Proton-Conducting Materials for a MEMS Fuel Cell, MIT S.M. Thesis, August 2006.

[485] D. Quinn, B.L. Wardle, S.M. Spearing, Residual Stress and Microstructure of As-deposited and Annealed Sputtered Yttria Stabilized Zirconia Thin Films, Journal of Materials Research 23 (2008) 609-618

[486] N. E. duToit, B.L. Wardle, S.G. Kim, Design Considerations for MEMS-scale Piezoelectric Vibration Energy Harvesters, Integrated Ferroelectrics 71 (2005) 121-160

[487] N. E. duToit, B.L. Wardle, Performance of Microfabricated Piezoelectric Vibration Energy Harvesters, Integrated Ferroelectrics 83 (2006) 13-23

[488] N. E. duToit, B.L. Wardle, Experimental Verification of Models for Microfabricated Piezoelectric Vibration Energy Harvesters, AIAA Journal 45 (2007) 1126-1137

[489] E.J. Garcia, B.L. Wardle, R. Guzman deVilloria, S. Wicks, K. Ishiguro, N. Yamamoto, A.J. Hart, Aligned Carbon Nanotube Reinforcement of Advanced Composite Ply Interfaces, AIAA-2008-1768, 49th AIAA Structures, Dynamics, and Materials Conference, Schaumburg, IL, April 7-10, 2008

[490] N. Yamamoto, B.L. Wardle, Thermal and Electrical Properties of Hybrid Woven Composites Reinforced with Aligned Carbon Nantoubes, AIAA-2008-1857, 49th AIAA Structures, Dynamics, and Materials Conference, Schaumburg, IL, April 7-10, 2008.

[491] B.L. Wardle, D.S. Saito, E.J. Garcia, A.J. Hart, R. Guzman deVilloria, Fabrication and Characterization of Ultra-High Volume Fraction Aligned Carbon-Nanotube-Polymer Composites, Advanced Materials, 20 (2008) 2707-2714.

[492] E.J. Garcia, B.L. Wardle, A.J. Hart, Joining Prepreg Composite Interfaces with Aligned Carbon Nanotubes, Composites Part A, 39 (2008) 1065-1070

- control over the material's CTE utilizing the negative CTE inherent to CNTs to counteract positive thermal expansion;
- fabrication time and cost improvements over typical C/C enhancements made possible by the nano-scale CNT scaffold for the carbon matrix;
- frictional/wear improvements and tailoring;
- enhance hydrophobicity;
- tailor of thermal conductivity, anisotropically, again made possible by incorporating aligned CNTs.

Currently, the majority of existing carbon/carbon composites is used for aircraft braking systems, with other important applications including brakes for automobiles, high-temperature thermal protection for the leading edges of the space shuttle wings, and nose cones for intercontinental ballistic missiles. [493] In such advanced C/C composites, a weave of carbon fibers (CFs) is laid up and impregnated with a phenolic resin. The resin is then carbonized and heat-treated at elevated temperatures to produce a porous carbon matrix, structurally supported by the CFs underneath, similar to how steel cables provide structural integrity in reinforced concrete. Aligned CNTs offer tremendous potential for improving the strength, toughness, and impact properties and tribological properties, as well as other relevant properties (thermal and hydrophobicity) of carbon-matrix composites. Nano-scale reinforcement provided by aligned CNTs can reduce the amount of free space in the matrix and increase the total interfacial region between reinforcement and matrix[494], thus creating structural reinforcement through the carbon matrix on two different length scales. The inherently nanostructured/nanoporous CNT forest, in turn, provides a more confined pyrolysis environment for the resin as it transforms into graphite than in a typical C/C material.

In the present work, existing C/C materials had their working surfaces modified with C/C/CNT composites fabricated as follows:

- pre-treatment of the C/C substrate on the working surface (blanket)
- growth of aligned CNTs on the surfaces of the blanket
- infiltration with phenolic resin
- pyrolysis.

This chapter focuses on the synthesis processes used to obtain aligned nanotube on C/C substrate and it is a preliminary study for the development of a new composite.

---

493 G. Savage, Carbon-Carbon Composites, Chapman & Hall, London, (1993)

494 R.A. Vaia, H.D. Wagner, Framework for Nanocomposites, Materials Today (Oxford, United Kingdom) 7 (2004) 32-37

3.2.2. Materials and Methods

In this work two different approaches have been applied to grow CNTs on C/C surface: barrier approach and non barrier approach.

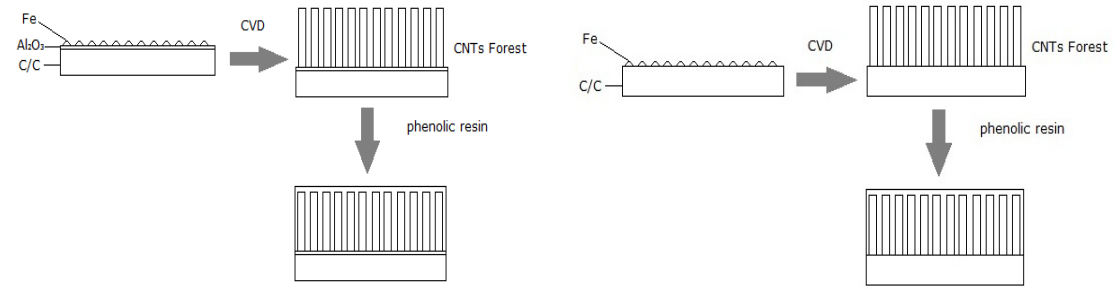

a b

Figure 3.2–1: Pattern of two different approaches applied: a) non barrier approach and b) barrier approach

Barrier approach (Figure 3.2–1 a) exploits an inert metal oxide for coating the substrate prior to catalyst application in order to prevent and protect it from damage. On the contrary, in non barrier approach (Figure 3.2–1 b), catalyst is directly applied on substrate surface.

General guidelines for optimizing process have been taken from one of Stephen Alan Steiner III's PhD thesis[495], where different techniques to apply barrier coating have been studied to grow carbon nanotubes on carbon fiber and a preliminary study about non barrier approach has been dealt with.

3.2.2.1. Preparation and Characterization of Substrate

Preliminary analyses have been done to characterize as received clutch material, to be used as substrate. Clutch has been received from supplier with a machined surface by machine tools. Discs are shown in Figure 3.2–2. Analyses have been conducted on 20 mm x 10 mm samples extracted from the as received clutch discs by abrasion cutting.

[495] S.A. Steiner III, Carbon Nanotube Growth on Challenging Substrates: Applications for Carbon-Fiber Composites, Doctor of Philosophy at the Massachusetts Institute of Technologies

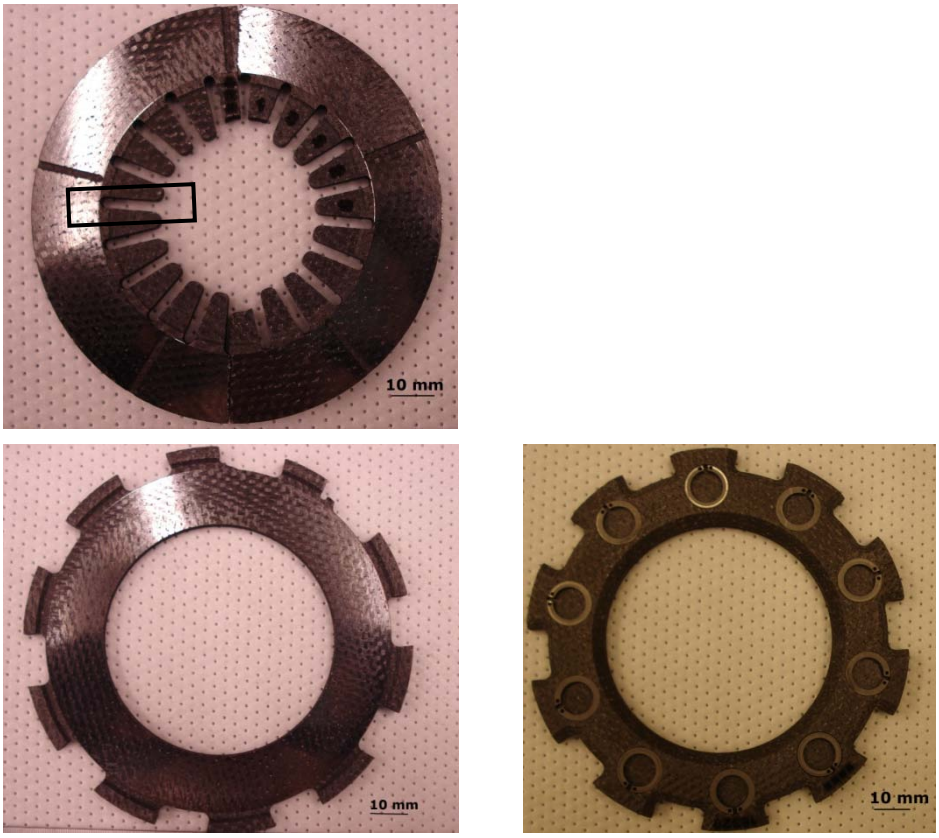

Figure 3.2–2: Clutch is constituted by two different disc repeated (a) disc one, (b) front and back of same disc, black rectangle show the dimension of samples .

In literature has been related CNT growth on several substrates, such as silicon wafer[496] and carbon fiber[497], which are specifically designed to favor carbon nanotube development. Hence, the major problem is due to the difficulties of growing aligned nanotubes on machined (carbon) substrates of industrial-like components, which present microvoids and cracks, instead of using almost defect-free planar substrates such as silicon wafer, as shown in Figure 3.2–3.

[496] W. Hu *et al.*, Growth of well-aligned carbon nanotube arrays on silicon substrates using porous alumina film as a nanotemplate, Appl. Phys. Lett. 79 (2001) 3083-3085

[497] A.R. Suraya *et al.*, Growth of Carbon Nanotubes on Carbon Fibers and the Tensile Properties of Resulting Carbon Fiber Reinforced Polypropylene Composites, Journal of Engineering Science and Technology 4 (2009) 400-408

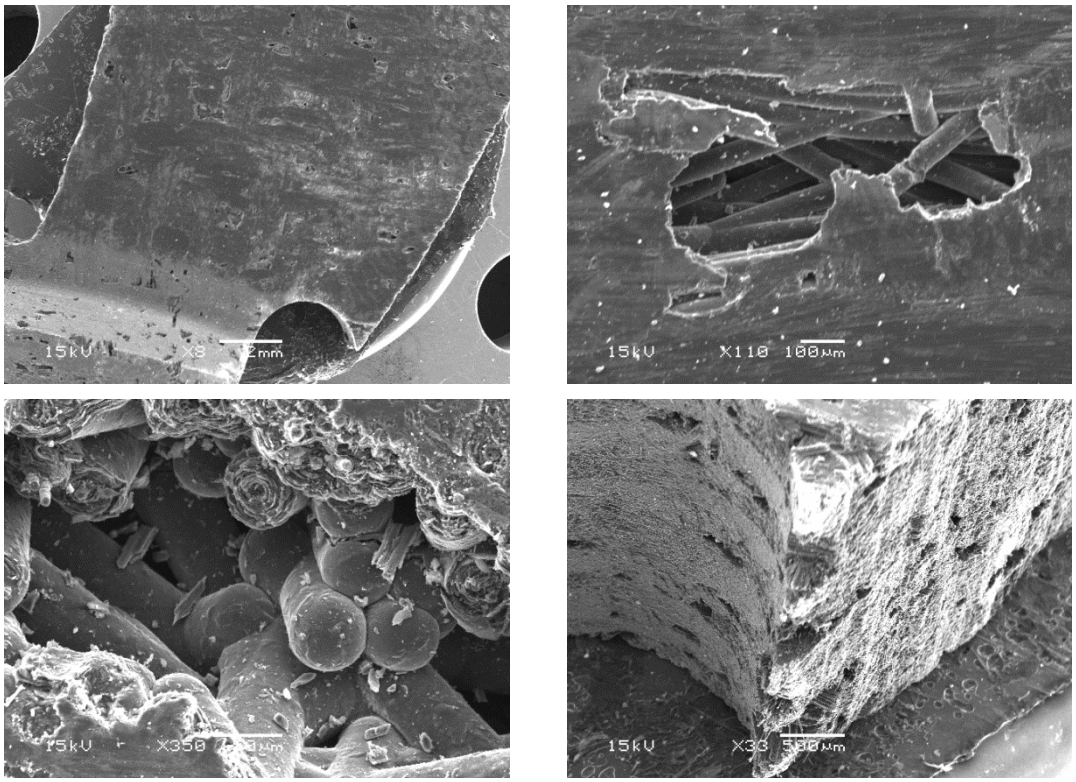

Figure 3.2–3: SEM images of as received samples, showing microvoids and cracks of machined surface

3.2.2.2. Pre-treatment on C/C substrate

As previously explained, before CNT growth on C/C clutch can properly occur, substrate must be pre-treated to guarantee a good adhesion between CNT and the substrate itself. Substrates as received have been exposed to different temperature, time and gas mixtures. Gases have been exploited Ar, He, CO_2 and mixture of them, temperature varies from 700 °C to 1100 °C and time from 1 hour to 5 hours. In order to investigate the substrate response at high temperature TGA, thermogravimetric analysis (TA Instruments (TGA) & PFEIFFER VACUUM (MS) Model TGA Q50 equipped with Thermostar mass spectrometer (PFEIFFER VACUUM) 953501.90), and BET analysis (Manufacters Micrometrics Model ASAP2020) have been performed. The former has been applied to determine weight variation on sample in relation to high temperature exposure in a controlled atmosphere. The latter is applied to measure the specific surface area of a material and hence to determine the gas effect on as received samples.

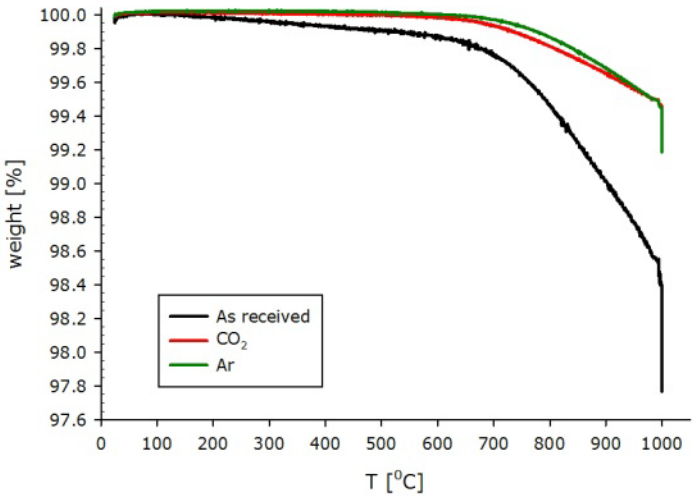

Figure 3.2–4: Thermogravimetric analysis of 3 different samples: as received (black line), etched by CO_2 (red line) and etched by Ar (green line)

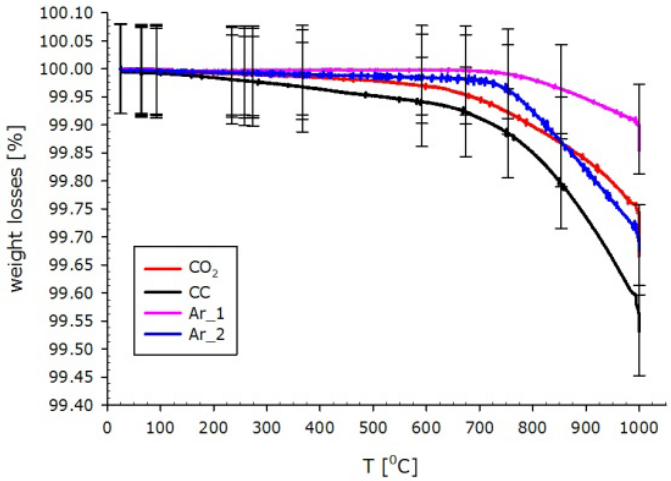

Figure 3.2–5: Thermogravimetric analysis of different treatment tried, as received sample (black line, CC), CO_2 etched (red line, CO2), Ar etched (pink Ar_2 and blue Ar_2 lines) at two different temperatures of 900 and 1100 °C (respectively)

TGA analysis before and after pre-treatment was performed from room temperature to 1000 °C at 10 °C/min. TGA plots in Figure 3.2–4 show that below the pre-treatment temperature (red line) and growing temperature there are no weight losses (below 700 °C, mismatches among plots are meaningless, because error bars are overlapped). In Figure 3.2–4, the curve indicated by "Ar" is obtained by TGA analysis of sample CC exposed to a pre-treatment of only Ar at the same temperature fixed during CO_2 etching

and the flow rate set adding together the values of two different gas flow rates, Ar and CO_2, employed during pre-treatment, (180 sccm + 20 sccm). Its behavior is similar to the sample treated with CO_2. TGA is repeated on a second sample set (Figure 3.2–5) both to confirm previous results and to demonstrate that the very small weight losses after 700 °C are only due to temperature and not to the kind of gas used. This seems to indicate a desorption process or reactivity (pyrolysis) not related to the kind of gas used. This indicates that the pre-treatment does not cause any effect on the substrate except for a possible continued pyrolisys. Furthermore in order to verify the homogeneity of as received samples different sets have been tested by TGA (Figure 3.2–6). As previously shown, the error bars overlapping confirms the similarity with respect to TGA of different samples taken from different parts of the clutch disc.

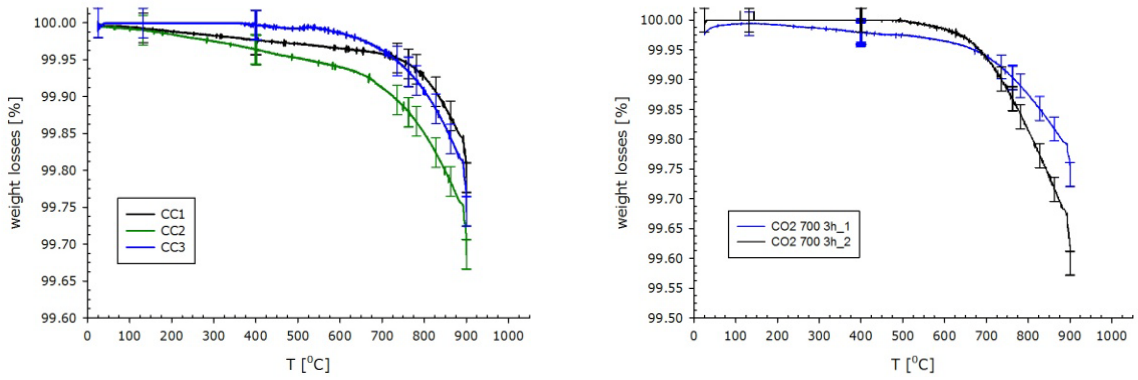

Figure 3.2–6: Sample treated at the same way to show result repeatability.

The pre-treatment performed on samples is expected to increase surface area. To verify this assumption, BET analysis was performed on several sample sets: in detail 3 sets of samples as received (without any treatment) and 3 set of samples which have been processed in CVD furnace with CO_2. Samples were degased under vacuum condition (10^{-5} Pa) at 150 °C for 3 hours. Analysis has been performed in Krypton @ 77.3 K beacuse samples show a surface area lower than 1 m^2. Results confirm that specific surface area [m^2/g] increases of 22.78% from as received to the CO_2 at T_1 for 3h etched sample, in agreement with literature results.[498]

Table 3.2-1: Surface area values for both as received and CO_2 etched samples.

[498] C. Zhou *et al.*, SWNT/PAN/SAN ternary composite: Pore Size Control and Electrochemical Supercapacitor Behavior, Polymer 47 (2006) 5831-5837

Set Sample	BET surface [m²/g]	Correlation Coefficient	BET surface [m²/g]	Correlation Coefficient	Increase
Set	As Received		CO_2		%
1	0.2334 ± 0.0004	0.9999908	0.2560 ± 0.0006	0.9999859	9.7
2	0.2355 ± 0.0014	0.9999039	0.3093 ± 0.0007	0.9999857	31.3
3	0.2750 ± 0.0018	0.9998853	0.3480 ± 0.0010	0.9999815	26.5
Average	0.2479 ± 0.0234		0.3044 ± 0.04619		22.6

To obtain reliable data three different sets of same samples have been measured. Results reported on

Table 3.2-1 have been plotted in Figure 3.2–7.

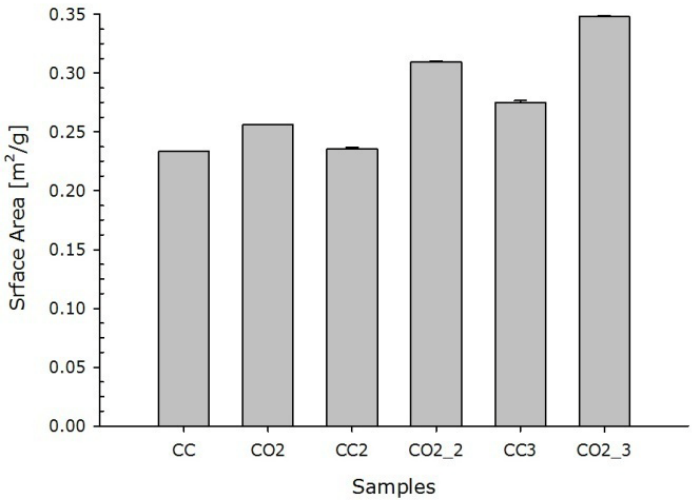

Figure 3.2–7: Surface area plot for different sample sets.

3.2.2.3. Barrier approach

As barrier coating material, alumina has been chosen according to Dr. Steiner's study. However, before coating substrate a pre-treatment must be performed to obtain a good adhesion between substrate and coating. Exposure of the substrate to different temperature and gas mixtures have been studied as pre-treatment. Two different deposition ways of alumina has been investigated. After barrier coating deposition a catalyst has been applied. As catalyst $Fe(NO_3)_3$ $9H_2O$ in 2-propanol IPA (Isopropyl alcohol) and two different ferrofluid has been probed, moreover different dipping times and solution aging time have been analyzed. CNTs growth occurred by CVD technique. In this procedure different time and two different temperatures have been investigated.

Flow chart summarizes parameters variation in barrier approach.

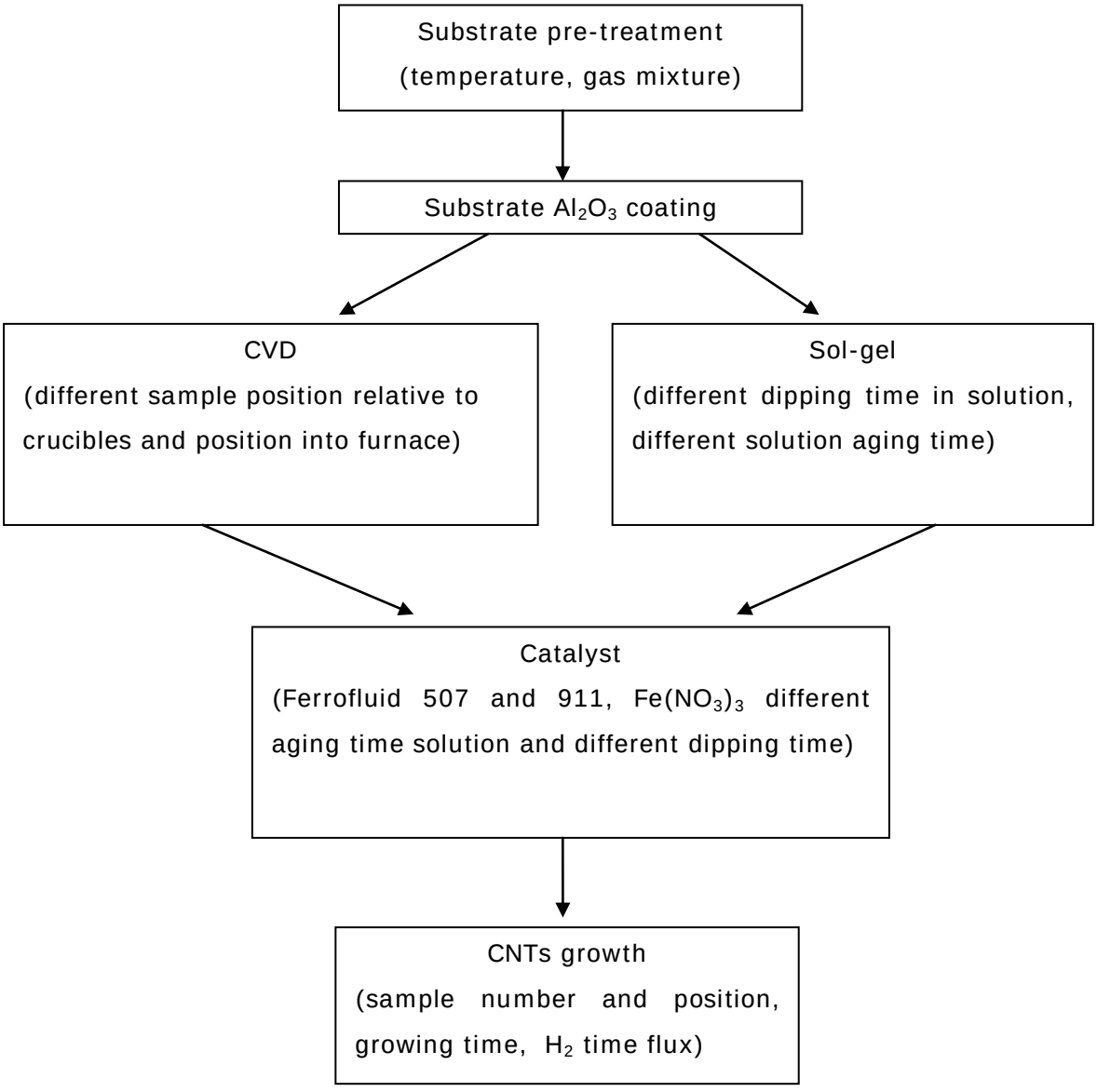

Two different deposition processes have been studied to coat the substrate with alumina: sol-gel and CVD technique. The former is obtained via Propylene-Oxide Assisted Gelation, while the latter exploits Aluminum triisopropoxide (ATI, $Al(OC_3H_7)_3$) as precursor. Among various sol-gel techniques[499], propylene-oxide-based formulation has been selected because it can control gel time in order to obtain a better process control. In this case, 2.96 g $AlCl_3 \cdot 6H_2O$ was dissolved in a mixture of 10.0 g (10.0 mL) deionized water and 7.89 g (10.0 mL) absolute ethanol. The mixture was stirred until the salt had fully dissolved. Next, 7.86 g (9.5 mL) propylene oxide was added slowly into the solution with stirring via syringe. The solution was then stirred another 5 minutes and allowed to solidify. Gel time was about 45 minutes; it could be further adjusted by increasing the amount of solvent used; however this results in an increase in porosity and its usefulness must be verified. The deposition process chosen is dip coating: samples are completely immersed into solution.

As already mentioned, the other deposition technique exploited in this work was CVD. The technique uses ATI as solid precursor, which is either sublimed or melted (melting point 128-133°C) to generate a vapor which is then delivered into the deposition chamber by a flow of an inert carrier gas, such as He or Ar. Solid precursors such as ATI are placed directly into a heated reaction chamber in proximity to the deposition target. In processes investigated, a ceramic crucible, an alumina crucible (Sigma-Aldrich part number Z561738-1EA), is filled with a fixed quantity of solid ATI. The crucible and a target substrate are then placed into a quartz process tube and heated with an electric clamshell furnace under a flow of an inert carrier gas such as He, N_2, or Ar. It was hypothesized that by setting the temperature profile of the furnace correctly, ATI would generate vapor (either as a liquid or solid), make its way to target substrates positioned throughout the quartz tube, and decompose via a surface-reaction-limited process to yield a conformal coating of alumina over the target, (in this case C/C composite). This is a line-of-sight process that deposits on the sample surface facing upward downstream of the crucible and has a typically spatially-varying thickness non-uniformity. In comparison with previous work,[500] alumina deposition process parameters was not modified. Sample arrangement in the furnace is expected to have influence on CNTs growth, due to possible different temperature distributions occurring in the furnace used. In case of sol-gel technique, this preliminary study is not required, due to the intrinsically homogeneous nature of the coating layer. Hence, different samples positions into furnace

[499] S.A. Steiner III, Carbon Nanotube Growth on Challenging Substrates: Applications for Carbon-Fiber Composites, Doctor of Philosophy at the Massachusetts Institute of Technologies

[500] Ibidem

have been studied to find the most suitable configuration able to provide a good alumina layer for further nanotube growth. Figure 3.2–8 (a) shows a sketch of relative position between target and samples, in detail samples could be place on a side of crucible or place over the crucible, in both case the coated surface was the top one. On the other hand Figure 3.2–8 (b) shows the different sample position inside the quartz tube (zone 1 or between zone 1 and 2), where samples could be arranged.

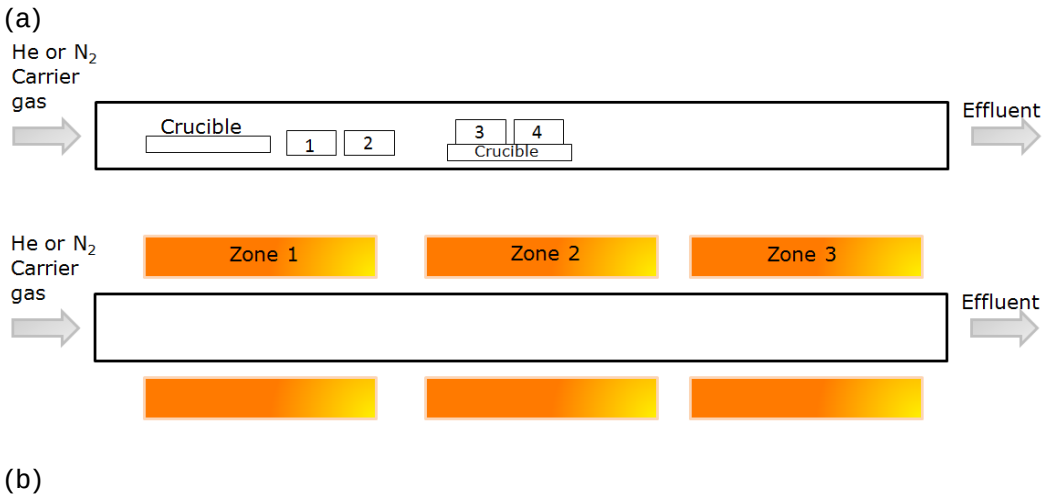

Figure 3.2–8: Possible variation in CVD alumina deposition

Different catalysts have been attempted: $Fe(NO_3)_3$ $9H_20$ in IPA and two different ferro solutions for growing CNTs at low temperature. In case of $Fe(NO_3)_3$ $9H_20$ in IPA different aging time of the solutions and different dipping time into solution have been investigated.

3.2.2.4. Non Barrier approach procedure

Another approach is focused on CNTs growth directly on C/C surface without any halfway layer. In this case more attention was focused on catalyst concentration, solution aging and dipping time. Flow chart shows the sequence to obtain CNTs on substrate.

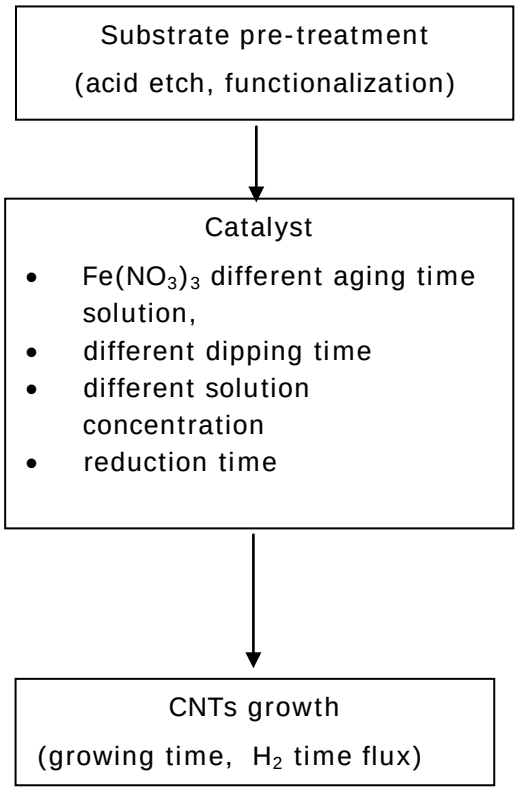

Alumina is a promoter of CNTs growth, but it may form an undesirable brittle layer between substrate and CNTs, so another approach that can avoid any in-between layer is desired. In non barrier approach, chemical surface treatments have been performed on the substrate to increase carbon fiber surface reactivity and surface energy, as well as to reduce the number of defects, in order to achieve a surface suitable to grow CNTs. The reactivity of the carbon fiber in an oxidizing atmosphere is dependent on the amount of order in its surface structure. [501]

Typical surface treatments fall into the following categories:

- dry gaseous oxidation,
- plasma treatment,
- electrolytic oxidation,
- liquid oxidation (chemical).

[501] Z. Wu *et al*. Nitric Acid Oxidation of Carbon Fiber and the Effect of Subsequent treatment in Refluxing Aqueous NaOH Carbon, Carbon 33 (1995) 597-605

Dry oxidation exploits air or oxygen or ozone as oxidizing gas. Surface layers burn away unevenly to create more active sites, but loss of fiber strength occurs if the treatment is extended. Low-pressure plasma treatments employ gases such as nitrogen, argon, oxygen, and air, among others. Plasmas contain highly energetic ions and radicals with very high average temperatures. Therefore, chemically inactive basal planes of graphite may be functionalized. Electrolytic oxidation is fast, uniform, and suitable for mass production and it exploits nitric, sulfuric, and phosphoric acids, dichromate, and permanganates.

Liquid chemical oxidations uses nitric acid, sulfuric acid, phosphoric acid, or hydrogen peroxide as the oxidizing agent. Using such technique, various densities of functional groups have been produced on carbon fibers as a function of reaction time. Oxidative treatments produce active sites by forming carbon-oxygen functional groups, increasing the surface roughness and surface area.[502] Some authors [503,504,505,506,507,508] recently described the effect of acid etch on carbon fiber. Nitric acid causes oxidation of carbon fiber, leading to obtain different amounts of surface acidic functional groups. The acidic capacity of these carbon fibers is proportional to the oxidation time. Nitric acid oxidation also causes a decrease of tensile strength, a weight losses and an increase of surface area in comparison with virgin fibers. Pits, crevasses, expanded microvoids have been formed upon oxidation.[509] For example[510], in the acidic medium, the graphite rod reveals +0.4 V (oxidation) and +0.3V (reduction) peaks upon the first anodic scan whereas the CF has peaks of +0.6V (oxidation) and +0.2V (reduction). In the case of the carbon fiber working electrode, not only was a rather large difference between the oxidation and reduction peaks observed, but also the charge under the curve was about 10 times greater than a graphite electrode of approximately the same size. After the electrochemical treatment in sulfuric acid, the fiber acquired the same amphoteric

---

502 Z. Wu *et al*. Nitric Acid Oxidation of Carbon Fiber and the Effect of Subsequent treatment in Refluxing Aqueous NaOH Carbon, Carbon 33 (1995) 597-605

503 Ibidem

504 Ibidem

505 M.B. Vázquez-Santos *et al.,* Effects of phosphoric acid as additive in the preparation of activated carbon fibers from poly(p-phenylene benzobisoxazole) by carbon dioxide activation Journal of Analytical and Applied Pyrolysis 95 (2012) 68–74

506 E. Bayramli, L. Toppare, N.K. Erinç, Investigations on the Electrochemical Surface Treatment of Carbon Fibers, Turk J Chem 25 (2001) 251-258

507 G. Li *et al.,* Interface correlation and toughness matching of phosphoric acid functionalized Kevlar fiber and epoxy matrix for filament winding composites, Composites Science and Technology 68 (2008) 3208–3214

508 Y.J. Kim *et al.*, Effects of sulfuric acid treatment on the microstructure and electrochemical performance of a polyacrylonitrile (PAN)-based carbon anode, Carbon 43 (2005)163–169

509 Z. Wu *et al*. Nitric Acid Oxidation of Carbon Fiber and the Effect of Subsequent treatment in Refluxing Aqueous NaOH Carbon, Carbon 33 (1995) 597-605

510 E. Bayramli, L. Toppare, N.K. Erinç, Investigations on the Electrochemical Surface Treatment of Carbon Fibers, Turk J Chem 25 (2001) 251-258

character when a certain amount of acidity occurred. The cyclic voltammetry studies indicate that in 50% sulfuric acid, oxidation and reduction of the carbon fiber surface are possible at +0.6 V and +0.2 V respectively. Electrochemical treatments of the fiber surfaces produced acidic surface groups in H_2SO_4 and NH_4CO_3 solutions, which were not present at the untreated surfaces. Chemical modifications on carbon fiber vary microstructure as functions of different heat treatment temperature and sulfuric acid treatment. Authors found [511] that the microstructure of the samples was not changed much by sulfuric acid treatment, although there were slight changes in interlayer spacing values, H/C ratio, crystallite size, and porosities. In case of phosphoric acid [512] the amount of surface functional groups of as-received and phosporic acid functionalized carbon fiber. The amount of oxygen functional groups on fiber surface was significantly changed by phosphoric acid functionalization moreover monofilament tensile strength was constant. [513]

As in previous method, substrate was treated before growing nanotubes, using CO_2 for the same time and at the same temperature of the optimum set obtained. Subsequently C/C substrate was hot acid etched using a blend of HNO_3, H_2SO_4 and H_3PO_4, at a fixed temperature for 3 hours. In this study, as pre-treatment, an hot acid (nitric, sulfuric and phosphoric acid at different concentration and T= 100°C) pickling has been chosen, in order to create more steps and pits on the surface carbon fibers, as well as to increase their chemical reactivity. Subsequent functionalization was performed using K_2CO_3 to neutralize surface. As catalyst iron has been chosen, but in this case $Fe(NO_3)_3$ $9H_2O$ has been dissolved in deionized water and both molar concentration and dipping time variation have been studied Then samples were dried in air and then iron nitrate were reduced to nanoparticles using furnace at determined temperature for different times (2-8 hours) using a fixed flow of inert gas. CNTs growth was performed by CVD technique at different growing time.

3.2.2.5. Growth procedure

CNT growth has been obtained in an atmospheric pressure CVD furnace (Figure 3.2–9). Most samples have been obtained via a standard CVD procedure with few parameters modified. Growth temperature, gas types and flow rate have been fixed; instead position into furnace, minutes of flowing of reactive gas. Only three sets have been grown

511 J. Kim *et al.*, Effects of sulfuric acid treatment on the microstructure and electrochemical performance of a polyacrylonitrile (PAN)-based carbon anode, Carbon 43 (2005)163–169

512 G. Li *et al.*, Interface correlation and toughness matching of phosphoric acid functionalized Kevlar fiber and epoxy matrix for filament winding composites, Composites Science and Technology 68 (2008) 3208–3214

513 Ibidem

exploiting another gas source and one inch furnace, keeping a lower temperature. All gases used were ultrahigh purity grade (Airgas, >99.999%). CVD growth of CNTs was performed inside a fused quartz tube (54-mm outer diameter, 50-mm inner diameter, 1.37-m length) heated by a three-zone split-hinge tube furnace (Lindberg/Blue M model HT55667C, 30- cm heated zone lengths,Figure 3.2–9). Due to the distance between thermocouples in this furnace and how a 54-mm process tube sits in this furnace, reported temperatures may underestimate actual process temperatures by ~80°C as determined by calibrations performed with in situ thermocouple instrument. Pre and post-treatment, etching with CO_2 and pyrolysis after resin infiltration respectively, have been performed in 25 mm furnace set up with fused quartz process tube (25 mm outer diameter, 22 mm inner diameter, 760 mm length) .

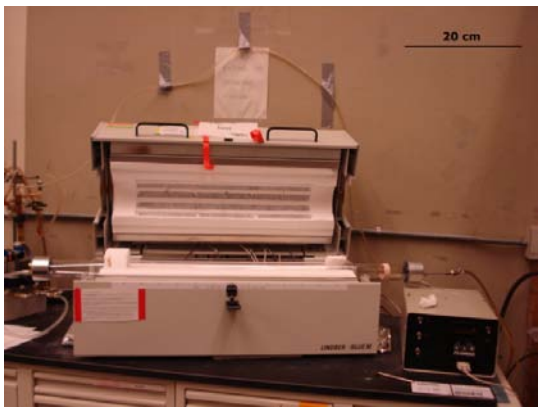

Figure 3.2–9: Furnace used to grow CNTs.

Furnace parameters have been changed one at a time in order to optimize the process for realizing aligned CNTs on carbon carbon substrates, only the sample position into furnace was not changed. All samples was put in the middle of zone 2 (Figure 3.2–8 (b)). After CNTs growth, samples have been characterized by SEM (JEOL Model JSM-6060)In some cases a FEG (field emission gun) was used (JEOL 2010 FEG Analytical Electron Microscope), due to its higher resolution.

Thanks to the kind industrial partnership of GeS Ferrari S.p.A. some data have been omitted to avoid any replications of experimental procedures. Table 3.2-2 and Table 3.2-3 relate all sample sets produced by two different approaches: barrier and no barrier method respectively.

Table 3.2-2: Barrier approach sample list

Set Name	CO_2 etching (n° samples inside the tube)	Al_2O_3 deposition	Catalyst	Growth (time, n° samples into tube)
A	12	CVD 4 samples to side of crucible	$Fe(NO_3)_3$	35 min, 4 samples
B	12	CVD 4 samples to side of crucible	$Fe(NO_3)_3$	30 min, 4 samples
C	12	CVD 4 samples to side of crucible	$Fe(NO_3)_3$	35 min, 4 samples
D	12	CVD 4 samples to side of crucible	$Fe(NO_3)_3$	35 min, 4 samples
E	12	CVD 4 samples to side of crucible	$Fe(NO_3)_3$	45 min, 4 samples
F	12	CVD 4 samples to side of crucible	$Fe(NO_3)_3$	35 min, 4 samples
G	4	CVD 4 samples to side of crucible	$Fe(NO_3)_3$	35 min, 4 samples
H	2	CVD 2 samples to side of crucible	$Fe(NO_3)_3$	35 min, 4 samples
I	1	CVD 1 samples to side of crucible	$Fe(NO_3)_3$	35 min, 4 samples
L	2	CVD upon crucibles two samples each	$Fe(NO_3)_3$	35 min, 2 samples
M	2	Sol Gel (for 1 h from preparation solution)	$Fe(NO_3)_3$	35 min, 2 samples
N	2	Sol Gel (after 1h dipping 6 times up to gelification)	$Fe(NO_3)_3$	35 min, 2 samples
P1	4	Sol Gel (after 1h dipping 12 times up to gelification)	911	35 min, 4 samples (T_{growth} 480 °C)
P2	4		$Fe(NO_3)_3$	30 min, 2 samples
P3	2		507	35 min, 4 samples (T_{growth} 480 °C)
P4	2		$Fe(NO_3)_3$	30 min, 2 samples

Set Name	CO_2 etching (n° samples inside the tube)	Al_2O_3 deposition	Iron particles	Growth (time, n° samples into tube)
Q1	4	CVD upon crucibles two samples each	507	35 min, 2 samples (T_{growth} 480 °C)
Q2	4		911	35 min, 2 samples (T_{growth} 480 °C)
Q3	2		$Fe(NO_3)_3$	30 min, 2 samples
Q4	2		$Fe(NO_3)_3$	30 min, 2 samples
R1	4 (different T)	Sol Gel (after 1h dipping 6 times up to gelification)	$Fe(NO_3)_3$ different aging time	60 min, 4 samples
R2				
R3		CVD upon crucibles two samples each		
R4				
S	4 (different t)	CVD upon crucibles two samples each (2 crucibles)	$Fe(NO_3)_3$ different aging time	45 min, 4 samples
T	4 (2 different following etch)	CVD upon crucibles two samples each (2 crucibles)	$Fe(NO_3)_3$ different aging time	45 min, 4 samples
V	4 middle (T_{CO2}, t_{CO2})	CVD upon crucibles two samples each (2 crucibles)	$Fe(NO_3)_3$ t_{opt}	45 min, 2 min H_2 flow, 4 samples

Table 3.2-3: Non barrier approach sample list

Set Name		Substrate Etching		Functionalization	$Fe(NO_3)_3$	$Fe(NO_3)_3$ Reduction time	Growth Gases and flowing time
		CO_2 (T_{CO2}, t_{CO2})	Acid etch	K_2CO_3			
A	A1	No	3h	1h	$t_{catalyst}$; $con_{catalyst}$	0.25 t_r	C_xH_y/H_2 45 min/t_{H2}
	A2	No	3h	1h	$t_{catalyst}$; $con_{catalyst}$	0.3 t_r	C_xH_y/H_2 45 min/ t_{H2}
	A3	Yes	3h	1h	$t_{catalyst}$; $con_{catalyst}$	0.3 t_r	C_xH_y/H_2 45 min/ t_{H2}
	A4	Yes	3h	1h	$t_{catalyst}$; $con_{catalyst}$	0.25 t_r	C_xH_y/H_2 45 min/ t_{H2}
B		Yes	4h	2h	$t_{catalyst}$; $con_{catalyst}$	0.28 t_r	C_xH_y/H_2 60 min/ t_{H2}
C	C1	Yes	3h	1h	$t_{catalyst}$; $con_{catalyst}$	No	C_xH_y/H_2 45 min/2 min t_{H2}
	C2	Yes	3h	1h	$t_{catalyst}$; $con_{catalyst}$	No	C_xH_y/H_2 30 min/ t_{H2}
D	D1	Yes	3h	1h	$t_{catalyst}$; $con_{catalyst}$	No	C_xH_y/H_2 10 min/ t_{H2}
	D2	Yes	3h	1h	$t_{catalyst}$; $con_{catalyst}$	No	C_xH_y/H_2 20 min/ t_{H2}
	D3	Yes	3h	1h	$t_{catalyst}$; $con_{catalyst}$	No	$C_xH_{0.5y}$ /CO_2 45 min
	D4	Yes	3h	1h	$t_{catalyst}$; $con_{catalyst}$	No	$C_xH_{0.5y}$ /CO_2 20 min
E		Yes	3h	1h	$t_{catalyst}$; $con_{catalyst}$	No	C_xH_y /H_2 4 min/ t_{H2}
F		Yes	3h	1h	$t_{catalyst}$; $con_{catalyst}$	No	C_xH_y /H_2 6 min/ t_{H2}
G		Yes	3h	1h	$t_{catalyst}$; $con_{catalyst}$	No	C_xH_y /H_2 8 min/ t_{H2}

Set Name	Etching		Functionalization	$Fe(NO_3)_3$	$Fe(NO_3)_3$ Reduction time	Growth Gases and flowing time
	CO_2 (T_{CO2}, t_{CO2})	Acid etch	K_2CO_3			
I	Yes	3h	1h	$t_{catalyst}$; $con_{catalyst}$	0.21 t_r	C_xH_y /H_2 15 min/ t_{H2}
L	Yes	3h	1h	$t_{catalyst}$; 0.01 $con_{catalyst}$	0.21 t_r	C_xH_y /H_2 15 min/ t_{H2}
M	Yes	3h	1h	0.04 $t_{catalyst}$; $con_{catalyst}$	0.21 t_r	C_xH_y /H_2 15 min/ t_{H2}
N	Yes	3h; conc1%	1h	$t_{catalyst}$; $con_{catalyst}$	0.21 t_r	C_xH_y /H_2 15 min/ t_{H2}
P	Yes	3h; conc10%	1h	$t_{catalyst}$; $con_{catalyst}$	0.21 t_r	C_xH_y /H_2 15 min/ t_{H2}
Q	Yes	3h	1h	0.5 $t_{catalyst}$; $con_{catalyst}$	0.21 t_r	C_xH_y /H_2 15 min/ t_{H2}
R	Yes	3h	1h	0.2 $t_{catalyst}$; $con_{catalyst}$	0.21 t_r	C_xH_y /H_2 15 min/ t_{H2}
S	Yes	3h	1h	0.25 $t_{catalyst}$; $con_{catalyst}$	0.21 t_r	C_xH_y/H_2 15 min/ t_{H2}
T	Yes	3h	1h	0.3 $t_{catalyst}$; $con_{catalyst}$	0.21 t_r	C_xH_x/H_2 15 min/ t_{H2}
U	Yes	3h	1h	$t_{catalyst}$; 0.5 $con_{catalyst}$	0.21 t_r	C_xH_y/H_2 15 min/ t_{H2}
Z	Yes	3h	1h	0.5 $t_{catalyst}$; 0.05 $con_{catalyst}$	0.21 t_r	C_xH_y/H_2 15 min/ t_{H2}
X	3h		1h	0.5 $t_{catalyst}$; $con_{catalyst}$	0.08 t_r	C_xH_y/H_2 15 min/ t_{H2}
Y	Yes	3h	1h	0.5 $t_{catalyst}$; 0.5 $con_{catalyst}$	0.08 t_r	C_xH_y/H_2 15 min/ t_{H2}
W	Yes	3h	1h	0.5 $t_{catalyst}$; 0.1 $con_{catalyst}$	0.08 t_r	C_xH_y/H_2 15 min/ t_{H2}
J	Yes	3h	1h	0.5 $t_{catalyst}$; 0.5 $con_{catalyst}$	0.08 t_r	C_xH_y/H_2 15 min/ t_{H2}
Q_1	Yes	3h	1h	0.5 $t_{catalyst}$; 5 $con_{catalyst}$	0.5 t_r	C_xH_y/H_2 15 min/ t_{H2}
Q_2	Yes	3h	1h	0.5 $t_{catalyst}$; 10 $con_{catalyst}$	0.5 t_r	C_xH_y/H_2 15 min/ t_{H2}

3.2.2.6. Infiltration for CC-C/CNTs composite realization

To obtain the new composite material, after CNT growth, the best samples sets obtained from each of two different barrier or non barrier approaches (set V and Q, respectively) have been infiltrated with resin, applying different procedures.

As infiltrating resin, commercial Durite at different concentration and a RF resin (52.3% Resorcinol, 47.6% Formaldehyde and 0.1% K_2CO_3) have been used. Durite SC-1008[514] is a phenolic laminating varnish specifically designed for applications where extended exposure at temperatures up to 260°C are required. Its physical properties are reported in Table 3.2-4.

Table 3.2-4: Durite Properties[515]

Properties	Test Method	Unit	Value
Solid,@ 135 C	IR-063	%	60-64
Viscosity, Brookfield	IR-111	cps	180-300
Ph, @ 25 C	IR-034		7.9-8.5
Specific Gravity	IR-026		1.07-1.10

The two different resins have been attempted for finding the right viscosity to completely infiltrate samples without damage the coating. Durite is too viscous, so different concentrations (from 90% to 15%) have been studied and they are compare to RF resin, which is a resin at low viscosity (about 35-75 cps [516]). The viscosity of a matured RF solution increases with increasing amount of formaldehyde, for example if formaldehyde resorcinol ratio is 3:1 the viscosity increase is sharp with rapid onset of gelation. [517]

Half of samples have been infused and cured once, the remaining samples, twice. Curing occurred in oven (Lindberg/Blue M, Gravity Oven, GO1350TCOMA-1) at 80 °C for different time (as shown in Table 3.2-5) and then pyrolysis was carried out at 600 °C in inert gas for 2h in the same furnace used for CVD, thus the a sort of CVI process could take place.

514 http://www.momentive.com/

515 Ibidem

516 http://www.specialchem4adhesives.com

517 H. Warson, C. A. Finch, Applications of Synthetic Resin Latices, Fundamental Chemistry of Latices & Applications in Adhesives Volume 1, pg 608, John Wiley & Sons Ltd., (2001)

Table 3.2-5: Curing time

Resin Type	One Infiltration	Twice Infiltration
Resorcinol	48h	24h+48h
15% Durite	24h	24h+24h
30% Durite	48h	24h+48h
60% Durite	72h	24h+72h
90% Durite	72h	24h+72h

Mechanical properties of CC-C/CNTs composite samples obtained have been investigated by nanoindentation, Open platform (CSM Instruments) equipped with the nanoindenter module was used to perform depth-sensing nano-indentation tests on the cross-section of composite. Parameters have been taken from different works.[518] [519] [520] This technique allows to determine several properties starting from the typical loading-unloading curve results, i.e load vs displacement (Figure 3.2–10).

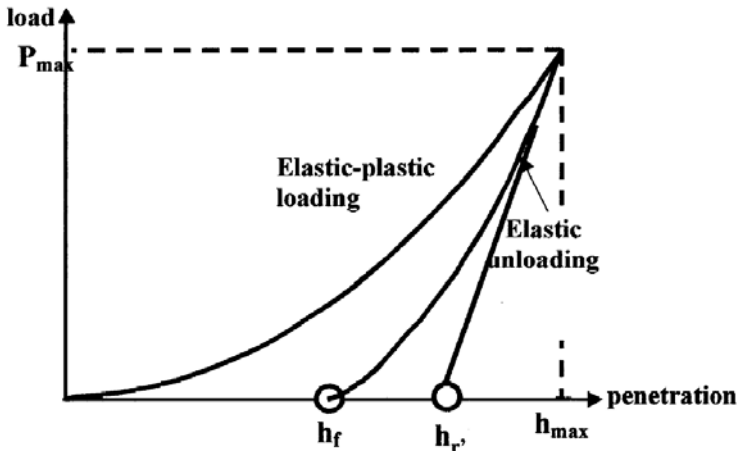

Figure 3.2–10: Typical loading/unloading curve for an instrumented (nano) indentation test

The loading portion of the curves results from elastic and plastic deformation, whereas on unloading the deformation is entirely elastic. Hardness is ordinarily defined by the mean apparent pressure of contact corresponding to maximum load. It is determined from the area of the residual print left on the specimen surface after unloading. The

[518] D T Marx, L Rwster, Mechanical properties of carbon—carbon composite components determined using nanoindentation, Carbon 37 (1999) 1679-1684

[519] P. Diss et al., Sharp indentation behavior of carbon/carbon composites and varieties of carbon, Carbon 40 (2002) 2567–2579

[520] S. Ozcan, P. Filip, Microstructure and wear mechanisms in C/C composite Wear 259 (2005) 642–650

Young's modulus is derived from the slope of the unloading curve. [521] Sample was mounted in resin, and polished to obtain a mirror like cross-section. A 50 mN force with linear loading/unloading rate of 40 mN/min was applied, the maximum load was held for 15 seconds. The indentations were performed using a Berkovich tip and the elastic modulus and Vickers hardness were calculated according to the Oliver and Pharr method[522].

3.2.3. Results

3.2.3.1. Barrier Method

In barrier approach method to deposit alumina on C/C substrate two different techniques have been applied (as discussed in paragraph 3.2.2.3). In the experimental conditions described, sol-gel deposition did not lead to well distributed and aligned CNTs growth, as shown in Figure 3.2–11. Figure 3.2–11 (a) shows how the alumina coating resulted severely cracked after deposition and gelation. Figure 3.2–11 (b) and (c) show samples without CNT growth and cracked coating, because excessive thickness of the deposition layer can be the case of seen defects. Indeed the propagation of isolated surface cracks across the film[523] is scaled to coating thickness, as reported by Hutchinson and Evans [524]

Figure 3.2–11 (d)-(e)-(f) represent samples with CNTs growth, but they are not well distributed and alignment was achieved not uniformly and only in few zones.

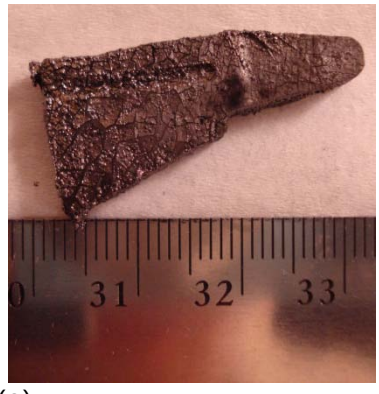

(a)

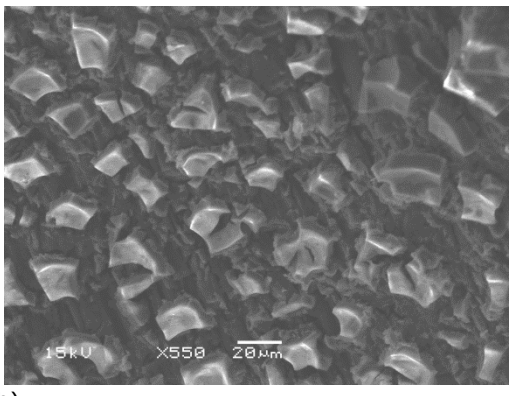

(b)

[521] P. Diss *et al*., Sharp indentation behavior of carbon/carbon composites and varieties of carbon, Carbon 40 (2002) 2567–2579

[522] W.C. Oliver, G.M. Pharr, An improved technique for determining hardness and elastic modulus using load and displacement sensing indentation experiments, Journal of Materials Research 6 (1992) 564-1583.

[523] J. W. Hutchinson, Stresses and Failure Modes in Thin Films and Multilayers, Technical University of Denmark, Notes for Academic Course, October 1996

[524] A.G. Evans, J.W. Hutchinson, The thermomechanical integrity of thin films and multilayers, Acta metall. mater., 43 (1995) 2507-2530

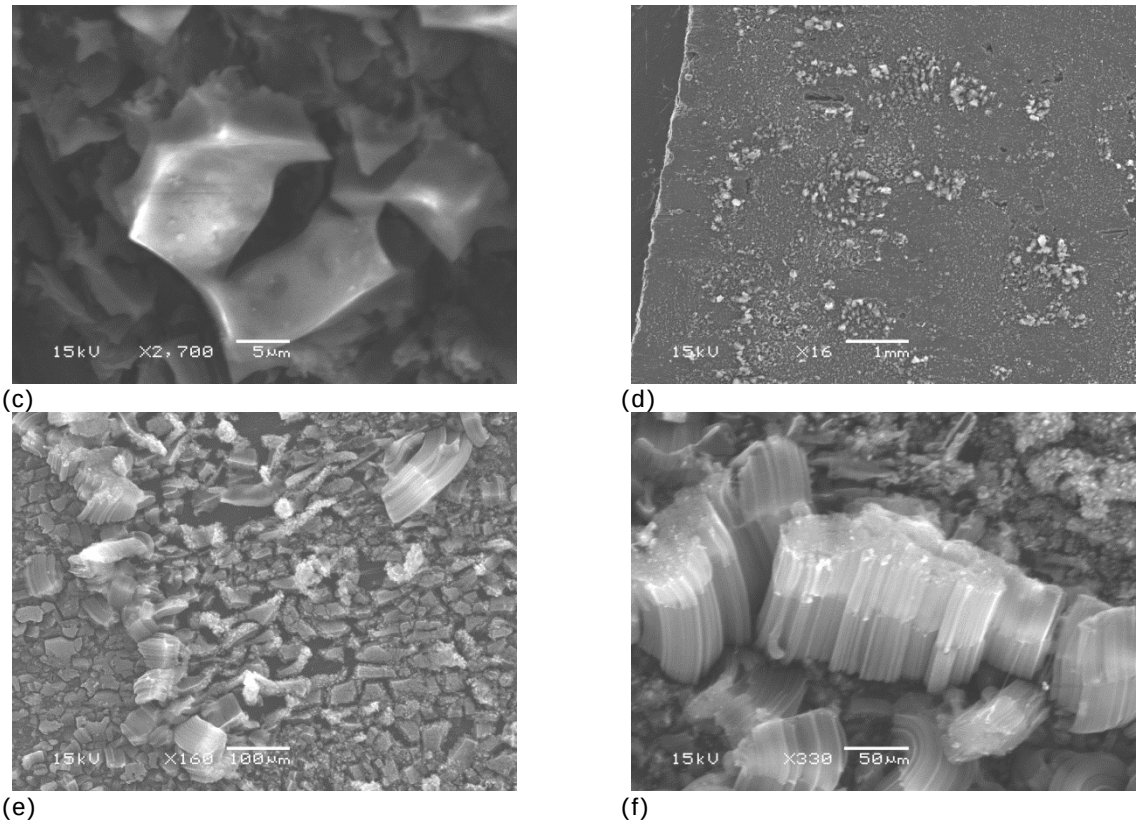

Figure 3.2–11: (a) Sample after sol-gel coat, (b)-(c) SEM images of sample set without CNTs growth, (d) SEM image showing not uniform CNTs growth, (e)-(f) SEM image at higher magnitude showing that CNTs are not uniform and only few nanotube are aligned

Also exploiting CVD as technique to deposit barrier layer several parameters must be changed to obtain aligned CNTs, such as concentration and time dipping in catalyst or growing time.

Some examples of failures have been reported in Figure 3.2–12. Figure 3.2–12 (a) – (b) shows samples obtained by: CO_2 etching of 4 samples, CVD Al_2O_3 deposition of 4 samples put to the side of crucible in zone 1, dipping for 20 minutes in catalyst solution after 1 aging hour and 35 minutes of growing process. Figure 3.2–12(c) – (d) displays samples underwent the same treatment of sample described previously (Figure 3.2–12 (a)-(b)), but in this case during CVD Al_2O_3 samples have been put placed not inside but lying on the crucible edge, in detail Figure 3.2–12(c) shows a quite good distribution all along surface with only a lack of growth in the middle of sample. Images in Figure 3.2–12 (e)-(f) display sample obtained growing CNTs into one inch furnace with different gas mixture. The last two images (Figure 3.2–12 (g) and (h)) show samples get using ferrocene 507 and 911 and keeping low temperature during growth.

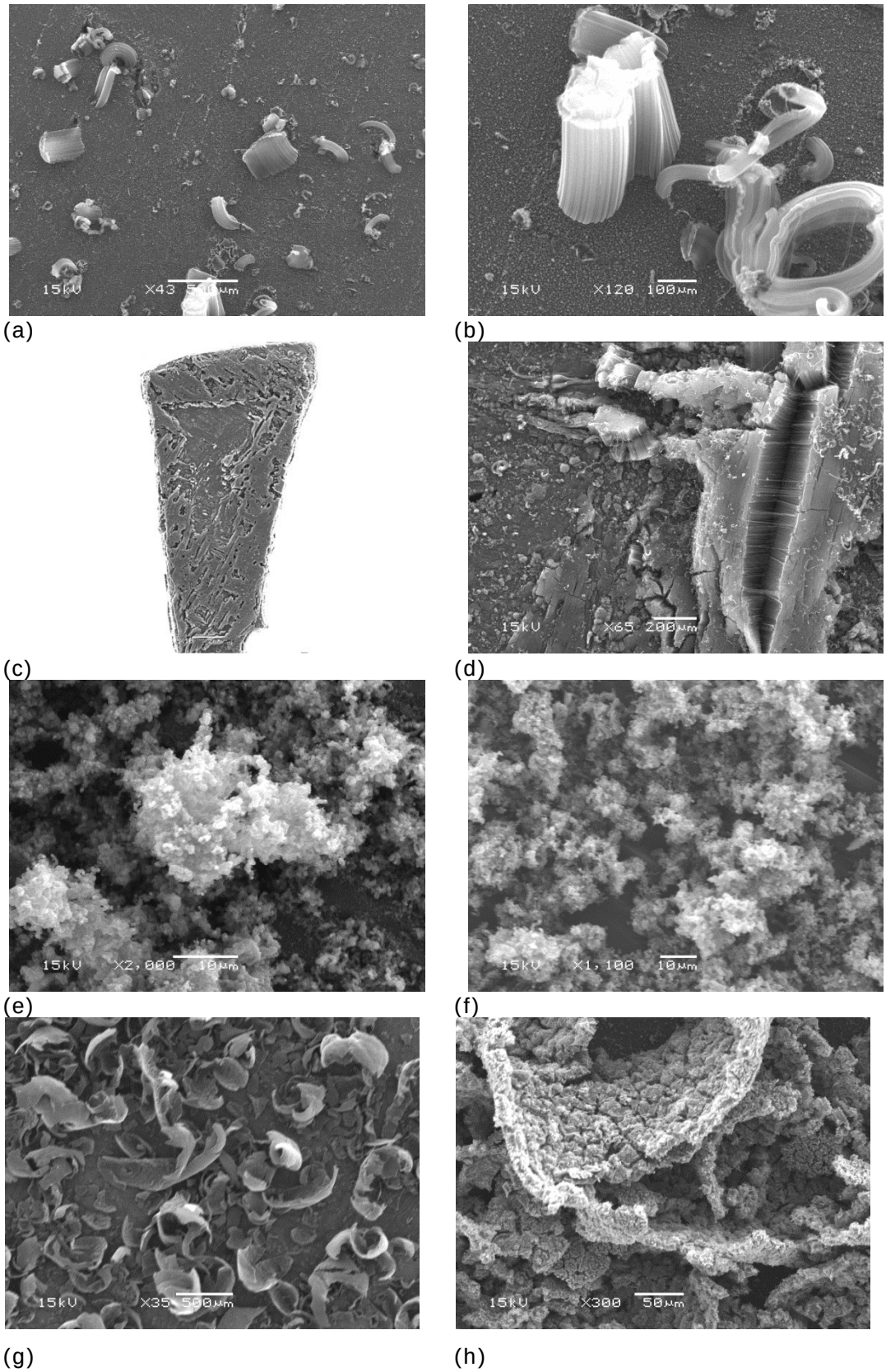

Figure 3.2–12: Examples of sample failures.

Among different sample positions studied for coating top surface with alumina, by CVD technique, it emerged that the best sample set to obtain aligned CNTs on substrate requires two samples put over each crucibles, positioned in zone 1, as shown in Figure 3.2–13. Afterwards samples coated with alumina (Figure 3.2–13 (a) and (b)) have been dipped into $Fe(NO_3)_3$ after 1 hour of aging for 10 minutes and then 45 minutes of growth, (Set V in Table 3.2-2). By means of the procedure above described, aligned CNTs on C/C substrare have been obtained.

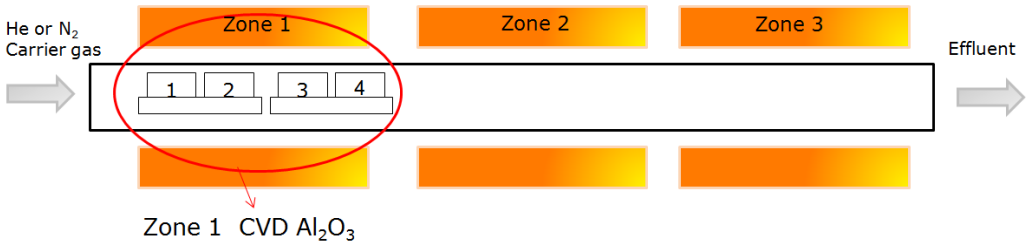

Figure 3.2–13: Outline of CVD furnace during alumina deposition.

(a) (b)

Figure 3.2–14: C/C substrate after alumina deposition

For the best set, the alumina coating thickness by CVD has been measured. Four silicon wafers have been used as substrates, being much more regular than the clutch disc parts, applying a duplication of best configuration studied to grow carbon nanotube (Figure 3.2–13). Each silicon wafer has been masked with another one to create a step which determines alumina coating thickness. Profilometer Analysis (Tencor P-16 Surface Profilometer) has been used.

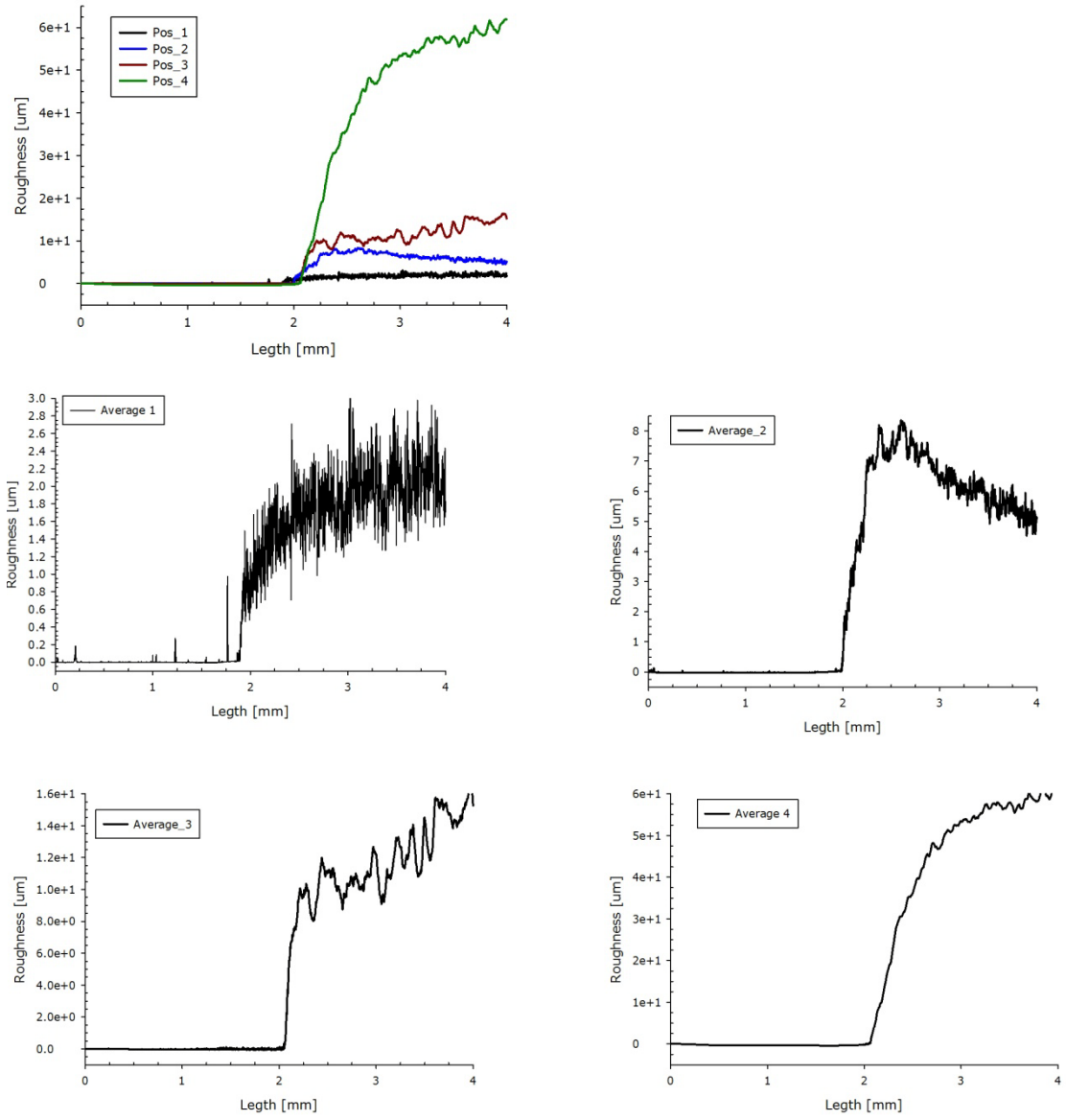

Figure 3.2–15: Profile plots at different furnace position of Silicon wafer coated by alumina

Figure 3.2–15 shows the roughness variation along silicon wafer samples, in detail from uncoated portion to coated one and the step in the middle (2 mm) pinpoints the Al_2O_3 coating thickness. Five profiles have been taken for each samples and plots reported have been obtained by average of all five measures. Different positions lead to different coating thickness: samples in position 4 are characterized by the highest thickness (~25 µm). This can be ascribed to two main reasons: position 4 is been distinguished by higher temperature than position 1, instead in zone 1 temperature was set about 150 °C, but zone 2 was at 700 °C, thus samples in position 4 was affected by higher temperature fixed in the near zone. Moreover the higher thickness of samples in position 4 could be ascribed to the carrier gas, whose flux goes from 1 to 4, possible carrying alumina from first crucible to the second.

Thickness varied from 1 μm to 25 μm. To double check results the same analysis has been also conducted on C/C samples, but using mechanical means (a scratch obtained by a blade) to selectively remove the alumina coating, instead of barriers prior to deposition. Figure 3.2–16 shows average profile of five scratches obtained from 3D profile on sample taken from position 3. The values resulted similar to previous ones.

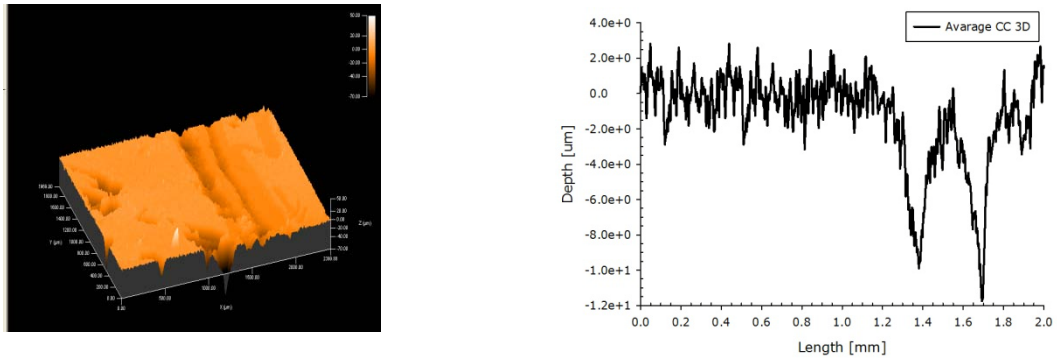

Figure 3.2–16: Profile plot of alumina on carbon substrate in position 3 measured by scratch

Figure 3.2–17 shows SEM images of a satisfactory CNTs alignment, probably thanks to more homogenous alumina layer formation, obtained using arrangement sketched in Figure 3.2–13.

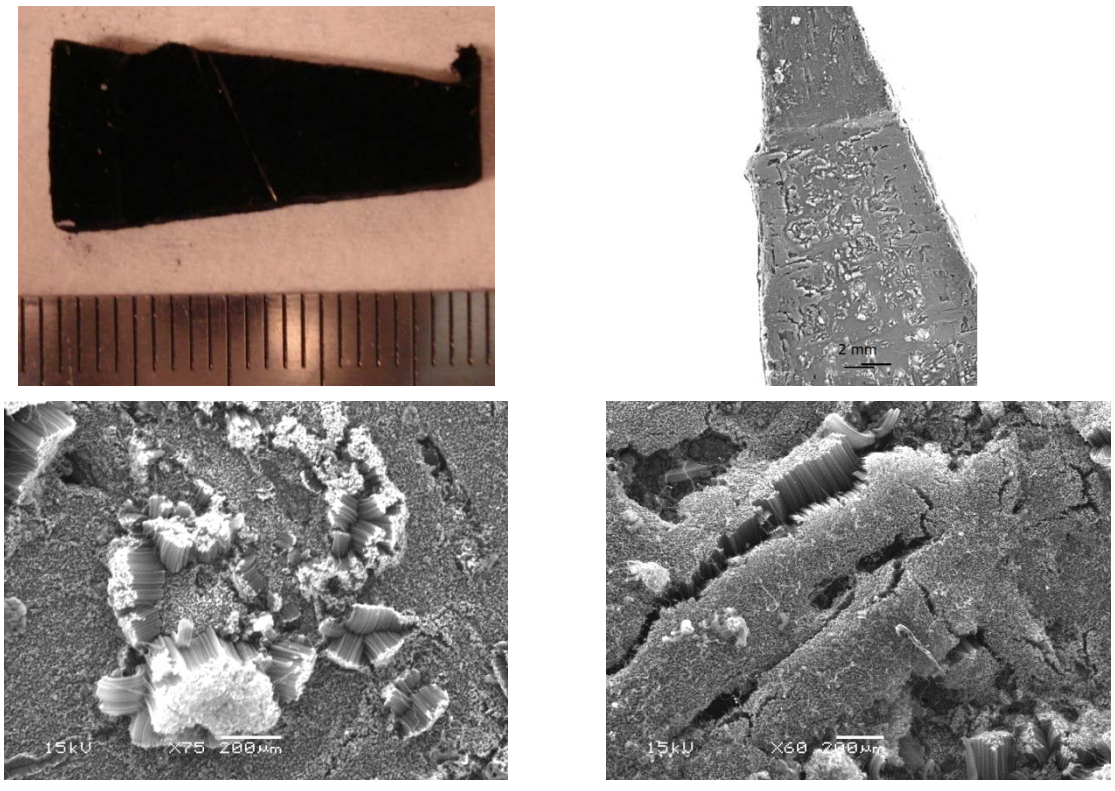

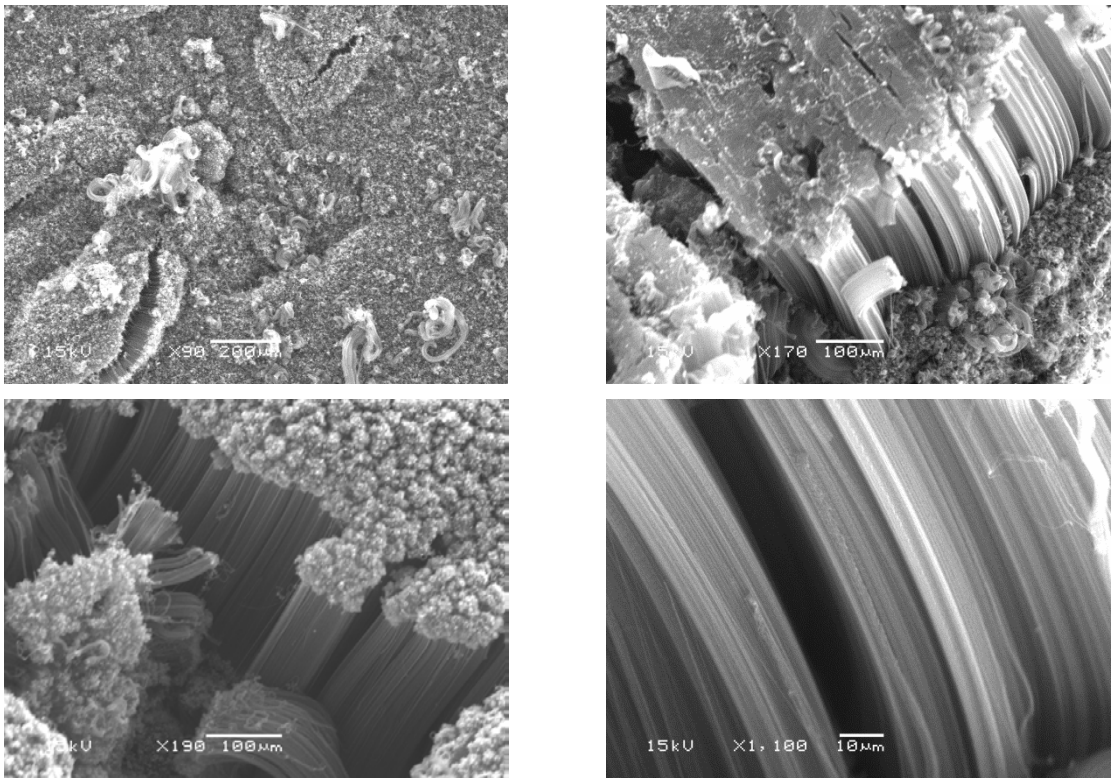

Figure 3.2–17: Set V SEM images, showing both uniform and aligned growth of carbon nanotubes.

From SEM image analysis, by means of a free software tool the average length was 124.9 µm. To measure geometric characteristic of aligned CNTs five measures for each image in all ten images have been taken. Measures have been repeated for three sets of samples obtained applying the same parameters of set V.

3.2.4. Non-barrier approach results

Results of the non-barrier approach on the clutch disc substrates show that without the intermediate layer no aligned nanotube growth occurs.

Nevertheless several different tests have been realized changing the different process parameters one by one, alignment was not reached. Figure 3.2–18 shows images taken from different sample sets. Samples obtained from A to G sets and X, Y sets show thin and tangled nanotube (as reported in Figure 3.2–18 (a)-(b)), set I shows large-dia. Nanotubes, while in L, M and T there is no growth (Figure 3.2–18 (c)-(d)), P and R show some moderate nanotube and growth (not homogenous) and S shows some growth along single fiber. The best results, as distribution and uniformity, seem to be obtained using procedure of set Q (Figure 3.2–18 (e)-(h)). In this case after 3 hours of acid etch, 1 hour in K_2CO_3, samples are dipped in $Fe(NO_3)_3$ for 12 hours and reduce at 800 °C in inert atmosphere, eventually growth process occurs in 15 minutes.

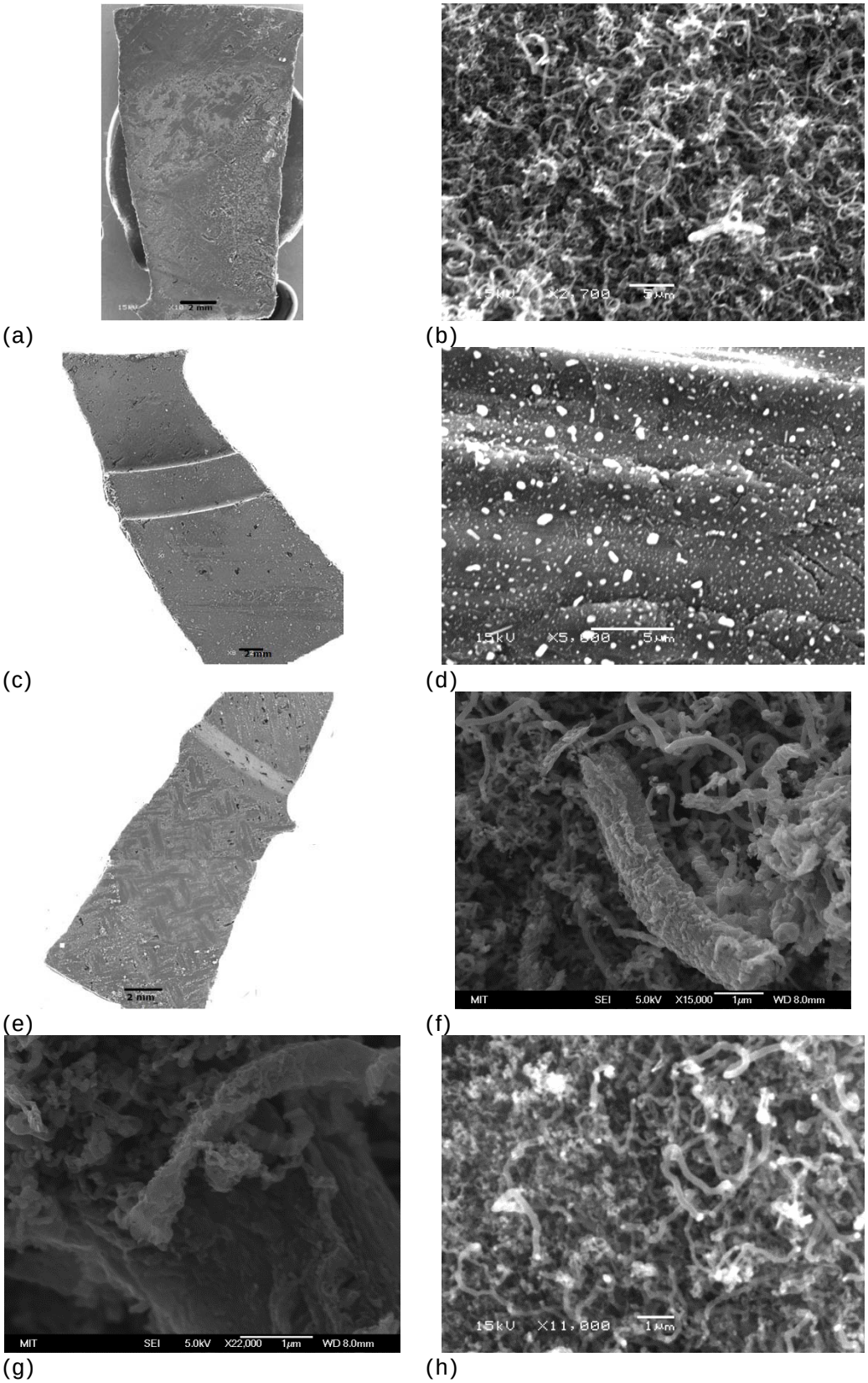

Figure 3.2–18: (a)-(b) SEM image of set B that show not uniform and thin growth of nanotube, (c)-(d) SEM image of set M without growth, (e)-(h) SEM images, (f)-(g) HRSEM images of set Q samples, they show uniform but tangled growth.

Image analysis for understanding the cause of CNT entanglment has been carried out. CNT lenght has been calculated for each samples at different flowing time of growing gas, each value was the result of the average data taken from five measures for each image in all five pictures.

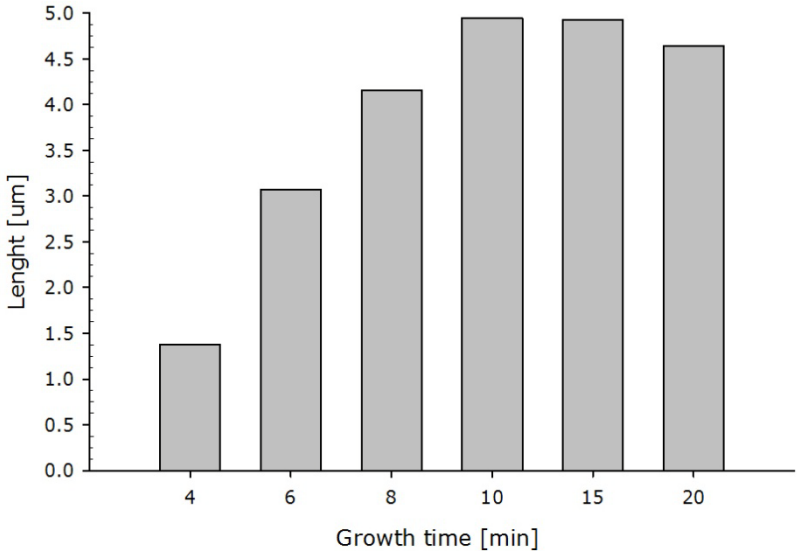

Figure 3.2–19: CNTs length in comparison with different flow time.

Bar plot in Figure 3.2–19 shows CNT length variation at different growth time, from 4 to 20 min. CNTs length increases from 4 to 15 min of C_xH_y flow, then it is constant. Trend agrees with theory [525]. Bronikowski [526] describes CNT bundle lengths as a function of the time for which they are exposed to CNT growth conditions.

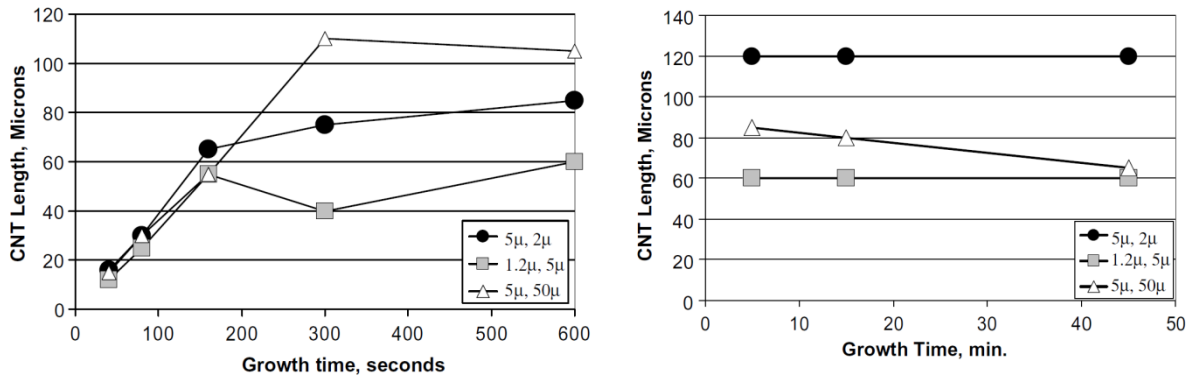

(a) (b)

[525] M.J. Bronikowski, CVD growth of carbon nanotube bundle arrays, Carbon 44 (2006) 2822–2832
[526] Ibidem

Figure 3.2–20: CNT length vs growth reaction time for short growth times. (a) CNT growth conditions: Fe catalyst thickness: 2.5 nm; temperature: 725 °C; pressure: 200 Torr; C_2H_4 flow: 500 sccm; H_2 flow: zero; (b) CNT growth conditions: Fe catalyst thickness: 2.5 nm; temperature: 725 °C; pressure: 200 Torr; C2H4 flow: 380 sccm; H2 flow: 190 sccm.

For all bundle arrays, as shown in Figure 3.2–20 (a) CNT length increases linearly with time for approximately the first 180 s of reaction; the slope of this line gives a growth rate of approximately 20 μm/min. The growth rate appears to decrease after the first 180 s, and drops to approximately zero by 300 s, so that the CNT length has stabilized after about 5 minutes. Figure 3.2–20 (b) shows the results of a second set of experiments in which CNT were allowed to grow up to 45 min. There is no significant difference in length between CNT 5 minutes and 45 minutes of CNT growth, indicating that growth has ended after 5 min of reaction time. The short growing time is probably due to metal particles inactivation, which means that the metal particles from which CNT nucleate remain catalytically active for only a short time after the carbon-containing feedstock is introduced. Possible mechanisms for the inactivation of catalytic, usually called “poisoning”, metal particle include either overcoating with carbon or conversion of the metal into a metal carbide or other coalescence phenomena. The end of growth after a few minutes is a phenomenon that we have observed consistently, independent of any other CVD parameters.[527]

In this study (Figure 3.2–21) growth seems to be linear and fast up to 10 minutes. The growth stop occurs after 10 minutes.

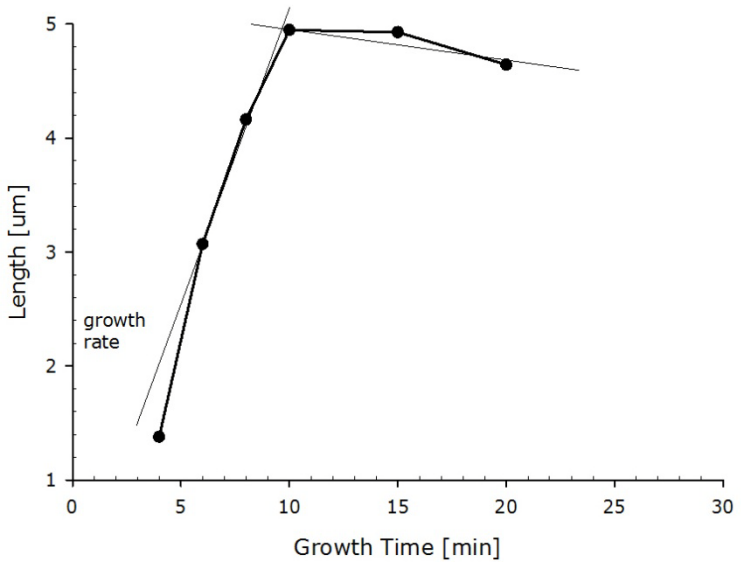

Figure 3.2–21: CNTs length at different time of growth

[527] M.J. Bronikowski, CVD growth of carbon nanotube bundle arrays, Carbon 44 (2006) 2822–2832

As discusses in previous chapter (paragraph 3.1.4.1) at lower catalyst concentrations (such as those used by Sinnott *et al*.) nanotube diameters increase with increasing catalyst concentrations, while at high concentrations (used by Bai *et al*.), larger metal particles form, which are not suitable for nanotube formation. Bai *et al*. suggest that the increased catalyst content creates a finer dispersion of catalyst particles as well as a carbon deficiency in the reaction zone, resulting in a smaller value of CNT average diameter. It would be generally expected that a higher catalyst concentration will lead to more and larger catalyst particles than a lower catalyst concentration. The larger catalyst particles will tend towards faster growth to the point at which they exclude themselves due to size, leading to a smaller CNT average diameter with the higher catalyst concentrations. On the other hand, at very low concentrations, the particles would be size-limited due to an unavailability of catalyst material, leading to a proportional relationship between catalyst concentration and CNT diameters. In literature[528,529] there are weakly and sometimes contrary correlation between catalyst particle diameter and CNTs diameter. A newly proposed theory[530] suggests that at very low catalyst concentrations, since catalyst particle size is limited by the availability of catalyst material and thus, directly proportional to the catalyst concentration, but is the concentration is increased, catalyst growth accelerates proportionately with size and many particles grow to exceed the threshold for CNT formation, leading to increased non-CNT contamination in the sample and CNT formation from the smaller catalysts. It is evident that there are trade-offs for catalyst concentration and growth time. As catalyst concentration increases, diameter decreases, but stability and structural perfection decrease, raising the reactivity of the CNT's. As growth time increases, the overall CNT array length increases.

Plot in Figure 3.2–22 shows CNT length variation, in three different cases. Set Q and X have the same catalyst molar concentration, but pyrolysis time change from t_r to 0.08 t_r. Set X and Y have the same pyrolysis time, but molar concentration split in half. Set Q and X have been characterized by same molarity, but pyrolysis time is reduced length increase. In detail length from set Q increase in 133% than set X. Applying the same pyrolysis time but reducing molarity set Y increase in 60% than set X. Thus, it is possible to conclude that changing pyrolysis time has more effect on length than modifying the catalyst concentration. Figure 3.2–22(a) and (b) show length variations in case of

528 S. Bai *et al*., Influence of ferrocene/benzene mole ratio on the synthesis of carbon nanostructures, Chemical Physics Letters 376 (2003) 83–89

529 G.S.B. McKee, C.P. Deck, K.S. Vecchio, Dimensional control of multi-walled carbon nanotubes in floating-catalyst CVD synthesis, Carbon 47 (2009) 2085-2094.

530 G.S.B. McKee, C.P. Deck, K.S. Vecchio, Dimensional control of multi-walled carbon nanotubes in floating-catalyst CVD synthesis, Carbon 47 (2009) 2085-2094

catalyst concentration increasing, from $conc_{catalyst}$ to 5 $conc_{catalyst}$ and 10 $conc_{catalyst}$. Especially increasing molar concentration lead to enhance the CNT growth, but there are not a linear correlation (31% from set Q to set Q_1, and 275% from set Q to set Q_2)

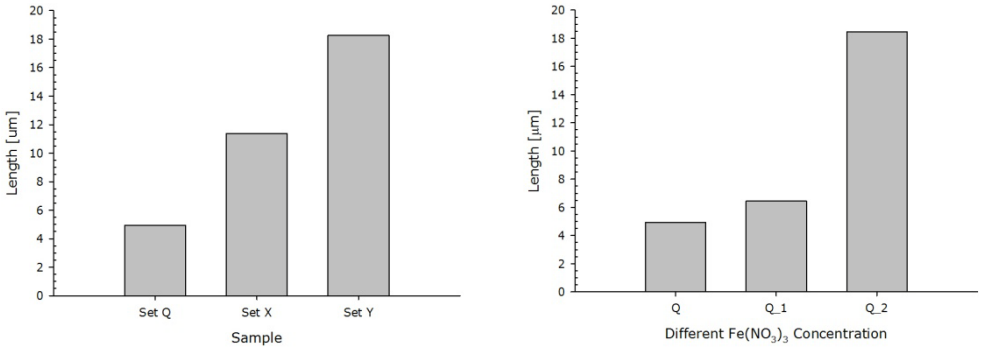

Figure 3.2–22: CNT lenght variation for different pyrolysis time and catalyst concentration

3.2.4.1. Infiltration for CC-C/CNTs composite realization

The best results of CNTs synthesis process are set V in case of barrier approach and set Q for direct approach. Thus several sets, applying the optimized parameter, have been manufactured.

The composite samples after infiltration, curing and pyrolysis (as described in paragraph 3.2.2.6) obtained are reported in Figure 3.2–23. Sample on the left was obtained infiltrating the barrier approach samples and on the right the non barrier approach.

One infiltration **Two infiltrations**

15% 15%

30%

30%

60%

60%

90%

90%

RF

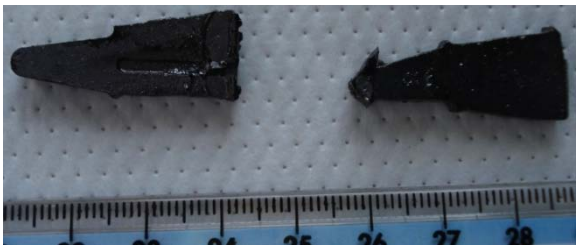

RF

Figure 3.2–23: Barrier and non barrier samples infiltrated by resin.

The most promising composite are samples obtained by a double infiltration of Durite at 60%, named D60 and B60. Subsequently image analysis and nanoindentation test have been performed on these samples. Figure 3.2–24 shows a sample sketch, to explain how sample have been investigated.

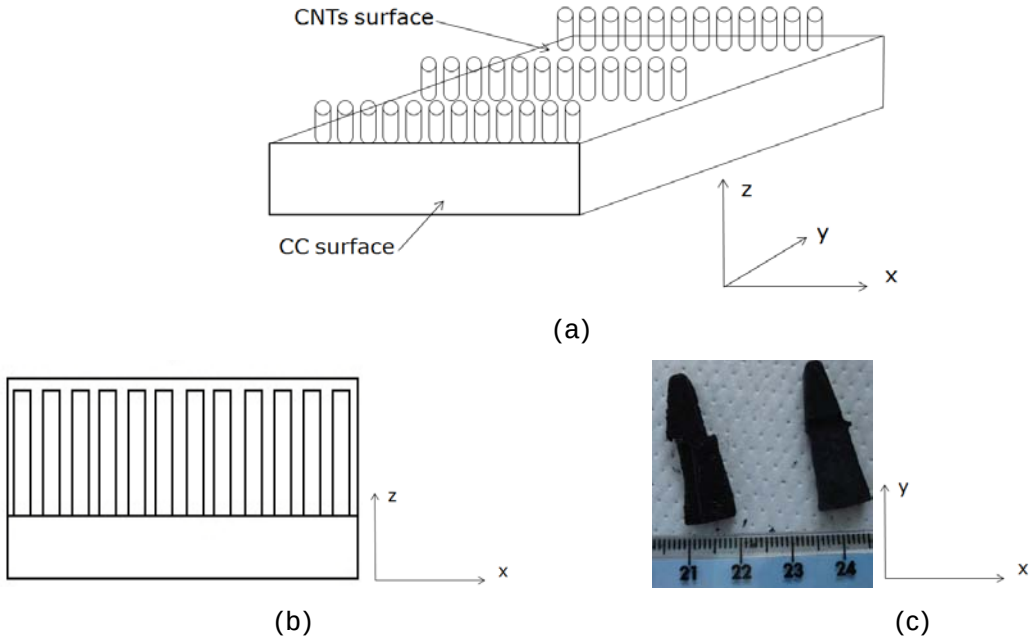

Figure 3.2–24: Sample sketch to show preparation method. (a) 3D configuration of final sample. (b) cross-section example (xz plane) and (c) coating surface plane (xy)

Figure 3.2–25 gathers SEM image of two different samples. Images (a) and (b) show the xz plane, cross-section in the core zone, CC. They highlight the presence of several voids and cracks on the surface. Figure 3.2–25 (c) and (d) show interface C/CNTs, where there are no voids and surface seems to be satisfactory solid and intact. Further investigation is require to qualify the level of integrity. The last two images (e) and (f) indeed show the cross-section core. In D60 sample, fibers have been pulled out, in the contrary B60 shows a more compact surface. SEM imaging reveals a porous matrix with high porosity, although more homogeneity at the micron-scale than the C/C material.

Image characterization results (Figure 3.2–25 (a)-(f)) indicate that the CNT/C surface seems to be well adhered to the C/C substrate, in detail Figure 3.2–25 (e)-(f) on right side. Indeed the macroscopic (cm-scale) surface of the C/C materials with CNT/C on the surface was untracked after pyrolysis (2 infusion) on both samples, Figure 3.2–26 (a)-(d) show the coating surface (xy plane) in case of D60 sample at different magnification, in detail several cracks and voids on all surface have been detected. Nevertheless C/CNT 'film' cross-sections survived the machining process and SEM imaging reveal that the interface remained intact and voids-free. Carbon fibers from the C/C substrate, on the

contrary, were pulled out by the cross sectioning operations. Hence it is possible to conclude that the C/CNT film is not bulked up enough after two infusion, it probably will be required more infusion or different infusion method. Coating thickness was about 38.4 µm for B60 sample and 26.9 µm for D60 samples, obtained by SEM image analysis.

D60 **B60**

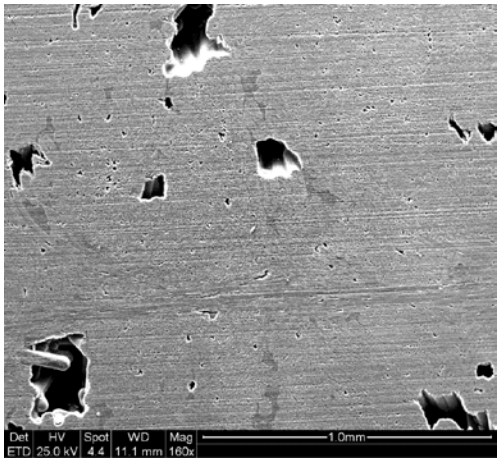

(a)

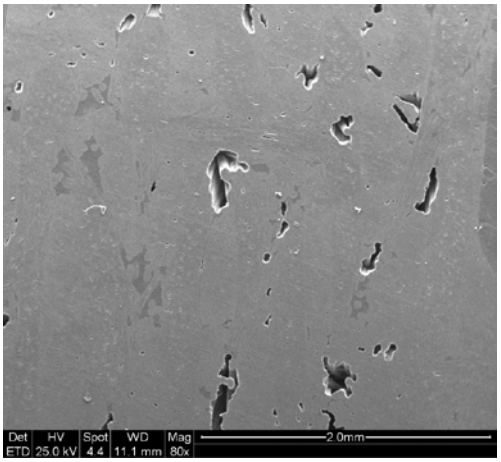

(b)

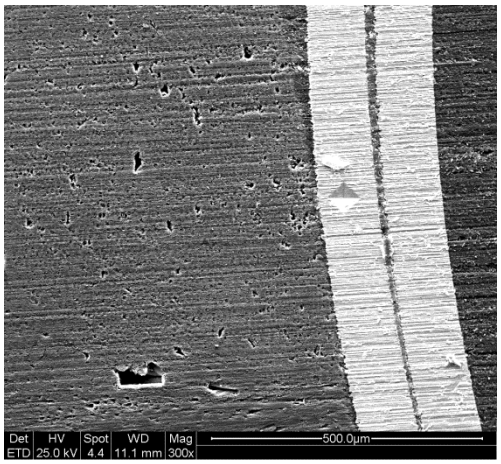

(c)

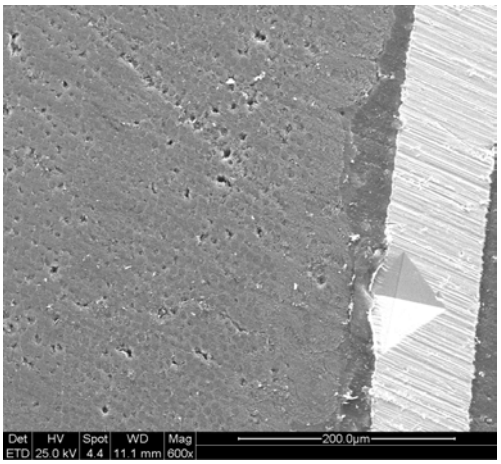

(d)

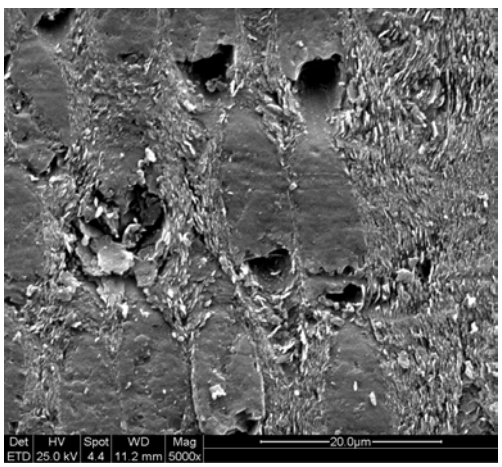

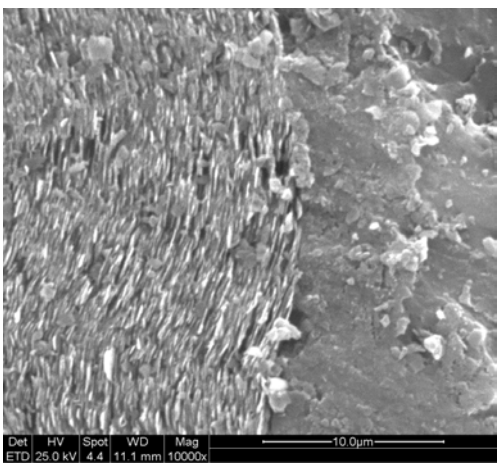

(e) (f)

Figure 3.2–25: SEM images of cross section (xz) plane (according to Figure 3.2–24) of two different samples, D60 (left) and B60 (right). CNT layers was on the right in (c), (d), (e) and (f).

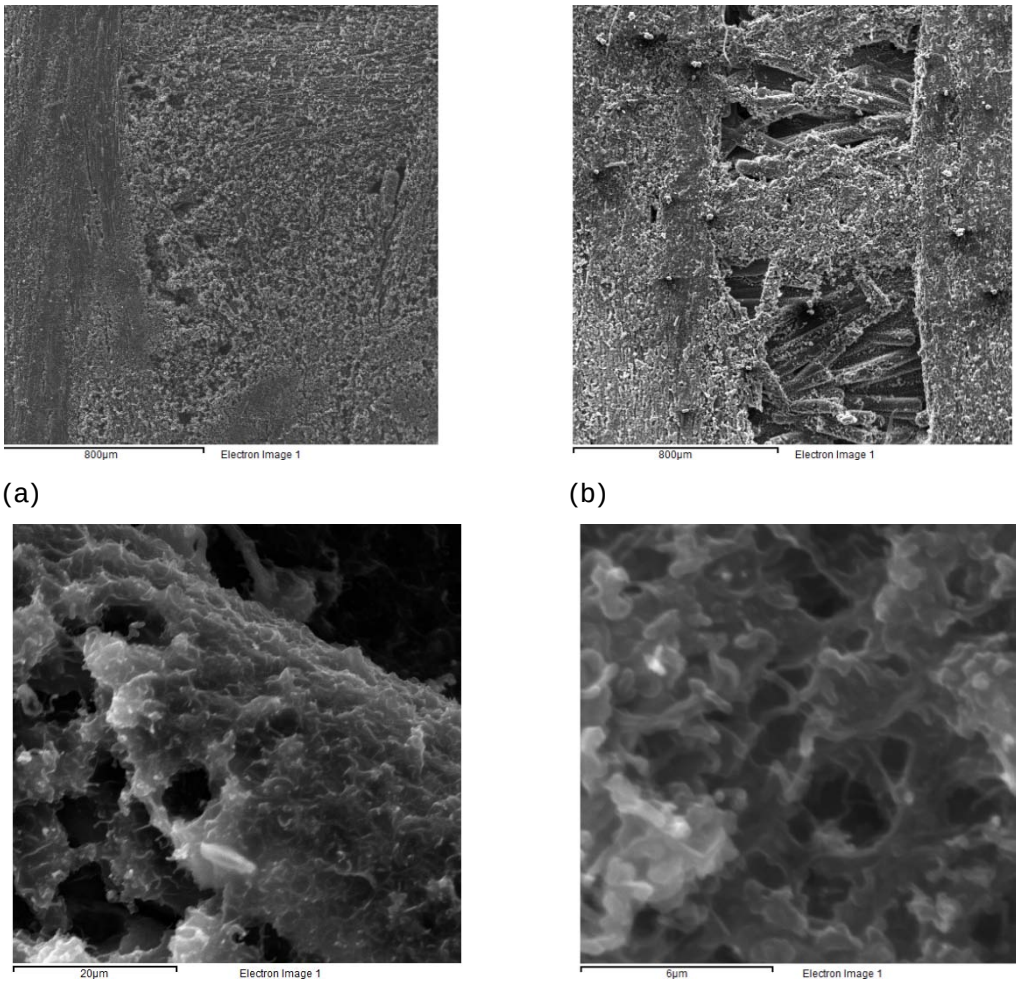

Figure 3.2–26: Unmodified coating surface (xy plane), according to Figure 3.2–24, of D60 sample to show CNT layer.

The indentations have been performed according to paragraph 3.2.2.6, The results obtained, in term of Young's Module and Vickers Hardness are reported in Table 3.2-6. Since the maximum indentation depth was lower than 1.8 µm, the ratio limit of 1/10[531] between maximum depth of penetration and layer thickness was respected.

[531] X. Cai, H. Bangert, Hardness measurements of thin films-determining the critical ratio of depth to thickness using FEM, Thin Solid Films 264 (1995) 59-71

Table 3.2-6: Vickers and Young's Modules [GPa] results

		B60		D60	
		HV	E	HV	E
CC/CNTs	Mean	123.53	17.36	90.41	12.72
	Std Dev	68.01	6.39	46.51	3.29
CC	Mean	159.77	20.98	107.89	14.85
	Std Dev	68.81	10.67	46.93	4.65

Figure 3.2–27 shows representative plots of indentation for each sample type, where (a) and (b) plots are referred to B60 sample and (c) and (d) to D60 sample. Plots (a) and (c) represent nanoindentation at C-CNTs interface and curves (b) and (d) loading and unloading curves on CC substrate.

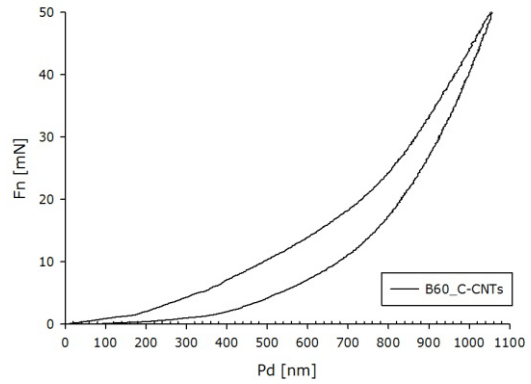

(a)

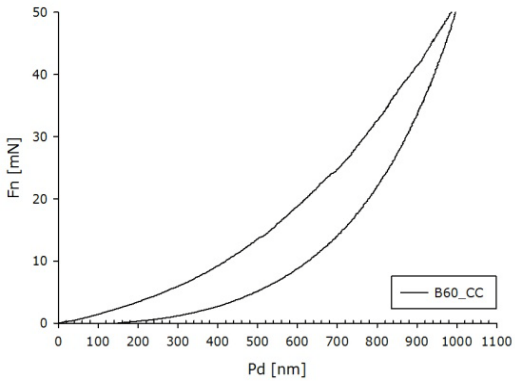

(b)

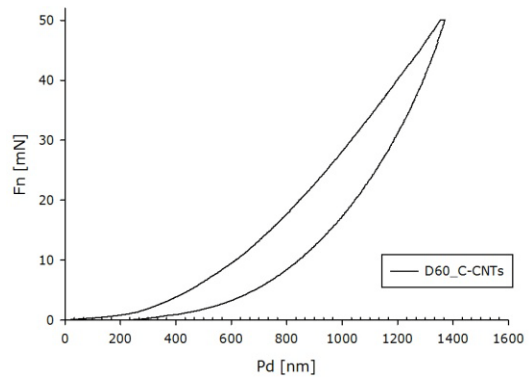

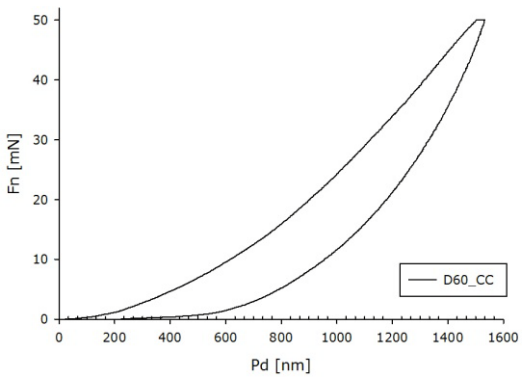

(c) (d)

Figure 3.2–27: Loading and unloading curves of samples B60 and D60 on CC bulk material and on C-CNTs interface, in detail (a) B60-C-CNTs, (b) B60-CC, (c) D60-C-CNTs, (d) D60-CC

Curves (Figure 3.2–27) reveal the elastic behavior of composite materials, this explains the reason why employing a traditional Vickers Hardness testers is not possible to see the indentation left from the test.

Nanoindentation reveals that the CNT/C film is softer (less hard) and more compliant than the C/C substrate. In case of barrier approaches hardness is 123 vs. 159 and modulus is 17 vs. 21 GPa for the CC/CNT and C/C materials respectively. In case of direct (non barrier) approaches, hardness is 90 vs. 108 HV and modulus is 13 vs. 15 GPa for the CC/CNT and C/C materials respectively. Barrier approach samples are harder than direct approach ones. Indeed in barrier approach the CNTs alignment has been reached, thus mechanical properties increased as expected, due to their anisotropic behaviour.[532] Instead by non barrier method entangled carbon nanotube have been obtained, thus an higher resin quantity with low mechanical properties and density have been infiltrated

Most nanoindentation works have been carried out on materials that are elastoplastic and much of the controversy surrounding the technique has involved interpreting the data in the elastoplastlc regime. A few authors [533] [534] reported a purely elastic response for a variety of carbons and chemical vapor deposited carbon matrices of a CC composite. Experimental results related in the thesis are in agreement, showing a behaviour that is almost completely elastic (Figure 3.2–27).

[532] Q. Zhang *et al.*, Hierarchical composites of carbon nanotubes on carbon fiber: Influence of growth condition on fiber tensile properties, Composites Science and Technology 69 (2009) 594–601

[533] P. Diss *et al.*, Sharp indentation behavior of carbon/carbon composites and varieties of carbon, Carbon 40 (2002) 2567–2579

[534] D T Marx, L Rwster, Mechanical properties of carbon—carbon composite components determined using nanoindentation, Carbon 37 (1999) 1679-1684

3.3. Conclusions

In this chapter, the synthesis of CNTs on carbon-matrix carbon-fiber composite has been described and optimized in terms of homogeneity of deposition and alignment of CNTs.

Both techniques were successfully developed. Well-adherent and well distributed CNTs on substrate have been achieved in both methods but desirable aligned CNTs have been get only by the barrier one.

The following steps optimize the CNT growth by barrier method:

- CO_2 etching at fixed temperature and time
- Al_2O_3 deposition by CVD
- $Fe(NO_3)_3$ in IPA deposited by dipping
- Growth process for 45 minutes

Steps to obtain CNTs by non-barrier method:

- CO_2 etching at fixed temperature and time
- Acid etch in a blend of HNO_3, H_2SO_4 and H_3PO_4 at fixed time and temperature
- Functionalization in K_2CO_3
- $Fe(NO_3)_3$ in water deposited by dipping
- Growth process for 15 minutes

Optimization studies of growth parameters yielded preliminary materials that were processed into carbon-CNT matrices via pyrolysis. From a preliminary image analysis and mechanical characterization it is possible to reveal that the macroscopic (cm-scale) surface of the C/C materials with CNT/C on the surface was uncracked after pyrolysis (2 infusion) on both samples and the cross-sections of the C/CNT 'film' survived the sample preparation machining process, revealing the interface to be intact and void free. Carbon fibers from the CC substrate, by contrast, were pulled out in places by the cross sectioning. In all cases porosity of the material from one infusion is too high revealing that further infusion studies need to be developed. Aligned CNT growth reached by the barrier method would perhaps be the most scalable, energy-efficient, cost-effective, gentle, and straightforward way to grow CNTs on carbon fibers, moreover both composite obtained seem to lead to good mechanical properties. Nanoindentation reveals that the CNT/C film is softer (less hard) and more compliant than the C/C substrate. In case of

barrier approaches hardness is 123 vs. 159 HV and modulus is 17 vs. 20 GPa for the CC/CNT and C/C materials respectively. In case of direct approaches hardness is 90 vs. 107 HV and modulus is 13 vs. 15 GPa for the CC/CNT and C/C materials respectively. Results clearly demonstrate that barrier approach samples are hardener than direct approach ones, and this can be ascribed mainly to the CNT alignment achievement and their anisotropic behaviour.[535] The results indicate that this is a promising approach for improving the mechanical, electrical and thermal properties of structural composites.

[535] Q. Zhang *et al.*, Hierarchical composites of carbon nanotubes on carbon fiber: Influence of growth condition on fiber tensile properties, Composites Science and Technology 69 (2009) 594–601

Chapter 4:
Conclusions & Future Developments

In automotive, aerospace and nuclear field, new materials, which are lightweight, high temperature resistant, or good wear resistant or able to dispose quickly heat along a preferred direction, are searched. Hybrid materials are good candidates for these applications because they combine the properties of several materials.

Lightweight intermetallic materials (in particular aluminides) and composites based on carbon show the more interesting features. For example, aluminides, thanks to high resistance to radiation damage and high temperature resistance are extensively applied in nuclear reactors, or in the gas and jet turbine engines and in the rotating components in the rear sections of engines, where temperature exceeds 1500 °C coupled with high loading stress. Carbon composites reinforced by carbon-nanotubes can be used for extreme friction and high temperature applications, like in high performance braking systems. Furthermore, for example, in aircraft wing they could provide de-icing and lighting protection strike, thanks to carbon nanotubes conductivity. Moreover, they could decrease weight and make army vehicle or airplane electromagnetically invisible.

Manufacturing techniques for such kind of hybrids are still defective, and in this framework, two different hybrid structures have been investigated in this thesis:

- intermetallics obtained by microwave assisted combustion synthesis technique, like Ni or Ti or complex aluminides. They have been investigated both to obtain freestanding elements, coatings on lightweight alloys and as brazing materials to join dissimilar materials, such as Titanium and Inconel;
- carbon fiber in carbon matrix reinforced by aligned carbon nanotubes. Aligned CNTs can provide interlaminar and intralaminar reinforcement in composites and electrical and thermal conductivity enhancement. A proper technique and different approaches to provide alignment during growth had to be investigated and optimized.

Concerning the first topic, combustion synthesis was activated by microwaves due to their peculiarity. Their ability to transfer energy instead of heat, their rapid and selective heating lead to controllably alter the cooling rate and consequently the final products microstructure. Nevertheless, the presence of electromagnetic field and the extremely high reaction speed make difficult to measure temperature during the process and thus monitor the process itself. For this purpose, the first part of the activity was focused on the simulation and experimental validation of a multiphysics model, which allows to study

simultaneously the progression of reactions and the temperature profile both in the reacting area and in surrounding base materials. For the first time a model, which couples three different application modes (i.e., chemical, electromagnetic and thermal/diffusion) has been developed. It is simplified due to the lack of reliable high temperature materials properties data and the need to reduce simulation computational resources. In spite of the assumptions and simplifications of the model, such as electromagnetic properties independent from temperature, the absence both of dimensional or density variation during or after the reaction and of interactions between metal powders and substrate, the model shows a good match between the temperatures simulated and measured in the case of NiAl synthesis on substrate of Ti.

The model was applied to study several systems:

- Titanium joining;
- joining between Ti and carbon or stainless steel;
- joining between Ti and Inconel;
- joining between SiC and NiAl;
- joining between SiC and $TiSi_2$

The model also allow to predict the extent of the heat affected zone during joining and it shows how the variation of synthesis conditions (i.e., MW forward power, MW ignition time, presence or absence of co-absorbers, dimension of substrates or pressed powders discs) define the joint microstructure. Furthermore, synthesis conditions proved to strongly influence the thickness of ternary layer, which was formed between intermetallic and base metal during joining reaction. The longer time of aluminides liquid phase existence, the higher maximum temperature of combustion synthesis and of surrounding parts reached led to thicker ternary layer. Increasing MW forward power reduces the reaction ignition time, thus surrounding materials are colder than in case of longer ignition time, therefore the intermetallic liquid phase has less time to react with the substrates decreasing the intermediate zone thickness. However, the ignition temperature of combustion synthesis has been reached without exposing the overall joining couple to high temperature, unlike in conventional brazing. In this way it is possible to contain possible unwanted transformations of substrate, like phase change and microstructural alterations as well as to reduce the extent of heat affected zone compared to conventional techniques. Tradeoff of these parameters allowed to optimize the joining process.

As far as the second topic is concerned, the efforts were focussed on obtaining aligned CNTs growth on non ideal substrates (not planar or single crystal surface), but substrates characterized by industrial surface finishing. Study focused on the optimization of two

experimental techniques for growing CNTs: barrier and non barrier approach. In case of barrier method, an inert metal oxide (Al_2O_3) has been deposited as intermediate layer between the substrate and the CNTs. Catalyst ($Fe(NO_3)_3$+IPA) deposited on such layer has been exploited to grow carbon nanotubes. Alternatively, in a more direct approach, catalyst ($Fe(NO_3)_3$ in deionized water) has been deposited directly on the substrate before growing CNTs. By barrier method 27 sample sets and by non barrier approach 31 sample sets have been produced. All samples were characterized by image analysis. In both cases it was possible to obtain well-adhered and well-distributed carbon nanotubes, but the first technique resulted better to reach a proper CNTs alignment. Aligned CNT growth reached by the barrier method would perhaps be the most scalable, energy-efficient, cost-effective, gentle, and straightforward way to grow CNTs on carbon fibers. Nevertheless, both techniques, after optimization of the deposition and growth parameters, lead to good mechanical properties, quantified in terms of surface hardness. The two most promising sets of CNTs coated samples, presenting the best alignment, distribution and adhesion, have been chosen to realize the final composite material. First of all, they have been infiltrated by resin. Two different resins have been used, one of these in four different concentrations; half of samples have been infiltrated once, the remaining samples twice. At a later stage, the samples have been cured in oven and pyrolised in inert gas for 2 hours. The results obtained by image analysis and mechanical characterization show a good adhesion between coating and substrate, but an excessively high porosity. This is probably due to unsatisfactory numbers of infiltrations. Hardness measurement, by nanoindentation test, demonstrated that barrier approach samples are harder than direct approach ones, and this can be mainly ascribed to the CNT alignment achieved and their anisotropic behaviour. The macroscopic (cm-scale) surface of the carbon composite materials with CNT/C on the surface was uncracked after pyrolysis and the cross-sections of the C/CNT 'film' revealed the interface to be intact and void free. Carbon fibers from the carbon-matrix carbon-fiber composite, by contrast, were pulled out in places by the cross sectioning operations, indicating loss of adhesion. Hence, approaches described are promising for improving the mechanical, electrical and thermal properties of aligned CNTs-reinforced structural composites. It was also demonstrated for the first time that by a proper selection of the process parameters it is possible to growth aligned CNTs on industrial substrates.

In conclusion, in this work, innovative hybrid materials have been prepared and their manufacturing process was investigated and optimized both by numerical simulation (intermetallics) and experimentally (CNTs). The main factors affecting the process yield and results have been determined and the use of numerical simulation proved to be an

essential tool in investigating extremely rapid processes occurring in high energy environments.

Anyway both hybrid structures need to be further improved and investigated. Future perspectives regarding the modeling of microwave activated combustion synthesis of intermetallic will involve the microwave and chemical modules refinement, which currently suffer from the lack of reliable temperature dependent materials properties data (i.e., dielectric and magnetic properties) and difficult to measure pre-exponential factor that is one of the most important value applied to describe the reaction kinetic in the chemical mode. Furthermore its extension to other aluminide synthesis, both as thick coating or as freestanding materials could be achieved. Regarding C/C/CNTs, the preliminary results achieved open the way to the manufacturing of new high performance composites. Optimization of infiltration process should be further investigated and thermo-mechanical properties should be systematically evaluated in order to scale up to a set of real components to be tested in high friction and wear applications.

References

[1] H. Ago *et al.*, Dispersion of metal nanoparticles for aligned carbon nanotube arrays, Applied Physics Letters, 77 (2000) 79-81

[2] E. Akman *et al.*, Laser welding of Ti6Al4V titanium alloys, Journal of Materials Processing Technology, 209 (2009) 3705-3713

[3] P.M. Ajayany, T.W. Ebbesenz, Nanometre-size tubes of carbon, Rep. Prog. Phys., 60 (1997) 1025–1062

[4] A.P. Aldushin, B.I. Khaikin, Combustion of mixtures forming condensed reaction products Combustion, Explosion, and Shock Waves, 10 (1974) 273-280

[5] V.I. Alexiadis *et al.*, Influence of the composition of Fe_2O_3/Al_2O_3 catalysts on the rate of production and quality of carbon nanotubes, Materials Chemistry and Physics 128 (2011) 96–108

[6] L. An *et al.*, Synthesis of nearly uniform single-walled carbon nanotubes using identical metal-containing molecular nanoclusters as catalysts, Journal of the American Chemical Society, 124 (2002) 13688–13689

[7] M. Arimondi *et al.*, Chemical Mechanism of the $Zr+O_2 \rightarrow ZrO_2$ Combustion Synthesis Reaction, The Journal of Physical Chemistry B, 101 (1997) 8059–8068

[8] A. Bachmatiuk *et al.*, Facilitating the CVD synthesis of seamless double-walled carbon nanotubes Nanotechnology, 18 (2007) 275619 (5pp)

[9] S. Bai *et al.*, Influence of ferrocene/benzene mole ratio on the synthesis of carbon nanostructures Chemical Physics Letters 376 (2003) 83–89

[10] E. Bayramli, L. Toppare, N.K. Erinç, Investigations on the Electrochemical Surface Treatment of Carbon Fibers, Turkish Journal of Chemistry, 25 (2001) 251-258

[11] A. Bayliss, B.J. Matkowsky, Modeling and numerical computation of a nonsteady SHS process, Combust. Plasma Synth. High-Temp. Mater., Conference 1990, 61-72

[12] A.R. Barron, Chemical Vapor Deposition, Connexions Web site. http://cnx.org/content/m25495/1.2/ Jul 13, 2009.

[13] O. Biceroglu, Thermal conductivity of sintered metal powders at room temperature Letters in Heat and Mass Transfer, 3 (1976) 183-191

[14] A. Biswas *et al.*, A study of selfpropagating high-temperature synthesis of NiAl in thermal explosion mode, Acta Materialia, 50 (2002) 757-773

[15] A.R. Boccaccini *et al.*, Electrophoretic deposition of carbon nanotubes, Carbon, 44 (2006) 3149–3160

[16] F. Booth, The theory of self-propagating exothermic reactions in solid systems, Transactions of the Faraday Society, 49 (1953) 272-281

[17] I. Boromei *et al.*, Oxidation behavior resistance of a duplex NiAl/Ti-Ni-Al coating by microwave assisted SHS on Ti substrate, EURO PM2009 Proceedings, EPMA, Copenhagen, Denmark, 3 (2009) 161-166

[18] I. Boromei *et al.*, Ni-Al-Ti Coatings Obtained by Microwave Assisted SHS: Oxidation Behaviour in the 750-900 C Range, Surface and Coatings Technology, 204 (2010) 1793–1799

[19] C.R. Bowen, B.Derby, Finite-difference modelling of self-propagating high-temperature syntheses of materials, Acta Metallurgica et Materialia, 43 (1995) 3903-3913

[20] P.J. Bridges, B. Magnus, Cost Effective Application of Titanium Alloys in Military Platforms, (2001) ISBN: 92-837-0026-0

[21] C.J. Brinker, G.W. Scherer, The physics and chemistry of Sol Gel Processing, Academic Press 1990 ISBN: 0-12-134970-5

[22] M.J. Bronikowski, CVD growth of carbon nanotube bundle arrays, Carbon 44 (2006) 2822–2832

[23] X. Cai, H. Bangert, Hardness measurements of thin films-determining the critical ratio of depth to thickness using FEM, Thin Solid Films 264 (1995) 59-71

[24] G.P Cammarota *et al.*, Ni–Al–Ti coatings obtained by microwave assisted SHS: Effect of annealing on microstructural and mechanical properties, Surface & Coating Technology 203 (2009) 1429-1437

[25] P. Capozzoli, Residual Stress and Electrochemical Properties of Proton-Conducting Materials for a MEMS Fuel Cell, MIT S.M. Thesis, August 2006

[26] F. Cesano *et al.*, Connecting carbon fiber by means of catalytically grown carbon nanofilaments: formation of carbon- carbon composites, Chemistry of Materials, 17 (2005) 5119-5123

[27] S. P. Chai, S. H. S. Zein and A. R. Mohamed, Synthesizing carbon nanotubes and carbon nanofibers over supported-nickel oxide catalysts via catalytic decomposition of methane, Diamond and Related Materials, 16 (2007) 1656-1664

[28] J.C. Charlier and S. Iijima , Growth Mechanisms of Carbon, Carbon Nanotubes Topics in Applied Physics, Volume 80, (2001) 55–81

[29] J.C. Charlier, S. Iijima, Growth Mechanisms of Carbon Nanotubes, Nature, 354 (1991) 55-81

[30] H.C. Chen, A.J. Pinkerton, L. Li, Fiber Laser Welding of Dissimilar Alloys of Ti–6Al–4V and Inconel 718 for Aerospace Applications, The International Journal of Advanced Manufacturing, 52 (2010) 977– 987

[31] L.H. Chen *et al.*, Growth of aligned carbon nanotubes on carbon microfibers by dc plasma-enhanced chemical vapor deposition, Applied Physics Letters, 88 (2006) 033103-033106

[32] Y.C. Chen, , K. Nakata, Microstructural characterization and mechanical properties in friction stir welding of aluminum and titanium dissimilar alloys, Materials & Design, 30 (2009) 469-474

[33] J. Cheng, R. Roy, D. Agrawal, Experimental Proof of Major Role of Magnetic Field Losses in Microwave Heating of Metal and Metallic Composites, J. Mater. Sci. Lett., 20 (2001) 1561–1563

[34] C.L. Cheung *et al.*, Diameter-Controlled Synthesis of Carbon Nanotube, The Journal of Physical Chemistry B, 106 (2002) 2429-2433

[35] H.C. Choi *et al.*, Delivery of Catalytic Metal Species onto Surfaces with Dendrimer Carriers for the Synthesis of Carbon Nanotubes with Narrow Diameter Distribution, Journal of Physical Chemistry B, 106 (2002) 12361–12365

[36] V. Choudhary, A. Gupta, Carbon Nanotubes - Polymer Nanocomposites, Chapter Polymer/Carbon Nanotube Nanocomposites Centre for Polymer Science and Engineering Indian Institute of Technology Delhi, India ISBN: 978-953-307-498-6

[37] T.V. Chow, H.C. Reader Understanding Microwave Heating Cavities, Artech House Microwave Library (2000) ISB: 1-58053-094-X

[38] K.S. Coleman, Nanotubes, Annu. Rep. Prog. Chem., Sect. A: Inorg. Chem., 104 (2008) 379-393

[39] E. Colombini *et al.*, Microwave ignited combustion synthesis of intermetallic compounds, modelling and experimental results, Metallurgia Italiana, 4 (2011) 29-34

[40] T. Czeppe, S. Wierzbinski, Structure and mechanical properties of NiAl and Ni3Al-based alloys, International Journal of Mechanical Sciences, 42 (2000) 1499-1518

[41] G. K. Day, Physical metallurgy of nickel aluminides, Sadhama, 28 (2003) 247–262

[42] K. Dawi *et al.*, F. High temperature oxidation of SiC under helium with low-pressure oxygen. Part 3: beta-SiC-SiC/PyC/SiC, Journal of the European Ceramic Society, 32 (2012) 485-494

[43] C.P. Deck, K. Vecchio, Growth mechanism of vapor phase CVD-grown multi-walled carbon nanotubes, Carbon, 43 (2005) 2608–2617

[44] P. Diss *et al.*, Sharp indentation behavior of carbon/carbon composites and varieties of carbon, Carbon, 40 (2002) 2567–2579

[45] S. Dong *et al.*, Synthesis of intermetallic NiAl by SHS reaction using coarse-grained nickel and ultrafine-grained aluminum produced by wire electrical explosion, Intermetallics, 10 (2002) 217-223

[46] W. B. Downs and R. T. K. Baker, Modification of the surface properties of carbon fibers via the catalytic growth of carbon nanofibers, Journal of Materials Research, 10 (1995) 625-633

[47] M.S. Dresselhaus, G, Dresselhaus, P. Avouris, Carbon Nanotubes: Synthesis, Structure, Properties, and Applications, Topics in Applied Physics, 80 (2001) ISBN: 3-540-41086-4

[48] N. E. duToit, B.L. Wardle, S.G. Kim, Design Considerations for MEMS-scale Piezoelectric Vibration Energy Harvesters, Integrated Ferroelectrics, 71 (2005) 121-160

[49] N. E. duToit, B.L. Wardle, Performance of Microfabricated Piezoelectric Vibration Energy Harvesters, Integrated Ferroelectrics, 83 (2006) 13-23

[50] N.E. duToit, B.L. Wardle, Experimental Verification of Models for Microfabricated Piezoelectric Vibration Energy Harvesters, AIAA Journal, 45 (2007) 1126-1137

[51] T.W. Ebbesen, Carbon Nanotubes, Annual Review of Materials Research, 24 (1994) 235-264

[52] T.W. Ebbesen, In Carbon Nanotubes: Preparation and Properiaes, (1997) Chapter IV page 139, CRC Press, Inc., Boca Raton, Florida, USA

[53] M. Endo, H.W. Kroto, Formation of carbon nanofibers, The Journal of Physical Chemistry, 96 (1992) 6941–4

[54] M. Eslamloo-Grami, Z. A. Munir, The mechanism of combustion synthesis of titanium carbonitride, Journal of Materials Research, 9 (1994) 431-435.

[55] I. Eswaramoorthi, L.P. Hwang, Synthesis and characterisation of larger diameter multi-walled carbon nanotubes over anodic titanium oxide template, Letters to the Editor Carbon ,44 (2006) 2330–2356

[56] A.G. Evans, J.W. Hutchinson, The thermomechanical integrity of thin films and multilayers, Acta Metallurgica et Materialia, 43 (1995) 2507-2530

[57] E.O. Ezugwu, Z.M. Wang, A.R. Machado, The machinability of nickel-based alloys: a review, Journal of Materials Processing Technology, 86 (1999) 1–16

[58] E.O. Ezugwu , Z.M. Wang, Titanium alloys and their machinability-a review, Journal of Materials Processing Technology, 68 (1997) 262-274

[59] S. Fan *et al.*, Self-Oriented Regular Arrays of Carbon Nanotubes and Their Field Emission Properties, Science, 283 (1999) 512-514

[60] A. Feng, O.A. Graeve, Z.A. Munir, Modeling Solution for Electric Field-Activated Combustion Synthesis, Computational Materials Science, 12 (1998) 137-155

[61] J.C. Feng, J. Cao, Z.R. Li, Microstructure Evolution and Reaction Mechanism during Reactive Joining of TiAl Intermetallic to TiC Cermet Using Ti–Al–C–Ni Interlayer, Journal of Alloys and Compounds, 436, (2007) 298–302

[62] M. Ferraris *et al.*, Joining of machined SiC/SiC composites for thermonuclear fusion reactors, Journal of Nuclear Materials, 375 (2008) 410-415

[63] W.I. Frankhouser *et al.*, Gasless Combustion Synthesis of Refractory Compounds, Noyes Publications, Park Ridge, New Jersey (1985) 5-60

[64] E.J. Garcıa *et al.*, Aligned Carbon Nanotube Reinforcement of Advanced Composite Ply Interfaces, AIAA-2008-1768, 49th AIAA Structures, Dynamics, and Materials Conference, Schaumburg, IL, April 7-10, 2008

[65] E.J. Garcia *et al.*, Fabrication and Multifunctional Properties of High Volume Fraction Aligned Carbon Nanotube Thermoset Composites, Journal of Nano System and Technology, 1 (2009) 1-11

[66] E.J. Garcia *et al.*, Fabrication and multifunctional properties of a hybrid laminate with aligned carbon nanotubes grown In Situ, Composites Science and Technology, 68 (2008) 2034–2041

[67] E.J. García *et al.*, Fabrication and Nanocompression Testing of Aligned Carbon-Nanotube–Polymer Nanocomposites, Advanced Materials, 19 (2007) 2151–2156

[68] E.J. Garcıa *et al.*, Fabrication of composite microstructures by capillarity-driven wetting of aligned carbon nanotubes with polymers, Nanotechnology, 18 (2007) 165602-165612

[69] E.J. Garcia, B.L. Wardle, A.J. Hart, Joining Prepreg Composite Interfaces with Aligned Carbon Nanotubes, Composites Part A, 39 (2008) 1065-1070

[70] V.H. Garcia, P.M. Mors C. Scherer, Modeling of the self-propagating reactions of nickel and aluminum multilayered foils, Acta Materialia, 48 (2000) 1201-1206

[71] S. Gedevanishvili, D. Agrawal, R. Roy, Microwave combustion synthesis and sintering of intermetallics and alloys, Journal of Materials Science Letters, 18 (1999) 665-668

[72] W. Gacitua E., A. Ballerini A., J. Zhang, Polymer Nanocomposites: Synthetic and Natural Fillers: a Review, Maderas.Ciencia y tecnologia, 7 (2005) 159-178

[73] S. Gennari *et al.*, SHS of NbSi2: A Comparison Between Experiments and Simulations, Monatshefte für Chemie - Chemical Monthly, 136 (2005) 1871–1875

[74] S. Gennari *et al.*, A new approach to the modeling of SHS reactions: Combustion synthesis of transition metal aluminides, Acta Materialia, 54 (2006) 2343–2351

[75] S. Gennari *et al.*, Combustion Modes and Reaction Paths of the Self-Sustained High-Temperature Synthesis of Intermetallic Compounds: A Computer Simulation Study of the Effect of Exothermicity, Journal of Physical Chemistry B, 108 (2004) 19550–19556

[76] S. Gennari *et al.*, Combustion Synthesis of Transition Metals Aluminides, Journal of Physical Chemistry B, 110 (2006) 7144-7152

[77] S. Gennari, *et al.*, Simulation Study of Wave Propagation Instabilities for the Combustion Synthesis of Transition Metals Aluminides, Journal of Physical Chemistry B, 110 (2006) 7144-7152

[78] S. Gennari *et al.*, Self-Propagating High-Temperature Synthesis of Intermetallic Compounds: A Computer Simulation Approach to the Chemical Mechanisms, Journal of Physical Chemistry B, 107 (2003) 732-738

[79] S. Gennari *et al.*, SHS (Self-sustained high-temperature synthesis) of intermetallic compounds: effect of process parameters by computer simulation, Intermetallics, 11 (2003) 1355-1359

[80] S. Gobbi *et al.*, High powder CO2 and Nd-YAG laser welding of wrought Inconel 718, Journal of Materials Processing Technology, 56 (1996) 333-345

[81] G. Golkar, S.M. Zebarjad, J.V. Khaki, Optimizing the ignition behavior of microwave-combustion synthesized Al2O3/TiC composite using Taguchi robust design method, Journal of Alloys and Compounds, 487 (2009) 751-757

[82] Q. Gong *et al.*, The effect of carbon nanotubes on the microstructure and morphology of pyrolytic carbon matrices of C–C composites obtained by CVI, Composites Science and Technology, 65 (2005) 1112–1119

[83] V. Gonzaga de Resende, Growth of carbon nanotube forests on carbon fibers with an amorphous silicon interface, Carbon, 48 (2010) 3635-3658

[84] Guest Editorial, Who should be given the credit for the discovery of carbon nanotubes, Carbon, 44 (2006) 1621

[85] I.E. Gunduz *et al.*, Investigations on the self-propagating reactions of nickel and aluminum multilayered foils, Applied Physics Letters, 93 (2008) 134101/1-134101/3

[86] M. Gupta, W.W.L. Eugene, Microwaves and metals, John Wiley and Sons, Singapore, 2007

[87] S. Han, Joining of Ceramics and Ceramic Matrix Composites for Nuclear Applications, Polytechnic of Turin, Turin, Italy, Ph.D. Thesis, 2012.

[88] A.P. Hardt, P.V. Phung, Propagation of gasless reactions in solids. Analytical study of exothermic intermetallic reaction rates, Combustion and Flame, 21 (1973) 77-89

[89] P.J.F. Harris, Carbon Nanotube and Related Structures New Materials for the Twenty-first Century, Cambridge University Press (2010) ISBN: 9780511605819

[90] K. Hata *et al.*, Water-Assisted Highly Efficient Synthesis of Impurity-Free Single-Walled Carbon Nanotubes, Science, 306 (2004) 1362-1364

[91] J.K. Hong *et al.*, Microstructures and mechanical properties of Inconel 718 welds by CO2 laser welding journal of materials, Journal of Materials Processing Technology, 201 (2008) 515-520

[92] M. Houlle *et al.*, Mechanical enhancement of C/C composites via the formation of a machinable carbon nanofiber interphase, Carbon, 46 (2008) 76 –83

[93] W. Hu *et al.*, Growth of well-aligned carbon nanotube arrays on silicon substrates using porous alumina film as a nanotemplate, Applied Physics Letters, 79 (2001) 3083-3085

[94] B. Huneau *et al.*, The ternary system Al-Ni-Ti Part I: Isothermal section at 900°C; Experimental investigation and thermodynamic calculation", Intermetallics, 7 (1999) 1337-1345

[95] J. W. Hutchinson, Stresses and Failure Modes in Thin Films and Multilayers, Technical University of Denmark, Notes for Academic Course, October 1996

[96] S. Iijima, P.M. Ajayan, T. Ichihashi, Growth model for carbon nanotubes, Physical Review Letters, 69 (1992)3100–3103

[97] T. Inoue *et al.*, Synthesis of diameter-controlled carbon nanotubes using centrifugally classified nanoparticle catalysts, Carbon, 45 (2007) 2164–2170

[98] S. Jayaraman *et al.*, Numerical predictions of oscillatory combustion in reactive multilayers, Journal of Applied Physics, 86 (1999) 800-809

[99] L. Jodin *et al.*, Influence of the Catalyst Type on the Growth of Carbon Nanotubes via Methane Chemical Vapor Deposition, Journal of Physical Chemistry B, 110 (2006) 7328-7333

[100] L. Jodin *et al.*, Growth of CNTs via Methane CVD, Journal of Physical Chemistry B, 110 (2006) 7328-7333

[101] J.R. Jokisaari, S. Bhaduri, S.B. Bhaduri Microwave activated combustion synthesis of bulk cobalt silicides, Journal of Alloys and Compounds, 394 (2005) 160–167

[102] J.R. Jokisaari *et al.*, Processing of single phase Mo5Si3 by microwave activated combustion synthesis, Materials Science and Engineering A, 323 (2002) 478–483

[103] M. Kajihara, Analysis of kinetics of reactive diffusion in a hypothetical binary system, Acta Materialia, 52 (2004) 1193–1200

[104] Y. Katoh *et al.*, Current status and critical issues for development of SiC composites for fusion applications, Journal of Nuclear Materials, 367-370 (2007) 659-671.

[105] K.L. Kepple, G.P. Sanborn, P.A. Lacasse, K.M. Gruenberg, W.J. Readyd, Carbon, 46 (2008) 2026 –203

[106] K.L. Kepple *et al.*, Improved fracture toughness of carbon fiber composite functionalized with multi walled carbon nanotubes, Carbon, 46 (2008) 2026 – 2033

[107] B.I. Khaikin, A.G. Merzhanov, Theory of thermal propagation of a chemical reaction front, Combustion, Explosion and Shock Waves, 2 (1966) 22-27

[108] R. Khare, S. Bose, Carbon Nanotube Based Composites: A Review, Journal of Minerals and Materials Characterization & Engineering, 4 (2005) 31-46

[109] H.S. Kim *et al.*, Synthesis of Aligned Few-Walled Carbon Nanotubes on Conductive Substrates, Journal of Physical Chemistry C Letters, 113 (2009) 17983–17988

[110] Y.J. Kim *et al.*, Effects of sulfuric acid treatment on the microstructure and electrochemical performance of a polyacrylonitrile (PAN)-based carbon anode, Carbon 43 (2005)163–169

[111] O.B. Kovalev, V.A. Neronov, Metallochemical Analysis of the Reaction in a Mixture of Nickel and Aluminum Powders, Combustion, Explosion, and Shock Waves, 40 (2004) 172–179

[112] O. Kubaschewski, C.B. Alcock, P.J. Spencer., Materials Thermochemistry, 6th Edition, Oxford; New York: Pergamon Press, 1993, p.299/315

[113] M. Kumar, Carbon Nanotubes - Synthesis, Characterization, Applications, Carbon Nanotube Synthesis and Growth Mechanism, Dr. Siva Yellampalli (Ed.), ISBN: 978-953-307-497-9

[114] M. Kumar, Y.I Ando, Chemical Vapor Deposition of Carbon Nanotubes: A Review on Growth Mechanism and Mass Production, Journal of Nanoscience and Nanotechnology, 10 (2010) 3739–3758

[115] G. Li *et al.*, Interface correlation and toughness matching of phosphoric acid functionalized Kevlar fiber and epoxy matrix for filament winding composites, Composites Science and Technology 68 (2008) 3208–3214

[116] H.P. Li, An investigation of the ignition manner effects on combustion synthesis, Material chemistry and Physics 80 (2003) 758-767

[117] W.Z. Li, *et al.*, Large-Scale Synthesis of Aligned Carbon Nanotubes, Science 274 (1996) 1701-1703.

[118] Y. Li *et al.*, Growth of single-walled carbon nanotubes from discrete catalytic nanoparticles of various size, Journal of Physical Chemistry B, 105 (2001)11424–11431

[119] M. Lieblich, J.L.González-Carrasco, G. Caruana, Thermal stability of an Al/Ni3Al composite processed by powder metallurgy, Intermetallics, 5 (1997) 515-524

[120] Leonelli *et al.*, Microwave Assisted Sintering of Green Metal Parts, Journal of Materials Processing Technology, 205 (2008) 489–496

[121] Leonelli, G. Poli, P. Veronesi, Simulazione numerica ed evidenza sperimentale della accelerata formazione di colli durante le fasi iniziali della sinterizzazione assistita da microonde di polveri metalliche, Metallurgia Italiana, 4 (2007) 27-34

[122] C. Leonelli, G. Poli, P. Veronesi, Optimisation of the microwave assisted SHS of intermetallics in single mode applicators

[123] O.A. Louchev, *et al.*, Growth mechanism of carbon nanotube forests by chemical vapor deposition, Applied Physics Letters, 80 (2002) 2752-2754

[124] Y. Luo *et al.*, Fabrication of high-quality carbon nanotube fibers for optoelectronic applications Solar Energy Materials & Solar Cells, 97 (2012) 78–82

[125] G. Lütjering, Influence of Processing on Microstructure and Mechanical Properties of (α+β)Titanium Alloys, Materials Science and Engineering A, 243 (1998) 32–45

[126] J. Ma *et al.*, Single Mode Microwave Heating of copper Powder Metal Compacts, Proceedings of the COMSOL User Conference 2006 Boston

[127] Maglia, Dynamic behaviour and chemical mechanism in the self-propagating high-temperature reaction between Zr powders and oxygen gas, Phys. Chem. Chem. Phys., 3 (2001) 489-496

[128] Magrez *et al.*, Striking Influence of the Catalyst Support and Its Acid–Base Properties: New Insight into the Growth Mechanism of Carbon Nanotubes, ACS Nano, 5 (2011) 3428–3437

[129] A. Magrez, Catalytic CVD Synthesis of Carbon Nanotubes: Towards High Yield and Low Temperature Growth, Materials, 3 (2010) 4871-4891

[130] A.G. Mamalis *et al.*, Nanotechnology and nanostructured materials: trends in carbon nanotubes, Precision Engineering, 28 (2004) 16–30.

[131] A.B. Mann *et al.*, Modeling and characterizing the propagation velocity of exothermic reactions in multilayer foils, Journal of Applied Physics, 82 (1997) 1178-1188

[132] D T Marx, L Rwster, Mechanical properties of carbon—carbon composite components determined using nanoindentation, Carbon, 37 (1999) 1679-1684

[133] C. Mattevi, *et al.*, In-situ X-ray Photoelectron Spectroscopy Study of Catalyst−Support Interactions and Growth of Carbon Nanotube Forests, Journal of Physical Chemistry C, 112 (2008) 12207–12213

[134] W. McCauley, J. A. Puszynski, Historical perspective and contribution of US researchers into the field of self-propagating high-temperature synthesis (SHS)/combustion synthesis (CS): Personal reflections, International Journal of Self-Propagating High-Temperature Synthesis, 17 (2008) 58-75

[135] G.S.B. McKee, C.P. Deck, K.S. Vecchio, Dimensional control of multi-walled carbon nanotubes in floating-catalyst CVD synthesis, Carbon, 47 (2009) 2085-2094

[136] W. Merchan *et al.*, Combustion synthesis of carbon nanotubes and related nanostructures, Progress in Energy and Combustion Science, 36 (2010) 696-727

[137] G. Merzhanov, Reviews: Fundamentals, achievements, and perspectives for development of solid-flame combustion, Russian Chemical Bulletin, 46 (1997) 1-27

[138] A.G. Merzhanov, The theory of stable homogeneous combustion of condensed substances, Combustion and Flame, 13 (1969) 143–156

[139] A.G. Merzhanov, Theory and practice of SHS: worldwide state of the art and the newest results, International Journal of Self-Propagating High-Temperature Synthesis, (1993) 113-158

[140] A.G. Merzhanov, Nonequilibrium theory of flame propagation. In: Combustion, Detonation, Shock Waves: Proc. of the Zel'dovich Memorial, Int. Conf. on Combust., Moscow, 12-17 Sept., 1994 / Ed. S.M. Frolov. V.1. Moscow: Russ. Section Combust. Inst. Publ., 1994, p.20-44; Advances in Combustion Science: In Honor of Ya.B.Zel'dovich /Eds. W.A.Sirignano, A.G.Merzhanov, L. De Luca. Aeronaut. and Astronaut. Publ., 1997, p.37-59 (Ser.: Prog. in Astronaut. and Aeronaut., V.173)

[141] A.G. Merzhanov, A.E. Averson, The present state of the thermal ignition theory: An invited review, Combustion and Flame 16 (1971) 89-124

[142] A.G. Merzhanov, New elementary models of the second kind, Dokl. Akad. Nauk SSSR

[143] A.G. Merzhanov, Theory of gasless combustion, Arch. Procesow Spalania, 5 (1974) 17–39

[144] A.G. Merzhanov, V. M. Shkiro, I. P. Borovinskaya, Synthesis of refractory inorganic compounds, USSR Pat. 255221, 1967; Fr. Pat. 2088668, 1972; US Pat. 3726643, 1973; UK Pat. 1321084, 1974; Jpn. Pat. 1098839

[145] M. Mir, A. Hosseini, G.H. Majzoob, A numerical study of vibrational properties of single-walled carbon nanotubes, Computational Materials Science, 43 (2008) 540–548

[146] R.W. Messler, Joining Advanced Materials, Advanced Materials Process, 2 (1995) 47–49

[147] R.W. Messler, Principle of Welding Processes: Physics, Chemistry and Metallurgy, Wiley-VHC, Verlag GmbH & Co. KGaA, 2004 DOI: 10.1002/9783527617487

[148] R.W. Messler *et al.*, Welding with Self Propagating High Temperature Synthesis, Welding Journal, 74 (1995) 37–44

[149] A.C. Metaxas, R.J. Meredith, Industrial Microwave Heating, Peter Peregrinus, London (1993) 97-102

[150] A. Moisala, A.G. Nasibulin and E.I Kauppinen, The role of metal nanoparticles in the catalytic production of single-walled carbon nanotubes—a review, . Journal of Physics: Condensed Matter, 15 (2003) S3011–S3035

[151] J.J. Moore, H. J. Feng, Combustion synthesis of advanced materials: Part I. Reaction parameters, Progress in Materials Science, 39 (1995) 243-273

[152] J.J. Moore, H. J. Feng, Combustion synthesis of advanced materials: Part II. Classification, applications and modelling, Progress in Materials Science, 39 (1995) 275-316.

[153] K. Morsi, Review: reaction synthesis processing of Ni-Al intermetallic materials, Materials Science and Engineering A 299 (2001) 1-15

[154] K. Morsi, The diversity of combustion synthesis processing: a review, J. Journal of Materials Science,47 (2012) 68-92,

[155] Z.A. Munir, U. Anselmi-Tamburini, The synthesis of high-temperature materials by combustion, Materials Science Reports, 3 (1989) 277-365

[156] Z.A. Munir, U. Anselmi-Tamburini, The synthesis of high -temperature materials by combustion, Division of Materials Science and Engineering, College of Engineering, University of California, Davis, CA 95616, USA (1988)

[157] G.D. Nessim, Properties, synthesis, and growth mechanisms of carbon nanotubes with special focus on thermal chemical vapor deposition, Nanoscale, 2 (2010) 1306–1323

[158] S. Noda, *et al.*, Millimeter-Thick Single-Walled Carbon Nanotube Forests: Hidden Role of Catalyst Support, Japanese Journal of Applied Physics, Part 2: Letters and Express Letters, 46 (2007) L399-L401

[159] B.V. Novozhilov, The theory of surface spin combustion, Pure and Applied Chemistry, 65 (1993) 309-316

[160] W.C. Oliver, G.M. Pharr, An improved technique for determining hardness and elastic modulus using load and displacement sensing indentation experiments, Journal of Materials Research, 6 (1992) 564-1583.

[161] R.L. Orban, M. Lucaci, Powder Metallurgy Impact on the Nanocrystalline NiAl Processing, Romanian Journal of Physics, 49 (2004) 885–892

[162] S. Ozcan, P. Filip, Microstructure and wear mechanisms in C/C composite, Wear, 259 (2005) 642–650

[163] O. Ozdemir *et al.*, Tribological properties of NiAl produced by pressure-assisted combustion synthesis, Wear, 265 (2008) 979–985

[164] C. Pascal, R.M. Marin-Ayral, J.C. Tedenac, Joining of Nickel Monoaluminide to a Superalloy Substrate by High Pressure Self-Propagating High-Temperature Synthesis, Journal of Alloys and Compounds, 337 (2002) 221-225

[165] J. Peng, J. Binner, S. Bradshaw, Microwave initiated self-propagating high-temperature synthesis of SiC, Journal of Materials Synthesis and Processing, 9 (2001) 363-368.

[166] A.C Pierre, Introduction to sol gel processing, Boston Dordrecht London, Kluwer Academic Publisher (1998) ISBN: 0792381211-9780792381211

[167] H.O. Pierson, Handbook of Chemical Vapor Deposition, Noyes Publications, Park Ridge, New Jersey, U.S.A., (1992) ISBN: 0-8155-1432-8

[168] G. Poli, R. Sola, P. Veronesi, Microwave-assisted combustion synthesis of NiAl intermetallics in a single mode applicator: Modeling and optimisation, Materials Science and Engineering A, 441 (2006) 149-156

[169] J. Prasek *et al.*, Methods for carbon nanotubes synthesis—review, Journal of Materials Chemistr, 21 (2011) 15872-15884

[170] J. Puszynski, J. Degreve, V. Hlavacek, Modeling of Exothermic Solid-Solid Noncatalytic Reactions, Industrial & Engineering Chemistry Research, 26 (1987) 1424-1434

[171] L. Qu, Y. Zhao, L. Dai, Carbon microfibers sheathed with aligned carbon nanotubes: Towards multidimensional, multicomponent, and multifunctional nanomaterials, Small, 2 (2006) 1052–1059

[172] D. Quinn, B.L. Wardle, S.M. Spearing, Residual Stress and Microstructure of As-deposited and Annealed Sputtered Yttria Stabilized Zirconia Thin Films, Journal of Materials Research, 23 (2008) 609-618

[173] B. Riccardi *et al.*, Issues of low activation brazing of SiCf/SiC composites by using alloys without free siliconJournal of Nuclear Materials, 329-333 (2004) 562-566.

[174] R. Rosa *et al.*, Energy Transfer in Microwave Assisted Combustion Synthesis of Inorganic Compounds, Proceedings of 13th International Conference on Microwave and RF Power Applications, AMPERE 13th, Toulouse, France, (2011) 169–172, ISSN 0832-7823

[175] R. Rosa *et al.*, Microwave Activated Combustion Synthesis and Compaction in Separate E and H Fields: Numerical Simulation and Experimental Results, Proceedings of CIMTEC 2010, 12th International Ceramics Congress, June 6-11, 2010, Montecatini Terme, Italy, Advances in Science and Technology, 63 (2010) 197–202

[176] R. Rosa *et al.*,, Microwave Assisted Combustion Synthesis in the Ti-Si-C System for the Joining of SiC: Numerical Simulation and Experimental Results, Journal of Materials Chemistry, Submitted

[177] R. Rosa *et al.*, Microwave assisted combustion synthesis of intermetallics based functionally graded materials: numerical simulation and experimental results, International Journal of Self-Propagating High-Temperature Synthesis, 18 (2009) 163-172

[178] R. Rosa, Microwaves as Ignition Source in the Combustion Synthesis of High Performances Materials, Doctor of Philosophy “High Mechanics and Automotive Design and Technology” at the University of Modena and Reggio Emilia (2010)

[179] R. Rosa *et al.*, Microwave Ignited Combustion Synthesis as a Joining Technique for Dissimilar Materials, Journal of Materials Engineering and Performance, 21 (2012) 725-732

[180] R. Rosa *et al.*, Ni-Al-Ti Coatings Obtained by Microwave Assisted Combustion Synthesis, Surface Engineering, 28 (2012) 91-95

[181] R. Rosa, P. Veronesi, Functionally Graded Materials Obtained by Combustion Synthesis Techniques: A Review, Chap. 2, Functionally Graded Materials, Nathan

J. Reynolds Ed., Nova Science Publishers Inc., New York, 2011, pp. 93–122, ISBN 978-1-61209-616-2

[182] R. Rosa *et al.*,, Microwave (MW)-assisted combustion synthesis of micrometric metallic powders for the preparation of intermetallicbased materials, PM2010 World Congress and Exhibition, Florence, Italy 10-14 October 2010, Proceedings Vol. 2, pp. 217-223, ISBN 978 1 899072 11 8.

[183] K.I. Rybakov *et al.*, Microwave Heating of Conductive Powder Materials, Journal of Applied Physics, 99 (2006) 023506-1 023506-9

[184] R. Saito *et al.*, Physical Properties of Carbon Nanotube, Imperial College Press, London (1998) ISBN 978-1860942235

[185] G. Savage, Carbon-Carbon Composites, Chapman & Hall, London, (1993)

[186] C.M. Seah, S.P. Chai, A.R. Mohamed, Synthesis of aligned carbon nanotubes, Carbon 49 (2011) 4613–4635

[187] H. Shah Hosseini, M. Shamanian, M., A. Kermanpur, Characterization of Microstructures and Mechanical Properties of Inconel 617/310 Stainless Steel Dissimilar Welds, Mater. Character., 62 (2011) 425–431

[188] K.G. Shkadinswi, B.I. Khaikin, A.G. Merzhanov, Propagation of a pulsating exothermic reaction front in the condensed phase, Combustion, Explosion, and Shock Waves, 7 (1971) 15-22

[189] S.B. Sinnott *et al.*, Model of carbon nanotube growth through chemical vapor deposition, Chemical Physics Letters, 315 (1999) 25–30

[190] H.Y. Sohn, X. Wang, Journal Mathematical and experimental investigation of the self-propagating high-temperature synthesis (SHS) of TiAl3 and Ni3Al intermetallic compounds, Journal of Materials Science, 31 (1996) 3281-32888

[191] S.A. Steiner III, Carbon Nanotube Growth on Challenging Substrates: Applications for Carbon-Fiber Composites, Doctor of Philosophy at the Massachusetts Institute of Technologies.

[192] Suhail Farooqi, Review of Single Step Techniques for Production of ACNT's, International Journal Of Engineering And Computer Science, 1 (2012) 23-27

[193] A.R. Suraya *et al.*, Growth of Carbon Nanotubes on Carbon Fibers and the Tensile Properties of Resulting Carbon Fiber Reinforced Polypropylene Composites, Journal of Engineering Science and Technology, 4 (2009) 400-408

[194] K. Tanaka, T. Yamabe, Fukui K. The Science and Technology of Carbon Nanotubes, Chapter 2 M. YUMURA Synthesis and Purification of Multi-Walled and Single-Walled Carbon Nanotubes, Elsevier, 1999 ISBN: 0080426964

[195] S. Takenaka *et al.*, Formation of carbon nanotubes through ethylene decomposition over supported Pt catalysts and silica-coated Pt catalysts, Carbon, 47 (2009) 1251–1257

[196] X.Y. Tao *et al.*, Large-scale CVD synthesis of nitrogen-doped multi-walled carbon nanotubes with controllable nitrogen content on a $Co_{1-x}Mg_xO$ catalyst, Diamond and Related Materials, 16 (2007) 425–430

[197] A. Tasha, D. Binh, S. Supapan, Effects of Catalyst Components on Carbon Nanotubes Grown by Chemical Vapor Deposition, Journal of Undergraudate Research in Physics (2012) 1-8

[198] K.B.K. Teo *et al.*, Catalytic Synthesis of Carbon Nanotube and Nanofiber, Encyclopedia of Nanoscience and Nanotechnology, Edited by H.S. Nalwa, Volume X, 1-22

[199] M.Terrones, *et al.*, Controlled Production of Aligned-Nanotube Bundles, Nature, 388 (1997) 52-55

[200] M.L. Terranova, V. Sessa, M. Rossi, The world of carbon nanotubes: an overview of CVD growth methodologies, Chemical Vapor Deposition, 12 (2006) 315–325

[201] E.T. Thostenson *et al.*,Carbon Nanotube/carbon fiber hybrid multiscale composites, Journal of Applied Physics, 91 (2002) 6034-6037

[202] E.T. Thostenson, Z. Ren, T.W. Chou, Composites Science and Technology 61 (2001) 1899–1912

[203] E.T. Thostenson, Zhifeng Ren, Tsu-Wei Chou, Composites Science and Technology, 61 (2001) 1899–1912

[204] S. C. Tsang, P. J. F. Harris and M. L. H. Green Thinning and opening of carbon nanotubes by oxidation using carbon dioxide, Nature, 362 (1993) 520 - 522

[205] R.A. Vaia, H.D. Wagner, Framework for nanocomposites, Materials Today (Oxford, United Kingdom) 7 (2004) 32-37

[206] A. Varma, J.P. Lebrat, Combustion Synthesis of Advanced Materials, Chemical Engineering Science, 47 (1992) 2179-2194

[207] M.B. Vázquez-Santos *et al.*, Effects of phosphoric acid as additive in the preparation of activated carbon fibers from poly(p-phenylene benzobisoxazole) by carbon dioxide activation Journal of Analytical and Applied Pyrolysis, 95 (2012) 68–74

[208] P.Veronesi *et al.*, Microwave assisted combustion synthesis of non-equilibrium intermetallic compounds, JMPEE, Journal of Microwave Power and Electromagnetic Energy, 44 (2010) 45-56

[209] P. Veronesi *et al.*, Microwave Activated SHS for the Joining of SiCf/ SiC Composites to Themselves and to SiC matrix, Proceedings of the Global Congress on Microwave Energy Applications GCMEA 2008 MAJIC 1st, August 4-8, 2008, Otsu Prince Hotel, Lake Biwa, Otsu, Japan, pp 713–716

[210] P. Veronesi *et al.*, Enhanced reactive NiAl coatings by microwave-assisted SHS, Compel: The International Journal for Computation and Mathematics in Electrical and Electronic Engineering, 24 (2008) 491-499

[211] B.Viswanathan, Frontiers in Chemestry, Chapter 5: Synthetic Strategies in chemist-SOL-GEL TECHNIQUES L.H. Kumar, National Centre for Caralysis Research Indian Institute of Technology, Madras, April 2008

[212] D. Vrel, J.M. Lihrmann, P. Tobaly, Contribution of solid-state diffusion to the formation of titanium carbide by combustion synthesis, Journal of Materials Synthesis and Processing, 2 (1994) 179-187

[213] L. Wang Controllable synthesis of carbon nanotubes with ultrafine inner diameters in ethanol flam Physica B: Condensed Matter, 398 (2007) 18–22

[214] B.L. Wardle, D.S. Saito, E.J. Garcia, A.J. Hart, R. Guzman deVilloria, Fabrication and Characterization of Ultra-High Volume Fraction Aligned Carbon-Nanotube-Polymer Composites, Advanced Materials, 20 (2008) 2707-2714.

[215] Warson, C. A. Finch, Applications of Synthetic Resin Latices, Fundamental Chemistry of Latices & Applications in Adhesives Volume 1, pg 608, John Wiley & Sons Ltd., (2001)

[216] M. Willert-Porada *et al.*, Microwave Sintering of High-Performance Ceramics: Material and Technological Aspects, CFI Ceramic Forum International, 75 (1998) 19-25

[217] C. Williams and J. Fernie, Novel joining and sealing processes for solid oxide fuel cells, 5th European Solid Oxide Fuel Cell Forum, Lucerne, Switzerland, 1-5th July 2002

[218] Z. Wu *et al.* Nitric Acid Oxidation of Carbon Fiber and the Effect of Subsequent treatment in Refluxing Aqueous NaOH Carbon, Carbon 33 (1995) 597-605

[219] S. Xie *et al.*, Carbon nanotubes arrays, Materials Science and Engineering A286 (2000) 11–15

[220] N. Yamamoto, Thermomechanical Testing of Materials and Structures for a Microfabricated Fuel Cell, MIT S.M. Thesis, August 2006

[221] N. Yamamoto, B.L. Wardle, Thermal and Electrical Properties of Hybrid Woven Composites Reinforced with Aligned Carbon Nantoubes, AIAA-2008-1857, 49th AIAA Structures, Dynamics, and Materials Conference, Schaumburg, IL, April 7-10, 2008

[222] J.M. Yang, The Mechanical Behavior of in-situ NiAl-Refractory Metal Composites, JOM 49 (1997) 40-43

[223] C.L. Yeh, W.H. Chen, C.C. Hsu, Formation of titanium silicides Ti5Si3 and TiSi2 by self-propagating combustion synthesis, J. Alloys Compds. ,432 (2007) 90-95

[224] J.M. Zazula, On Graphite Transformations at High Temperature and Pressure Induced by Absorption of the LHC Beam, LHC Project Note 78 / 97 January 18, 1997

[225] A.A. Zenin, A.G. Merzhanov, G.A. Nersisyan, Investigation of the thermal-wave structure in self-propagating high-temperature systhesis, Fiz. Goreniya Vzryva, 17 (1981) 79–90

[226] Zhang *et al.*, Effect of isotropic interlayers on the mechanical and thermal properties of carbon/carbon composites, Materials Letters 64 (2010) 1536–1538

[227] Y. Zhang *et al.*, Imaging as-grown single-walled carbon nanotubes originated from isolated catalytic nanoparticles, Applied Physics A, 74 (2002) 325–328

[228] X. Zhang *et al.*, Rapid growth of well-aligned carbon nanotube arrays, Chemical Physics Letters, 362 (2002) 285–290

[229] Q. Zhang *et al.*, Hierarchical composites of carbon nanotubes on carbon fiber: Influence of growth condition on fiber tensile properties , Composites Science and Technology, 69 (2009) 594–601

[230] P. Zhu , J.C.M. Li, C.T. Liu, Reaction mechanism of combustion synthesis of NiAl Materials Science and Engineering A, 329-331 (2002) 57–68

[231] S. Zhu *et al.*, Carbon nanotube growth on carbon fibers Diamond and Related Materials, 12 (2003) 1825–1828

List of Publications

- G. D. Chen, F. Fachin, **E. Colombini**, B.L. Wardle and M. Toner
  Nanoporous micro-element arrays for particle interception in microfluidic cell separation
  Lab on Chip, (2012), 12 (17) 3159-3167

- R. Rosa, **E. Colombini**, P. Veronesi, G. Poli, C. Leonelli
  Microwave ignited combustion synthesis as a joining technique for dissimilar materials
  Journal of Materials Engineering and Performance, (2012) 21, (5), 725-732

- **E. Colombini**, R. Rosa, P. Veronesi, M. Cavallini, G. Poli, and C. Leonelli
  Microwave ignited combustion synthesis as a joining technique for dissimilar materials: modeling and experimental results.
  Journal of SHS, (2012) 21 (1) 25-31

- **E. Colombini**, R. Rosa, P. Veronesi, A. Casagrande
  Microwave ignited combustion synthesis of intermetallic compounds, modeling and experimental results
  La Metallurgia Italiana, (2011), 103 (4) 29-34

- P.Veronesi, R.Rosa, **E.Colombini**, C.Leonelli, G.Poli, A.Casagrande
  Microwave Assisted Combustion Synthesis of Non-equilibrium Intermetallic Compounds
  Journal of Microwave Power and Electromagnetic energy, (2010) 44 (1) pp.46-56

- R.Rosa, P.Veronesi, S. Han, V. Casalegno, M. Salvo, **E. Colombini**, C. Leonelli, M. Ferraris
  Pressure-less microwave assisted combustion synthesis in the Ti-Si-C system for the joining of SiC: numerical simulation and experimental results,
  J. Mater. Chem. (Royal Society of Chemistry) Accepted

- P. Veronesi, R. Rosa**, E. Colombini**
  Control of the Microstructure of Powder Metallurgy Products by Microwave Heating, chapter submitted for publication on the volume
  Microwave Power Engineering with Advanced Computer Modeling, CRC Press.

- S. Gaiani, P. Veronesi, **E. Colombini**, G. Poli
  Evoluzione della tessitura Cristallografica durante la deformazione plastica di leghe di titanio alfa laminate a freddo
  La Metallurgia Italiana Accepted

- P. Veronesi, S. Gaiani, **E. Colombini**, G. Poli
  Recycling of alpha titanium technological scrap for exhaust system part manufacturing
  Journal of cleaner production, Submitted

Abstract contributions presented at national and international conferences

34° AIM: 7/9 Novembre 2012, Brescia (Italia)

R. Sola, **E. Colombini**, P. Veronesi, G. Poli, G.Parigi
Tempra laser di 40CrMnMo7 pre-nitrurato in plasma: influenza delle condizioni di trattamento

TITANIUM 2011 Conference: 2/5 October 2011, San Diego, CA (USA) Proceeding

E. Colombini, S. Gaiani, P.Veronesi, A.Balestri
Surface Modification of alphaTi alloys to increase high temperature wear resistance

SHS 2011- XI International Symposium: 5/9 September 2011, Atene (Grecia)

E. Colombini, R. Rosa, P. Veronesi, C. Leonelli, G. Poli
Microwave ignited combustion synthesis as a joining technique for dissimilar materials: modeling and experimental results (Premio come migliore presentazione orale e lavoro di ricerca)

R. Rosa, P. Veronesi, **E. Colombini**, M. Michelazzi, C. Leonelli, A.R. Boccaccini
Innovative combination between Combustion Synthesis and Electrophoretic Deposition Techniques

R. Rosa, P. Veronesi, **E. Colombini**, C. Leonelli, G. Poli
β-NiAl coated γ–TiAl intermetallic based alloy by contemporary combustion synthesis (Poster)

33° AIM: 11/13 Novembre 2010, Brescia (Italia)

E. Colombini, R. Rosa, P. Veronesi, A. Casagrande
Microwave assisted combustion synthesis of intermetallic compound: a multiphysics simulation and experimental validation

Publications appeared on abstracts of national and international conferences

54th AIAA/ASME/ASCE/AHS/ASC Structures, Structural Dynamics, and Materials Conference and Co-located Events: 8/11 April 2013

I. Stein, H. Vincent, S. Steiner , **E. Colombini**, BL Wardle
Processing and Mechanical Property Characterization of Aligned Carbon Nanotube Carbon Matrix Nanocomposite

34° AIM: 7/9 Novembre 2012, Brescia (Italia)

S. Gaiani, P. Veronesi, **E. Colombini**, G. Poli
Evoluzione della tessitura cristallografica durante la deformazione plastica di leghe di titanio alfa laminate a freddo

EUROMAT 2011: 12/15 Settembre 2011, Montpellier (France)

E. Colombini, R. Rosa, P.Veronesi, G. Poli
Microwave assisted combustion synthesis of aluminides: multiphysics simulation

R. Rosa, **E. Colombini**, P. Veronesi, G. Poli, C. Leonelli
Microwave ignited combustion synthesis as joining technique for dissimilar materials

ICMAT 2011: 26 Giugno-1 Luglio 2011, Suntec (Singapore)

P. Veronesi, A. Boccaccini, R. Rosa, **E**. **Colombini**, C. Leonelli
Microwave processing of glass-matrix composites in predominant magnetic or electric field

Publications appeared on proceeding of national and international conferences

2012 International Microwave Symposium, 7-22 Giugno 2012, Montreal (QC)

P. Veronesi, R. Rosa, **E. Colombini**
Rapid Microwave Sintering of Protective ZrO2 Coatings on Reactive Metal Powder Compacts (art. no. 6259780)

PM 2011: 9-12 Ottobre 2011, Barcelona (Spagna)

R. Rosa, R. Sola, **E. Colombini**, P. Veronesi and C. Leonelli
Microwave Ignited Combustion Synthesis of Metal and Intermetallic Matrix Composites, Vol.3 , p.141, Sintering, ISBN: 978-1-899072-23-1

Titanium 2011 Conference: 2/5 October 2011, San Diego, CA (USA)

S. Gaiani, **E. Colombini**, P. Veronesi, F. Mantovani
Comparison Between Different Titanium Welding Technologies

Titanium 2012 Conference Proceeding 5/8 October 2012, Atlanta GA (USA)

S. Gaiani, **E. Colombini**, P. Veronesi, R. Rosa
Optimization of the chemical milling of investment cast titanium alloys